# Metrology Enabled Tooling for the Assembly of Aero-Structures

Martin, Oliver

*Award date:*
2016

*Awarding institution:*
University of Bath

# Metrology Enabled Tooling for the Assembly of Aero-Structures

submitted by

O. C. Martin

for the degree of Doctor of Philosophy

of the

University of Bath

Department of Mechanical Engineering

December 2015

**Summary**

Metrology and Tooling are considered as discrete disciplines within Manufacturing Engineering, however, assembly tooling often acts as a checking mechanism. Assembly tooling has the primary function of controlling part location during assembly; with a secondary requirement as a *quality gate*. In-tool checks are manual mechanical checks of the assembly, these gauging checks assume the tooling has the correct, nominal geometry. Tooling conformance is certified periodically; however these intervals can be up to three years. Further examination of the metrology requirements within the aerospace industry with respect to large scale assembly tooling identify a requirement to: reduce manual metrology checks, reduce tooling recertification time, and enable greater automation.

Currently, there is a lack of integration between metrology and Wing-box assembly tooling. This research investigates how to increase manufacturing confidence with respect to tooling conformance; and, ultimately improve the manufacturing process for aero-structures, through the increased and enhanced use of metrology in the assembly tooling environment.

The Metrology Enhanced Tooling for Aerospace (META) framework has been created to provide a robust framework for deploying metrology in the tooling environment. The major elements of the framework are subsequently detailed and demonstrated in three chapters: i) large volume metrology networks, for the measurement of tooling structures; testing instrument performance, quantifying and improving the uncertainty estimation, and ultimately, establishing a rapid measurement process for assembly tooling; ii) embedded metrology systems demonstrates how local measurement systems can be utilised to replace and improve on, traditional in-tool checks; and iii) metrology feedback presents an example of an automated tooling pick-up that manipulates the assembly to achieve the design intent.

The contributions can be summarised as: firstly, the creation of the META framework for the deployment of metrology in assembly tooling environment, accommodating and facilitating a number of the future tooling and assembly requirements. Secondly, the establishment of a generic commissioning methodology and measurement strategy for the rapid measurement of assembly tooling to increase tooling confidence. The research output was demonstrated in a case study, through a combination of physical measurement and digital automation simulation to prove the process time was greatly decreased from current methods.

*For Ma & Pop*

## Acknowledgements

This PhD has been sponsored by Airbus UK, and the EPSRC Innovative Manufacturing Research Centre at the University of Bath (Grant Reference GR/R67507/0).

First and foremost I would like to thank the University of Bath and in particular, my supervisors: Prof. Stephen T. Newman and Dr. Vimal Dhokia, for taking me on so late in the day, giving their time generously, and for seeing the process through. In addition, thanks to Paul Maropoulos for starting my PhD with me. I would like to thank all the other members of the university that have helped me along the course of my research, including (but not limited to): Prof. Patrick Keogh, Dr. Jody Muelaner and Dr. Zheng Wang. Lastly, to Helen Liang for emotional support, motivational chats, and everything else. Through the Metrology Assisted Assembly hub of Airbus UK, I have had the pleasure of working with other universities on projects that helped shape and contribute to my research; I would like to thank them for their support, in particular: Prof. Svetan Ratchev & Dr. Tony Smith of the University of Nottingham; and Prof. Stuart Robson of University College London. Alongside the academic input, I have received much industrial steer and relevance to my research through engaging with Airbus UK. The engineers were patient, welcoming and enthusiastic. I would like to thank them all, especially: Mark Summers, Dave Tomlinson, Amir Kayani, Jon Wright, Abdul El-Nounu, Mike Toutt, Kerion McGloughlen & Gaz Edwards. I would also like to mention a couple of hardware vendors that have always been kind and helpful, lending both equipment and time readily: including Jon Kimber (Hexagon Metrology), Keith Noble & Darren Robbins (Faro), Nicolas Tanala (V-STARS/NTI), Kevin Hawley (GOM) and especially Craig Green (Horst Witte/Solve Metrology).

I would like to thank Ben Adeline (INSPHERE) for his support and the Friday *write-up days*. A special thanks to Craig Davey (INSPHERE) for reading my work, running with me, and keeping me honest. Most importantly, thanks to my family, for keeping me motivated and looking after Lucy, and for giving me a reason. Finally, I would like to give a special acknowledgement and big thank you to Aliya for putting up with me during the worst of it and picking me up when I needed it most.

# Contents

# List of Figures

# List of Tables

# Abbreviations

| | |
|---|---|
| A/C | Aircraft |
| ADM | Absolute Distance Measurement |
| ALCAS | Advanced Low-Cost Aircraft Structures |
| AMM | Assemble-Move-Measure |
| ASME | American Society of Mechanical Engineers |
| AT901 | Absolute Tracker 901 |
| AUK | Airbus United Kingdom |
| BLADE | Breakthrough Laminar Aircraft Demonstrator in Europe |
| BSI | British Standards Institution |
| CAD | Computer Aided Design |
| CAM | Computer Aided Manufacture |
| CCD | Charge-Coupled Device |
| CMM | Co-ordinate Measurement Machine |
| CMOS | Complementary Metal-Oxide-Semiconductor |
| CTE | Co-efficient of Thermal Expansion |
| DFA | Design for Assembly |
| DFM | Design for Manufacture |
| DMT | Digital Master Tooling |
| DMU | Digital Mock-Up |
| DPV | Digital Planning Validation |
| DSLR | Digital Single-Lens-Reflex |
| EDM | Electronic Distance Meter |
| ERS | Enhanced Reference System |
| FAL | Final Assembly Line |
| FMS | Flexible Manufacturing System |
| FOV | Field of View |
| FRS | Floor Reference System |
| FTI | Flight Test Instrumentation |

| | |
|---|---|
| GD&T | Geometric Tolerancing and Dimensioning |
| GUI | Graphical User Interface |
| GUM | Guide to the Expression of Measurement Uncertainty |
| HAHC | High Accuracy and High Capacity |
| HMT | Hard Master Tooling |
| ICY | Inter-changeability |
| IdMRC | Innovative Design and Manufacturing Research Centre |
| IEC | International Electrotechnical Commission |
| IFM | Interferometer |
| IML | Inner Mould Line |
| INBD | Inboard |
| ISO | International Organisation of Standardisation |
| KC | Key Characteristic |
| LED | Light Emitting Diode |
| LIMA | Laboratory for Integrated Metrology Applications |
| LOS | Line-of-Sight |
| LR | Long-Range |
| LS | Least Squares |
| LVM | Large Volume Metrology |
| LVMC | Large Volume Metrology Conference |
| MAA | Metrology Assisted Assembly |
| MADA | Metrology Assisted Determinate Assembly |
| MAF | Main Assembly Fixture |
| MAJ | Main Assembly Jig |
| MAST | Metrology & Assembly Systems & Technologies |
| MBD | Model-Based Definition |
| MCS | Monte Carlo Simulation |
| MP | Measurement Plan |
| MPE | Maximum Permissible Error |
| MR | Mid-Range |
| MScMS | Mobile Spatial co-ordinate Measuring System |
| MSN | Milestone Number |
| NGCW | Next Generation Composite Wings |
| NIST | National Institute of Standards and Technology |
| NPL | National Physical Laboratory |
| NMG | Numerical Master Geometry |
| NRC | Non-Recurring Cost |

| | |
|---|---|
| NRK | New River Kinematics |
| OIML | International Organisation of Legal Metrology |
| OML | Outer Mould-Line |
| OTBD | Outboard |
| OTP | Optical Tooling Point |
| PCMM | Portable Co-ordinate Measurement Machine |
| PDF | Probability Density Function |
| PI | Physik Instrumente |
| PLM | Product Lifecycle Management |
| POI | Position of Interest |
| QA | Quality Assurance |
| QC | Quality Control |
| RAG | Red, Amber & Green |
| RBO | Rigid Body Offset |
| RBT | Rigid Body Transform |
| RFA | Robotics in Fixture-less Assembly |
| RFV | Random Fuzzy Variables |
| RP | Reference Point |
| R&T | Research and Technology |
| SA | SpatialAnalyzer |
| SDK | Software Developers Kit |
| SLR | Single-Lens-Reflex |
| SPC | Statistical Process Control |
| STBD | Starboard |
| TCP | Tool Centre Point |
| TOA | Time of Arrival |
| TRL | Technology Readiness Level |
| UDP | User Datagram Protocol |
| UoB | University of Bath |
| UCL | University College London |
| UKAS | The United Kingdom Accreditation Service |
| UoN | University of Nottingham |
| USMN | Unified Spatial Metrology Network |
| VB | Visual Basic |
| VC# | Visual C-Sharp |
| VC++ | Visual C++ |
| VIM | Basic and General Terms |

| | |
|---|---|
| VIML | International Vocabulary of Terms in Legal Metrology |
| VLM | Vocabulary of Legal Metrology |
| VMS | Vision Measurement Software |
| VR | Virtual Reality |
| V-STARS | Video Self-calibration Triangulation and Resection System |
| wMPS | workspace Measuring and Positioning System |
| ZPC | Zero-Point-Clamp |

# Symbols

| | | |
|---|---|---|
| $c_i$ | = | Sensitivity coefficient |
| $d$ | = | Displacement |
| $d_o$ | = | Deadpath distance (offset) |
| $\delta_o$ | = | Uncertainty associated with deadpath |
| $\epsilon$ | = | Uncertainty associated to the azimuth encoders |
| $\epsilon_o$ | = | Uncertainty associated to the alignment offset of azimuth encoders |
| $k$ | = | Coverage factor |
| $i_c$ | = | Instrument uncertainty from the calibration certificate |
| $i_r$ | = | Instrument's resolution or fidelity of measurement |
| $n_c$ | = | Cosine error |
| $n_m$ | = | Average of the uncertainty magnitude associated to measured points |
| $n_n$ | = | Magnetic nest uncertainty |
| $n_r$ | = | Axis runout variance |
| $n_t$ | = | Spherically Mounted Retro-reflector (SMR) mechanical centring tolerance |
| $\omega$ | = | Uncertainty associated with refractive index |
| $P$ | = | Position |
| $P^*$ | = | 'True' position |
| $p_{spec}$ | = | V-STARS specification uncertainty |
| $p_t$ | = | Retro-reflector 1.5" split bearings mechanical centring tolerance |
| $p_{tp}$ | = | Temperature probe uncertainty |
| $p_{vb}$ | = | Variance output from the V-STARS bundle adjustment algorithm |
| $\phi$ | = | Elevation (measured) |

| | | |
|---|---|---|
| $\phi^*$ | = | 'True' Elevation |
| $r$ | = | Radial distance (measured) |
| $r^*$ | = | 'True' radial distance |
| $\rho$ | = | Uncertainty associated to the zenith encoders |
| $\rho_o$ | = | Uncertainty associated to the alignment offset of zenith encoders |
| $\sigma$ | = | Standard deviation |
| $t_t$ | = | Tooling ball manufacturing tolerance |
| $\theta$ | = | Azimuth (measured) |
| $\theta^*$ | = | 'True'Azimuth |
| $U_c$ | = | Expanded uncertainty |
| $u_c$ | = | Standard uncertainty |
| $x_c, y_c, z_c$ | = | Measured centre offset |
| $x_r, y_r, z_r$ | = | Runout variance |
| $Y_{x,y,z}$ | = | 3D measurand |

# Chapter 1

# Introduction

## 1.1 Research Need

In the Engineering community, tooling can include a wide spectrum of manufacturing aids, in the context of this thesis, tooling is used to refer to *Assembly Tooling*; this encompasses both *jigs* and *fixtures*.

Traditional 'monolithic' aerospace assembly tooling consists of large, static steel structures secured to the reinforced-concrete factory floor; these tools are configured for one aircraft type only. This traditional build philosophy controls all the features by: common jig location, master jig datum, jig setting, certification points, build slips and pin diameters (Tomlinson and Singh, 2008). The positional, dimensional and geometric accuracy of the assembly is implied from the tooling. That is to say, if the tooling is correct and the components are positioned correctly within the tooling, then the assembly is correct. These mechanical measurements and checks ensure the build tolerances are maintained throughout the assembly process.

The manufacturing positional tolerances of the tooling interfaces and location pins/slips must be less than the assembly tolerances; ideally <10% although this is rarely possible at the dimensional scale of a wing-box assembly. Monolithic jigs and fixtures are very expensive, have lead times in excess of 24 months (Millar and Kihlman, 2009) and have little ability to accommodate product variation and design changes. Expense and long lead times are driven by the tight assembly tolerances. As an example: a metallic wing build can have assembly tolerances in the order of $\pm 0.3\,\text{mm}$, globally; the tooling is constructed with a setting tolerance of around $\pm 0.15\,\text{mm}$ consuming up

to 50 % of the assembly tolerance budget.

The assembly tooling primarily controls the: position, location and form of the required assembly; however, this tooling has an additional function as a checking mechanism, acting as a *quality gate* for the completed assembly. Part and assembly verification involves manually rotating pins and moving slips to ensure that the assembly is correctly positioned and held within the fixture. It follows that metrology is intrinsically linked to tooling. The tool setting and recertification is a manual and time consuming process, consequently, massive structures are needed to achieve the rigidity and stability required to maintain the tooling tolerances for multiple years without recertification. There is an associated risk that out of tolerance assemblies could go undetected between recertification periods.

Fixture manufacture times and non-recurring costs (NRCs) could be reduced if assembly fixtures moved away from traditional *hard* tooling and moved towards *soft* tooling, that is: away from large, rigid structures and towards reconfigurable or flexible tooling. Figure 1-1 describes this current and future state of aerospace assembly/manufacture.

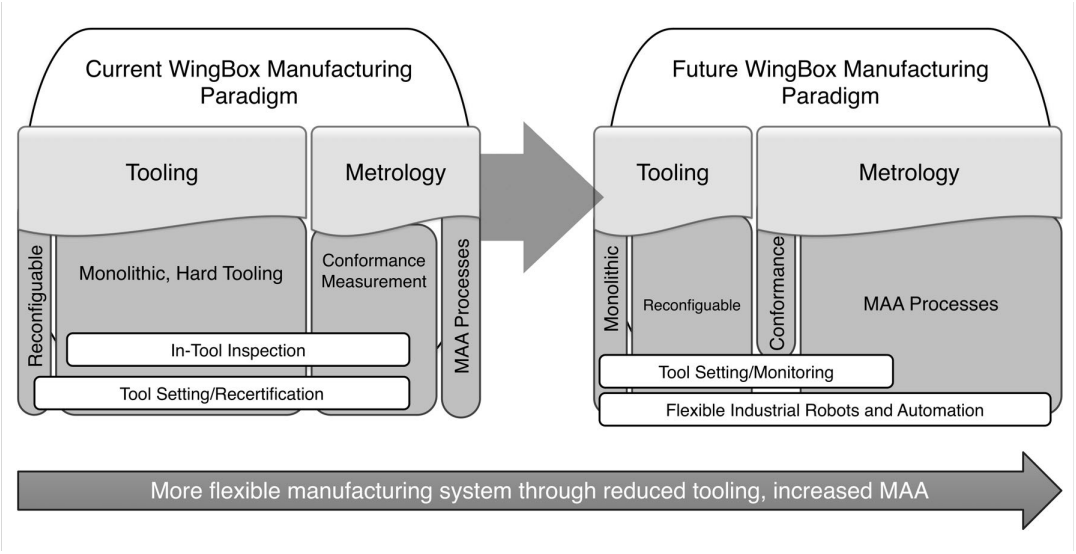


Figure 1-1: The research landscape: illustrating the interaction between metrology and tooling within Wing-box assembly manufacture, with the current [left] and future [right] states

In order to achieve this paradigm shift a strong metrological infrastructure is required to maintain the required tolerances within the tooling and the assembly process;

this research addresses this need.

## 1.2 Knowledge Gaps

Historically, metrology and assembly tooling are considered as closely related, but discrete disciplines within manufacturing engineering. The existing research associated to the metrology challenges within large aerospace assembly tooling is limited; as such, the research gaps are significant and in some cases fundamental. Much of the metrology knowledge in the context of large scale assembly tooling remains within industry practices, and has not been disseminated through publication.

Industrial tooling practices give an alternative perspective on the knowledge gaps, that have little or no academic exposure. One such area, is the verification of assembly tooling condition. Due to the complexity and scale of Wing-box assembly tooling, the time to check the fixture is extensive; consequently, the tools have long periods of time between certifications (years).

However, it is apparent from the available literature that assembly tooling employs metrology as an enabling technology to build and verify the tooling, but does not yet have an integrated approach to embedding into aerospace Wing-box assembly tooling. Consequently, tooling structures are dominated by mechanical gauging with no in-process digital metrology. More fundamentally still, estimating the co-ordinate measurement uncertainty when certifying tooling structures remains undocumented. This is of particular importance when considering the challenging relative tolerances over the manufacturing scale.

## 1.3 Research Aims

This research explores the implicit links between metrology and tooling, the overlap, and more importantly, how the two disciplines can mutually benefit from an integrated approach. The overall aims can be summarised as:

- To increase manufacturing confidence with respect to tooling conformance;
- To improve the manufacturing process for aero-structures, specifically: the assembly of wing-boxes through the novel deployment of metrology within the tooling environment.

## 1.4 Research Objectives

Following the identification of the knowledge gaps and research aims, these research aims will be achieved through the following *objectives*:

i) To create a generic framework for the integration of metrology and assembly tooling; accommodating the multi-disciplinary, high resource needs of aerospace wing-box manufacture.

ii) To define the sources of uncertainty on large scale, multi-instrument measurement networks in non-controlled environments.

iii) To establish a method for the rapid measurement of Wing-box assembly tooling.

iv) To reduce the dependency on manual, mechanical in-tool checks for component placement and assembly conformance. Quantify the associated uncertainty for integrating these techniques

## 1.5 Thesis Structure

The thesis is divided into 9 major chapters. The Chapter 1 introduces the research need, aims and objectives. Chapter 2 provides a review of metrology, dimensional uncertainty and Wing-box assembly tooling academic literature. In Chapter 3 a complimentary review from an industrial perspective of aircraft Wing-box assembly is provided.

In Chapter 4 a framework is introduced and outlined for Metrology Enhanced Tooling for Aerospace, entitled the META framework. The following chapters 5, 6 and 7 detail the major functionality and demonstration of the framework, namely: large volume metrology networks, embedded metrology systems and metrology feedback. Chapter 8 discusses the research findings and limitations in order to formulate the conclusions and future work found in Chapter 9.

# Chapter 2

# Review of Large Volume Metrology, Dimensional Uncertainty, and Aerospace Wing-box Assembly Literature

## 2.1 Introduction

This chapter researches the historical and current knowledge that is relevant to the intended field of contribution. Broadly the three main areas are: *Metrology*, *Assembly Tooling* and the *Digital Environment*. Greater emphasis and fidelity has been given to the review of *Metrology* as this is an established field of research.

The metrology sections The sections related to Metrology, are from Section 2.2 to 2.8; *Large Volume Metrology* is first discussed as a precursor for contextualising the subsequent Sections 2.3: *Dimensional Uncertainty*; and Section 2.4, a review of the inter-relationship between *Uncertainty and Tolerance*. Sections 2.5 and 2.6 introduce the mathematics used when deploying the measurement systems introduced in Section 2.2. Section 2.5: *Position and Location* describes the mathematical models used for determining co-ordinate definitions from triangulation technologies and multi-lateration techniques. *Network Adjustments* (Section 2.6) takes the co-ordinate definitions from multiple measurement stations and bundles the information for optimised co-ordinate definitions with a reduction in dimensional measurement uncertainty.

Networked instruments and sensors are further detailed in Section 2.7, *Data Fusion.* Finally, *Metrology Assisted Assembly (MAA)* is reviewed. This section navigates through the relatively recent field of MAA. The research contained within this thesis: *Metrology Enabled Tooling for the Assembly of Aero-Structures* is perhaps best described as a new sub-group contained within MAA.

Tooling is a generic term, consequently the literature review specifically examines tooling within the context of aerospace Wing-box assembly. *Aerospace Wing-box Assembly Tooling* (Section 2.9) examines the functional and ergonomic requirements as well as the considerations for design for manufacture and assembly. Automated tooling is also included for completeness although at the Wing-box assembly level this is limited.

Lastly, the *Digital Environment* (Section 2.10) is briefly reviewed with respect to its use and application to the tooling digital mock-up (DMU) environment and metrology software.

## 2.2 Large Volume Metrology

Aerospace components are often too large to be practically measured within a conventional, gantry-style, Co-ordinate Measurement Machine (CMM), instead Large Volume Metrology instruments are employed. Large Volume Metrology (LVM) is defined by the National Physical Laboratory (NPL) as measurements larger than one metre, or: that the metrology has to be brought to the component and not vice-versa (NPL, 2014). This section explores the available metrology instruments and their associated operational technologies, for the measurement of large aerospace components, such as wing-boxes.

### 2.2.1 Spherical Co-ordinate Metrology Systems

Spherical co-ordinate measurement systems produce Cartesian coordinates $(x, y, z)$ from the polar information: radial distance, azimuth and zenith/elevation (Figures 2-13 & 2-14). Interferometers or ADMs measure the radial distance and the angles (azimuth and zenith) are calculated from rotary encoders.

**Fundamental Technologies**

Combining the following fundamental technologies (or at least the principal concepts) gives rise to a spherical coordinate measurement system.

*Fringe Counting Interferometers* measure linear displacement in one-dimension; the measured displacement is a relative measurement and not an absolute one. The basic operation of an interferometer begins with splitting a coherent light source into two; one beam is reflected back to a sensor internally and is the stable reference beam, the other beam is reflected from a target back to the sensor along the same path as the reference beam. The two beams recombine before the sensor and as the target moves the reflected beam shifts phase with respect to the reference beam. Fringe counting interferometers count the interference fringes created when the reference beam combines with the reflected beam (from the target), this is analogous to a linear encoder counting grate intervals. A simple binary model would only consider total constructive and total destructive interference; when both the reference and reflected light source are reunited in-phase they are constructively interfering (intense light), but when the reflected beam is shifted by half the wavelength ($\lambda/2$) of the light source then total destructive interference is experienced (dark): this produces interference fringe patterns which cycle between light and dark over half the wavelength. For visible light the wavelength is between 400-700nm, and so the fringe patterns are spaced 200-350nm apart; this gives us our basic unit of measurement. However, as the light shifts between these binary states the interface fringes create intensity gradients, these fringe patterns can be further analysed and measurements can be interpolated with uncertainties of less than 1/1000 of a fringe (Schodel, 2009). Figure 2-1 illustrates the fringe patterns experienced when the reference and reflected beam recombine.

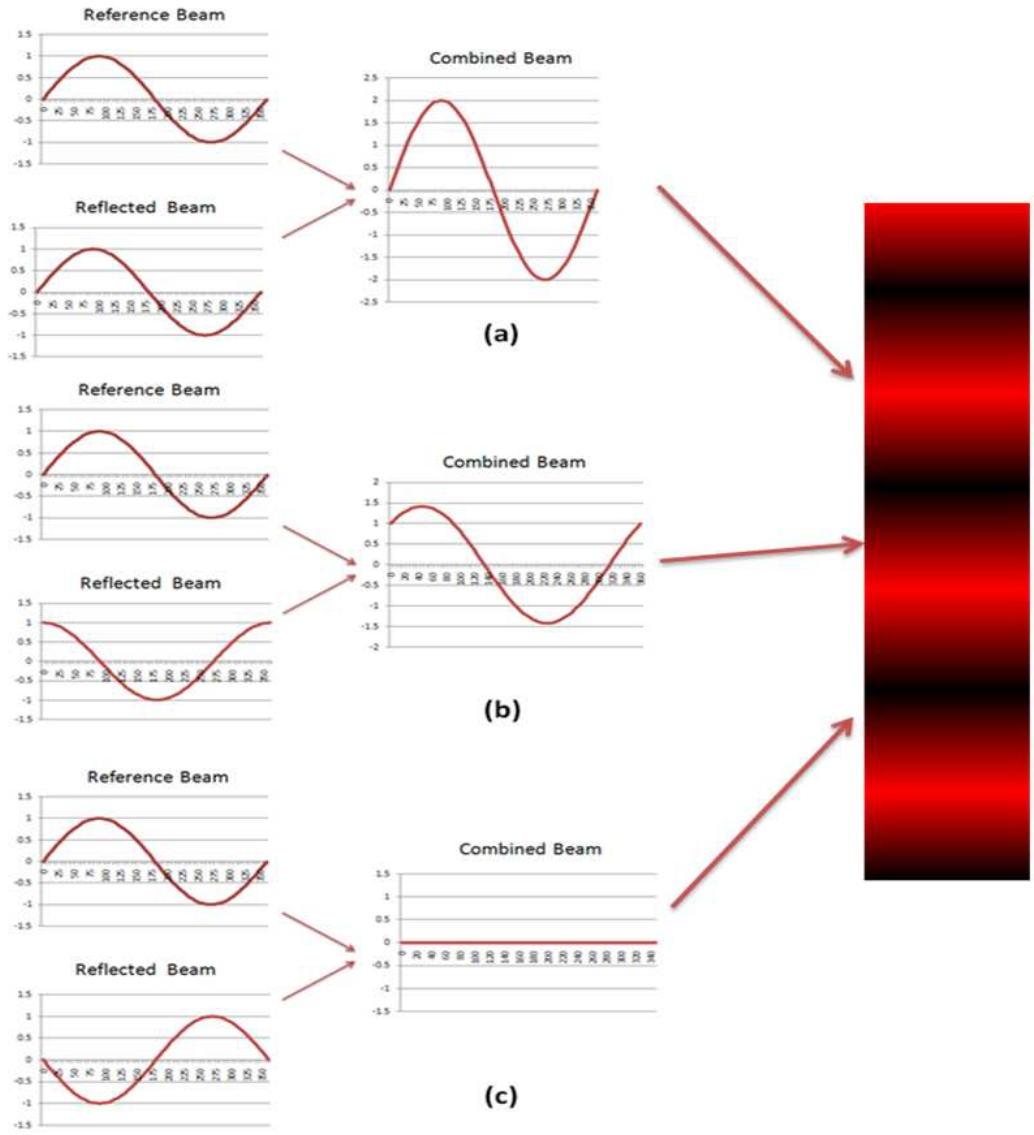


Figure 2-1: Superposition of waves showing: (a) total constructive interference; (b) constructive interference; (c) total destructive interference

Interferometers are capable of displacement measurement, the measurement must be continuous from a reference point, hence, the line of sight must not be broken during measurement. Fringe counting interferometers are of a high accuracy and are used in the calibration of gauges; traditionally, they are the principal technology in laser trackers due to the speed and accuracy of dynamic measurement. In a controlled laboratory environment their accuracy can reach the sub-nanometre scale (Schodel, 2009), how-

ever their factory performance is limited by environmental factors - for non-laboratory applications the refractive index of air is the main source of uncertainty (Schwenke et al., 2002). The refractive index is profoundly affected by temperature gradients, humidity, concentration of carbon dioxide and pressure (Flack and Hannaford, 2005): in a factory environment all these factors are likely to be non-uniform, and hence difficult to measure, predict, model and most importantly, *compensate*.

*Absolute Distance Measurement (ADM)* in its simplest form, can be based on the time of flight or time of arrival (TOA) principle; by measuring the TOA and knowing the speed of light, the distance can be easily calculated. However this method is limited to the accuracy of time measurement, for example: a resolution of 1 nanosecond will give rise to a distance resolution of 30cm (Hirai et al., 2009). Hence a very accurate method of time measurement is required to obtain reasonable/suitable results. Modulation methods can give rise to more accurate ADM systems (Kyle et al., 1997); here we can obtain practical/factory measurements of the sub-millimetre level. Although this accuracy is not quite as high as the fringe counting interferometer's accuracy, in a factory environment they are comparable; a recent product launched from Leica: the AT401 is quoted in a white paper (*Leica Absolute Tracker AT401: White Paper*, 2010) as having a Maximum Permissible Error, MPE of 10 µm over 80m; which out performs fringe counting interferometry techniques over the same distance. However, ADM technology still requires a period of stability to record a measurement. ADM does have the additional advantage of being able to measure a distance even after the line of sight is broken; hence laser trackers use ADMs to complement their fringe counting interferometers as a backup system if the beam is broken during the measurement.

*Linear and Rotary Encoders* use the same basic conceptual principle: a scale which is effectively many slots (or grates) at given intervals is read by a photo sensor (Figure 2-2). This sensor detects the 'light and dark' intervals created from the encoded disk (or scale - for linear encoder) obstructing the line of sight from the Light Emitting Diode (LED) to the sensor (Bolton, 1999). The increments are counted (similar to the interference fringes counted in interferometric techniques), and relative displacement can be calculated.

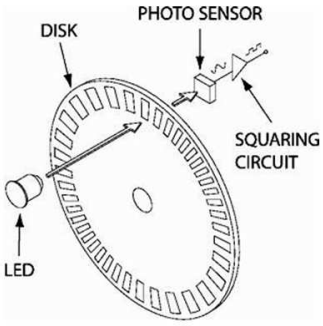


Figure 2-2: Basic elements of an incremental rotary encoder

This is relative displacement needs a reference point in order to make measurements, analogous to the fringe counting interferometer. However, using more sensors and encoders can to give rise to an absolute measurement system (Sugo, 2007).

### Laser Trackers

An established technology within the aerospace industry with a Technology Readiness Level (TRL) of 9 (Muelaner and Robson, 2008), the laser tracker is the dominant metrology system in the commissioning and re-certification of traditional tooling within aerospace.

Laser trackers require a Spherically Mounted Retro-reflective (SMR) target (see Figure 2-3) ; SMR targets reflect a light beam back along the same path it was projected; with an acceptance angle of around $\pm 30^o$ (*Leica Geosystems: Red-Ring Reflectors Specification (RRR)*, 2010). Accurately centred and repeatable SMRs are expensive and fragile, so repeatable magnetic SMR nests are placed so that one SMR can be mounted in them when necessary - this adds a significant amount of time to the measurement process. This [system] holds obvious limitations in terms of mounting the SMR nests without affecting the tooling or work piece. The fringe counting interferometer (IFM) is the principal distance measurement technology due to its speed and accuracy, oppose to ADM systems that require a period of stability to make accurate measurements. The rotary encoders measure the azimuth and zenith, in combination with the IFM or ADM which measures the radial distance; this enables the target to be tracked through space. This ability to track provides the user with real-time measurement information. The tracker's IFM samples at $3000Hz$ and averages these samples to give a measurement

read-out at $1000Hz$ (*Leica Geosystems: PCMM System Specifications*, 2009). Often the laser tracker is equipped with an ADM as a back-up for when the laser beam is broken.

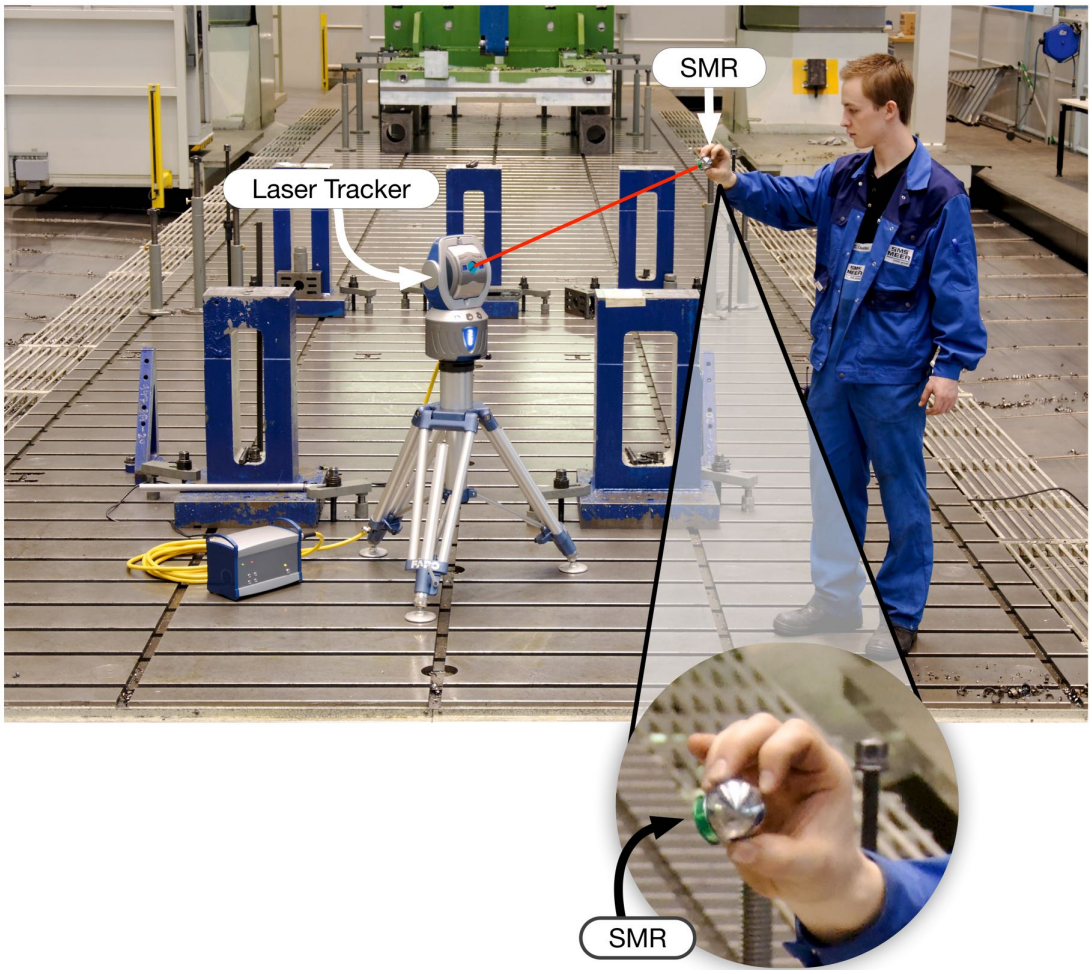


Figure 2-3: An image of a laser tracker in operation and the SMR target [Modified from (Faro, 2015)]

Optimum levels of accuracy are restricted in a factory environment due the temperature gradients, humidity, etc. that contribute to an unpredictable refractive index. It is important to note that the rotary encoders are a greater source of uncertainty especially over long distances, as a small encoder error becomes increasingly significant as measurement distance increases. Accuracy can be increased through multiple measurements of the target. Multiple measurements enable regression analysis calculations such as least-squares estimation to be performed, reducing the positional uncertainty

of a point's location (Section 2.5). Multiple measurements of a single position will yield differing co-ordinate definitions (due to measurement uncertainty), the position's definition can be essentially averaged and a new co-ordinate definition established with less associated uncertainty than that of a single measurement. This requires either: multiple laser trackers or the subsequent repositioning of one laser tracker (multi-hopping) - the techniques are either expensive capital cost (the former) or expensive in time (the latter).

As a typical system, Leica Geosystems state (*Leica Geosystems: PCMM System Specifications*, 2009) that the 3D uncertainty over the working volume of the Absolute Laser Tracker *AT901* is:

$$15\mu\text{m} + 6\mu\text{m/m (with a confidence level of } 2\sigma \approx 95\%) \tag{2.1}$$

**Laser Radar**

Laser radar is a relatively new technology - launched 2000 (Glazebrook, 2006) - and subsequently, has not had the industrial exposure that the laser tracker has, hence laser radar holds a TRL 3 (Tomlinson and Singh, 2008). It is an expensive technology, in the order of twice that of the laser tracker. The key difference to that of a laser tracker is that the laser radar does not need SMR targets to reflect the beam. It employs a frequency modulated infrared laser, and compares the up-sweep and down-sweep signals (Metris, 2009) from the reflected light, to enable ADM; hence no specific targets are required. However, targets are important to indicate datum points and specific measurements accurately, for example these could be tooling balls, tooling holes, or any definable feature. It follows that the laser radar can be used to accurately (sub-millimetre) scan surfaces and features over large distances - a capability unique to this technology.

Additionally, the laser radar can be automated to find the desired targets - although this can be achieved with a laser tracker the limitations introduced by the necessity of SMR targets in terms of acceptance angles and cost hinder the employment of a laser tracker in this manner.

The stated manufacturer's (Metris, 2009) uncertainty for laser radar is:

$$10\mu\text{m/m (with a confidence level of } 2\sigma \approx 95\%) \tag{2.2}$$

#### Total Station

Total Stations are based on the traditional Theodolite chassis (2.2.2) with an additional ranging capability (Section 2.2.2), using an Electronic Distance Meter (EDM).

Total Stations are an evolutionary product improvement, and are essentially spherical coordinate measurement machines widely used in Ship Building, Geo-surveying and Civil Engineering. They can target prisms, SMRs or be reflector less, however due to their legacy applications the targeting accuracy has not been optimised for accuracy. Total stations have much larger operational envelopes of around 1km, and are robust systems designed for harsh environments. Their stated (Leica Geosystems, 2014*a*) uncertainty is:

$$600\mu\text{m} + 1\mu\text{m/m (with a confidence level of } 2\sigma \approx 95\%) \tag{2.3}$$

### 2.2.2 Triangulation Systems

The following systems are based on the principles introduced in section 2.5.1.

#### Theodolites

Theodolites are an established technology for surveying, and a simple employment of the triangulation technique described in Section 2.5.1. A Theodolite is a passive optical instrument that measures the angle of the sighted target; once the target has been measured from two stations, which are a known distance apart the targets distance can be established. Their stated (Leica Geosystems, 2014*b*) uncertainty is:

$$0.5 arcseconds \text{ (with a confidence level of } 2\sigma \approx 95\%) \tag{2.4}$$

#### Photogrammetry

Photogrammetry essentially uses images or photographs taken from multiple positions (two or more) to triangulate the point of interest in 3D space, the position of the target is derived primarily from angular information which is calculated from the individual sensors (Figure 2-4), film or Charge-Coupled Devises (CCDs). However, in order compute this calculation a dimensional scale is required (Mikhail et al., 2001) and is often

introduced into images.

The algorithms used for the sorting, combining and triangulation of the images is known holistically as the bundle adjustment, the speed of the bundle depends on the computational processing speed and the efficiency of the algorithm/program; which is unique to each manufacturer. Images are capable of capturing many targets at once; this is only limited by field of vision and line of sight. The points of interest are often use targets; either by using active targets (*e.g.* LEDs) or passive targets (*e.g.* retro-reflective adhesive targets or printed coded/un-coded targets (Figure 2-5)) attached onto the surface. Targets can also be projected onto a free-form surface; from this large number of targets, a point-cloud of the surface geometry can be generated.

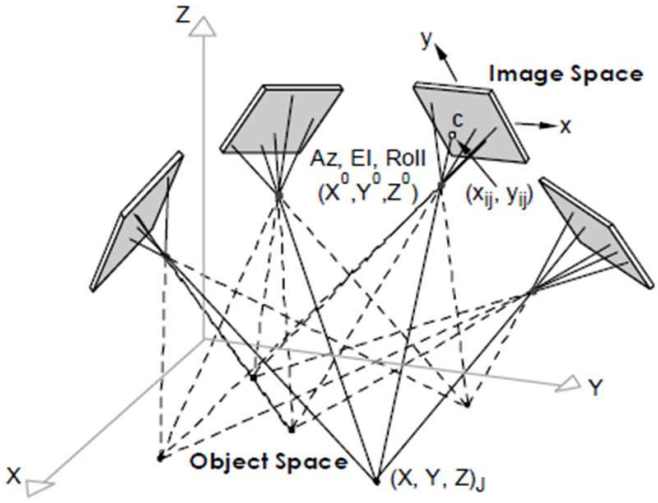


Figure 2-4: Illustrating the principle of photogrammetry (*Geodetic Systems Inc*, 2010)

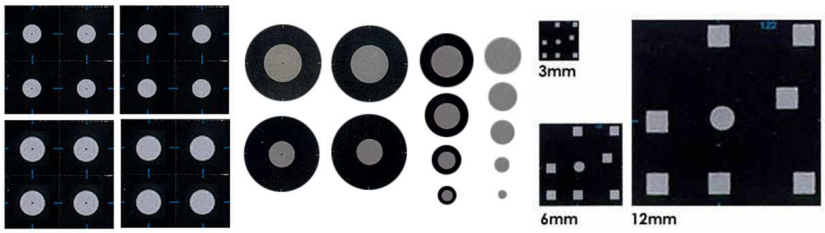


Figure 2-5: Photogrammetry targets, un-coded (left, middle) & coded (right) (*Geodetic Systems Inc*, 2010)

Many systems are available within photogrammetry with varying degrees of accuracy and cost. The rise in availability of high resolution digital cameras and the fall in computational costs gives potential for photogrammetry to become a much lower cost solution than laser based systems. The measurement volume can be substantial by adding more cameras or taking more images by using a roving (off-line photogrammetry) camera system. An example of a commercially available system (Geodetic Systems, 2014) is the Video Self-calibration Triangulation and Resection System (V-STARS) from Geodetic Systems Inc. (GSI); using a single INCA3 camera and taking multiple images from different positions this system can produce measurements with uncertainties of:

$$10\mu\text{m} + 10\mu\text{m/m (with a confidence level of } 2\sigma \approx 95\%) \tag{2.5}$$

Multi-camera systems enable dynamic measurement of many targets (online photogrammetry), however these online systems have greater measurement uncertainty than the offline counterparts. For example the V-STARS/M uses a stereo pair of the INCA3 cameras and has double the uncertainty of the roving INCA3 camera configuration. The dynamic measurements are in the order of a couple of hertz; higher speed cameras have greater associated uncertainty and/or do not give 'real-time' updates but record the data (at a high speed/frequency) and post-process the images. An important difference between photogrammetry and laser based systems - apart from being able to make simultaneous measurements - is that photogrammetry is more environmentally robust. Laser based systems gain uncertainty due to refractive index variation (due to environmental factors), and may not detect this increased error. However although photogrammetry is an optical system too, thermal gradients, humidity, etc. will affect the measurement, but as photogrammetry takes many images around the measurand the bundle adjustment will ignore spurious data and quantify optical variations within the measurement uncertainty. Additional sources of uncertainty in photogrammetry are the associated lens distortions and the subsequent error mapping of these.

*PosEye* is a proprietary technology owned by MEEQ. PosEye has two modes of operation; firstly it can be used like a conventional photogrammetry system, with a camera/sensor and targets; alternatively the system can be essentially reversed, that is, the camera is the point of interest/target obtaining its 6DOF position by referencing into a constellation of known points; coined: Star Gazing. The sensors used are low cost, low resolution and not metrology specific; this reduces the cost, and the low resolution enables higher frequency of operation/monitoring. MEEQ believe PosEye

can achieve an accuracy of 50-300 µm depending on using either 1000-100 measurements respectively, and can reach a frequency of around 50-69 Hz (MEEQ, 2007). It should be noted that there is no quoted uncertainty associated with the statement of accuracy. The Star Gazing technique is particularly suited to machine/robot control - although a camera/sensor is required for each point of interest. PosEye has been deployed commercially in Volvo to re-certify a fixture; but the technology/company is still in its infancy with a TRL 1/2.

### iGPS

The Indoor Global Positioning System (iGPS) is a technology exclusively owned by Nikon Metrology[1]. The system consists of transmitters and receivers (or sensors) - the former being stationary 'beacons' (Figure 2-6) and the latter performing the measurements. The system is based on triangulation. The beacons transmit a rotating beam consisting of two fanned lasers which are mutually orthogonal; additionally a unique reference beam rotates at a different speed to the fanned sweep beam, this [second] beam acts as a unique identifier to the transmitting station. The Azimuth and Elevation angle can be calculated by the receiver via the pluses detected from the fanned laser beams. It requires more than one transmitter in order to locate the receiver via a bundle adjustment, however subsequent transmitters can reduce the uncertainty by 15, 10 and 5 percent by having three, four or five transmitters, respectively (Sharke, 2003). Including fixed sensors or monuments in the network (and therefore the bundle adjustment), allows the system self correct and re-calibrate the drift caused by movements of the stations (Muelaner and Robson, 2008). Adding more transmitters also creates redundancy in the system - therefore line of sight issues are minimised or resolved completely.

[1]Metris became a subsidiary of Nikon on 21/10/09, and has subsequently been rebranded as Nikon Metrology 10/11/2009

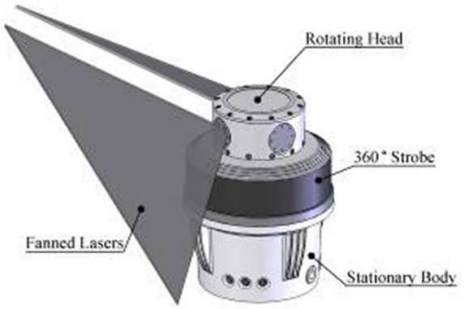


Figure 2-6: iGPS Transmitter (Muelaner et al., 2010)

Although not similar to the traditional NAVSTAR[2] GPS (Anon, 2009) in terms of technology: it does hold a resemblance in that it allows many receivers to be placed in a working environment without compromising - or indeed affecting - the transmitting systems. This enables many receivers to work within an environment completing independent tasks without overloading the system. This workspace can be as large as needed, just by adding more transmitters.

Nikon Metrology (Nikon Metrology, 2010) states that the iGPS system is capable of achieving an accuracy of:

$$200\mu\text{m (with a confidence level of } 2\sigma \approx 95\%) \tag{2.6}$$

however, a study funded by Airbus, the University of Bath(Muelaner et al., 2010) and National Physical Laboratory (NPL) showed that in a four station network the uncertainty achieved was between:

$$0.8 - 1.1\text{mm (with a confidence level of } 2\sigma \approx 95\%). \tag{2.7}$$

It should be noted that this experiment used an older software version than is currently released.

[2]NAVSTAR is the satellite system operated by the U.S Air Force however it is employed by commercial GPS systems, e.g. car satellite navigation

### 2.2.3 Portable Co-ordinate Measurement Machines

Large, complicated components or assemblies inherently have hidden or partially hidden features such as a deep recess or a blind bore, this causes line-of-sight problems within large volume optical metrology systems. For these measurements manufacturers have developed Portable Coordinate Measurement Machines (PCMMs).

#### Large Volume Metrology Tactile Probing

These PCMMs work in conjunction with the LVM system, such as: laser tracker, photogrammetry, etc, to create tactile probing devices. The probes are calibrated and their dimensions are known to the operational software. Multiple targets on the probe enable the metrology system to calculate both position and orientation of the probe, that is to say: 6 Degrees of Freedom (DOF) can be described; this allows accurate definition of the probe's point. Probes that work in this manner are present in systems which allow multiple targets to be located at once: for example photogrammetry or iGPS. Probes relying on a laser tracker as the primary location method, adopt an additional metrology technology in order to establish orientation (pitch, roll and yaw), for example the Leica T-Probe uses both a laser tracker and photogrammetry. Additionally some PCMM probes allow scanning heads to be utilised - enabling free form point-cloud data to be gathered.

Airbus Broughton, already utilises the Leica T-Probe within their tooling systems (Leica Geosystems, 2009) for setting, inspecting and recertification of tooling. Additionally, probes can be adapted and fitted to a robot's end effector or feature of interest enabling 6DOF positional information to be obtained. The PCMMs intrinsically introduce more uncertainty to the system that is being used as the platform. Probes have offsets and so do not obey Abbe's Law, thus increasing uncertainty further. The Leica T-Products use a photogrammetry system that has a hight uncertainty than the laser tracker; subsequently this introduces uncertainty in the probe's orientation - magnified by the probe offset. Leica states a T-Probe with a 110 mm stylus will have an uncertainty (*Leica Geosystems: PCMM System Specifications*, 2009) of:

$$30\mu\text{m} + 10\mu\text{m/m (with a confidence level of } 2\sigma \approx 95\%) \tag{2.8}$$

#### Articulated Arms

Articulated Arm CMMs are at the lower limits of the LVM envelope with typical working volumes of between*1200-3700mm*. Articulated arm CMMs have a series of stiff linkages creating around 8DOF, with a probe or laser scanner at the terminus. Between the linkages are rotary encoders within each joint. The kinematics of the articulated arm CMM is well understood, as it is similar to robotic kinematic models, and the probe position can be extrapolated from the encoder values. The systems can measure the probe's centre with a typical uncertainty of (Faro, 2014):

$$16 - 60\mu\text{m at } 1200\text{mm} - 3700\text{mm (with a confidence level of } 2\sigma \approx 95\%) \tag{2.9}$$

## 2.3 Dimensional Uncertainty

The measurement requirements during the construction and setting of large assembly tooling, places high demands on on instrumentation. Due to the scale of the measurements (10m+) the measurement uncertainty is of a significant magnitude. This section researches dimensional uncertainty and the current landscape.

### 2.3.1 Definition

The British Standard (BS): PD6461-1(1995): BASIC AND GENERAL TERMS (VIM) (BSI, 1995*a*) formally defines uncertainty (of measurement) as:

> "parameter, associated with the result of a measurement, that characterises the dispersion of the values that could reasonably be attributed to the measurand.
>
> **NOTE 1** The parameter may be, for example, a standard deviation (or a given multiple of it), or the half-width of an interval having a stated level of confidence.
>
> **NOTE 2** Uncertainty of measurement comprises, in general, many components. Some of these components may be evaluated from the statistical distribution of the results of series of measurements and can be characterised by experimental standard deviations. The other components,

which also can be characterised by standard deviations, are evaluated from assumed probability distributions based on experience or other information.

**NOTE 3** It is understood that the result of the measurement is the best estimate of the value of the measurand, and that all components of uncertainty, including those arising from systematic effects, such as components associated with corrections and reference standards, contribute to the dispersion"

A more recent International Organisation of Standardisation (ISO), Standard: VIM, ISO/IEC Guide 99:2007 (*ISO/IEC Guide 99:2007 International vocabulary of metrology – Basic and general concepts and associated terms (VIM)*, 2007) has been developed, but not adopted by British Standard Institution (BSI) as a published document (BSI, 1995*c*). Hence, for this document the above [BS] definition for uncertainty has been adopted.

### 2.3.2 Uncertainty Discussion

The primary British Standard relating to determining measurement uncertainty is BS PD6461-1(1995): GUIDE TO THE EXPRESSION OF UNCERTAINTY IN MEASUREMENT (GUM) (BSI, 1995*b*), this has been superseded by the joint ISO and International Electrotechnical Commission (IEC) Guide: 98-3:2008 (*ISO/IEC Guide 98-3:2008 Uncertainty of measurement – Part 3: Guide to the expression of uncertainty in measurement (GUM)*, 2008) which is essentially a re-issue of the GUM British Standard with minor corrections, however this ISO/IEC guide has not been adopted by the BSI (BSI, 1995*b*). The GUM outlines that a measurement should always be accompanied by the associated uncertainty of the measurement; this stated uncertainty of a system is, in turn, accompanied by a confidence level; in the form:

$$a\mu\text{m} + b\mu\text{m/m (at a confidence level of } k\sigma). \tag{2.10}$$

In written terms this translates as: the true value of the measurand lies within the interval of $a$ plus $b$ or every additional metre of the measurement (where $a$, $b$ and $k$ are numerical values); this is stated with a confidence level of $k\sigma$ ($k$ is known as the coverage factor). The confidence level correlates to a percentage of 68.26%, 95.46 % and 99.74% for $1\sigma$, $2\sigma$ and $3\sigma$ respectively, based on Gaussian distributions (or Normal

distributions); this effectively indicates the likelihood that the true value of the measurand falls within the stated uncertainty interval. GUM defines the *Standard Uncertainty* ($u_c$) as a single standard deviation: that is, expressed at the $1\sigma$ level; when using a coverage factor greater than 1 we refer to the quantity as the *Expanded Uncertainty* ($U_c$). In tolerance and measurement critical applications such as those experienced in the aerospace industry, a $3\sigma$ or 99.74% confidence level may be applied. The GUM standard adopted a paradigm of indirect measurement; where the functionally related quantities of the measurand could be quantified in isolation to obtain the value of the measurand: hence, allowing us to propagate the uncertainty of measurement (Rossi, 2009).

Measurement uncertainty is formulated by examining the measurement process and identifying the constituent sources of uncertainty and propagating the uncertainty appropriately. Generic sources of uncertainty include: the measurement instrument (repeatability, resolution, calibration, etc.), stability of the measurand, environmental effects (thermal, pressure, humidity, etc.), measurement process (parallax error, sine errors, etc) and operator variations, to name a few (Bell, 2001). The possible sources of uncertainty can only be truly identified when specific measurement processes are scrutinised. The GUM classifies uncertainty into two groups: *Type A* and *Type B* uncertainty; Type A is an uncertainty that varies randomly, which in turn can be analysed through statistical methods from observations; Pavese (2009) comments that: *the current Type A evaluation seems only to involve the replication of measurements for a purpose and furthermore that the GUM standard only recognises systematic errors as random variables with zero expectation: this assumption is not always valid.* Type B uncertainty is evaluated using methods other than the statistical analysis of observation, such as calibration certificates. It should be noted that once an uncertainty is documented, the subsequent use of the uncertainty information is considered as a Type B contribution, even if the uncertainty was originally determined with both Type A and Type B quantities (Kirkup and Frenkel, 2006).

Systems are often a combination of Type A and B quantities, this is referred to as the combined standard uncertainty (where, $k = 1$) or combined expanded uncertainty (where, $k > 1$), the measurand $Y$ is a function of $N$ number of quantities ($X_i$) such that:

$$Y = f(X_1, X_2, \ldots, X_N). \tag{2.11}$$

The combined standard uncertainty ($u_c$) of independent quantities is given by:

$$u_c^2(y) = \sum_{i=1}^{N} \left( \frac{\delta f}{\delta x_i} \right)^2 u^2(x_i). \tag{2.12}$$

where $u_c$ is the positive square root. The modelling methodology presented in GUM is criticised for underestimating uncertainty in certain applications, for example when Type A uncertainties with a t-distribution with a low number of degrees of freedom contributes significantly to the uncertainty budget (Vilbaste et al., 2010). An alternative way of evaluating the propagation of the individual components of uncertainty is presented in the ISO/IEC Standard Guide 98-3:2008 (*ISO/IEC Guide 98-3:2008/Suppliment 1:2008 Propagation of distributions using a Monte Carlo method*, 2008) which explores the propagation of distributions by using Monte Carlo simulation; this supplement is consistent with GUM. Monte Carlo Simulation (MCS) combines distributions by sampling from the Probability Density Functions (PDFs) of the associated components of uncertainty that contribute to the overall, combined uncertainty. MCS is a simple method that uses computational power instead analytical mathematics; this provides a generic approach, whereas a bespoke mathematical model may need to be constructed for each component in the analytical approach. Additionally, if a component of uncertainty is difficult to model, empirical data can be used to determine the PDF. However, in most cases MCS can only offer a reinterpreting of our measurement model based on the measurement equation, values and uncertainty model (Steele and Douglas, 2009). The evaluation of uncertainty is not limited to MCS or the GUM formula (Equation 2.12), for example research is ongoing using Random Fuzzy Variables (RFV) for the expression and propagation of uncertainty in two dimensions (Pertile et al., 2009)

Stated uncertainty can be considered as a magnitude, that is, without direction. However uncertainty may be associated to a vector, for example: the direction of measurement; subsequently, quoting uncertainty as in Equation 2.10 may not be wholly appropriate. Consider the following: Figure 2-7 shows the average (mean) measurement of a set of measurements along a line, the associated measurement variation - the measurement repeatability - is a Gaussian distribution and for simplicity, can be considered to be equivalent to the measurement uncertainty; beneath the distribution is a simple MCS of 250 measurements. The simulation has based the measurement position along the axis of measurement within the bounds of the uncertainty/measurement distribution. This measurement could have been conducted with a one-dimensional instrument, such as a ruler, and could be adequately defined/stated with Equation 2.10

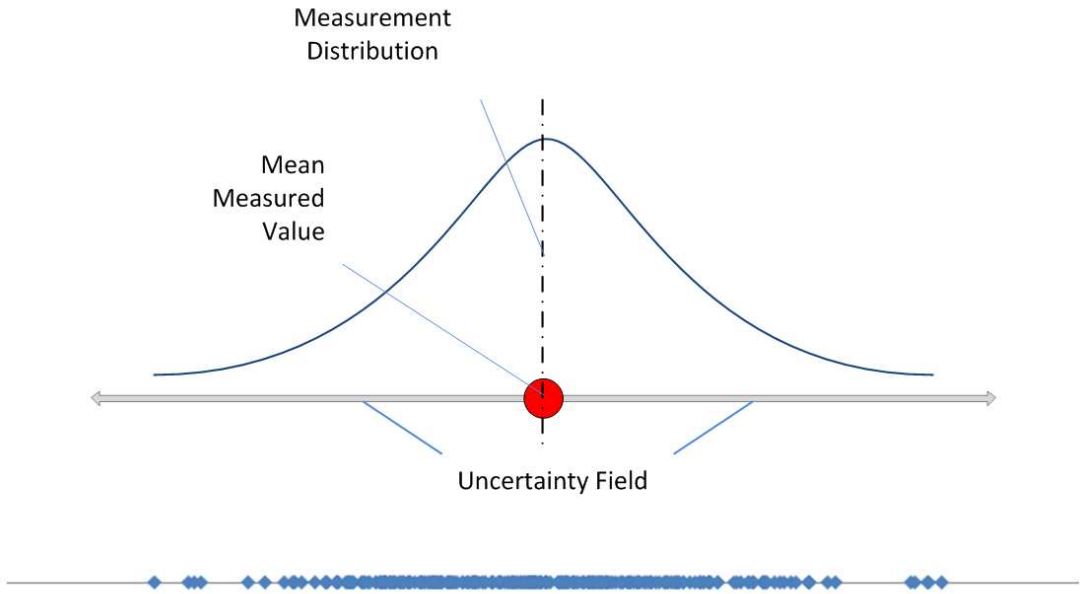


Figure 2-7: Single dimensional measurement and the distribution of the associated uncertainty

Figure 2-8 shows a measured value taken using an instrument that measures in two orthogonal axes $(x, y)$, each axis is identical and so too are their associated uncertainties (standard deviations), consequently the measurement distributions are equal. We can now infer that the true value of the measurand lies in the $x, y$ plane of measurement, in a circular distribution, the stated confidence level will determine the radius of the uncertainty field, this has been verified through a MCS which is shown on the right with 3000 samples. The measurement system could be a bore alignment system or a $x, y$ positioning table; with equal uncertainties Equation 2.10 is still an applicable and relevant way of describing the system's capability.

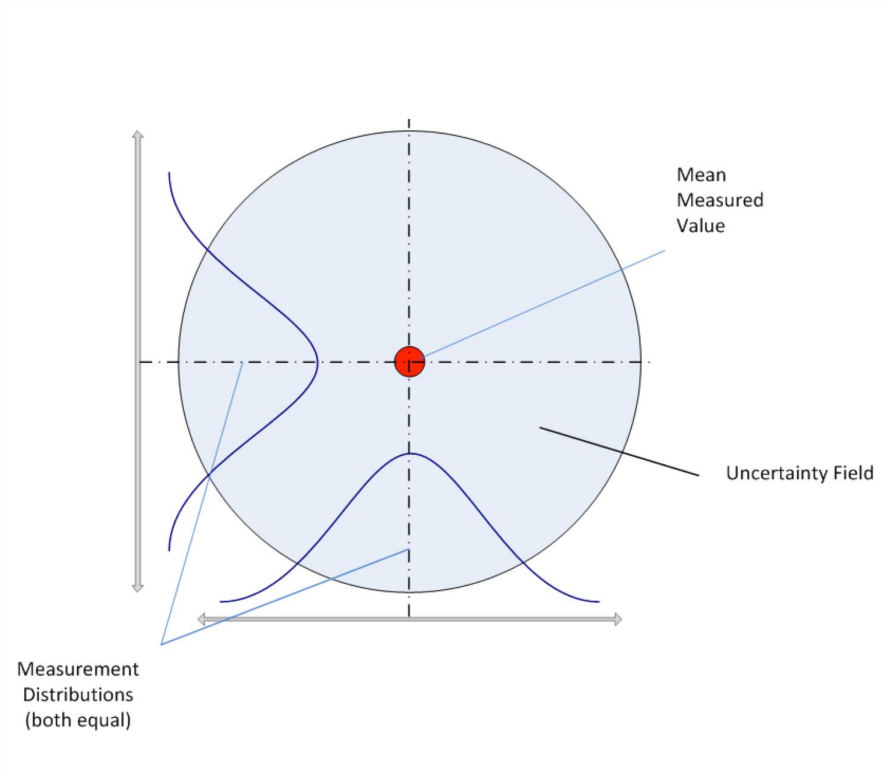


(a) Theoretical 2D measurement with equal uncertainty distributions

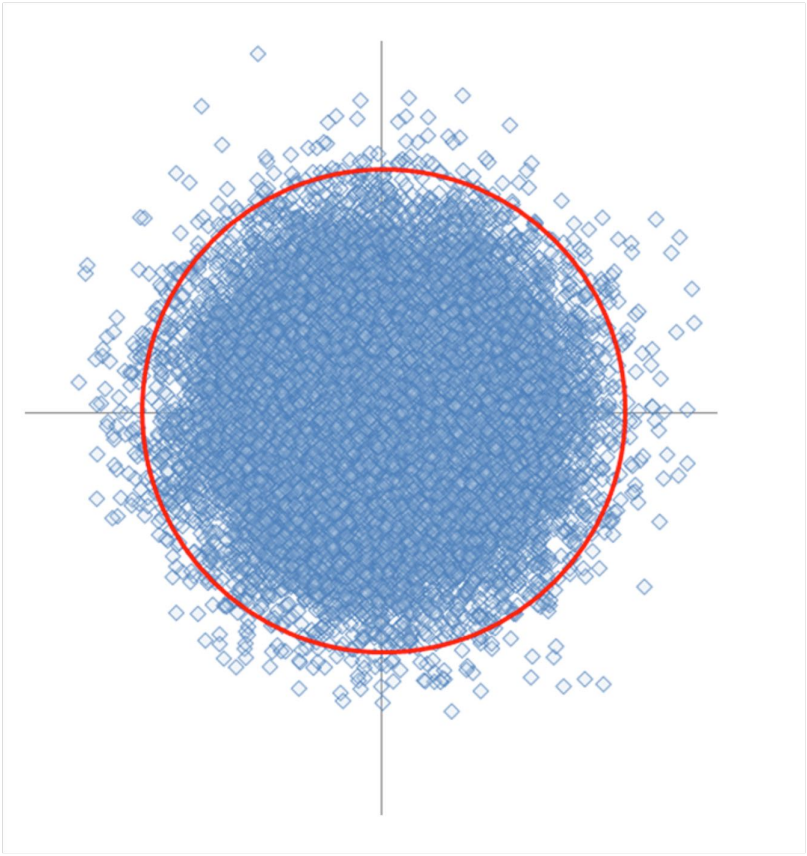

(b) Monte Carlo Simulation of 2D measurement with equal uncertainty distributions

Figure 2-8: Two dimensional measurement with equal normal uncertainty distributions

Figure 2-9 is representative of a system similar to that in the above example; however, this example illustrates a system with two distinct components of measurement and unequal associated uncertainties. As a result when the distributions are plotted we see an elliptical shape on the measurement plane, in the background are the MCS samples, and their density in the plane of measurement. The measurement systems could be one of those described above, the important differentiation to note is that the uncertainty cannot be described by Equation 2.10 and remain representative of the systems capability; this argument readily extends to three dimensions. In the case of unequal component uncertainties a magnitude accompanied by a vector is more appropriate, in measurement network adjustment (Section 2.6) the covariance matrix essentially provides this information, but is unwieldy in practice.

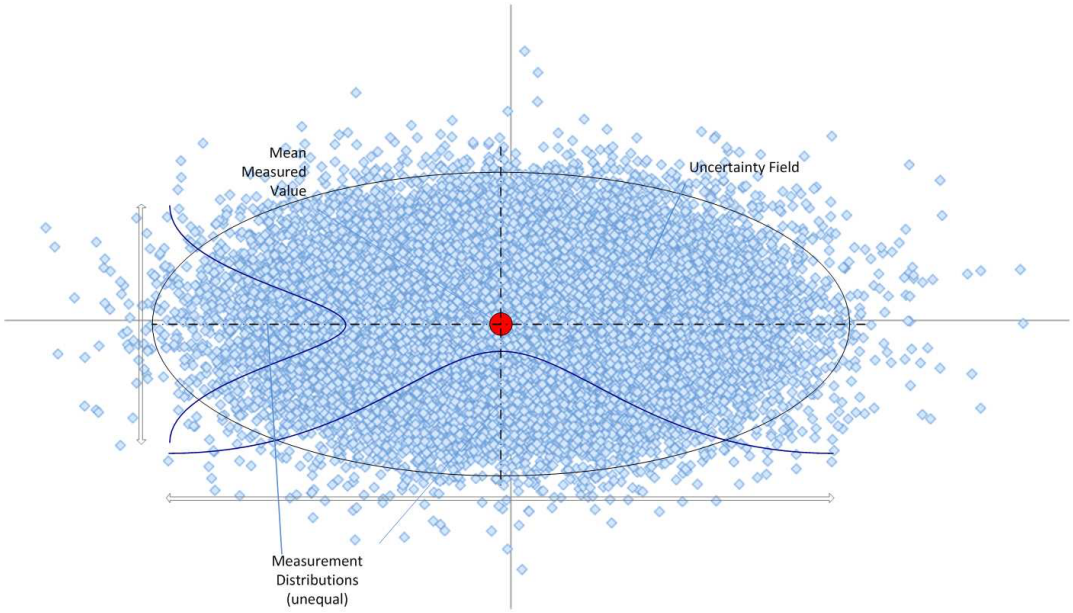


Figure 2-9: Two dimensional measurement with unequal uncertainty distributions

### 2.3.3 Associated Standards

Section 2.3 introduced the BS PD6461-1 (1995): GUIDE TO THE EXPRESSION OF UNCERTAINTY IN MEASUREMENT (GUM) (BSI, 1995*b*) in relation to the uncertainty of measurement. This is a generic standard referring to metrology across a wide spectrum and not specifically for dimensional metrology; this standardises the expression and propagation of uncertainty in a common format and ensures traceability back to fundamental standards. GUM forms Part 3 of the General Metrology set of 4 standards, Parts 1, 2 and 4 of the set are: BS PD6461-1 (1995): BASIC AND GENERAL TERMS (VIM) (BSI, 1995*a*), BS PD6461-2(1980): VOCABULARY OF LEGAL METROLOGY (VLM) (BSI, 1980) and BS PD6461-4(2004): PRACTICAL GUIDE TO MEASUREMENT UNCERTAINTY (BSI, 2004), respectively. ISO/IEC standards (*ISO/IEC Guide 99:2007 International vocabulary of metrology – Basic and general concepts and associated terms (VIM)*, 2007; *ISO/IEC Guide 98-3:2008 Uncertainty of measurement – Part 3: Guide to the expression of uncertainty in measurement (GUM)*, 2008; *ISO/IEC Guide 98-1:2009 Uncertainty of measurement – Part 1: Introduction to the expression of uncertainty in measurement*, 2009) are more current but have not been adopted by the BSI, generally the ISO/IES standards are corrections and updates of the BSI doc-

uments, however a supplement has been developed to include methods in uncertainty propagation with use of Monte Carlo methods (*ISO/IEC Guide 98-3:2008/Suppliment 1:2008 Propagation of distributions using a Monte Carlo method*, 2008); additionally, the International Organisation of Legal Metrology (OIML) has issued the latest VLM standard: International Vocabulary of terms in Legal Metrology (VIML) (International Organization of Legal Metrology, 2000). The United Kingdom Accreditation Service (UKAS), have produced a practical document, providing guidelines to the application of these standards (UKAS, 2012).

Specific BSI or ISO/IEC calibration standards for LVM systems (other than CMM calibration) do not currently exist, however the American Society of Mechanical Engineers (ASME) has created a standard: ASME B89.4.19-2006: PERFORMANCE EVALUATION OF LASER-BASED SPHERICAL CO-ORDINATE MEASUREMENT SYSTEMS (*ASME B89.4.19-2006 Performance Evaluation of Laser-Based Spherical Coordinate Measurements Systems*, 2006). B89 describes a method designed to exercise the laser tracker's ranging and angle sensors with the use of a reference standard, the USA based National Institute of Standards and Technology explores the B89 standard, Muralikrishnan et al. (2009) identifies areas for improvement in the tests and analysis to ensure the identification of geometric and systematic errors. On the other hand the National Physical Laboratory (NPL) has presented an alternative method than B89 for determining the alignment and encoder errors method, without the use of additional equipment (Hughes, Sun, Forbes and Lewis, 2010); this method measures a constellation of points from multiple stations. The measurement data can subsequently bundled and a simultaneous parameter estimation can be made - based on the laser tracker uncertainty model. Industrially, Airbus UK (AUK) has an internal instrument performance checks (known as field checks), that are carried out prior to using the laser tracker, the document is know as CPR1037 (Jones, 2010). Although less rigorously applied than the B89 or NPL simultaneous parameter estimations, the Airbus Standard CPR1037 is a quick process that gives a good indication that the instrument is performing as expected.

## 2.4 Uncertainty & Tolerance

### 2.4.1 Uncertainty & Tolerance Relationship

It is important that uncertainty is considered during measurement to ensure that tolerances are achieved. However, as uncertainty is a statistical parameter a confidence interval is required in order to assess that a tolerance is achieved. Assuming that

the tolerance band is greater than the measurement uncertainty (within a confidence interval), there are four cases to consider (Figure 2-10):

1. `Out of Tolerance`: Both the measured value and the associated uncertainty is out of tolerance
2. `Indeterminate`: The measured value is out of tolerance however, the associated uncertainty overlaps the tolerance boundary
3. `Indeterminate`: The measured value is within tolerance however, the associated uncertainty overlaps the tolerance boundary
4. `In Tolerance`: Both the measured value and the associated uncertainty is within tolerance

Considering measurement uncertainty with respect to manufacturing tolerances ensures that components/assemblies that are out of tolerance are not accepted, and in-tolerance components/assemblies are not rejected! Smaller measurement uncertainty reduces the likelihood of an indeterminate conclusion. However, wing assembly fixture checks, setting procedures and re-certifications, are applications that have tight tolerances relative to the measurement distances. The associated uncertainty of large volume measurement instruments' occupies a significant proportion of these setting tolerances, and the stated confidence level has a considerable impact on the determination of tolerance requirements. As an example, a setting tolerance could be in the order of $\pm 250\,\mu m$ over a 15m fixture (*e.g.* A320), from the manufacturers stated instrument uncertainty (Equation 2.1) alone (not including other uncertainty contributions), the uncertainty over this distance is $105\,\mu m$ at a $2\sigma$ level (42% of tolerance budget) and $157.5\,\mu m$ at a $3\sigma$ level (63% of tolerance budget). The impact of the statistical confidence level is illustrated in Figures 2-11 & 2-12; Figure 2-11 shows that with a high confidence level, the measurement outcome is more likely to be indeterminate, as opposed to Figure 2-12 where a reduction in the confidence level, yields a more definitive conclusion.

Tolerances are conventionally stated as an absolute figure/requirement, this is acceptable when a measurement instrument/process has an associated uncertainty an order of magnitude less than the tolerance requirement. However, in large volume applications, where instruments related processes have a combined measurement uncertainty that consumes a large proportion of the tolerance budget, it is perhaps more appropriate for the tolerance requirement to be accompanied by a confidence level; this would help inform the measurement strategy and reduce ambiguity.

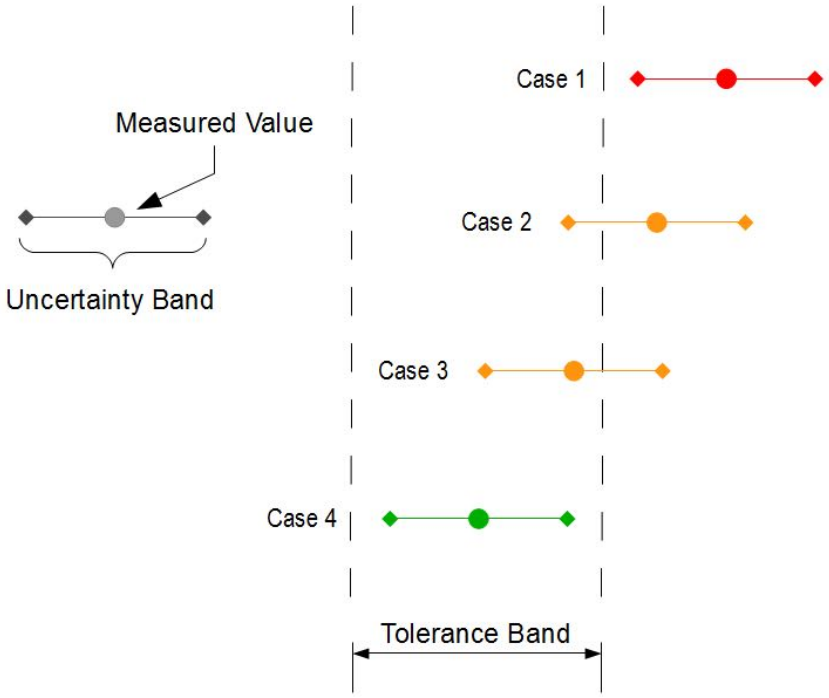


Figure 2-10: Uncertainty in relation to tolerance bands

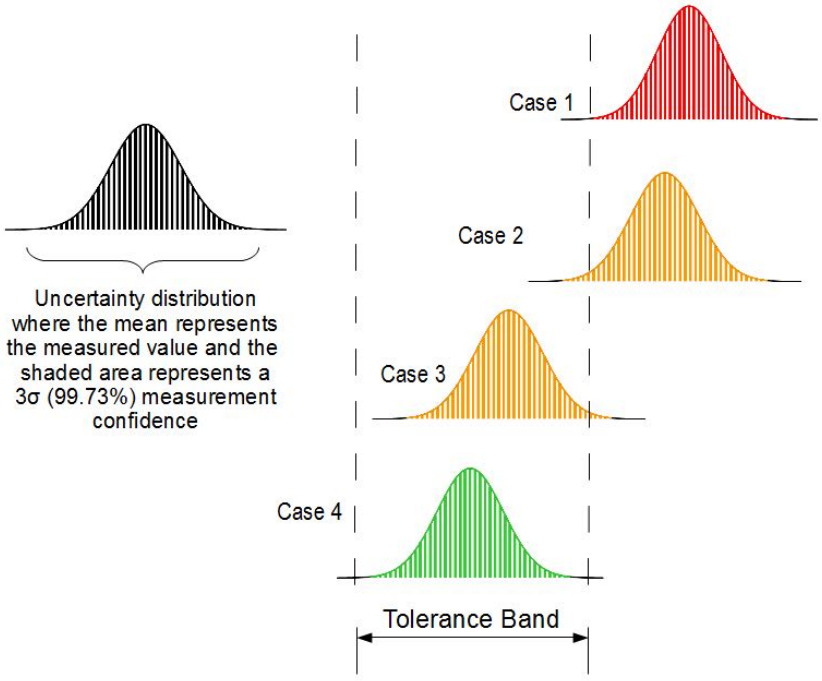


Figure 2-11: 3-Sigma uncertainty distributions in relation to tolerance bands

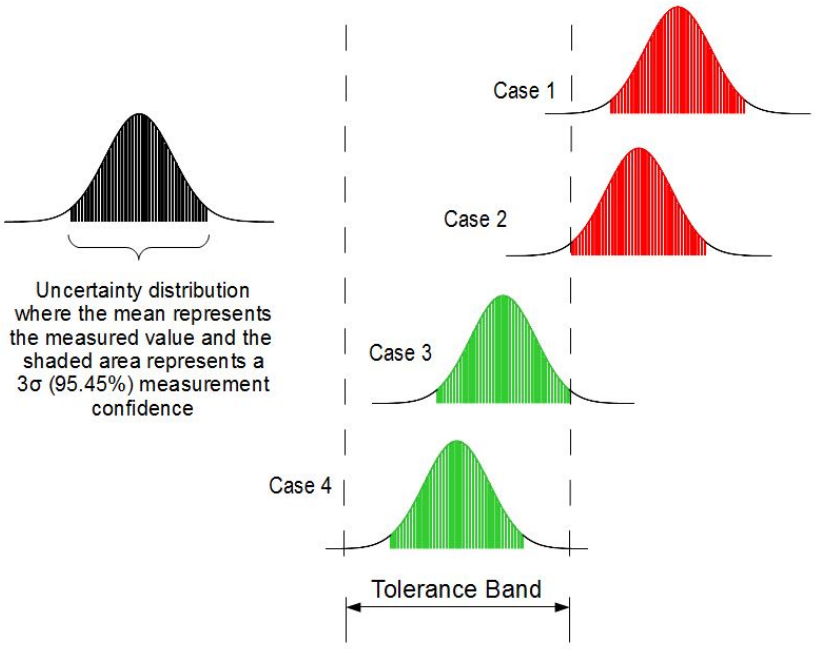


Figure 2-12: 2-Sigma uncertainty distributions in relation to tolerance bands

### 2.4.2 Laser Tracker Uncertainty Model

The laser tracker is an important technology within LVM and the aerospace sector, it is discussed in Section 2.2.1. It is the instrument used for the construction and validation of Wing-box assembly tooling. This section examines how the measurement uncertainty for this spherical co-ordinate measurement system can be described.

Spherical co-ordinate measurement systems produce Cartesian coordinates $(x, y, z)$ from the polar information: radial distance, azimuth and zenith/elevation (Figure 2-13). Interferometers (IFMs) and/or Absolute Distance Meters (ADMs) measure radial distance and the angles (azimuth and zenith) are calculated from rotary encoders.

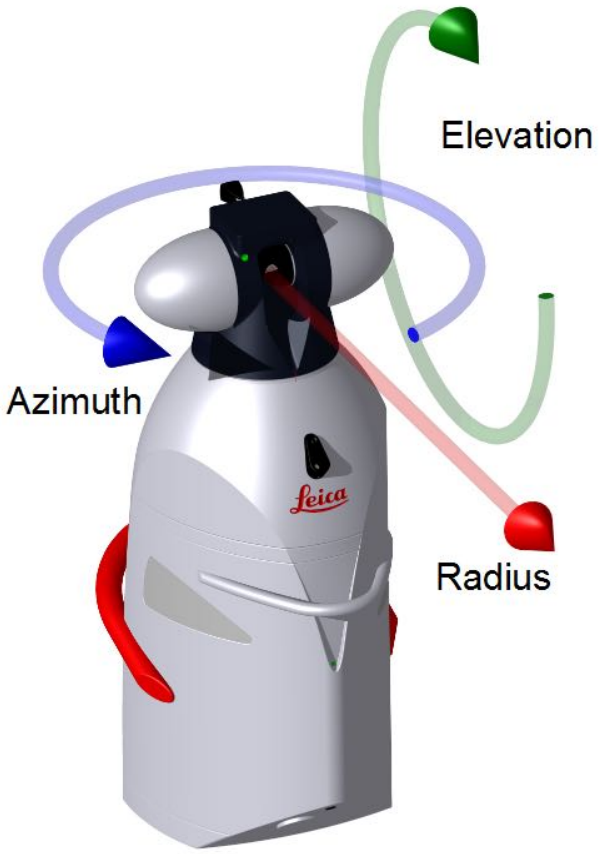


Figure 2-13: Laser tracker identifying the measurement sensors

Figure 2-14 and Equations 2.13 & 2.14 describe the spherical coordinate system and Cartesian coordinate system relationship.

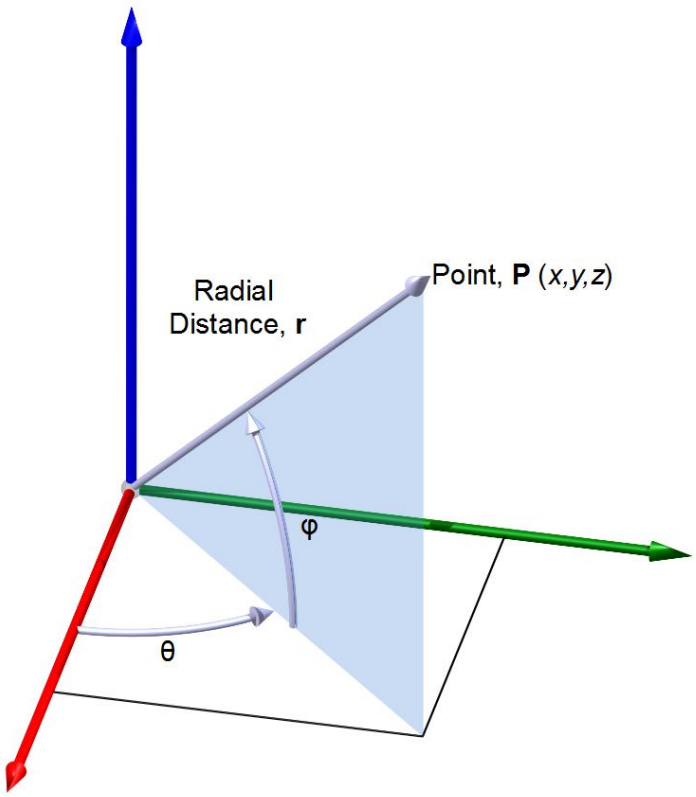


Figure 2-14: Spherical co-ordinate system

Where:

$$r = \sqrt{x^2 + y^2 + z^2}, \theta = \tan^{-1}(\frac{y}{x}), \phi = \sin^{-1}(\frac{z}{r}), \tag{2.13}$$

and the $x, y, z$ Cartesian co-ordinates of a point ($\mathbf{P}$) are described as:

$$x = r\cos\theta\cos\phi, y = r\sin\theta\cos\phi, z = r\sin\phi. \tag{2.14}$$

The uncertainty of measurement for the laser tracker can be generically characterised

by the following equations, which have been adapted from (Forbes and Harris, 2009), for generality:

Let the *true* position, $\mathbf{P}^*$ be given by: $\mathbf{P} = [r^*, \theta^*, \phi^*]^T$ where $r^*, \theta^*, \phi^*$ are the *true* radial distance, azimuth and zenith respectively; from Equation 2.14 the Cartesian format of the spherical co-ordinates are as follows:

$$\mathbf{P} = [r^* \cos\theta^* \cos\phi^*, r^* \sin\theta^* \cos\phi^*, r^* \sin\phi^*]^T. \tag{2.15}$$

The estimated value of the measured radial distance ($r$) is a function of the measured displacement ($d$), refractive index uncertainty ($\omega$) and deadpath ($d_o$). The refractive index uncertainty causes variation in the laser path. The deadpath is the distance between the interferometer and the datum position (where the counter is equal to zero) (Flack and Hannaford, 2005). Hence the measured radius can be defined as:

$$r = (1 + \omega_0)(d_0 + d), \tag{2.16}$$

The deadpath ($d_0$) can be expressed as the sum of the 'true' deadpath value ($d_o^*$) and the uncertainty associated to the deadpath ($\delta_o$), such that:

$$d_0 = d_0^* + \delta_o \tag{2.17}$$

Similarly the displacement ($d$) can be expressed as the sum of the 'true' displacement ($d^*$) value and the uncertainty associated to the ($\delta$), such that:

$$d = d^* + \delta \tag{2.18}$$

The uncertainty parameters $\omega$ and $\delta_o$ are elements of different Gaussian distributions with zero mean values. Whereas, the uncertainty associated with distance measurement, $\delta$ has both a component of noise (Gaussian with a zero mean) and a statistical component of uncertainty that is proportional to the true radial distance. The azimuth angular measurement ($\theta$) can be described as a function of the alignment/offset ($\epsilon_o$) of the vertical axis encoder, and the azimuth encoder uncertainty ($\epsilon$):

$$\theta = \theta^* + \epsilon_o + \epsilon \tag{2.19}$$

The zenith angular measurement ($\phi$) can be described as a function of the alignment/offset ($\rho_o$) of the vertical axis encoder, and the azimuth encoder uncertainty ($\rho$):

$$\phi = \phi^* + \rho_o + \rho. \tag{2.20}$$

We can define these seven components of uncertainty dispersions as offsets ($\omega_o, \delta_o, \epsilon_o, \rho_o$) and shape/positional dispersions ($\delta, \epsilon, \rho$).

## 2.5 Position & Location

Measurement instruments can often be networked together; this can be achieved by using the same instrument in different positions or multiple instruments in differing positions. This process may be necessary in order to make the measurement (e.g. Photogrammetry); alternatively the measurement network could reduce the measurement uncertainty through an optimisation process; or the network could be employed to increase the working volume of measurement and improve line-of-sight issues. Although an in-depth discussion on positioning and location techniques is beyond the scope of this research, we introduce two fundamental concepts: Triangulation and Multilateration.

### 2.5.1 Triangulation Principles

Triangulation requires three pieces of information, two angles and a distance, as an example, consider Figure 2-15:

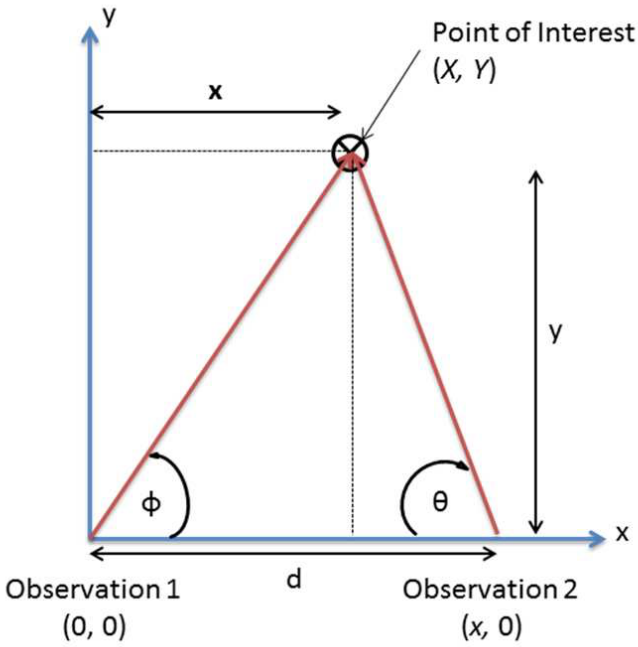


Figure 2-15: Triangulation: an example

Let observation 1 be the origin; then the y co-ordinate can be ascertained by:

$$d = \frac{y}{\tan\phi} + \frac{y}{\tan\theta} \tag{2.21}$$

Rearranging and using trigonometric identities gives:

$$y = \frac{d\sin\phi\sin\theta}{\sin(\phi+\theta)}) \tag{2.22}$$

Subsequently, the x coordinate can be calculated:

$$x = d - \frac{y}{\tan\theta} \tag{2.23}$$

### 2.5.2 Multilateration Principles

Multilateration techniques rely on distance measurement and not the angular information required for triangulation. As a specific example, consider the three instruments in Figure 2-16, as there are only three measurements the technique is known as *trilateration*.

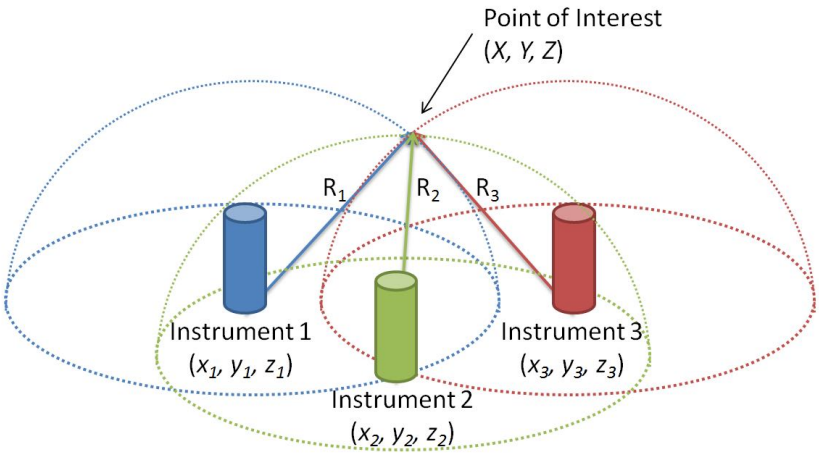


Figure 2-16: Trilateration principle

The equation that describes a sphere in Cartesian terms generates the following equations for the distance measurement from the first, second and third instrument respectively:

$$R_1^2 = (X - x_1)^2 + (Y - y_1)^2 + (Z - z_1)^2; \tag{2.24}$$

$$R_2^2 = (X - x_2)^2 + (Y - y_2)^2 + (Z - z_2)^2; \tag{2.25}$$

$$R_3^2 = (X - x_3)^2 + (Y - y_3)^2 + (Z - z_3)^2. \tag{2.26}$$

The positions of the 3 instruments form a plane; we can let this plane lie in $z = 0$. For the purposes of simplifying the calculations we can let Instrument 1 form the origin, then:

$$R_1^2 = X^2 + Y^2 + Z^2. \tag{2.27}$$

Orientating the co-ordinate frame such that instrument 2 lies on the x-axis and letting the distance along the $x$ axis from instrument 1 to instrument 2 equal $D_{2x}$:

$$R_2^2 = (X - D_{2x})^2 + Y^2 + Z^2. \tag{2.28}$$

Letting $(D_{2x}, D_{2y})$ represent the offset of instrument 3 relative to instrument 1 (Figure 2-17), gives:

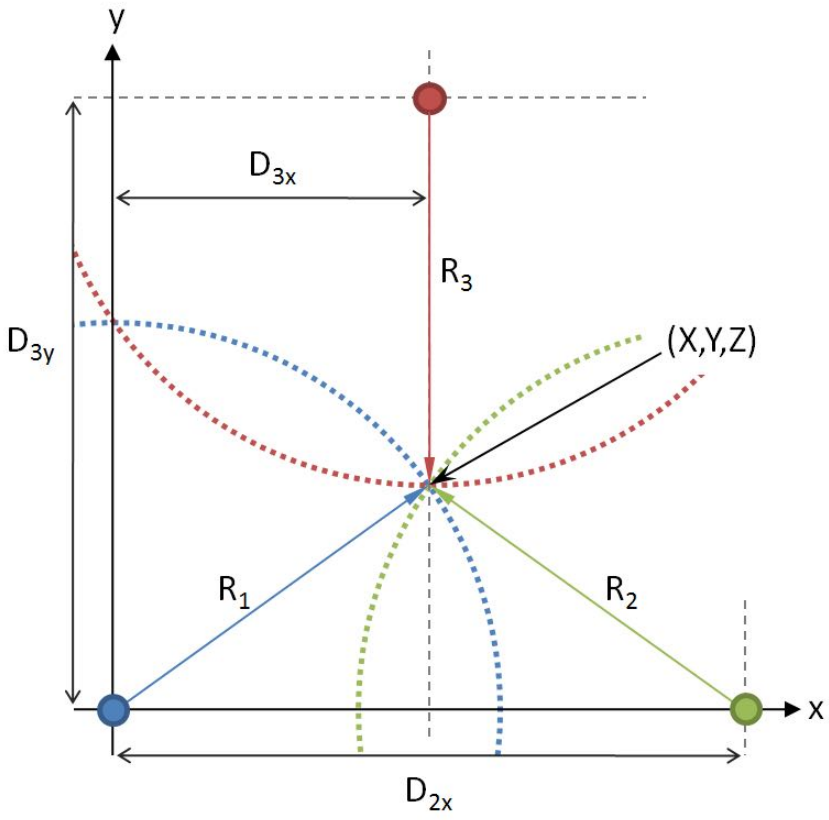


Figure 2-17: Plan elevation of trilateration example

$$R_3^2 = (X - D_{3x})^2 + (Y - D_{3y})^2 + Z^2. \tag{2.29}$$

In order to solve we first subtract equation 2.28 from equation 2.27 and simplify:

$$R_1^2 - R_2^2 = 2XD_{2x} - D_{2x}^2. \tag{2.30}$$

Rearranging for $X$ yields:

$$X = \frac{R_1^2 - R_2^2 + D_{2x}^2}{2D_{2x}}. \tag{2.31}$$

We can now substitute equation 2.31 into equation 2.27, giving:

$$R_1^2 = \left(\frac{R_1^2 - R_2^2 + D_{2x}^2}{2D_{2x}}\right)^2 + Y^2 + Z^2; \tag{2.32}$$

that is:

$$Y^2 + Z^2 = R_1^2 - \left(\frac{R_1^2 - R_2^2 + D_{2x}^2}{2D_{2x}}\right)^2; \tag{2.33}$$

Expanding equation 2.29 for the third sphere gives:

$$R_3^2 = X^2 - 2XD_{3x} + D_{3x}^2 + Y^2 - 2YD_{3y} + D_{3y}^2 + Z^2 \tag{2.34}$$

We can now substitute equation 2.33 into the expanded equation 2.34 for the third sphere and simplify to give:

$$Y = \frac{R_1^2 - R_3^2 - 2XD_{3x} + D_{3x}^2 + D_{3y}^2}{2D_{3y}} \tag{2.35}$$

We can now use the $X$ co ordinate obtained from equation 2.31 to solve equation 2.35, and subsequently use the $X$ and $Y$ values to solve for $Z$ in equation 2.27; this will yield two possible solutions and additional information can be used to determine which value is appropriate - such as earth's position, relative to the co-ordinate frame. The co-ordinate values can subsequently be transformed into the co-ordinate frame required for the application.

This example assumes a perfect distance measurement, i.e. without noise; consequently the intersection of the spheres is exact. In reality there is noise - uncertainty of measurement - present in the physical measurement, this leads to a volume of positional ambiguity: it is common practice to find the centroid of this volume (Munoz et al., 2009). This volume of positional ambiguity can be considered as the instrument network uncertainty; it is important to note that this is unlikely to be the total

measurement uncertainty; but rather a contributing component of uncertainty.

Although trilateration only deals with the specific case of a three instrument network, the fundamental principles remain for more than three instruments; the algorithms do however become more involved and so too does the handling of uncertainty.

## 2.6 Co-ordinate Fitting & Network Adjustment

Co-ordinate fitting is regularly required within metrology applications; for example: locating instruments to reference points or co-ordinate systems, data fitting, 'best-fitting', *etc.* This is closely related to network adjustment computations. Measurement networks are widely used in large assembly tooling applications to negotiate line of issues and reduce the measurement uncertainty of the co-ordinate definition of point measurements.

*Network Adjustment* is the general term for combining sets of co-ordinate measurement data taken from either: a single instrument that has been moved multiple times, multiple instruments each obtaining a set of measurements, or a combination of both. Network adjustment is a generic term used for resolving: theodolite networks, geo-surveys, laser tracker networks and photogrammetric networks - to name a few. Sometimes referred to as a *Bundle Adjustment*, the calculations detailed in this chapter outline the basic principles that are routinely undertaken by metrology software packages. The adjustment computations, combine the data sets via common measurement points, subsequently a new set of point co-ordinates in computed. The new set of *adjusted* point coordinates represent the mean position (or centroid), based on minimising the residuals in the data sets, these residuals can be regarded as a consequence of measurement uncertainty - *noise*.

This chapter briefly explores the least squares regression method for fitting co-ordinate data. This gives an appreciation of the computational requirements for network adjustments and the expected outputs/metrics for further discussion. The information presented in the following sections has been extracted, interpreted and condensed from Luhmann et al. (2006) and Ghilani (2010).

### 2.6.1 2D Co-ordinate Fitting Using Least Squares

#### Equal-Weight Least Squares Solution of a Linear System

Consider a 2D scenario, and the application of an equal-weight Least Squares (LS) solution of a linear system. A system of 2D observations can be described in the following form:

$$AX = L + V, \tag{2.36}$$

where:

$$A = \begin{bmatrix} a_{11} & a_{12} & \dots & a_{1n} \\ a_{21} & a_{22} & \dots & a_{2n} \\ \vdots & \vdots & \ddots & \vdots \\ a_{m1} & a_{m2} & \dots & a_{mn} \end{bmatrix} X = \begin{bmatrix} x_1 \\ x_2 \\ \vdots \\ x_n \end{bmatrix} L = \begin{bmatrix} l_1 \\ l_2 \\ \vdots \\ l_m \end{bmatrix} V = \begin{bmatrix} v_1 \\ v_2 \\ \vdots \\ v_m \end{bmatrix}. \tag{2.37}$$

In the context of co-ordinate metrology and co-ordinate fitting, we use the *measured* points to populate the $A$ matrix; the *control* points for $L$; our unknown parameters for $X$; and the $V$ matrix describes the fit residuals. Then general least squares solution is given by:

$$X = (A^T A)^{-1} A^T L = N^{-1} A^T L, \tag{2.38}$$

where, $N$ is the *Normal* matrix.

#### Weighted Least Squares Solution of a Linear System

The instrument uncertainty associated to the system of observations, can be utilised to *weight* our regression fit. The more confident of a point's co-ordinates (lower uncertainty) the higher we can weight the observation, from a mathematics perspective, the uncertainty is commonly termed *variance*. It follows that the weights are inversely proportional to the associated point uncertainty/variance; such that:

$$w_i = \frac{\sigma_0^2}{\sigma_i^2} = \frac{1}{\sigma_i^2}, \tag{2.39}$$

where, $\sigma_i^2$ is the observation's associated variance/uncertainty, with a *unit reference variance* ($\sigma_0^2 = 1$).

The weighted, uncorrelated observations can be expressed as:

$$WAX = WL + WV, \tag{2.40}$$

and the least squares solution of which is given by:

$$X = (A^T WA)^{-1} A^T WL = N^{-1} A^T WL. \tag{2.41}$$

In Equation 2.41 the *Normal Matrix*, $N$, is defined as: $N = (A^T WA)$, and the *Weight Matrix*, $W$ is given by:

$$W = \begin{bmatrix} \frac{\sigma_0^2}{\sigma_{x1}^2} & 0 & \dots & 0 \\ 0 & \frac{\sigma_0^2}{\sigma_{x2}^2} & \dots & 0 \\ \vdots & \vdots & \ddots & \vdots \\ 0 & 0 & \dots & \frac{\sigma_0^2}{\sigma_{xn}^2} \end{bmatrix} = \begin{bmatrix} \frac{1}{\sigma_{x1}^2} & 0 & \dots & 0 \\ 0 & \frac{1}{\sigma_{x2}^2} & \dots & 0 \\ \vdots & \vdots & \ddots & \vdots \\ 0 & 0 & \dots & \frac{1}{\sigma_{xn}^2} \end{bmatrix}. \tag{2.42}$$

**2D Coordinate Fitting**

2D co-ordinate fitting can be achieved via the application of the LS solution; it is a conformal co-ordinate transformation (linear system) with four unknowns: *a, b, c,* and *d*, these are related to the four transformation parameters: *S, θ, $T_x$* and *$T_y$* that is: *scale, rotation, x-translation* and *y-translation* respectively. From Equation 2.36, $AX = L + V$, we have:

$$A = \begin{bmatrix} x_a & -y_a & 1 & 0 \\ y_a & x_a & 0 & 1 \\ x_b & -y_b & 1 & 0 \\ y_b & x_b & 0 & 1 \\ \vdots & \vdots & \vdots & \vdots \\ x_m & -y_m & 1 & 0 \\ y_m & x_m & 0 & 1 \end{bmatrix} X = \begin{bmatrix} a \\ b \\ c \\ d \end{bmatrix} L = \begin{bmatrix} X_a \\ Y_a \\ X_b \\ Y_b \\ \vdots \\ X_m \\ Y_m \end{bmatrix} V = \begin{bmatrix} v_{X_a} \\ v_{Y_a} \\ v_{X_b} \\ v_{Y_b} \\ \vdots \\ v_{X_m} \\ v_{Y_m} \end{bmatrix}. \tag{2.43}$$

Populating $A$ with the *measured* points and $L$ with the *control* points, $V$ contains the residuals after the regression. $X$ holds the parameters $a, b, c$ and $d$, these are related to the transformation parameters, $S$, $\theta$, $T_x$ and $T_y$, such that:

$$\theta = \tan^{-1} \frac{b}{a}, \tag{2.44}$$

and

$$S = \frac{a}{\cos \theta}. \tag{2.45}$$

These parameters can be found by using Equation 2.38:

$$X = (A^T A)^{-1} A^T L. \tag{2.38}$$

Subsequently, the residuals ($V$) can be found by rearranging equation 2.36 such that:

$$V = AX - L. \tag{2.46}$$

A numerical example of equal-weighted 2D coordinate fitting can be found in Appendix B.

### 2.6.2 3D Co-ordinate Fitting Using Least Squares

#### Equal-Weight Least Squares Solution of a Non-Linear System

The 3D case of co-ordinate fitting requires the application of a non-linear solution; firstly, we look at the equal-weight least squares solution of a non-linear system linearized by a Taylor series approximation which is given by:

$$JX = K + V, \tag{2.47}$$

where:

$$J = \begin{bmatrix} \frac{\delta F_1}{\delta x_1} & \frac{\delta F_1}{\delta x_2} & \dots & \frac{\delta F_1}{\delta x_n} \\ \frac{\delta F_2}{\delta x_1} & \frac{\delta F_2}{\delta x_2} & \dots & \frac{\delta F_2}{\delta x_n} \\ \vdots & \vdots & \ddots & \vdots \\ \frac{\delta F_m}{\delta x_1} & \frac{\delta F_m}{\delta x_2} & \dots & \frac{\delta F_m}{\delta x_n} \end{bmatrix} X = \begin{bmatrix} dx_1 \\ dx_2 \\ \vdots \\ dx_n \end{bmatrix} K = \begin{bmatrix} l_1 - F_1(x_1, x_2, \dots, x_n) \\ l_2 - F_2(x_1, x_2, \dots, x_n) \\ l_3 - F_3(x_1, x_2, \dots, x_n) \end{bmatrix} V = \begin{bmatrix} v_1 \\ v_2 \\ \vdots \\ v_n \end{bmatrix}. \tag{2.48}$$

In the context of co-ordinate metrology and co-ordinate fitting, we use the *measured* data to populate the *Jacobian*, $J$, matrix; the *control* points for $K$; our seven transformation parameters are the unknown parameters contained within $X$ (see *Equal-Weight 3D Coordinate Fitting*); and the $V$ matrix describes the residuals. The solution is given as:

$$X = (J^T J)^{-1} J^T K = N^{-1} J^T K. \tag{2.49}$$

An initial approximation for the unknowns should be used, the solution should be iterated, applying the corrections after each iteration. This is repeated until convergence.

### Weighted Least Squares Solution of a Non-Linear System

The weighted solution is important when considering the instrument uncertainty, similarly to the 2D system of equations/observations, the weighted observations are described by:

$$WJX = WK, \tag{2.50}$$

which has a solution:

$$X = (J^T W J)^{-1} J^T W K = N^{-1} J^T W K. \tag{2.51}$$

### 3D Coordinate Fitting

There are seven parameters to consider during a 3D transformation (Ghilani, 2010): *scale, x-rotation, y-rotation, z-rotation, x-translation, y-translation* and *z-translation*:

$S$, $\theta_1$, $\theta_2$, $\theta_3$, $T_x$, $T_y$ and $T_x$, respectively. The rotation matrix is derived from three sequential rotations about a single axis, the rotation about the $x - axis$ ($\theta_1$) and is given by:

$$X_1 = R_1 X_0, \tag{2.52}$$

where:

$$X_1 = \begin{bmatrix} x_1 \\ y_1 \\ z_1 \end{bmatrix} R_1 \begin{bmatrix} 1 & 0 & 0 \\ 0 & \cos\theta_1 & \sin\theta_1 \\ 0 & -\sin\theta_1 & \cos\theta_1 \end{bmatrix} X_0 = \begin{bmatrix} x \\ y \\ z \end{bmatrix}. \tag{2.53}$$

The second rotation about the $y - axis$, $\theta_2$ is defined as:

$$X_2 = R_2 X_1, \tag{2.54}$$

where:

$$X_2 = \begin{bmatrix} x_2 \\ y_2 \\ z_2 \end{bmatrix} R_2 = \begin{bmatrix} \cos\theta_2 & 0 & -\sin\theta_2 \\ 0 & 1 & 0 \\ \sin\theta_2 & 0 & \cos\theta_2 \end{bmatrix}. \tag{2.55}$$

The final rotation about the $z - axis$, $\theta_3$ is:

$$X = R_3 X_2, \tag{2.56}$$

where

$$X = \begin{bmatrix} X \\ Y \\ Z \end{bmatrix} R_3 = \begin{bmatrix} \cos\theta_3 & \sin\theta_3 & 0 \\ -\sin\theta_3 & \cos\theta_3 & 0 \\ 0 & 0 & 1 \end{bmatrix}. \tag{2.57}$$

The single rotation matrix, $R$, becomes:

$$X = R_3 R_2 R_1 X_0 = R X_0, \tag{2.58}$$

hence:

$$R = \begin{bmatrix} r_{11} & r_{12} & r_{13} \\ r_{21} & r_{22} & r_{23} \\ r_{31} & r_{32} & r_{33} \end{bmatrix}, \tag{2.59}$$

where:

$$\begin{aligned} r_{11} =& \ \cos(\theta_2)\cos(\theta_3), \\ r_{12} =& \ \sin(\theta_1)\sin(\theta_2)\cos(\theta_3) + \cos(\theta_1)\sin(\theta_3), \\ r_{13} =& -\cos(\theta_1)\sin(\theta_2)\cos(\theta_3) + \sin(\theta_1)\sin(\theta_3), \\ r_{21} =& -\cos(\theta_2)\sin(\theta_3), \\ r_{22} =& -\sin(\theta_1)\sin(\theta_2)\sin(\theta_3) + \cos(\theta_1)\cos(\theta_3), \\ r_{23} =& \ \cos(\theta_1)\sin(\theta_2)\sin(\theta_3) + \sin(\theta_1)\cos(\theta_3), \\ r_{31} =& \ \sin(\theta_2), \\ r_{32} =& -\sin(\theta_1)\cos(\theta_2), \\ r_{33} =& \ \cos(\theta_1)\cos(\theta_2). \end{aligned} \tag{2.60}$$

The mathematical model is completed by multiplying by a scaling factor, $S$, and adding on the translations, $T_x$, $T_y$ and $T_z$, to give:

$$\begin{aligned} X &= S(r_{11}x + r_{21}y + r_{31}z) + T_x, \\ Y &= S(r_{12}x + r_{22}y + r_{32}z) + T_y, \\ Z &= S(r_{13}x + r_{23}y + r_{33}z) + T_z. \end{aligned} \tag{2.61}$$

Populating $X$ with the unknown transformation parameters and the *Jacobian*, $J$, matrix, gives:

$$\begin{bmatrix} \left(\frac{\delta X}{\delta S}\right)_0 & 0 & \left(\frac{\delta X}{\delta \theta_2}\right)_0 & \left(\frac{\delta X}{\delta \theta_3}\right)_0 & 1 & 0 & 0 \\ \left(\frac{\delta Y}{\delta S}\right)_0 & \left(\frac{\delta Y}{\delta \theta_1}\right)_0 & \left(\frac{\delta Y}{\delta \theta_2}\right)_0 & \left(\frac{\delta X}{\delta \theta_3}\right)_0 & 1 & 0 & 0 \\ \left(\frac{\delta Z}{\delta S}\right)_0 & \left(\frac{\delta Z}{\delta \theta_1}\right)_0 & \left(\frac{\delta Z}{\delta \theta_2}\right)_0 & \left(\frac{\delta X}{\delta \theta_3}\right)_0 & 1 & 0 & 0 \end{bmatrix} \begin{bmatrix} dS \\ d\theta_1 \\ d\theta_2 \\ d\theta_3 \\ dT_x \\ dT_y \\ dT_z \end{bmatrix} = \begin{bmatrix} X - X_0 \\ Y - Y_0 \\ Z - Z_0 \end{bmatrix} \tag{2.62}$$

### 2.6.3 Network Adjustment

The least-squares methods introduced in the above section can be used to combine co-ordinate measurements from multiple observations by arbitrarily *fixing* a data set and treating them as the *control points*. Once the observations from each measurement station have been combined, a *composite* point group can be generated. The composite point group represents the most likely 'true' position of the measurand, based on the measured observations and, in the weighted case, the associated uncertainty. Each point co-ordinate definition within the composite group should be accompanied by an associated uncertainty, this could be in the form of $x, y, z$ values, or, more accurately, the co-variance matrix. This network adjustment process is employed within the large aerospace assembly tooling community to create reference systems, known as either: Jig Reference Systems (JRS), Floor Reference Systems (FRS) or Enhanced Reference Systems (ERS). These reference systems are used for accurately building jigs and fixtures, and subsequent processes, providing an accurate method for locating measurement systems (see Chapter 3).

The network adjustment method for defining the ERS was adopted by Airbus UK (AUK). AUK tooling has tight manufacturing requirements due the the tight tolerances associated with wing-box assembly. AUK have employed SpatialAnalyzer's Unified Spatial Metrology Network (USMN) as their network adjustment tool, this uses an algorithm based on weighted least-squares, the weights are related to the respective instruments' uncertainty parameters (Calkins, 2002)). AUK have standardised their internal USMN process (Forster, 2007) to ensure consistence across the business. In addition to utilising the instrument uncertainty parameters, consideration is also given to the temperature of the tooling. Reduction in the effects caused by thermal expansion is achieved by scaling each instrument using a linear expansion model, before applying the network adjustment. A similar methodology has been developed and published by the jig and fixtures manufacturer ElectroImpact Inc., detailing a methodology for creating a control point network (equivalent to reference system), with consideration for jigs that 'float' with the expansion (Christensen and Flynn, 2012). Further accuracy improvements to the co-ordinate definition of the reference system points can be made by introducing calibrated length bars into the USMN/network adjustment (Calkins and Sandwith, 2007).

Other, non-commercial, multi-instrument network adjustments such as the Bayesian approach developed by the National Physical Laboratory (NLP) (Forbes, 2012) and the Mahalanobis distance method (Predmore, 2010), give a reduction in the associated

uncertainty to the points generated through the adjustment, when compared to the UMSN algorithm (Predmore, 2010). However, this reduction is at the single digit micron-level, this is of little significance when generating measurement data that spans tens of metres. Developments in large scale network measurements that could be adapted for aerospace assembly fixtures, could further drive down the reference network uncertainty, to a negligible level. For example, the ATLAS detector at CERN, used a single laser source to generate many frequency scanning interferometers (FSI) which can be deployed through fibre optics. This enabled the creation of a geodetic grid of interferometers at a low-cost and high accuracy to monitor the detector (Gibson et al., 2005). The NPL are currently developing the FSI technique for generic applications (NPL, 2014)

## 2.7 Data Fusion

Instrument networks are used for a number of reasons, mainly: reducing measurement uncertainty, increasing the measurement volume and providing complementary technologies to enhance data collection. Due to the expense of measurement instruments, instrument networks are usually roving or multi-hop systems using a single instrument many times. Instrument hardware networks have many challenges; using the data from each instrument in the most efficient way is paramount. Different measurement instruments have differing strengths, data management has to have an awareness of such attributes and respond appropriately. Multi-sensor data fusion is a method for centrally combining and processing data from a number of different sensors (Huang et al., 2007). The data fusion can be described as either: complementary, competitive and cooperative (Durrantwhyte, 1988). *Complementary* if sensors are independent but can offer additional information by complementing one another; *competitive* if the sensors are independently measuring the same area/targets in order to eliminate random error and reduce measurement uncertainty; and *co-operative* sensors are independent but different from each other and the combination of sensors provides a level of information that each sensor cannot achieve alone. Within dimensional metrology, examples of such multi-sensor data fusion include: field of image fusion, tactile and optical coordinate metrology, coherent and incoherent optical measuring techniques, computed tomography and scanning probe microscopy (Weckenmann et al., 2009). It is likely that the future of multi-sensor data fusion will become increasingly important as higher levels of integration with fast processing speeds become a necessity for large volume metrology and automation.

## 2.8 Metrology Assisted Assembly

Metrology Assisted Assembly (MAA) - sometimes referred to as *measurement* assisted assembly (MAA) - is defined by Muelaner et al. (2013) as: using measurement to guide assembly operations, including: predictive processes, assemble-move-measure (AMM), active tooling and closed-loop control. This definition suggests that MAA is inherent in many processes. As a consequence, this section will introduce a number of examples where metrology/measurement is a large component of the research development, within the context of manufacturing and assembly.

As part of the growing requirement for MAA, in-process measurement and control there is a increasing need for full-field measurement systems. Metrology-driven automation has been identified as a key area for growth (Jamshidi et al., 2010). These systems provide a metrological environment, and begin to move away from traditional "point and shoot" type instruments, similar to the iGPS system (see Section 2.2.2). These measurement systems aim to have multi-target measurement capability (required for 6DOF) the research-based solution from DIGEP-Politecnico di Torino, the: Mobile Spatial co-ordinate Measuring System (MScMS), this system uses ultrasound and multi-lateration to determine the co-ordinate measurement. The lower cost MScMS was benchmarked against the more mature and commercially available iGPS system Maisano et al. (2009), the system was shown to perform at the sub-ten-millimetre level; which is not sufficient for most tooling requirement, except for the initial positioning of primary tool structure. The second generation Mobile Spatial co-ordinate Measuring System (MScMS-II) uses photogrammetric methods and triangulation for position and location (Franceschini et al., 2014) which is perhaps a more robust method to employ within the MAA context and the intended industrial applications. These distributed metrology systems are enablers for the further, and wider adoption of MAA processes. For example the control of tooling and robotics (see Section 2.9.5) requires 6DOF measurement data at a sufficiently high frequency, and a low feedback latency close to real-time. Although possible with current technologies such as a laser tracker (see Section 2.2.1), line-of-sight issues are a major concern, in addition the cost is prohibitive as the metrology system is five to ten times the cost of the automation. The metrology system is also dedicated to the automation system. Affordable, accurate and ubiquitous metrology systems would provide a platform for the realisation of many automation prospects. Distributed metrology systems have been used to control robotics as a tool for manufacturing, with iGPS (Norman et al., 2013) and research-based technologies such as Tianjin University's workspace Measuring and Positioning System (wMPS)

(Xue et al., 2014).

Measurement is often considered in the context of product conformance and Quality Control (QC), and not as an in-process tool. For example the Metrology Assisted Determinate Assembly (Muelaner and Maropoulos, 2010) philosophy requires in-process measurement data to drive downstream manufacturing operations. However current distributed metrology systems are unable to achieve aerospace, specifically: wing and associated tooling tolerances at an affordable and robust level. However iGPS has been used in practice with Boeing to assemble fuselage sections (Mei and Maropoulos, 2014), however it should be noted that the tolerance requirement for the fuselage is significantly relaxed when compared to wing-level aerodynamic criteria.

## 2.9 Aerospace Wing-Box Assembly Tooling

The following section explores the broad issues encountered when considering the design of assembly jigs and fixtures in aerospace. Tooling is traditionally an empirically taught and heuristically based field with experience and learning passed on from master to apprentice over a period of years (Rong et al., 2005); as each fixture is esoteric, broad theories of fixturing that apply across the spectrum of applications are not practical. Therefore a review of industrial practices within aircraft assembly tooling (Section 3) is perhaps the most appropriate vehicle to understanding the industrial requirements and the gaps in knowledge and understanding that exist.

### 2.9.1 Functional Requirements

The terms jigs and fixtures are often used interchangeably when referring to work holding (Boyes, 1980); strictly speaking there is a distinction between the terms: jigs hold and locate the workpiece whilst guiding a material removal operation; whereas fixtures only hold and locate workpiece or assembly (Pollock, 1988). Aerospace Wing-box assembly fixtures can be thought of as both a means for validation and verification; the tooling not only places the component correctly for assembly but checks the assembly is correct. The fixture must locate and control all six degrees of freedom on both a component and assembly level. The fixture acting as a quality gate is a key driver for hard tooling as it is difficult to get stable and repeatable positional accuracies when employing modular tooling (Leopold et al., 2008). This traditional tooling philosophy carries inherent problems as the tooling is typically only re-certified once every three

years (Tomlinson and Singh, 2008) after its initial commissioning. Ensuring that the tooling remains stable between certifications is another driver for monolithic structures as any movement between certifications could allow a number of concessions to go undetected. The assembly and components need to be held rigid with a stability that ensures the relative and global positions of the parts; this requirement further drives monolithic tooling. Future developments in creating stiffer components, greater sub-assembly rigidity or more accurate and quicker Finite Element Analysis (FEA) models (Burley et al., 1999) are essential in order to reduce the levels of assembly tooling. Alternatively, advances in metrology systems may contribute to tooling reductions. Metrology systems either have to have increased capability in terms of feature recognition or develop enhanced datum structures that are capable of describing and monitoring any part/assembly distortions during handling, assembly and machining operations; it is important that these new technologies and developments are cost effective. Including manufacture and maintenance of assembly jigs and fixtures it is estimated at 10% of the overall manufacturing costs for each air frame (Burley et al., 1999) or at approximately 5% of the total build cost (Rooks, 2005). The size and complexity of the assembly fixtures creates typical construction times of more than 6 months (Plut and Bone, 1997). Flexible tooling could result in a reduction in tooling lead times, however with relatively high Non-Recurring Costs(NRCs) it is estimated that a fixture has to be reconfigured 4-5 times before it becomes economically competitive to conventional tooling (Kihlman, 2002), after which is it significantly cheaper than monolithic tooling. Eventually, the assembly process would benefit from the development of jigless/fixture-less manufacture, this would depend heavily on metrology to define and drive the assembly; this would still require some form of work holding; for example the work holding could be replaced with sensor-guided robots (Bone and Capson, 2003).

There is a need to increase automation in the aerospace sector to satisfy the forecast increase in production volume and further reduce health and safety risks to the operators. There are significant obstacles to overcome before automation can be fully embraced by the aerospace sector. Automation requires an accurate method of referencing back into the local (component) or global (assembly) co-ordinate system. The future of Wing-box Assembly holds additional considerations, such as the use of Composite Materials replacing the traditional Aluminium based components.

Composite materials hold new challenges that are integrally linked to metrology. Composites cannot be treated like their metallic counterparts, as they are not as susceptible to in-fixture machining processes often used to achieve the required Wing-box

assembly tolerances. Additionally, damage to composites induced through the assembly processes are 'hidden' and could potentially go unnoticed. Clamping forces could cause such damage; research into the development of clamping force optimisation techniques is progressing using swarm intelligence based techniques (Deng and Melkote, 2006).

### 2.9.2 Ergonomic Requirements

In addition to a fixture holding and checking the assembly, a fixture also has to satisfy the ergonomic requirements of the build, allowing for the human factors associated with the operators. An example of this would be the orientation of the build: vertical or horizontal, i.e. the wing skins perpendicular to the floor (vertical) or parallel to the floor (horizontal). Both have advantages and disadvantages, a vertical build is a more efficient use of factory floor space, and allows easy access to both sides of the build, but the operators need to work at height; on the other hand a horizontal build uses up more floor space, causes a greater level of sag during the assembly, but avoids working a height and allows for different access to that of the vertical build. Millar and Kihlman (2009) demonstrated a Reconfiguable and Flexible (ReFlex) fixture, which illustrated how an active 'picture-frame' tooling configuration could move between vertical and horizontal build configurations, coined: *ergonomically active*; albeit on a relatively small scale. Additionally, a horizontal build is likely to cross fewer thermal gradients than a vertical build. Virtual Reality (VR) can aid the design jigs and fixtures, enabling the operators/tool designers to explore the ergonomic considerations before committing to a final design(Rajan et al., 1999).

### 2.9.3 Concurrent Engineering

Long lead times associated with the design and manufacture of the assembly fixtures means that fixtures (in excess of 24 months (Millar and Kihlman, 2009)) have to begin before the aircraft geometry and assembly strategy has been finalised. This does not however constitute concurrent engineering in the traditional sense as the information stream is typically one-way, that is, feeding into the tool designers. Subsequently, late design changes impact the fixture design, which may already be in the late stages of manufacture. Employing a concurrent engineering strategy from the offset may enable the late design changes to be predicted and accommodated for; additionally the tooling design team could work in a more integrated manner with aircraft design team to build in better datum structures and points of reference for key characteristics. A novel

concurrent engineering strategy for aircraft tooling collaborative design - based on the organisational structure and working principle of human body - uses a model based on neuron-endocrine-immunity as a working principle (Li et al., 2009); this system is divided into controller and controlled objects so that it can monitor and discern the product changes in good time, adjust, and restructure the aircraft tooling design process flexibly, including the overall coordinates and optimising the tooling design.

### 2.9.4 Design for Manufacture & Assembly

Design for Manufacture and Assembly (DFM/A) could change future fixturing requirements. DFM/A is a design philosophy that not only considers the products functionality, but integrates the manufacturing and assembly mechanism required to produce the product (Molloy et al., 1998); for example, integrating a determinate assembly philosophy - where components can only fit together in the correct position and orientation. DFM/A could have large implications on the assembly fixturing needs, as an example determinate assembly would require work holding but not accurate or bulky fixturing; as the components would locate relative to one another. This is essentially fixture-less assembly.

### 2.9.5 Reconfigurable, Flexible & Automated Tooling

This section examines the current landscape of research conducted within reconfigurable, flexible and automated tooling; this has a close relationship with the research presented within this thesis. Reconfigurable, flexible and automated tooling, are large contributors to the broader area of *Flexible Manufacturing Systems* (FMS), of which Metrology Assisted Assembly (MAA) is an enabling technology. Mei and Maropoulos (2014) are proponents of the Digital Master Tooling (DMT) philosophy to facilitate the move away from hard tooling, and the Hard Master Tooling (HMT) towards FMS and more specifically, flexible tooling. They describe the effective synergy between advanced optically based metrology and tooling in an integrated digital and physical measurement environment. Reconfigurable and flexible tooling are often considered concurrently with automation; although not intrinsically linked, flexible tooling solutions often provide appropriate platforms for introducing automation. As an example, Kihlman (2002) outlines within his thesis, the: Affordable Reconfigurable Tooling (ART) framework, employing a system of reconfigurable tooling elements, assembled in a similar way to scaffolding, named BoxJoint. Kihlman proposed that laser trackers

could provide the metrological feedback, while serial robots position or re-position passive pick-ups within a flexible 'picture frame' tooling arrangement. An alternative, and perhaps more intuitive use of standard industrial robots is to deploy robots in place of fixturing, this is coined Robotics in Fixture-less Assembly (RFA), (Corona-Castuera et al., 2005). This RFA solution has limitations based on robotic repeatability and absolute positioning accuracy. Typically repeatability is tens of micrometres, whereas positioning, is at the millimetre level. It has been suggested that an exoskeleton of encoders could be retro-fitted to a standard robot serial axis industrial robot to create High Accuracy and High Capacity (HAHC) automation (Muelaner et al., 2011). Alternatively live metrology feedback can negate the requirement for accurate automation, but often at a prohibitive cost; as an example Kihlman developed ART further, introducing automated pick-ups, guided directly by a 6DOF laser tracker (Kihlman et al., 2004); this automated tooling is also known as *Active Tooling*.

Much of the research into active tooling has predominately been focussed on machining fixtures; however, where possible, common themes have been identified. In a recent review paper Bakker et al. (2013) broadly splits active tooling into three areas: i) Sensor-based fixture design, ii) Automatically reconfigurable fixtures, and iii) Active fixtures. These can be described as:

**Sensor-based fixture design** aims to automatically sense the part and/or assembly, ensuring correct location within the fixture.

**Automatically reconfigurable fixtures** change the position of pick-ups to account for product variants, with differing tooling requirements.

**Active fixtures** is a broad term for fixtures that include features such as: variable clamping forces, actuation and sensing.

Commercially available, flexible tooling turnkey solutions offered by companies such as Advanced Integration Technology (AINT) and NOVA-TECH Engineering. However this tends to be for loading and positioning components, such as fuselage/wing join-up, and not an adaptive process.

## 2.10 Digital Environment

Historically, the digital environment provided a platform for component and assembly product design, with increased functionality, the digital environment can be used for

digital simulation as a virtual prototype enabling verification of product functionality before the physical realisation of the intended product (Maropoulos and Ceglarek, 2010). The digital factory is an extension of this and is described by Bracht (Bracht and Masurat, 2005) [as] *an environment where all the computer-aided tools necessary for the planning of new products and production plants as well as for the operation of the factories are networked through a central database.*

### 2.10.1 Tooling Digital Mock-Up

The Digital Mock-Up (DMU) of the tooling is driven from the CAD geometry of the components that are to be assembled in the fixture; the digital environment is paramount in the fixture design procedure. Additional considerations which impact the design fixture is the factory layout and build philosophy, as this determines the amount of fixturing, the design of the fixtures and the expectation of the fixtures. The use of integrated digital tools such as the CATIA/DELMIA product family provides a platform for Product Lifecycle Management (PLM) including: factory layout, ergonomic/human factors, robotic programming and simulation, clash detection, etc. using a product, process and resource model: the effectiveness of this PLM in Bombardier Belfast is reported in (Butterfield et al., 2007). DaimlerChrysler report (Wöhlke and Schiller, 2005) on the additional benefits of Digital Planning Validation (DPV) designed to run in parallel to the digital planning stages; this enables the designer to check the manufacturability of a product in terms of its geometry and associated assembly processes. Currans (Curran et al., 2007) uses the digital factory to aid cost effectiveness by implementing direct operating costs and manufacturing costs into the development tools (Curran et al., 2007). Furthermore, Boeing are developing tools that allow a user to interface through a VR environment with the CAD geometry analysing real-time clashes, visualising and manipulate the model in real-time (Mizell, 1994).

### 2.10.2 Metrology Software

This section briefly explores metrology software, focusing on generic capabilities found within third party large volume metrology software and not an exhaustive review of software solutions. Manufacturers create their own software to complement their respective hardware; for example, Faro: CAM2, Nikon: iSPACE, Leica Geosystems: PC-DMIS. However, there are standalone, third-party softwares that have developed additional functionality with broader instrument interfaces. Generally speaking, in-

tegration of systems within a manufacturer's product range can be accomplished by employing their own software. Difficulties occur when systems from different manufacturers require integration. Third party software developers can often accommodate more system interfaces. An established example of a LVM program - that Airbus UK employs for its LVM activities - is SpatialAnalyzer (SA) by New River Kinematics (NRK); this software provides a 3D environment in which a metrological system can be based; utilising a multitude of instruments from many different manufacturers. Additional post-measurement analysis tools can also be employed; for example network uncertainty evaluation or a CAD data comparison (Figure 2-18).

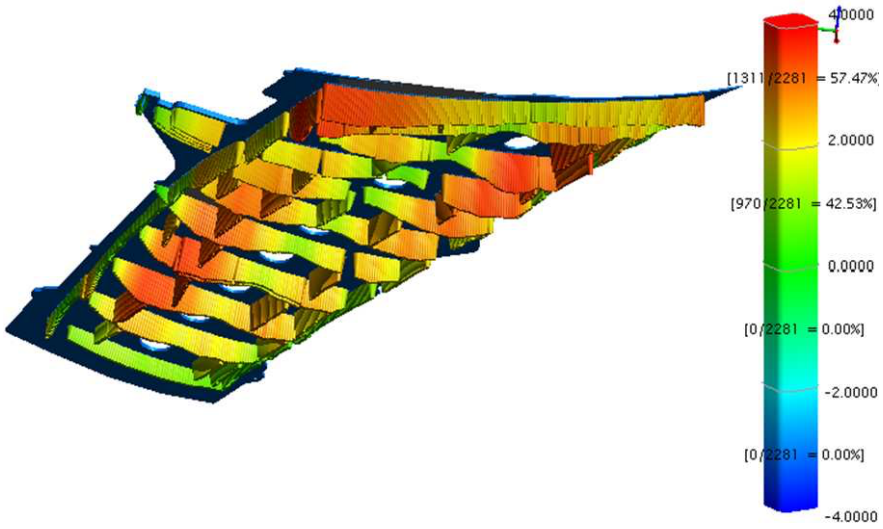


Figure 2-18: Example of measured data to nominal CAD geometetry within SpatialAnalyzer

Software that interfaces with a multitude of instruments includes (but is not limited to):

- Verisurf (*www.verisurf.com*)
- SpatialAnalyzer (*www.kinematics.com*)
- Metrolog (*www.metrologic.fr*)
- BuildIT (*www.builditsoftware.com*)
- Polyworks (*www.innovmetric.com*)

The main differences between the packages tends to be derived from the historical development path, hence the graphical user interface and experience is a matter of personal choice. For example: Verisurf is based on a Computer Aided Manufacture (CAM) platform, Polyworks has a reverse engineering and scanning inspection background, and SpatialAnalyzer (SA) was developed specifically for large volume metrology.

As these software platforms have literally thousands of functions, it is difficult to explicitly give a definitive comparison between packages. A better approach is to develop a build philosophy and assembly method, and then assess each package against the requirements of the build. The appropriate software considerations are detailed below:

i) *Compare/Build to CAD*: This function is the ability to compare measured data to the CAD nominal geometry of the design intent. Typically this is carried out as inspection task. However, if the software enabled CAD comparison and measurement system are capable of dynamic operation then adjustments (manual or automated) can be performed based on the deviations from CAD; this can described as: *Building to CAD*. This is particularly useful during: tool setting, assembly alignments and concession re-work.

   Many software packages can import native CAD formats and some can import Model Based Definition (MBD) data within the files: importing G,D&T information, surface finish, annotations, etc. The ability to orientate your instrument(s) correctly to CAD, measure and subsequently compare to nominal is paramount functionality in a Metrology Assisted Assembly (MAA) philosophy. The software packages named above all provide this feature to varying degrees. Large-scale assemblies/builds rarely have reliable features to perform a traditional 3, 2, 1 location fit. For example as planes are unlikely to adequately 'flat' due to the large scale and material compliances. Hence, a higher level of control when fitting to nominal geometry is important, especially when measuring freeform surfaces.

   Comparing to CAD is a straightforward inspection operation and is similar across platforms, with graphical representation varying between software packages. Building to CAD functionality varies between vendors again, with the graphical interface and usability being a matter of personal choice.

ii) *Instrument Interfaces*: within large volume assembly multiple instruments (from multiple vendors) are likely to contribute to the build process (see Section 2.2 & 2.7), this could be in parallel or sequential. A harmonised software approach enhances the assembly process and data management. It is therefore important

that the software platform accommodates a number of different instruments, with the ability to simultaneously drive two or more instruments. The number and variety of instrument interfaces differs amongst software platforms, so too does licensing. This is a consideration to be explored after the instrument selection process has been completed, as the software platform should not inform this choice but rather based on instrument capability and appropriateness.

iii) *Uncertainty Analysis*: the handling of instrument uncertainty varies between software platforms, some do not include uncertainty calculations at all. The uncertainty calculations within these interfaces is based on the instrument uncertainty not process uncertainty as described in Section 2.3. However, SA does have the ability to quantify the level of uncertainty when fitting geometric features to measured points.

The level of control of the uncertainty parameters associated to instruments also varies amongst the platforms; that is, how the uncertainty parameters are calculated and/or assigned to instruments. Uncertainty may also be calculated when constructing geometry or bundling instruments.

iv) *Bundle/Network Adjustment*: this is the ability combine multiple instruments and the associated measurements together to reduce the uncertainty of those measured points, see Section 2.7. This creates a network of instruments, either by having multiple instruments or by moving a single instrument to multiple locations (or a combination of the two).

The bundle adjustment algorithms vary amongst manufacturers, some are generic as described in Section 2.6, others are proprietary algorithms. Some bundles use the instrument uncertainty parameters to weight the bundle adjustment, others are un-weighted. A bundle can be a minimising calculation or in the case of SpatialAnalyzer - use a Monte Carlo Simulation (MCS) within their Unified Spatial Metrology Network (USMN) function to compute the network uncertainty.

v) *Reverse Engineering*: this is the ability to create CAD geometry from measured data. Reverse engineering capability varies greatly between software packages, with Polyworks having the strongest suite of reverse engineering tools. However there are other specific reverse engineering software packages also available such as Geomagic (*www.geomagic.com*) or Rapidform (*hwww.rapidform.com*).

Although reverse engineering is not an essential part of traditional assemblies, there is a growing requirement to aid interface management by measuring the

actual interface and reverse engineer the mating component; for subsequent processes such as fettling.

vi) *Scripting*: This is the ability to 'programme' the software in order to automate or semi-automate measurement processes. The ease of scripting and the flexibility is something that varies between manufacturers for example VeriSurf records a measurement process that can be replayed as a measurement plan.

The scripting or measurement plan interface is an important consideration, for example the ability to lock down all the controls or simplify the graphical user interface (GUI) for shop-floor operators is often useful to avoid excessive training or a mistake when using the software. Some providers will also allow access to the Software Developers Kit (SDK), this means that one can build bespoke software interfaces, and call functions from the metrology platform. This truly locks down the process, but is perhaps more suited to high through-put production. These bespoke software interfaces are offered by some vendors such as BuildIT and SpatialAnalyzer at an additional cost.

## 2.11 Review Summary

The literature review presented within this chapter has been carried out to establish a robust overview of the current landscape; from which we can draw a number of conclusions and knowledge gaps, as follows.

The metrology requirements for aerospace and the associated tooling fall into the area of *Large Volume Measurement* (Section 2.2). This section outlined the operation and instrument uncertainty for measurement systems that: i) are currently used within industry; ii) have exploitation potential; or, iii) are utilised within this body of research; from which we can infer that:

- Measurement is discrete point, target based.
- The current landscape is dominated by laser tracker technologies.
- Instrument associated uncertainty is significantly large when compared to the tooling and assembly tolerances.
- From this literature review instrument performance in an *industrial environment* can be drastically different from the manufacturers statement.

- Comparable LVM technologies with advantages exist but are not being deployed in assembly tooling environments due to lack of industrial exposure (TRL).

Secondly, research and discussion around *Dimensional Uncertainty* (Section 2.3), highlighted that it is an important and fundamental concept to understand. In the context of large scale of assembly tooling and aerospace structures the relationship and interaction between *Uncertainty and Tolerance* (Section 2.4) is of significance. The magnitude of the measurement uncertainty is comparable to that of the build/assembly tolerances. Thus, not considering the measurement uncertainty could lead to widespread product non-conformance. This section identified the following:

- GUM standards do not easily accommodate 3D co-ordinate measurements.
- Process uncertainty is large, and even more significant in relation to tooling and assembly tolerances, than just instrument considerations.
- Uncertainty is rarely considered during laser tracker operations (tool setting).

Determining the co-ordinate *Position and Location* from the native sensors of the measurement instrument systems is presented in Section 2.5, namely triangulation and multi-lateration techniques. Subsequently, the basic principles of *Co-ordinate Fitting and Network Adjustment* (Section 2.6) is introduced. These principles are important when considering large scale metrology challenges. This combining of sensors is generically known as *Data Fusion* and is discussed in Section 2.7.

- Process uncertainty is even more significant in relation for assembly tolerances
- GUM standards do not easily accommodate 3D LVM networks.
- Measurement uncertainty estimation of LVM networks is largely undocumented.
- At best, instrument uncertainty is considered during reference network generation
- The use of complementary metrology technologies can reduce measurement uncertainty.

Within the current landscape, a significant proportion of the research presented in the following chapter out could be described as a sub-division of *Metrology Assisted Assembly* (Section 2.8). Metrology Assisted Assembly is a newly established area of

manufacturing, shifting metrology away from the traditional inspection capacity and moving measurement systems in-process to drive assembly operations. Subsequently, MAA has significant knowledge gaps, in relation to the scope of this research they are:

- A lack of an integrated approach towards metrology and aerospace Wing-box assembly tooling.
- Metrology practices and process with respect to tooling are not publicly documented.

This review of the literature and examination of the state-of-the-art within *Aerospace Wing-box Assembly Tooling* (Section 2.9) has illustrated the esoteric nature. There exists little information that is formally documented and readily available within the area of assembly tooling, and more specifically aerospace wing-box assembly tooling. Explicitly there remains:

- No publicly documented metrology requirements, limitations or process with regard to large scale tooling to tooling.

This enforces that tooling is a largely heuristic - "master and apprentice" - discipline within manufacturing engineering functions. It follows, that the most appropriate way to examine aerospace assembly tooling requirements is through the use of a *Review of Industrial Practices within Aircraft Wing-box Assembly Tooling* (Chapter 3). This will allow the specific academic challenges and industrial requirements - both, technical and business drivers - to be extracted.

The *Digital Environment* was discussed in Section 2.10 for completeness. This section explores the digital tools for the creation of tooling and the simulation and use of metrology systems. The section highlighted that:

- Software tools for simulating the tooling and metrology resources does not currently exist.
- Metrology software has limited uncertainty analysis capability, at best quantifing instrument associated software and not the measurement process.

## 2.12 Research Gaps

Following the *Review of Large Volume Metrology, Dimensional Uncertainty, and Aerospace Wing-box Assembly Literature* the main research gaps have emerged, relating to:

- Methods for quantifying the co-ordinate uncertainty for a large volume metrology processes, with particular reference to industrial multi-instrument networks;
- An integrated approach towards metrology and aerospace Wing-box assembly tooling, to further Metrology Assisted Assembly (MAA)
- Examination of the metrology requirements within the aerospace industry with respect to large scale assembly tooling.

# Chapter 3

# Review of Industrial Practices within Aircraft Wing-box Assembly Tooling

## 3.1 Introduction

The *Review of Large Volume Metrology, Dimensional Uncertainty, and Aerospace Wing-box Assembly Literature* (Chapter 2), identified the gap (Section 2.12) that exists when exploring Wing-box assembly tooling with respect to the metrology requirements. The industrial requirements for the assembly tooling and the subsequent need for metrology is best examined though a review of current industrial practices.

This review introduces the assembly tooling and metrology requirements for Wing-box assembly tooling at Airbus UK (AUK). As an example, the Airbus A380 Trailing Edge (Section 3.2) provides focus as a representative assembly tool, in terms of Wing-box scale and challenges.

The assembly tools in Airbus have two main functions:

i) To locate and hold the components during the manufacturing and assembly process to achieve the Key Characteristic (KC) tolerances, this includes holding the parts rigid during manufacturing operations such as drilling and fettling.

ii) To verify the build tolerances and act as a quality control (*post-assembly*)

Typically the assembly tolerances are approximately 300 µm, within this build tolerance the tooling is assigned around 150 µm of the allowable tolerances, good practice dictates that the tooling should consume around 10% of the build tolerance, however this is not possible due to the large scale of the fixtures and so the tooling occupies around 50% of the build tolerance. The scale of the assembly tooling ensures that the tooling has to be measured in an industrial environment. This limits the achievable uncertainty by: choice of measurement system (hardware limitations), low environmental control (refractive index) and material compliance/stability.

A well designed fixture should also enhance the assembly process by creating an ergonomic and intuitive working environment, allowing easy access where appropriate. An ideal fixture would also contribute to a lean manufacturing environment.

The components and/or sub-assemblies are located in the tooling using their key characteristics. Once located in the fixture the components then undergo an assembly process, after which, the new assembly is checked in-fixture for conformance and in particular their Inter-changeability (ICY) requirements; this is important for when the part or sub-assembly moves to another fixture or is moved to the Final Assembly Line (FAL). The verification of the KCs and ICYs is paramount in ensuring that the Aircraft tolerances are met, which in turn, ensures the aircraft's aerodynamic criteria are maintained.

The aerodynamic criteria are descended from the aircraft's Numerical Master Geometry (NMG) which in turn is a numerical interpretation from the aeroplane's initial aerodynamic shape, conceived for manufacture. The NMG defines the KCs of the aeroplane's geometry, the ICY ensures that all the important interfaces between parts and sub-assemblies are compatible; the KCs and ICY is checked and implied from the tooling. Figure 3-1 highlights important Wing-box features, indicating where metrology plays a key role.

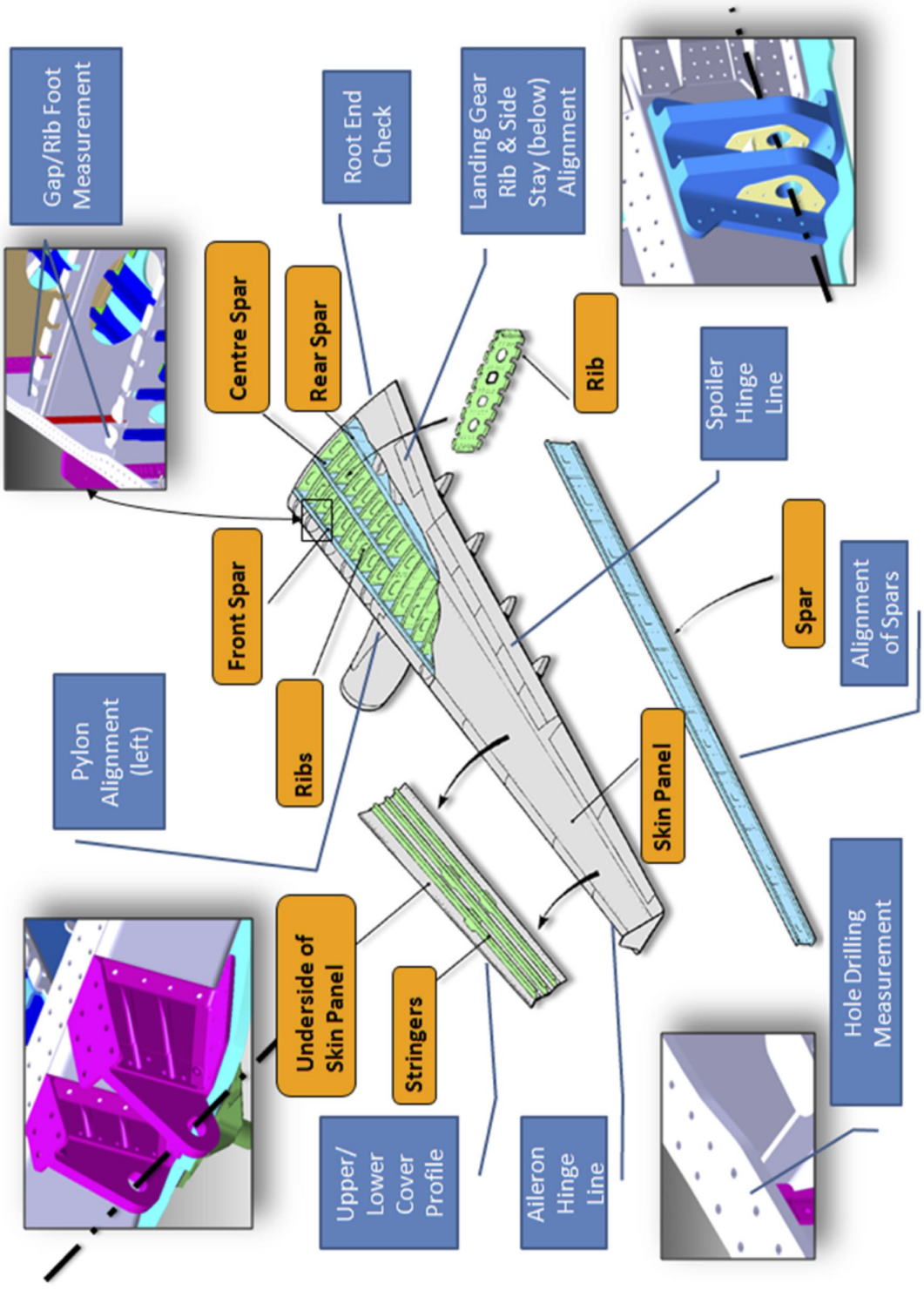


Figure 3-1: Wing terminology (in orange) and metrology requirements (in blue)

## 3.2 Airbus A380 Trailing Edge

The A380 Trailing Edge sub-assembly provides an example of how the tooling controls the ICY and KCs during the assembly process. This example focuses on the setting and checking of the rear spar, hinge brackets and gear rib in the sub-assembly; these components are considered by using simplified CAD geometry (Figure 3-2), related back to the physical tooling features to further understanding.

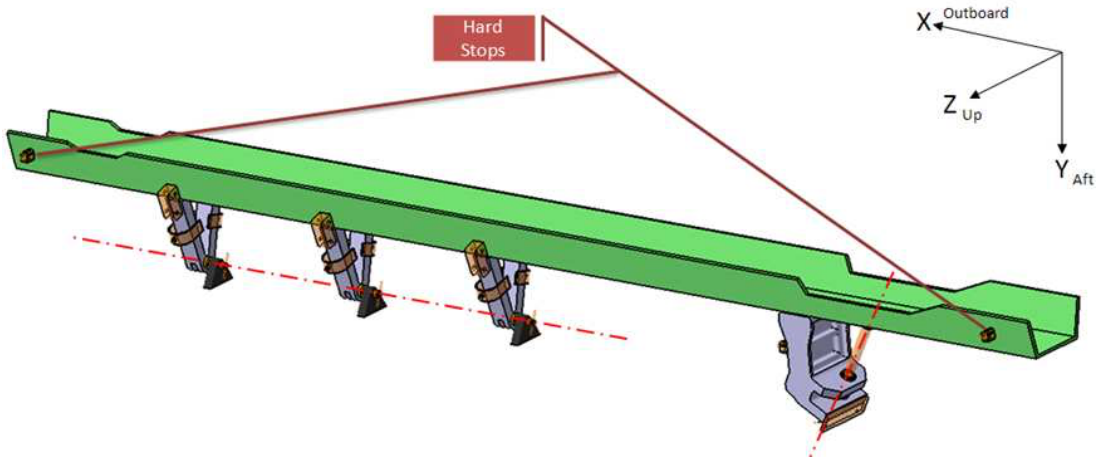


Figure 3-2: Simplified trailing edge sub-assembly

### 3.2.1 Hinge Brackets

Figure 3-3 gives a broad overview of the hinge line tooling. The hinge brackets have two ICY requirements, the hinge line co-axiality, both locally (between brackets) and globally (overall wing NMG), the second ICY requirement is the step condition between the bracket and the upper cover interface. The step condition on the lower cover is met by fettling appropriately.

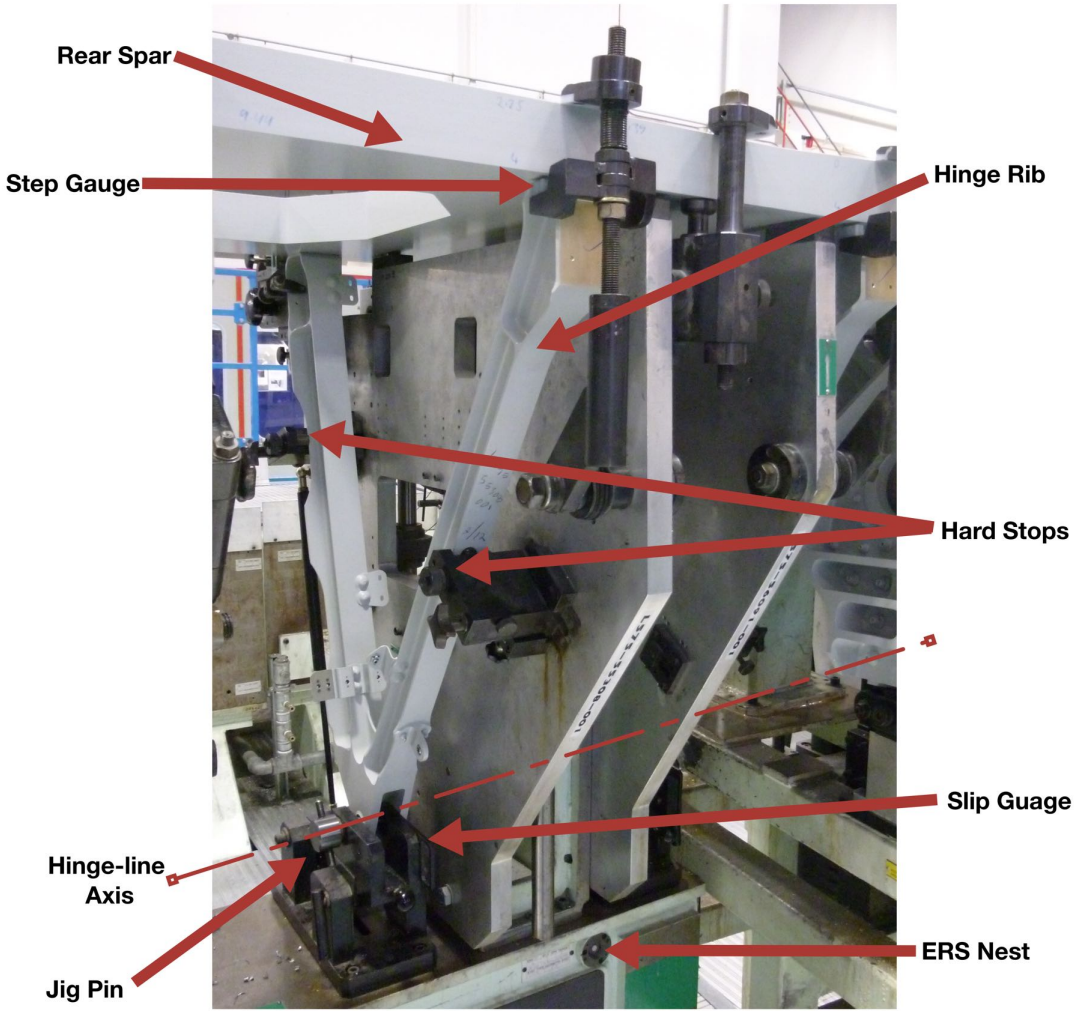


Figure 3-3: A380 hinge bracket overview

The hinge line is constrained from the hinge bore with a pin controlling co-axiality (constraining: $Y$, $Z$, $R_Z$ and $R_Y$). In turn, this is then tightened back against a gauge plate and a slip gauge (constraining: $X$), to ensure the hinge brackets' normality to the hinge line; this process requires experience and judgement which is likely to vary from operator to operator.

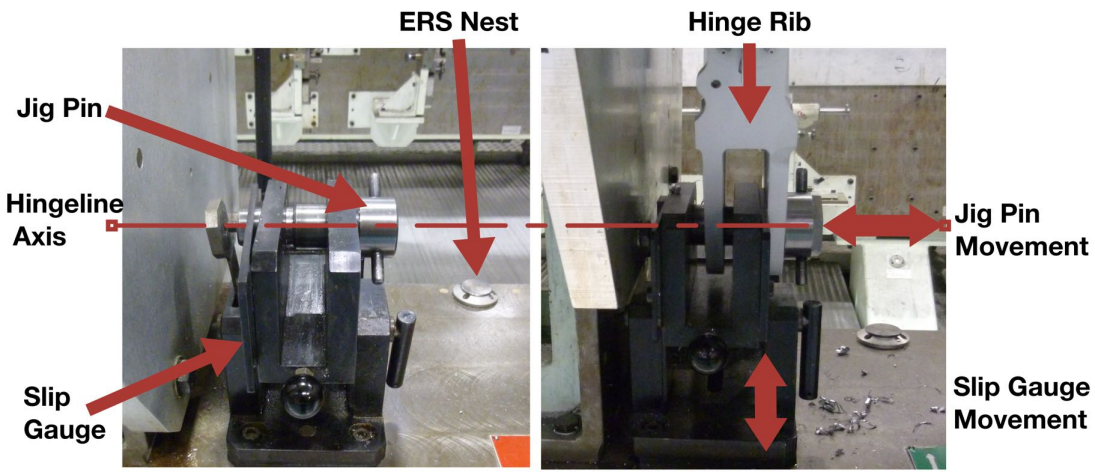


Figure 3-4: A380 hinge-line setting/check

The pin and slip gauge are also used for checking the conformance of the sub-assembly in the fixture: the assembly is 'correct' if the pin can be rotated and the slip gauge (nominally 7.8mm) can move freely *post-assembly* (Figure 3-4). Again, these checks use operator experience and judgement, and are subsequently subjective and time consuming.

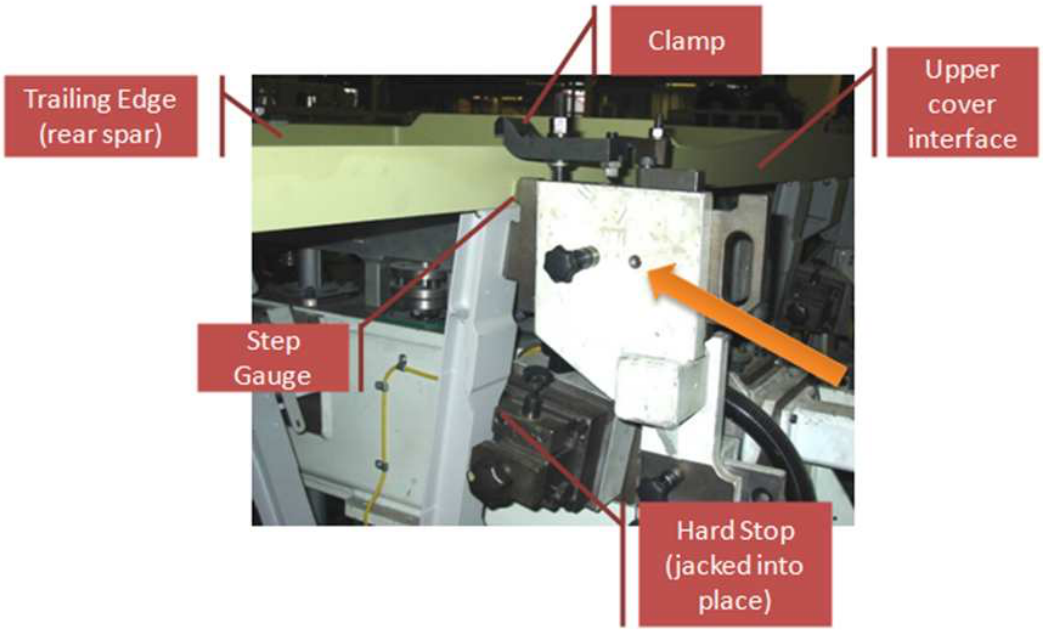


Figure 3-5: A380 step condition

Figure 3-5 examines the second ICY requirement: the step condition between hinge bracket and rear spar upper cover interface. This step condition is satisfied by using a step gauge to align the interface within a tolerance of 150 µm (*pre-assembly*), the top of the rear spar is then clamped and hard stops are jacked onto the hinge bracket (constraining: $R_X$). The upper cover step is of particular importance as it determines the upper cover profile, and therefore aero-efficiency.

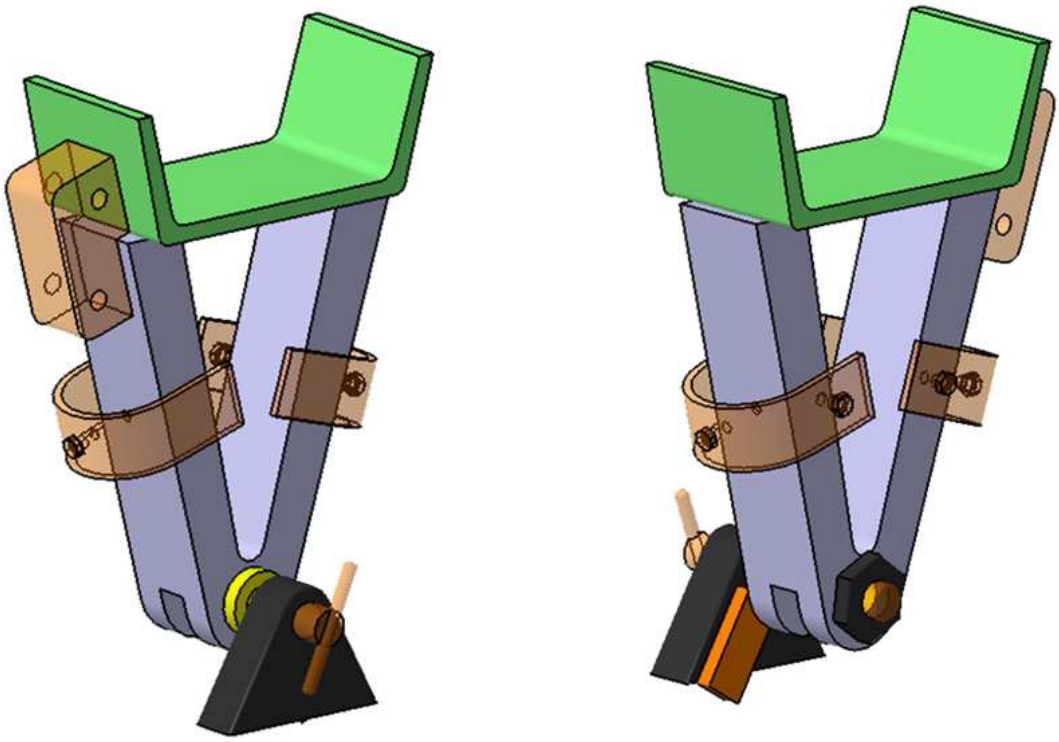

Figure 3-6: Hinge bracket simplified geometry

Figure 3-6 is representative of the tooling used in the A380 Trailing Edge sub-assembly; this simplified geometry allows clear identification of the tooling constraints. Figure 3-7 indicates how the tooling controls the component placement and constrains the assembly.

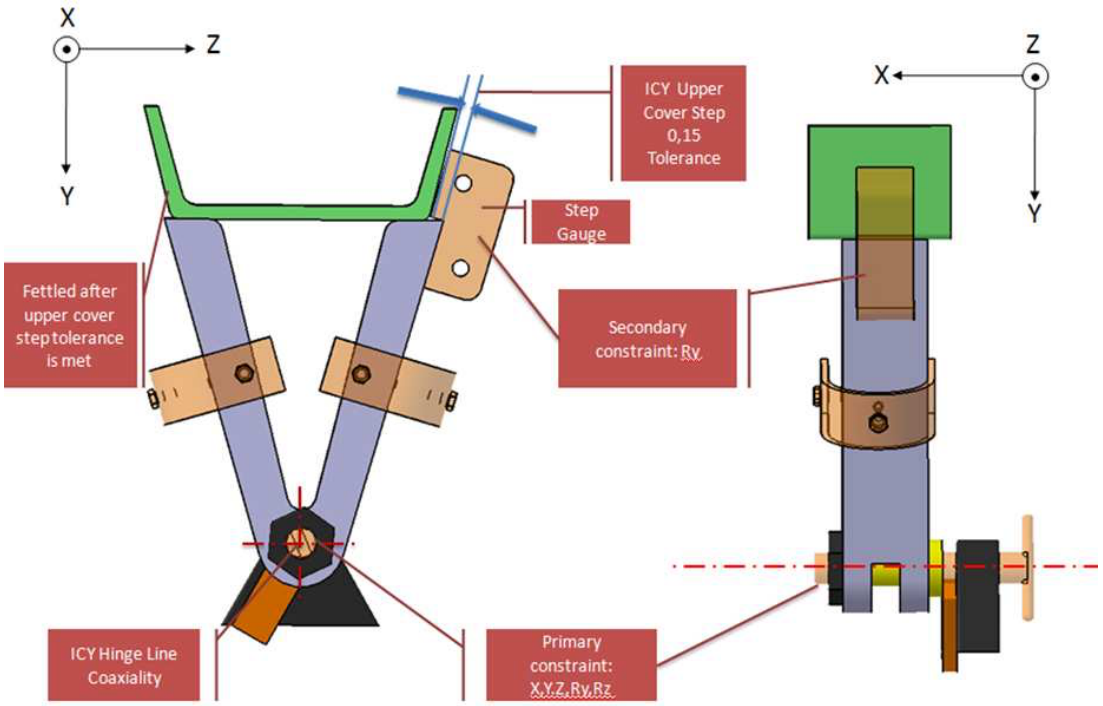


Figure 3-7: Simplified tooling constraints

### 3.2.2 Gear Rib Setting

The gear rib has complex KC and ICY requirements, and related geometry. Figure 3-8 identifies the key features of the gear rib tooling; two of the KCs: Point A (centre point of the spherical bearing) and Point B (centre point of the internal bore) are in free space, and create the ICY Axis for the Pintle. The second ICY is the aft flange of the gear rib that interfaces with the Shroud Box, a KC tooling hole is held with a hard stop, wound into the nominal position and subsequently pinned.

The simplified geometry in Figure 3-9 and Figure 3-10 identifies the tooling that controls the gear rib during assembly. This begins with the spherical bearing being assembled before the Spar is placed in the assembly; subsequently the gear rib is constrained with the tooling Pintle, this orientates the spherical bearing (KC Point A) with the Hinge Bore (KC Point B). The hinge bore has a tight tolerance bush, to avoid damaging this bush an additional tooling bush is installed; damage can occur when the tooling Pintle is installed and removed via actuators. The control of these two KCs ensures the ICY of the Pintle Axis (constraining: $X$, $Z$ and $R_X$). The Shroud Box

interface flange is clamped against hard stops (constraining: $R_Y$). Lastly, the Pintle-Axis rotation is constrained with a hard stop wound and pinned into a tooling hole on the gear rib shoulder (constraining: $R_Y$ and $Y$).

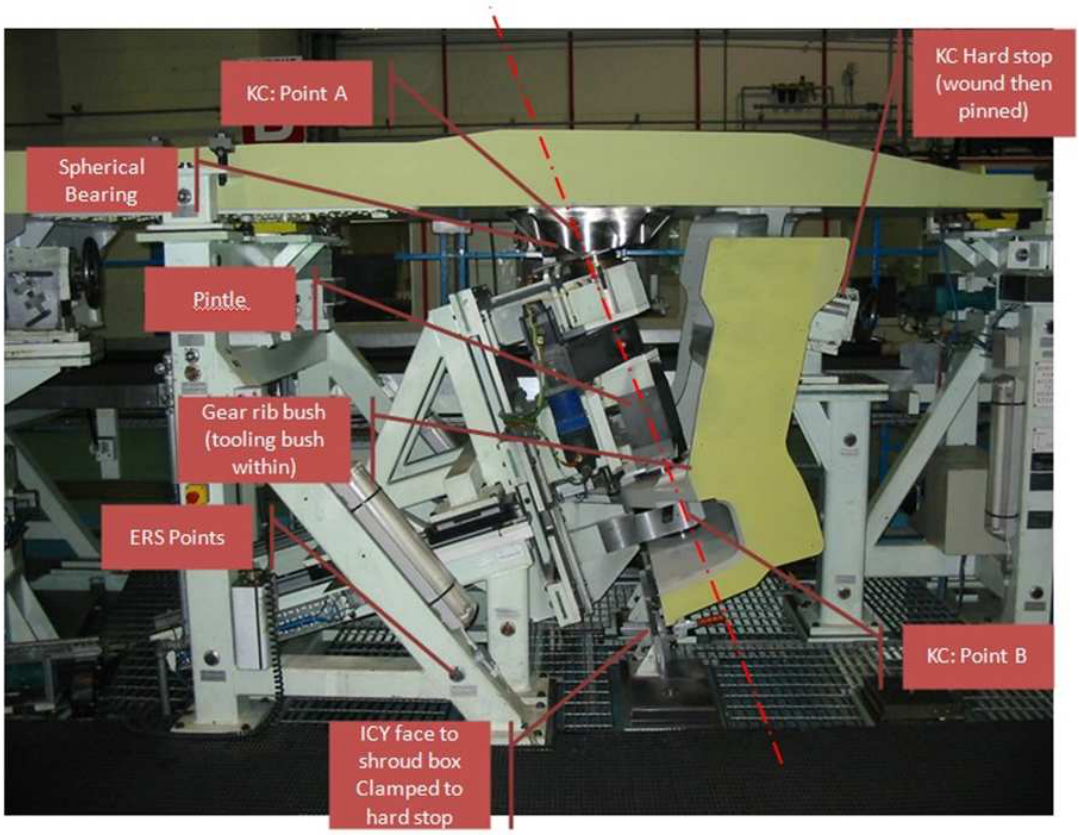


Figure 3-8: A380 gear rib, spar and assembly tooling

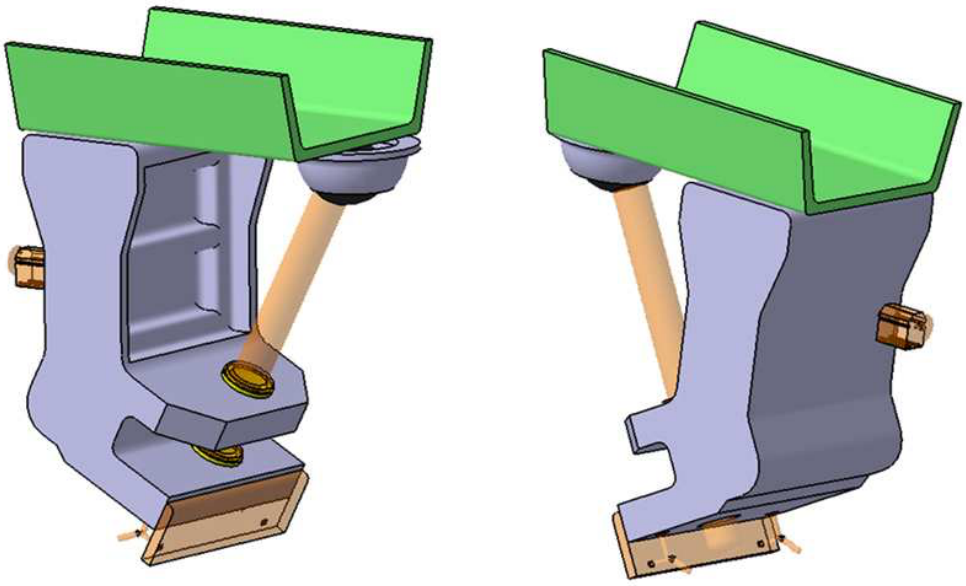

Figure 3-9: Gear rib simplified geometry

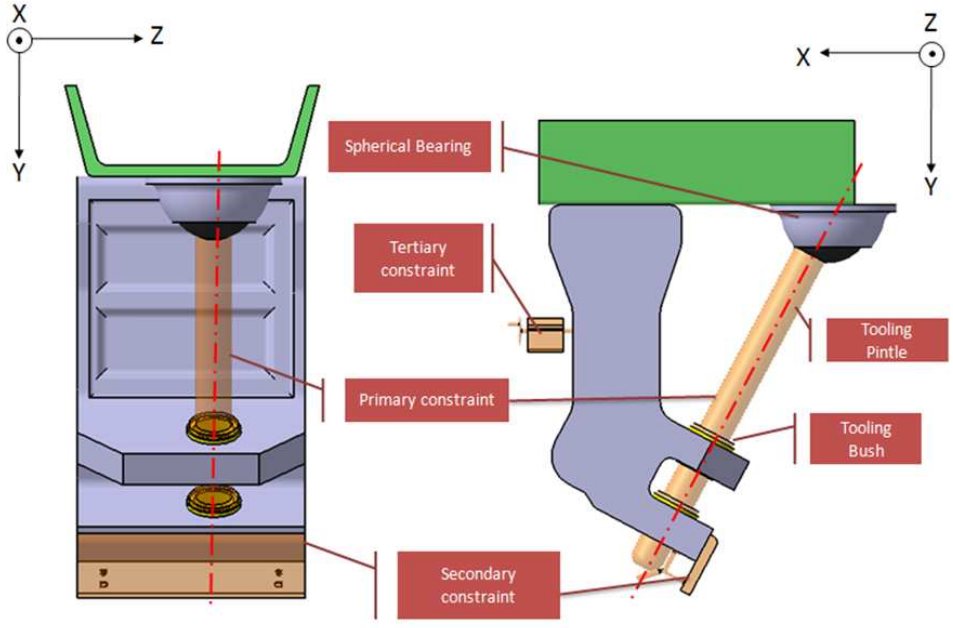


Figure 3-10: Simplified tooling constraints

Conformance of the Pintle Axis is checked with slip gauges, identified in Figure 3-11, this is a manual operation, hence time-consuming and subjective.

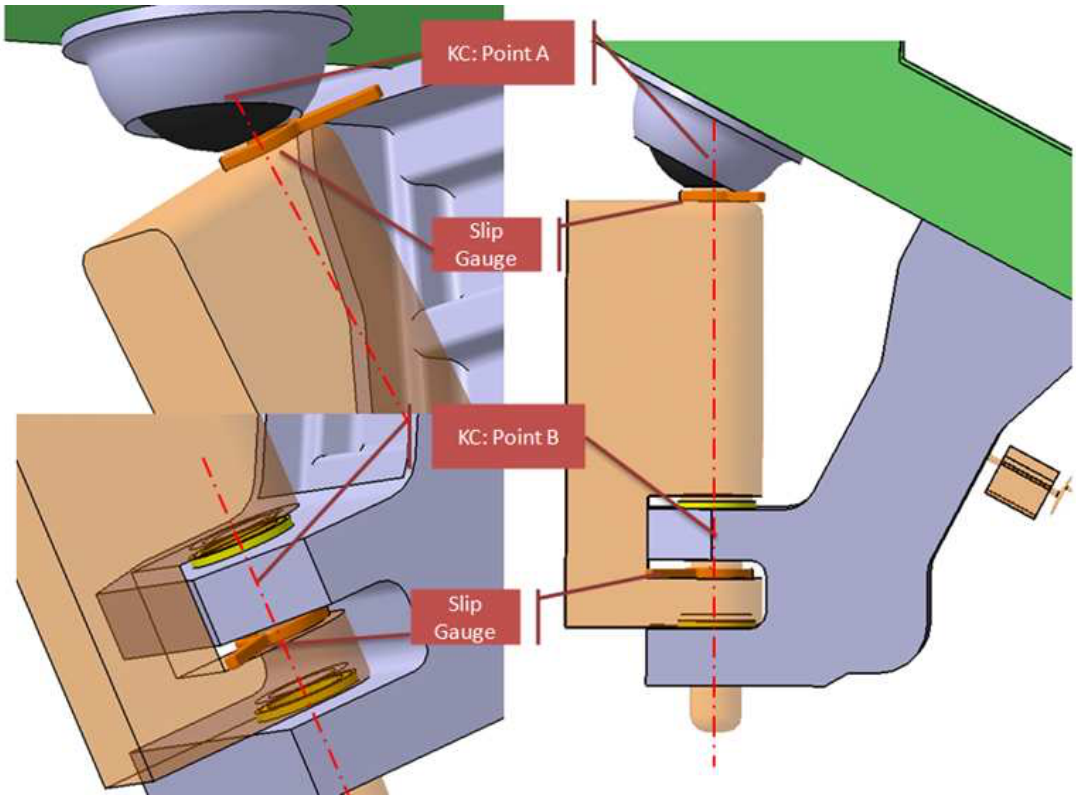


Figure 3-11: Slip gauges in gear rib tooling

### 3.2.3 Rear Spar Setting

The rear spar on the A380 is set after the gear rib, side stay (not shown) and hinge brackets are nominally positioned, the spar sits on these components and is located by the gear rib (in the X). The degrees of freedom (DOF) of the spar: $X, Y, R_x, R_y$ and $R_z$ are consequently arrested. $R_y$ is further constrained against two hard stops at each end (Figure 3-2); this essentially constrains $Z$ displacement. $Z$ displacement is further controlled by the hinge brackets' hard stops. The spar is a long and thin component, hence a large potential for deformation is present during assembly. The rear spar bends and twists, following the interfaces of the components it sits on as these components' KC and ICY requirements dominate the build sequence.

## 3.3 Recertification

Jig and fixture commissioning - building and setting - is a time consuming process. In order to avoid subsequent re-setting operations the tools have sufficient stability to be checked periodically. This periodic check is known as *Recertification*. The assumption that the tooling is stable and as a result accurately positioned may be a source of error since the fixture is only re-certified once every three years. In general the recertification process:

- Takes place once every three years on a typical, monolithic fixture
- Usually takes weeks depending on the amount of re-work required
- Re-work is expensive both in terms of expertise and (more importantly) the expense of taking the fixture out of production for a substantial time.

The time consumed to re-certify a fixture will become even more paramount as production rates are likely to increase in the future. The current recertification process (Figure 3-12) inspects several different points of interest highlighted on a *Sheet 800*. A Sheet 800 documents and describes the following:

- Reference Points (RP): are the primary tool datum. RPs are machined tooling holes on the main structure of the tooling with known co-ordinate definitions relative to the tooling and wing co-ordinate frames.
- Enhanced Reference System (ERS): this is an extended reference system from the co-ordinate definition of the tooling reference points. The ERS points are arbitrarily placed SMR nests around the tooling, this decreases line of sight issues when measuring the RPs alone.
- Optical Tooling Points (OTP): these are theoretical points used in the definition of critical tooling detail relative to the RPs/ERS points. Typically the OTPs are in free space (taking into account the SMR and facility tooling offsets) close to where the tool interfaces with components. The OTPs are used to ensure the flags and pick-ups are correctly positioned.

The initial stage of the recertification process is to prepare the tool: add vector bars, sine bars, uncover nests, place targets, remove panels for line of sight and other auxiliary tooling/processes used for the recertification; this stage in itself is time consuming and potentially hazardous, as personnel need to work at height and in confined areas.

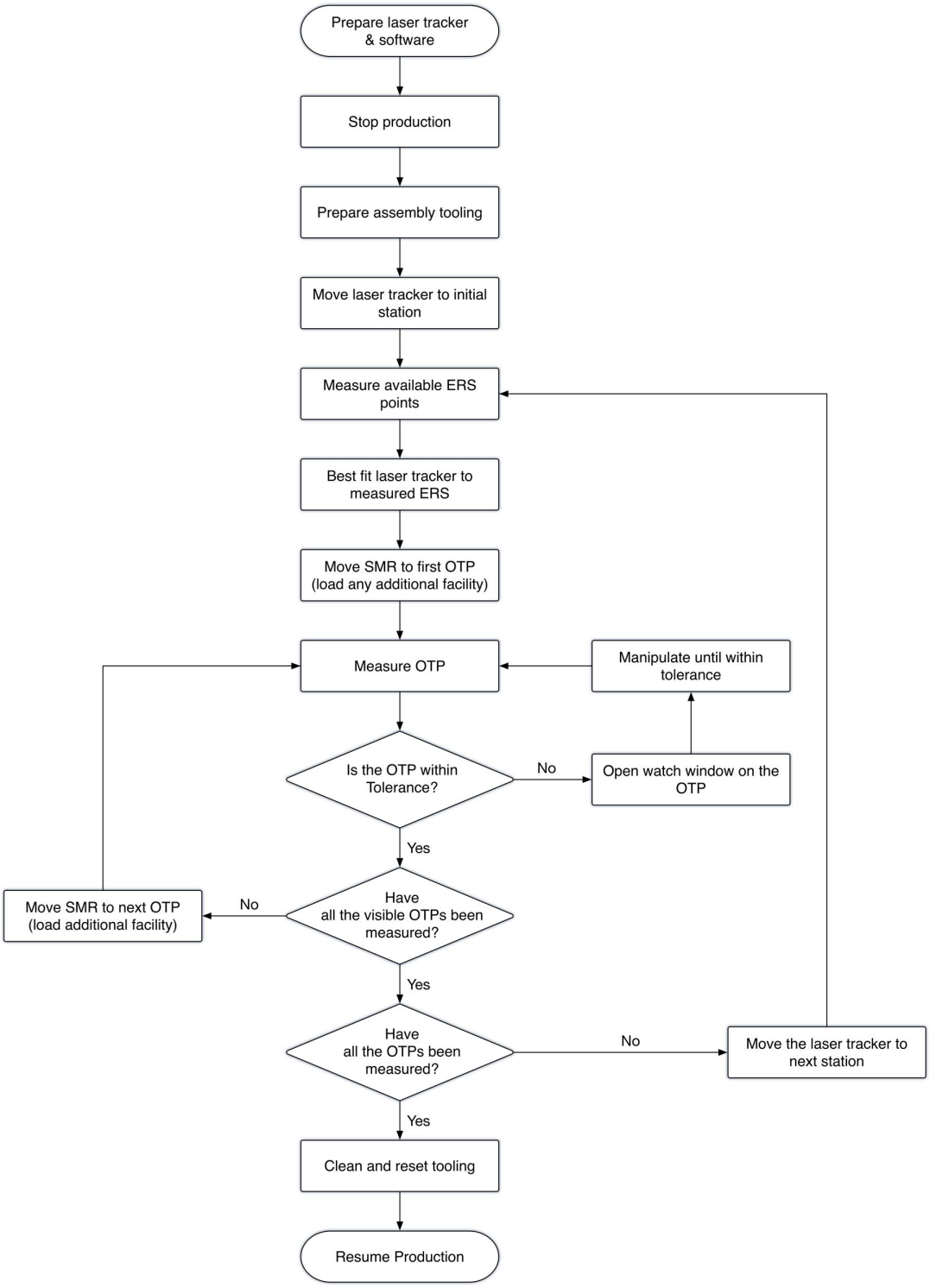


Figure 3-12: The current manual recertification process

The commissioning of the fixture uses a laser tracker network to reduce line-of-sight issues and reduce the measurement uncertainty; this is essential as the volume of measurement is large and the environment unstable and so accuracy needs to be as high as practically possible. The software used for this measurement is SpatialAnalyzer (SA), within which the Unified Spatial Metrology Network (USMN) function is used to create an optimised composite point group. USMN is achieved by using the information from each measurement station and the associated components of uncertainty for each point; the USMN algorithm computes the optimum positions for each point - that is, the position with the least associated uncertainty. The position of each point within the composite group is fed into the Sheet 800 for future reference and use.

Subsequent recertification of the fixture involves using a laser tracker taking measurements of the OTPs, as these are the work holding interfaces; a various number of stations are necessary as not all OTPs can be seen from one station. The ERS are also measured to establish the coordinate frame, and locate the instrument; the measured OTP information is checked against the original USMN/ Sheet 800 data. If the OTPs are within tolerance then the fixture can return to production; otherwise re-work is required. Re-work involves rectifying the out of specification points - this utilises the dynamic measurement capability of the laser tracker to watch points in real-time: enabling the user to move the out of specification point into the correct position whilst receiving metrological feedback. Once all the points are within tolerance of the nominal point positions the tool can return to production.

## 3.4 Airbus Future Requirements

The future requirements of Airbus provides additional direction to ongoing research areas, as well as expanding the envelope of the accepted academic/industrial knowledge. As a business Airbus focusses on manufacturing efficiency (reduction in cost to Airbus), meeting customer demand, higher manufacturing quality to achieve fuel efficiency targets (reduction in cost to Customer), as well as legislative pollution targets.

### 3.4.1 Increased Production Rates

An increased production rate indicates that the assembly process is going to have to accelerate as well as an increase in facility size. To increase the speed of production, either: a much increased workforce is required or more automation and less manual

checks are going to have to be introduced. Additionally, this large increase in production rate means that the time margins for concession rework becomes narrower than currently available. Embedding metrology within the tooling environment could enable an increase production rate in the following ways:

- Reduce manual metrology checks
- Enable greater automation
- More robust component placement
- Detect concessions earlier
- Reduce/eradicate recertification times
- Increase in SPC data collection

### 3.4.2 Reduced Ramp-Up Time

A subsequent requirement of the increase in production rate is a reduction in the ramp-up time. The ramp-up time relates to the time from beginning production of a new Wing-box (or product variant) to the point where full production rate is achieved. Essentially this ramp-up time is the learning curve for assembling a new product, resolving any issues that may arise during the production process. Employing a greater metrology presence within the tooling could reduce the ramp-up time by:

- Ensuring component/sub-assembly placement is correct
- Enable automation
- Reduce tooling reliance
- Detect assembly error
- Increase in SPC data collection

### 3.4.3 Reduce Jig Recertification Time

As production rates increase, the impact of taking tooling out of use for recertification will increase. One solution would be to build a parallel set of tooling to move the

assemblies to when the other fixtures are being certified, however this is excessively expensive. Embedding metrology into the fixtures could provide a monitoring or checking system that could reduce recertification times, or in the case of a monitoring system: eradicate the need for recertification altogether. Additionally this would provide an increase in SPC data collection.

## 3.5 Review Summary

It is important to recognise the purpose of tooling and not be distracted by the tooling itself; when examining part and assembly verification we are interested in the workpiece being 'correct' not the tooling. Such a heavy emphasis on the tooling is a result of difficult-to-measure component features; hence the tooling determines the position of KCs and ICY from a secondary measurement; measurement of the tooling and not the sub-assembly/assembly. Manual operations rely heavily on judgement and specialist training; inherently these methods introduce a potential for human error and an increased measurement uncertainty. It is important to recognise that here the tooling serves as a quality control method; it holds build tolerances and is used to check the assembly is correct, from which, Statistical Process Control (SPC) data can be extracted.

Aerospace fixtures have broadly two metrology requirements: 1) fixture setting and recertification and 2) assembly conformance, where the success of 2) is largely dependant on task 1). Measurement systems employed for both these must have a low uncertainty of measurement to ensure build tolerances are maintained. Section (2.2) illustrates that the state of the art LVM is capable of satisfying the uncertainty requirements, but at a significant financial cost. Laser trackers are employed throughout the current Wing-box assembly; largely used for fixture certifications and to a lesser extent assembly operations, the laser tracker's low uncertainty of measurement, large working volume, speed of measurement and dynamic tracking are favourable as well as its established industrial exposure.

Extensive use of the laser tracker is not without limitations as the recertification tasks typically take weeks (Tomlinson and Singh, 2008); the main reasons for this are: the tracker can only measure one point at a time, the target has to be moved to each point of interest manually, the system has to be multi-hopped to avoid line-of-sight issues and additional facility tooling for targeting (e.g. sine & vector bars) is required. The recertification process has requirements that make other systems unsuitable, such

as dynamic tracking for watching pick-ups back to their nominal positions. Consequently, the Laser radar and single roving camera photogrammetry systems are not suitable; iGPS can track points, but the high uncertainty voids its use for fixture rework. Dual photogrammetry systems are capable of the requirements but have not been introduced due to their lack of exposure in this application, and their expense.

The assembly process uses mechanical metrology to ensure the components are both positioned and assembled correctly. This uses operators' judgement and experience, ultimately this is a subjective process. Laser trackers are occasionally used to check features and watch components into their CAD nominal positions. Technology is readily available that can be deployed to aid these measurement processes, increasing measurement repeatability and confidence in the measurement processes. However, these are often expensive solutions and still rely on some level of pre-setting and calibration.

Additionally, it is worth noting that suppliers of components are likely to use different fixturing methods and configurations than Airbus, holding and controlling differing features; this can create residual stresses that can cause distortions and hence non-conformance on jig releases. For example if co-axiality is forced on the hinge line, then on removal from the tooling the sub-assembly's hinge line will spring to a position of least stress - creating difficulties at the next assembly stage.

# Chapter 4

# Metrology Enhanced Tooling for Aerospace (META) Framework

## 4.1 Introduction

The Metrology Enhanced Tooling for Aerospace (META) Framework has been developed through this research as a template for the deployment of Metrology Enabled Tooling for the Assembly of Aero-Structures. This chapter presents the META framework, subsequently the following chapters examine elements of the framework through research activities, bench-level and industrial trials.

The literature review (Chapter 2) indicated that the key requirement for large-scale assembly is to overcome the constraints associated with the physical size of products and assemblies and the corresponding dimensional and form tolerances ((Maropoulos et al., 2008)). Firmly embedded metrology systems within the manufacturing processes are still not a reality as most systems are extrinsic of the tooling, and not embedded within it. To place metrology systems within the control loop of a manufacturing cell prerequisites such as: autonomous operation, high reliability, high speed measurement, and flexibility are paramount (Gooch, 1998). This exploitation of technologies is stifled due to the lack of integration with core design and assembly processes. The META framework addresses this gap as an integrated approach towards metrology and aerospace Wing-box assembly tooling, to further Metrology Assisted Assembly (MAA).

From the review of industrial practices within aircraft Wing-box assembly tooling (Chapter 3), it is evident that advances in large volume metrology and tooling

are increasingly important in order to achieve the future manufacturing requirements. Broadly, the three key industrial requirements highlighted: 1) increased production rates, 2) reduced Ramp-up and 3) reduction of jig recertification; can all be achieved or supported through increased use of large volume metrology.

The META Framework aims to address the industrial needs:

- Reduce manual metrology checks & reduce tooling reliance
- Enable greater automation
- More robust component placement & detect assembly error
- Detect concessions earlier
- Reduce/irradiate recertification times
- Increase in SPC data collection

The above academic and industrial gaps can be bridged through the development of metrology enhanced tooling. In turn, metrology enhanced tooling relies on the effective synergy of complimentary interfaces accommodated by a strong software platform. These hybrid systems could utilise many metrology technologies, for example: a macro co-ordinate system could be set-up using photogrammetry or a network of lasers; this would effectively surround and monitor key characteristics of the tooling. Localised metrology would sit within this larger metrological environment - laser radar, PCMMs, actuators, sensors, arms, scanners, etc - providing fine measurement of difficult features, freeform surfaces, tooling pick-ups, part location and verification. This environment could potentially provide the prerequisite of any automation attempt, determining the sources and magnitude of any dimensional variations of the components that are currently being experienced during the manual assembly stage (Saadat and Cretin, 2002). Webb et al. (2009) suggest the integration of multiple metrology systems for metrology assisted assembly by employing a de-centralised service-oriented software architecture.

## 4.2 Functional Requirements

The META Framework has three functional requirements:

1. *primary* functions: checking the positions of the tooling, components and assemblies,
2. *secondary* functions: aiming to enhance the assembly process directly; and,
3. *tertiary* functions: collection of data for future learning, statistical analysis and documentation.

These function sets are detailed in Figure 4-1.

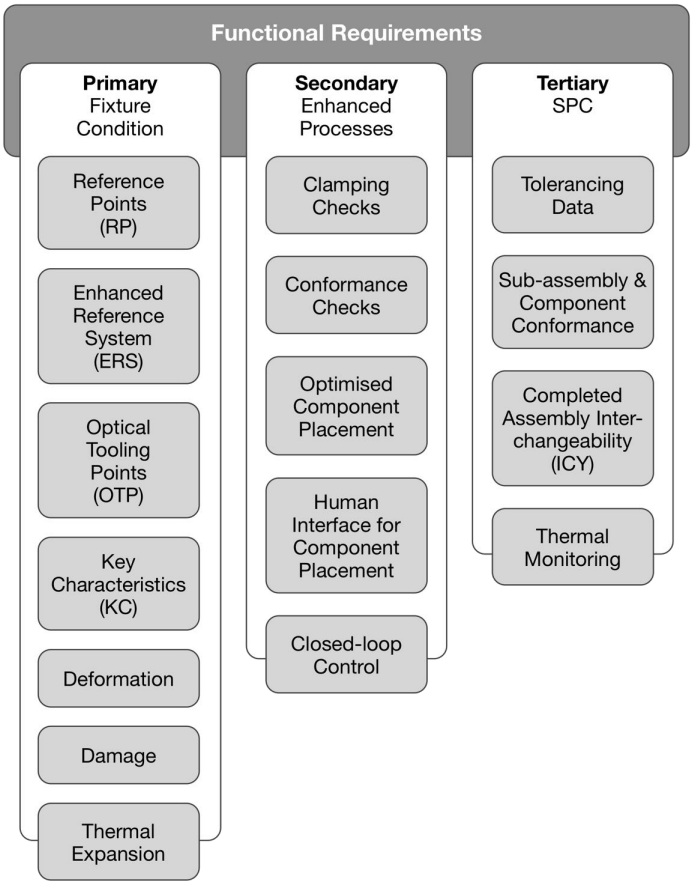


Figure 4-1: Functions of the META framework

The META frameworks primary functions require a periodic metrology system to monitor the key characteristics of the tooling and assembly which are in an essentially

static configuration. This monitoring eliminates the need to re-certify fixtures periodically, removing the need to take the fixture out of production. Current practice can take weeks to re-certify and re-work a fixture, causing down-time that will have increasing impact as production rates increase.

Automated control of tooling (Section 7) does not require real-time feedback as the movements can be iterative, unlike a material removal operation. Machining operations and automation where an iterative loop is not appropriate must have direct closed loop feedback from the instrument (for example a laser tracker) and not through the core software; as any latency in the feedback/control loop could produce a concession at best, and a scrap part/assembly at worst.

The tertiary function is to enable the collection of manufacturing data and information. This information could not only enhance the tooling and assembly during operation - informing downstream manufacturing and assembly operations (data-driven manufacture), but also begin a large scale data collection for the use of Statistical Process Control (SPC), providing learning for future optimisation of the assembly processes. SPC is particularly relevant as the manufacturing rates increase, helping to produce process capability charts and increase process confidence, and reducing non-value adding conformance checks.

## 4.3 META Framework

The META framework (Figure 8-1) illustrates the effective synergy of complimentary instruments. The framework manages interfaces from multiple instruments, analyses the data and responds accordingly.

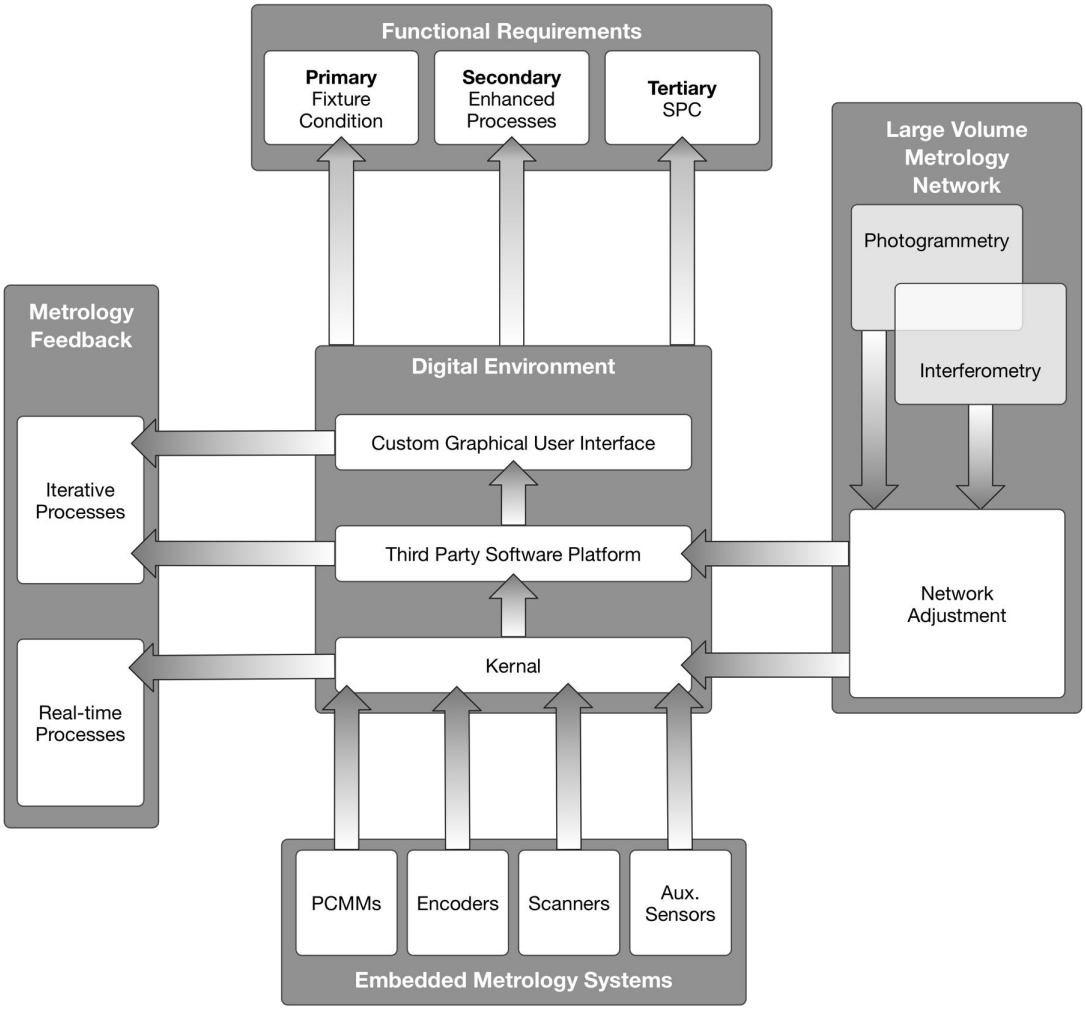


Figure 4-2: META framework

Examining each element set of the framework in turn:

**Digital Environment:** This includes: 1) the Graphical User Interface (GUI); a 2) Third Party Software Platform: and the 3) Kernal.

The *Graphical User Interface* (GUI) presents a simplified front-end of the software. Current practice engages specialist metrology and tooling engineers for many of the operations/functions that the META framework addresses; a simplified software interface with minimal user input would reduce the need for specialists and enable factory operators to carry out the operations.The GUI is built in a standard Microsoft Windows programming language such as Visual C Sharp

(VC#), Visual C++ (VC++) or Visual Basic (VB). This would allow calculations to be carried out within the coded GUI, with the added ability to utilise Software Developers Kits (SDKs) from manufacturers and software vendors, that is: a *Third Party Software Platform*. Subsequently, the GUI front-end could use all the power of the native programming language as well as using metrology platforms such as SpatialAnalyzer to add flexibility for completing more complex operations or provide continuity with the metrology engineers and organisational standards. Lastly the *Kernal* is included for completeness as direct communication between hardware may be required for real-time positioning processes, see: Metrology Feedback below.

**Functional Requirements:** these are described above in Section 4.2.

**Metrology Feedback:** is dependent on the required response time of the operation. For example, a material removal operation requires real-time feedback, here it is necessary to interface directly with the instrument/kernel. However near real-time feedback operations, such as human manipulation of components/flags/pick-ups or non-time critical automation (such as that presented in Chapter 7) can have metrological feedback via the integration software/GUI, where latency is acceptable.

**Embedded Metrology Systems:** are located globally via the Large Scale Measurement Network. The local metrology systems include instruments (laser trackers, PCMMs, Scanners) and sensors (temperature, strain, linear displacement, encoders, etc.) to provide greater data fidelity where required within the tooling/assembly environment. This could be to check specific features (such as steps or gaps), collect environmental data (temperature), or drive automation (laser tracker, bore-alignment), etc. (Chapters 6 & 7).

**Large Volume Metrology Network:** current LVM technology (Section 2.2) does not present a cost-effective, highly accurate large volume metrology monitoring environment. In the absence of a real-time, highly accurate, ubiquitous LVM system; the large scale metrology network is likely to be configured as described in *Large Volume Multi-Instrument Networks* (Section 5.3) or an automated periodic measurement as outlined in *Automated Measurement of Aircraft Wing-box Assembly Tooling* (Section 5.4). Both methods use laser tracker measurements (interferometry) to give scale to the photogrammetric bundle adjustment.

## 4.4 Chapter Summary

The Metrology Enhanced Tooling for Aerospace (META) framework presents a generic map for the interaction of metrology within the tooling environment. The interaction path is dependent on the desired functional output.

The elements of the framework can be tested in isolation. These discrete elements provide interim solutions that can readily be applied to existing and future aerospace assembly tooling. Chapters 5, 6 & 7, examine elements of the framework through research activities, bench-level and industrial trials illustrated in Figure 4-3.

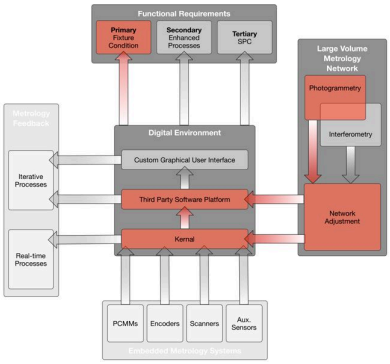


**Chapter 5:**
5.2: Photogrammetry & Laser Tracker Performance Testing

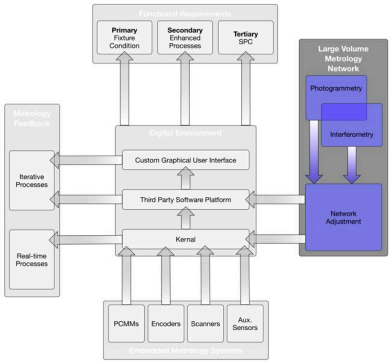


**Chapter 5**
5.3: Large Volume Multi-Instrument Networks

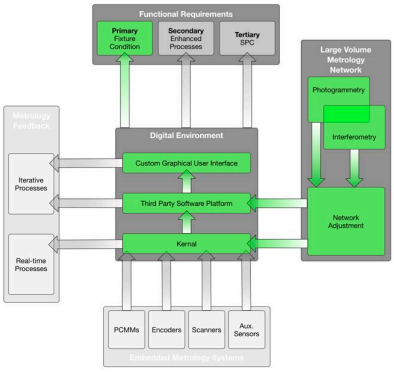


**Chapter 5:**
5.4: Automated Measurement of Aircraft Wingbox Assembly Tooling

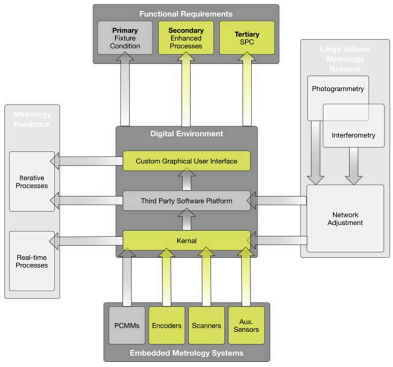


**Chapter 6:**
Embedded Metrology Systems

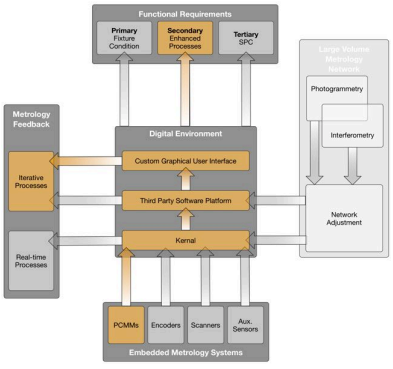


**Chapter 7:**
Metrology Feedback

Figure 4-3: The elements of the META framework utilised in each chapter

# Chapter 5

# Large Volume Metrology Network

## 5.1 Introduction

The research presented in this chapter will establish a method for the measurement of fixture condition: identified as the primary function of the META Framework. This is presented in three sections:

**Section 5.2:** *Photogrammetry & Laser Tracker Performance Testing*, examines the suitability of photogrammetry as an alternative metrology instrument for the measurement of assembly tooling structures.

**Section 5.3:** *Large Volume Multi-Instrument Networks*, determines the associated uncertainty considerations for laser tracker and photogrammetry systems being used as complementary technologies for large volume measurements.

**Section 5.4:** *Automated Measurement of Aircraft Wing-box Assembly Tooling*, details a process for the measurement of fixture condition employing the outcomes from the previous sections.

## 5.2 Photogrammetry & Laser Tracker Performance Testing

The META framework requires large volume metrology networks for achieving the functional requirements, particularly the primary function: the verification of fixture condition. This section is an assessment of the suitability of photogrammetry as an alternative technology for the measurement of fixture condition (see Figure 5-1).

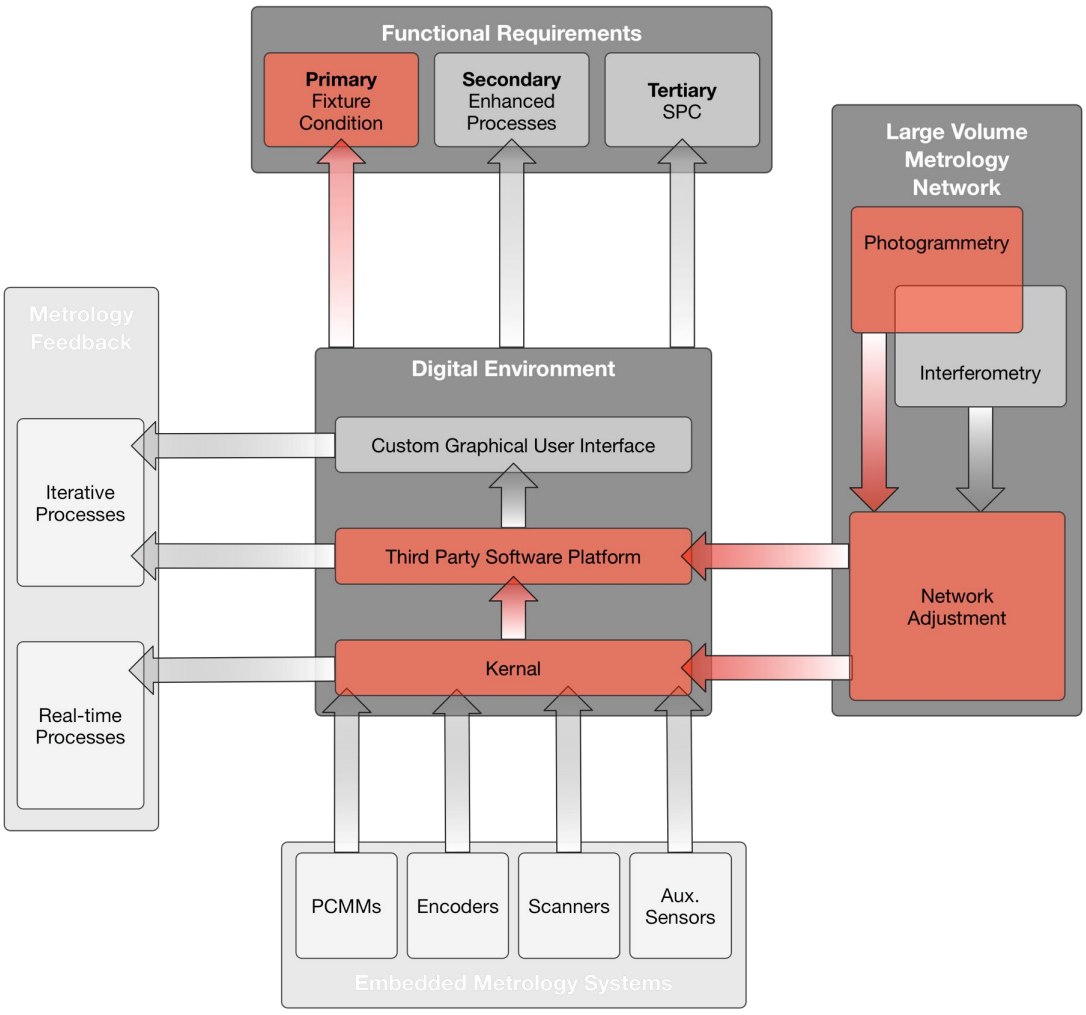


Figure 5-1: META framework elements explored in this section

At present, high accuracy measurement within large scales aerospace assembly tool-

ing is dominated by laser tracker technologies (Peggs et al., 2009), often networked data sets are used to reduce measurement uncertainty. The aerospace sector utilises laser tracker systems for the assembly tool setting and conformance tasks required for wing-level manufacture (Chapter 3). In part, this is due to the dynamic measurement capability of laser trackers. However, many static point measurements are required in these tooling conformance applications and from the literature review (Chapter 2.2), photogrammetry systems could provide an attractive alternative, as they have the following advantages:

- Simultaneous multiple-target measurement,
- Quick measurement time,
- Lower operator skill level,
- Inexpensive measurement targets.

These benefits are offset by the systems' accuracy and cost. The cost is comparable to laser trackers, however, the accuracy is invariably considered to be not as good as laser trackers, even though in certain operating environments comparable accuracy levels are attained. As computational costs reduce, and readily available digital cameras rise in standard - in terms of mechanical construction, sensors and lenses - photogrammetry could provide a far more cost effective alternative to laser tracker measurement systems. This section compares the capability of two imaging systems: 1) the V-STARS INCA3 from Geodetic Systems Inc. (GSI) and, 2) a Nikon D700 digital SLR fitted with a 28mm Nikkor lens and Vision Measurement Software (VMS). The V-STARS system is representative of a state of the art commercial photogrammetric system built around a custom designed imaging system and software, whereas the second system utilises an off-the-shelf 12MP digital camera and lens in combination with research based photogrammetric software; costing an order of magnitude less than the commercial system.

Manufacturers state an instrument's performance in terms of measurement uncertainty, however this is often assessed and determined in a controlled environment and not an industrial setting; consequently, an independent verification of a measurement system's capability in an environment similar to that of the intended application environment is required to achieve confidence in an instrument's performance; especially for tolerance critical operations, such as those found in aerospace.

### 5.2.1 Methodology

The evaluation will determine the measurement uncertainty of static measurements in an environment and volume similar to the intended industrial application, that is, the conformance measurement of wing-level tooling structures within aircraft manufacture.

The evaluation is considered in two parts:

1. *Co-ordinate Measurement Evaluation*: A reference network of discrete points will be established with an accurately determined co-ordinate definition. In turn, the photogrammetry systems will re-measure the reference network. The measurement uncertainty is determined by using a method of co-ordinate comparison; comparing the measured co-ordinates with a reference network with a quantified associated uncertainty (Muelaner et al., 2009; Hughes, Forbes, Sun, Maropoulos, Muelaner, Jamshidi and Wang, 2010). Subsequently the total uncertainty of measurement will be determined by constructing uncertainty budgets in accordance with the BSI standard: Guide To The Expression Of Uncertainty In Measurement (GUM) (BSI, 1995*b*).

   The discrete point measurement gives rise to an uncertainty estimation based in an environment similar to the industrial deployment; however it does not simulate the practical issues experienced when measuring wing-level assembly tooling.

2. *Tooling Point Measurement Evaluation*: To simulate the practical limitation experienced when measuring wing-level assembly tooling, the photogrammetry systems will measure a sub-set of Optical Tooling Points (OTPs) on a demonstration wing-box assembly fixture (two-thirds scale).

The result will inform the suitability of photogrammetry to measure within fixture geometries with an appropriate level of uncertainty.

### 5.2.2 Co-ordinate Measurement Evaluation

#### Establishing a Reference Network

The reference network is a constellation of 11 points within an approximate volume of 13.5m x 8m x 3m. Repeatable magnetic target nests are used to hold 1.5" targets such as SMRs, tooling balls or split bearings; this allows the same point in space to be measured by each instrument.

The repeatability of magnetic target holding nests was experimentally evaluated. The magnetic nest repeatability was determined by placing a tooling ball in the nest and measuring the runout in each axis with a digital dial indicator ten times for five different nests, this totalled a 150 runout measurements.

The tooling ball has a 3D co-ordinate variation ($Y_{x,y,z}$) that can be combined such that the 3D or spherical positional variation:

$$Y_{x,y,z} = \sqrt{x_r^2 + y_r^2 + z_r^2} \tag{5.1}$$

Where the axial components of uncertainty can be expressed as:

$$\begin{aligned} x_r &= i_c + i_r + t_t + x_c && (5.2)\\ y_r &= i_c + i_r + t_t + y_c && (5.3)\\ z_r &= i_c + i_r + t_t + z_c && (5.4)\\ & && (5.5) \end{aligned}$$

Where:

| | | |
|---|---|---|
| $x_r, y_r, z_r$ | = | Runout variance |
| $i_c$ | = | Instrument uncertainty from the calibration certificate, this is reported at 1.5 µm, with a 2 sigma coverages factor ($k = 2$). Hence can be treated as Type B and a normal distribution; the standard uncertainty ($u(i_c)$) is 0.75 µm |
| $i_r$ | = | Instrument's resolution or fidelity of measurement, the 0.5 µm 'rounding' error can be considered as having a rectangular distribution (equal probability) hence the standard uncertainty is $0.5/\sqrt{3} = 0.29$ µm |
| $t_t$ | = | Tooling ball sphericity manufacturing tolerance, 0.5 µm can be considered as having a rectangular distribution (equal probability) hence the standard uncertainty is $0.5/\sqrt{3} = 0.29$ µm |

$x_c, y_c, z_c$ = Measured centre offset, Type A uncertainty determined through multiple measurements

Generalising we have:

$$n_r = i_c + i_r + t_t + n_c \tag{5.6}$$

Where,

$n_r$ = Axis runout variance, Type A uncertainty determined through multiple measurements

$n_c$ = Cosine error attributable to the plunger alignment and deflection in each axis, defined as:

$$n_c = n_m(1 - cos\theta) \tag{5.7}$$

Where,

$n_m$ = Measured value

Such that:

$$n_r = i_c + i_r + t_t + n_m(1 - cos\theta) \tag{5.8}$$

$$n_c = n_m(1 - cos\theta) \tag{5.9}$$

The sensitivity coefficient is defined as:

$$c_i = \frac{\delta n_c}{\delta \theta} = n_m sin\theta \tag{5.10}$$

The measured values ($n_m$) of centring deviation have a zero mean. Substituting $n_m$ with the calculated RMS of the measured values: 2.23 µm gives an average stroke length experiences, and estimating a extreme worst-case plunger deflection of ±0.261 80 rad (i.e. at 3 sigma), gives a variance of 0.087 27 rad. Now:

$$c_i = 2.23sin(0.26180) = 0.577\mu m \text{ rad}^{-1} \tag{5.11}$$

The standard uncertainty is determined in Table 5.2.

| Standard uncertainty component $u(x_i)$ | Source $X_i$ | Value of standard uncertainty $u(x_i)$ | Sensitivity coefficient $c_i = \frac{\delta f}{\delta x_i}$ | $u_i(n) = \lvert c_i \rvert u(x_i)$ |
|---|---|---|---|---|
| $u(i_c)$ | Inst. Unc | 0.75 µm | 1.0 | 0.75 |
| $u(i_r)$ | Inst. Res | 0.29 µm | 1.0 | 0.29 |
| $u(t_t)$ | Tooling ball tol. | 0.29 µm | 1.0 | 0.29 |
| $u(n_c)$ | Cosine error | 0.087 27 | 0.577 | 0.05 |
| | | | | $u_c^2(n_r) = \Sigma u_i^2(n_r) = 0.73\,\mu\text{m}^2$ |
| | | | | $u_c(n_r) = 0.86\,\mu\text{m}$ |

Table 5.2: Uncertainty contributions for isolated axis measurement

3D co-ordinate variation ($Y_{x,y,z}$):

$$Y_{x,y,z} = \sqrt{x_r^2 + y_r^2 + z_r^2} \tag{5.12}$$

and the observed uncertainties in each axis are broadly equal, then

$$Y_{x,y,z} = \sqrt{3 \cdot n_r^2} = \sqrt{3} \cdot n_r \tag{5.13}$$

and the combined standard uncertainty for the position becomes:

$$u(Y_{x,y,z}) = \sqrt{3} \cdot u(n_r) = 1.48\mu m \tag{5.14}$$

The magnetic target nests uncertainty can subsequently be used as a component of the overall combined uncertainty of measurement for the reference network. The reference points are accurately measured using a Leica AT401 laser tracker. Each point is measured 10 times from different stations (Figure 5-2). The co-ordinate definitions from each measurement location are combined using a weighted least squares regression, with the intent to minimising the associated point uncertainty based on the instruments' uncertainty characteristics (Muelaner et al., 2010). The weighted network adjustment is in turn based on the three main components of the laser tracker uncertainty model (Section 2.4.2), that is, the two angular encoders and radial distance measurement. Subsequently the uncertainty associated with each point was computed via a Monte Carlo simulation. The constellation of points was computed with an average magnitude uncertainty of 11.8 µm at 1 $\sigma$ (a confidence interval of 68.26%). This analysis was carried out with SpatialAnalyzer software as the algorithms have been verified by the national measurement institutes NIST ((Shakarji, 2015)) and PTB ((Wendt and Gerwien, 2015)).

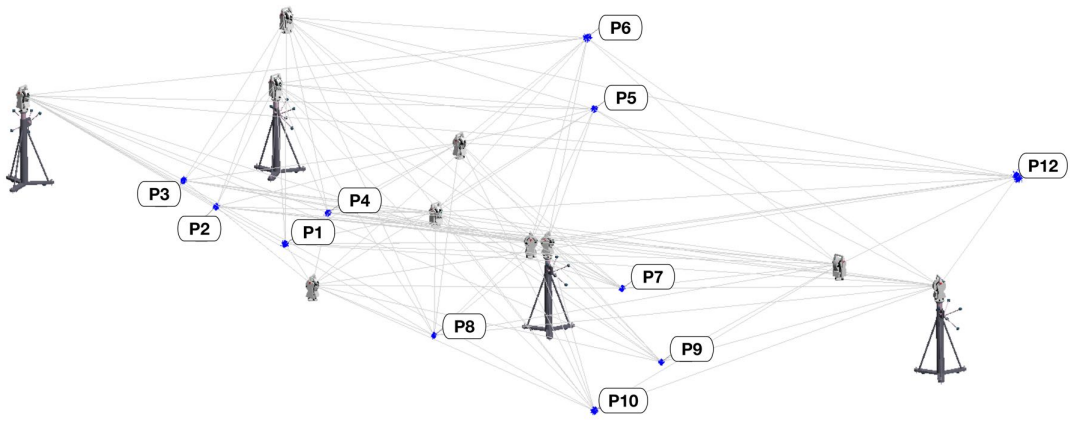


Figure 5-2: Graphic representation of the laser tracker measurement positions for the reference network

Measurement errors attributable to variations in the refractive index and temperature during the data acquisition has not been explicitly compensated in the network adjustment. As a result any errors arising from this will be seen in the network residuals and internal correlations between measurements and parameters. The computed uncertainty includes a number of uncertainty contributions, including the instrument

parameters in ranging and angular uncertainty, but also the uncertainty associated to the Spherically Mounted Retro-reflector (SMR) target and magnetic nests. These variations are implicit within network adjustment and subsequent Monte Carlo simulation-based uncertainty evaluation. However the number of measurement samples is limited, and therefore cannot be thought of as a robust characterisation of these components of uncertainty. As a consequence the SMR and magnetic nests have been explicitly included within the uncertainty budget (Table 5.3).

The co-ordinate definition ($n$) of the points in the reference network can be expressed as:

$$n = n_m + n_t + n_n \tag{5.15}$$

Where:

$n_m$ = This uncertainty source is an average of the uncertainty magnitudes associated to each of the points in the reference network. It has been determined using a Monte Carlo simulation approach on the adjusted network based on the two angular and ranging uncertainties of the laser tracker. This is a statistically determined variance and the standard uncertainty can be obtained by treating this as a normal distribution.

$n_t$ = The Spherically Mounted Retro-reflector (SMR) has a mechanical centring tolerance of 6 µm, with an equal probability applied to the tolerance band. Hence we can assume a rectangular distribution, and obtain the standard variance as such:

$$\frac{6}{\sqrt{3}} = 3.46\mu m \tag{5.16}$$

$n_n$ = The 1.5" magnetic nest allows repeatable placement of the SMR, the uncertainty source was experimentally determined (See Table 5.2)

| Standard uncertainty component<br><br>$u(x_i)$ | Source<br><br>$X_i$ | Value of standard uncertainty<br><br>$u(x_i)$ | Sensitivity coefficient<br><br>$c_i = \frac{\delta f}{\delta x_i}$ | $u_i(n) = \lvert c_i \rvert u(x_i)$ |
|---|---|---|---|---|
| $u(n_m)$ | Network measurement | 11.80 µm | 1.0 | 11.80 |
| $u(n_t)$ | Targeting manufacturing Tolerance | 3.46 µm | 1.0 | 3.46 |
| $u(n_n)$ | Nest manufacturing tolerance | 1.48 µm | 1.0 | 1.48 |
| | | | | $u_c^2(n) = \Sigma u_i^2(n) = 153.44\,\mu m^2$<br>$u_c(n) = 12.39\,\mu m$ |

Table 5.3: Uncertainty contributions for static reference network measurement

**Commercial Photogrammetric System Uncertainty Analysis**

There are three approaches to estimate the measurement uncertainty in this case, they are:

1. Pre-measurement: a system specification estimate: based on the manufacturers information and combining with the additional known sources of uncertainty.
2. Post-measurement: an estimate of the measurement uncertainty based on the instrument metrics and combining the additional known sources of uncertainty - without knowledge of the reference network
3. Post-measurement: an estimate of the measurement uncertainty based on knowledge of the reference network i.e. a co-ordinate comparison.

**System specification estimate**

The uncertainty of the photogrammetric measurement ($p$), from a pre-measurement perspective can be expressed as:

$$p = p_{spec} + p_t + n_n + p_{tp} \tag{5.17}$$

Where:

$p_{spec}$ = The V-STARS specification is given as: 5 µm+5 µm/m at 1 sigma, using the mean inter-point distance of 7.248 m, gives an average of 41.24 µm at 1σ.

$p_t$ = the retro-reflective 1.5" split bearings have a mechanical centring tolerance of 6 µm, with an equal probability applied to the tolerance band. Hence we can assume a rectangular distribution, and obtain the standard variance as such:

$$\frac{6}{\sqrt{3}} = 3.46\mu m \tag{5.18}$$

$p_{tp}$ = The constellation of measurements is scaled using a linear expansion model based on average readings from a temperature probe. This probe has a level of associated uncertainty (0.5 °C), which in turn has a dimensional impact on the co-ordinate definitions. The sensitivity co-efficient ($c_i$) is generically defined as:

$$c_i = \frac{\delta f}{\delta x_i} = \frac{\delta f}{\delta X_i}\bigg|_{X_1 = x_1 \ldots X_N = X_1} \approx \frac{\Delta f}{\Delta X_i} \tag{5.19}$$

hence, the linear expansion model given by:

$$\Delta L = \Delta T \alpha L \tag{5.20}$$

becomes,

$$\frac{\Delta L}{\Delta T} = \alpha L = c_i \tag{5.21}$$

Substituting the mean inter-point distance and a thermal co-efficient of expansion of concrete gives:

$$\begin{aligned} c_i &= 7.248362682m \times 9.9 \times 10^{-6^\circ}\mathrm{C}^{-1} && (5.22)\\ &= 81.89 \times 10^{-6} m^\circ\mathrm{C}^{-1} && (5.23)\\ &= 81.89 \mu m^\circ\mathrm{C}^{-1} && (5.24) \end{aligned}$$

The standard uncertainty is determined in Table 5.4.

| Standard uncertainty component<br>$u(x_i)$ | Source<br>$X_i$ | Value of standard uncertainty<br>$u(x_i)$ | Sensitivity coefficient<br>$c_i = \frac{\delta f}{\delta x_i}$ | $u_i(n) = \lvert c_i \rvert u(x_i)$ |
|---|---|---|---|---|
| $u(p_{spec})$ | V-STARS specified uncertainty | 41.24 µm | 1.0 | 41.24 |
| $u(p_t)$ | Targeting manufacturing Tolerance | 3.46 µm | 1.0 | 3.46 |
| $u(n_n)$ | Nest manufacturing tolerance | 1.48 µm | 1.0 | 1.48 |
| $u(p_{tp})$ | Temperature probe uncertainty | 0.5 °C | 81.89 µm/°C | 40.95 |
| | | | | $u_c^2(n) = \Sigma u_i^2(n) = 3391.41\,\mu\mathrm{m}^2$<br>$u_c(n) = 58.24\,\mu\mathrm{m}$ |

Table 5.4: Uncertainty contributions for pre-measurement estimate of V-STARS commercial photogrammetric system

**Post-measurement without knowledge of the reference network**

The reference network was re-measured using the V-STARS INCA3 camera (Figure 5-3), using additional scale bars to give independent scale for the bundle adjustment, without any knowledge of the reference networks co-ordinates. The V-STARS INCA3 is a purpose built metric camera with a 8MP CCD sensor, with a 21mm focal length, and a 77° x 56° field of view.

Figure 5-3: Graphic representation of the V-STARS INCA3 (blues cubes) measurement positions for the reference network

Here we quantify the measurement uncertainty as if we have no knowledge of the reference network. This replicates a typical photogrammetry measurement. The photogrammetry systems measurement of the reference network contains the following components of uncertainty such that:

$$p = p_{vb} + p_t + n_n + p_{tp} \tag{5.25}$$

Where:

$p_{vb}$ = This variance is an output from the V-STARS bundle adjustment algorithm and is a metric for the *quality* of the measurement. This is a root-mean square (RMS) value of the residual errors experienced when bundling the images together with the 1m scale bars as constraints.

Table 5.5 shows the combined the standard uncertainty:

| Standard uncertainty component $u(x_i)$ | Source $X_i$ | Value of standard uncertainty $u(x_i)$ | Sensitivity coefficient $c_i = \frac{\delta f}{\delta x_i}$ | $u_i(n) = \lvert c_i \rvert u(x_i)$ |
|---|---|---|---|---|
| $u(p_{vb})$ | V-STARS Bundle Adjustment RMS | 22.00 µm | 1.0 | 22.00 |
| $u(p_t)$ | Targeting manufacturing Tolerance | 3.46 µm | 1.0 | 3.46 |
| $u(n_n)$ | Nest manufacturing tolerance | 1.48 µm | 1.0 | 1.48 |
| $u(p_{tp})$ | Temperature probe uncertainty | 0.5 °C | 81.89 µm/°C | 40.95 |
| | | | | $u_c^2(n) = \Sigma u_i^2(n) = 2174.67\,\mu m^2$ |
| | | | | $u_c(n) = 46.63\,\mu m$ |

Table 5.5: Uncertainty contributions for post-measurement uncertainty estimate with knowledge of the reference network

**Post-measurement with knowledge of the reference network**

The uncertainty evaluation is based on a six degrees of freedom (6DOF) un-weighted least-squares regression; using the network of points from the laser tracker network as a reference and 'best-fitting' the constellation of points measured using the INCA3; Table 5.6 summarises the best-fit residual errors. Figure 5-4(a) shows the individual co-ordinate discrepancies in each axis, for each reference point. Figure 5-4(b) shows the magnitudes of the co-ordinate discrepancies and an indication of the levels of the overall 3D measurement uncertainty present. The magnitude of the standard deviation from this least-squares fit is 43 µm; the standard deviation is similar in each axis and shows a good 3D agreement. Table 5.7 compares the inter-point distances of the two data sets - the maximum point to point distance is 14.5 m - this compares the *shapes* of the two data sets. Here the standard deviation is 41 µm; which is close to the standard deviation of the least-squares fit, and is therefore consistent with the measurement.

| Best-Fit Transformation | | | | |
|---|---|---|---|---|
| Results | $X$ | $Y$ | $Z$ | Mag |
| Max Error | 0.0423 | 0.0488 | 0.0387 | 0.0525 |
| RMS Error | 0.0235 | 0.0269 | 0.0201 | 0.0410 |
| StdDev Error | 0.0246 | 0.0282 | 0.0211 | 0.0430 |

Table 5.6: V-STARS/S best-fit with reference network points

| Differences between inter-point distances, *mm* | | | | | | | | | | | |
|---|---|---|---|---|---|---|---|---|---|---|---|
| | P1 | P2 | P3 | P4 | P5 | P6 | P7 | P8 | P9 | P10 | P11 |
| P1 | 0.000 | -0.019 | -0.041 | -0.059 | -0.032 | -0.057 | -0.005 | 0.028 | 0.032 | 0.061 | 0.065 |
| P2 | | | -0.011 | -0.004 | 0.026 | 0.006 | 0.050 | 0.036 | 0.054 | 0.066 | 0.101 |
| P3 | | | | -0.022 | -0.045 | -0.057 | -0.020 | -0.026 | -0.007 | 0.025 | 0.033 |
| P4 | | | | | -0.022 | -0.012 | -0.027 | -0.063 | -0.029 | -0.001 | 0.038 |
| P5 | | | | | | 0.017 | -0.020 | -0.039 | -0.030 | 0.011 | 0.067 |
| P6 | | | | | | | -0.039 | -0.055 | -0.058 | -0.015 | 0.041 |
| P7 | | | | | | | | -0.018 | -0.009 | 0.024 | 0.053 |
| P8 | | | | | | | | | 0.033 | 0.061 | 0.065 |
| P9 | | | | | | | | | | 0.037 | -0.005 |
| P10 | | | | | | | | | | | 0.003 |
| P11 | | | | | | | | | | | 0.000 |
| | | | | | | | | | | St. Dev | 0.041 |
| | | | | | | | | | | Maximum | 0.101 |

Table 5.7: Inter-point distance differences

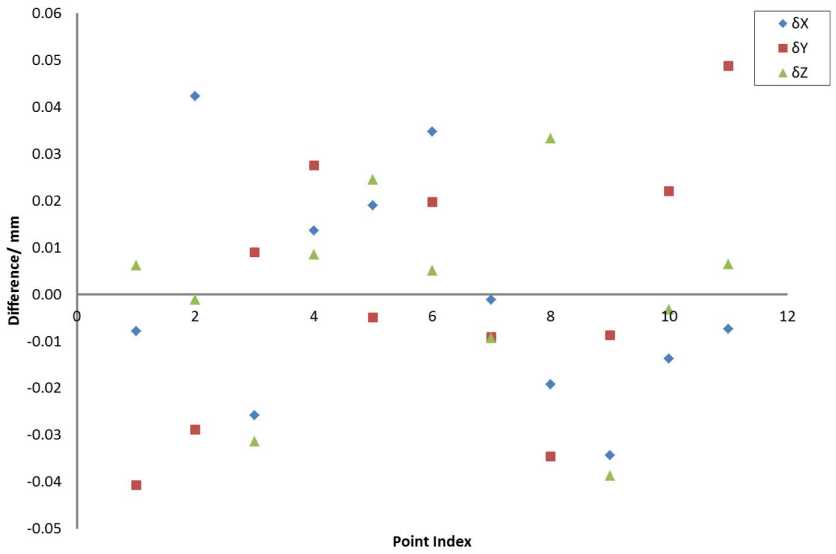


(a) Differences in each co-ordinate axis

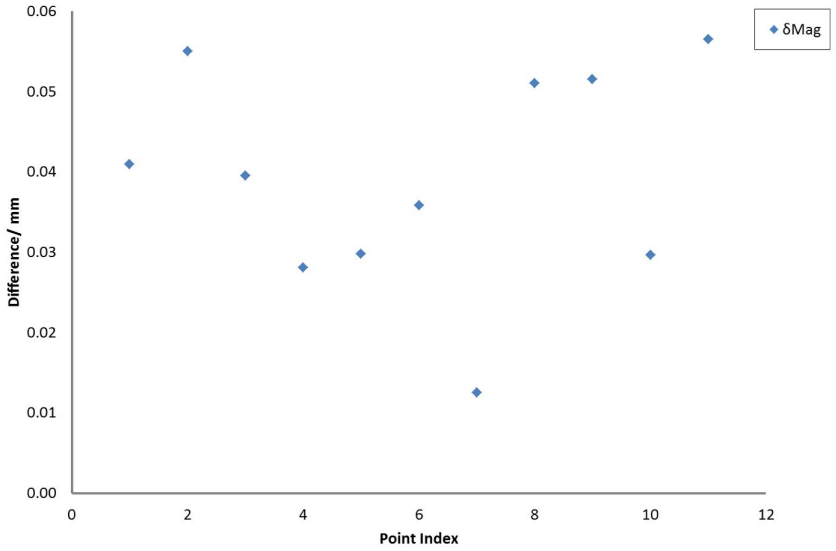


(b) Magnitude of Differences

Figure 5-4: Comparison of V-STARS/S co-ordinates after un-weighted least-squares regression with the reference network co-ordinates

To establish the system's absolute uncertainty, and tracing the measurement back to our reference standard, we have to add-in the reference standard uncertainty and the best-fit residuals such that:

$$p = p_f + n \tag{5.26}$$

| Standard uncertainty component<br><br>$u(x_i)$ | Source<br><br>$X_i$ | Value of standard uncertainty<br><br>$u(x_i)$ | Sensitivity coefficient<br><br>$c_i = \frac{\delta f}{\delta x_i}$ | $u_i(n) = \lvert c_i \rvert u(x_i)$ |
|---|---|---|---|---|
| $u(p_f)$<br>$u(n)$ | 6DOF fit residuals<br>Reference standard network uncertainty | 41.23 µm<br>12.53 µm | 1.0<br>1.0 | 41.23<br>12.53 |
| | | | | $u_c^2(n) = \Sigma u_i^2(n) = 1856.92\,\mu m^2$<br>$u_c(n) = 43.09\,\mu m$ |

Table 5.8: Uncertainty contributions for post-measurement uncertainty estimate with knowledge of the reference network

V-STARS estimated uncertainty vary based on:

| | |
|---|---|
| System specification and associated contributions | :58.24 µm |
| V-STARS bundle adjustment RMS and associated contributions | :46.63 µm |
| V-STARS Fit quality to reference network | :43.09 µm |

**Off-the-shelf Photogrammetric System Uncertainty Analysis**

The off-the-shelf photogrammetric system comprised of a Nikon D700 digital SLR fitted with a 28mm Nikkor lens and Vision Measurement Software (VMS). The measurement was processed using a self-calibrating photogrammetric adjustment. The off-the-shelf photogrammetric system has only two approaches to estimate the measurement uncertainty as there is not a formal system specification. The two options for the uncertainty estimate are:

1. Post-measurement: an estimate of the measurement uncertainty based on the instrument metrics and combining the additional known sources of uncertainty - without knowledge of the reference network

2. Post-measurement: an estimate of the measurement uncertainty based on knowledge of the reference network i.e. a co-ordinate comparison.

**Post-measurement without knowledge of the reference network**

Here we quantify the measurement uncertainty as if we have no knowledge of the reference network. This replicates a typical photogrammetry measurement. The system measured the reference network, the bundle adjustment metrics can be used to estimate the measurement uncertainty, such that:

$$p = p_{vmsb} + p_t + n_n + p_{tp} \tag{5.27}$$

Where:

$p_{vmsb}$ = This variance is an output from the VMS bundle adjustment algorithm and is a metric for the *quality* of the measurement. This is a root-mean square (RMS) value of the residual errors experienced when bundling the images together with the 1m scale bars as constraints. The variance is a statistical parameter with a normal distribution.

The uncertainty estimate can be determined in Table 5.9:

| Standard uncertainty component | Source | Value of standard uncertainty | Sensitivity coefficient | $u_i(n) = \lvert c_i \rvert u(x_i)$ |
|---|---|---|---|---|
| $u(x_i)$ | $X_i$ | $u(x_i)$ | $c_i = \frac{\delta f}{\delta x_i}$ | |
| $u(p_{vb})$ | VMS Bundle Adjustment RMS | 97.58 µm | 1.0 | 97.58 |
| $u(p_t)$ | Targeting manufacturing Tolerance | 3.46 µm | 1.0 | 3.46 |
| $u(n_n)$ | Nest manufacturing tolerance | 1.48 µm | 1.0 | 1.48 |
| $u(p_{tp})$ | Temperature probe uncertainty | 0.5 °C | 81.89 µm/°C | 40.95 |
| | | | | $u_c^2(n) = \Sigma u_i^2(n) = 34\,659.31\ \mu m^2$ |
| | | | | $u_c(n) = 105.89\ \mu m$ |

Table 5.9: Uncertainty contributions for post-measurement uncertainty estimate without knowledge of the reference network

**Post-measurement with knowledge of the reference network**

A 6DOF least squares regression is applied to the resultant co-ordinate definitions, fitting the dataset to the reference points. The residuals are given in Table 5.10 and the inter point distance deviations in Table 5.11. Figure 5-5 shows the values are approximately four times larger than the V-STARS residuals.

| | Best-Fit Transformation | | | |
|---|---|---|---|---|
| Results | $X$ | $Y$ | $Z$ | Mag |
| Max Error | 0.1512 | 0.2611 | 0.1383 | 0.2838 |
| RMS Error | 0.0819 | 0.1274 | 0.0916 | 0.1771 |
| StdDev Error | 0.0859 | 0.1336 | 0.0961 | 0.1857 |

Table 5.10: Digital SLR best-fit with reference network points

| Differences between inter-point distances (mm) | | | | | | | | | | | |
|---|---|---|---|---|---|---|---|---|---|---|---|
| | P1 | P2 | P3 | P4 | P5 | P6 | P7 | P8 | P9 | P10 | P11 |
| P1 | 0.000 | 0.028 | -0.301 | -0.013 | 0.061 | -0.242 | 0.132 | 0.038 | 0.074 | -0.083 | 0.012 |
| P2 | | | -0.323 | -0.048 | 0.126 | -0.109 | 0.205 | 0.090 | 0.174 | -0.004 | 0.102 |
| P3 | | | | 0.052 | 0.158 | 0.028 | 0.019 | -0.205 | -0.069 | -0.281 | -0.100 |
| P4 | | | | | 0.200 | 0.107 | 0.228 | 0.089 | 0.264 | 0.092 | 0.233 |
| P5 | | | | | | -0.091 | 0.023 | 0.089 | 0.121 | 0.007 | 0.078 |
| P6 | | | | | | | -0.289 | -0.230 | -0.236 | -0.364 | -0.224 |
| P7 | | | | | | | | 0.134 | 0.133 | 0.050 | 0.074 |
| P8 | | | | | | | | | 0.128 | -0.019 | 0.108 |
| P9 | | | | | | | | | | -0.048 | -0.019 |
| P10 | | | | | | | | | | | -0.006 |
| P11 | | | | | | | | | | | 0.000 |
| | | | | | | | | | | St. Dev | 0.155 |
| | | | | | | | | | | Maximum | 0.364 |

Table 5.11: Inter-point distance differences

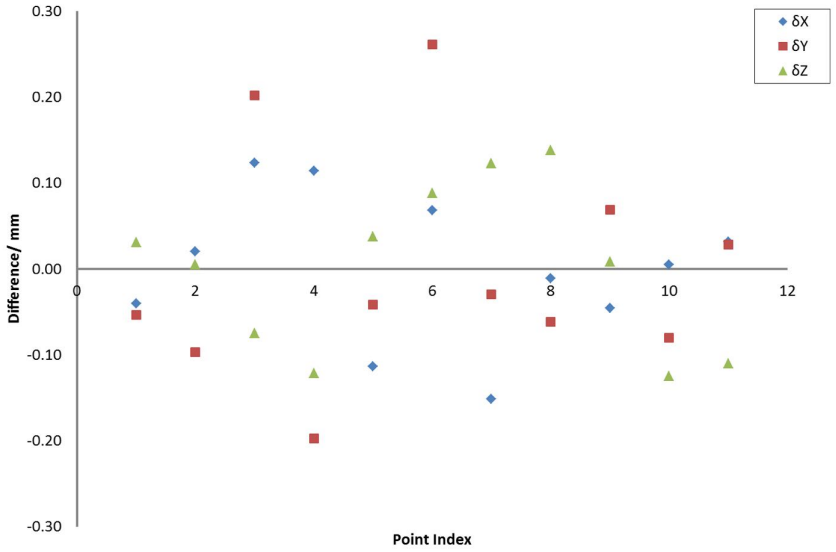


(a) Differences in each co-ordinate axis

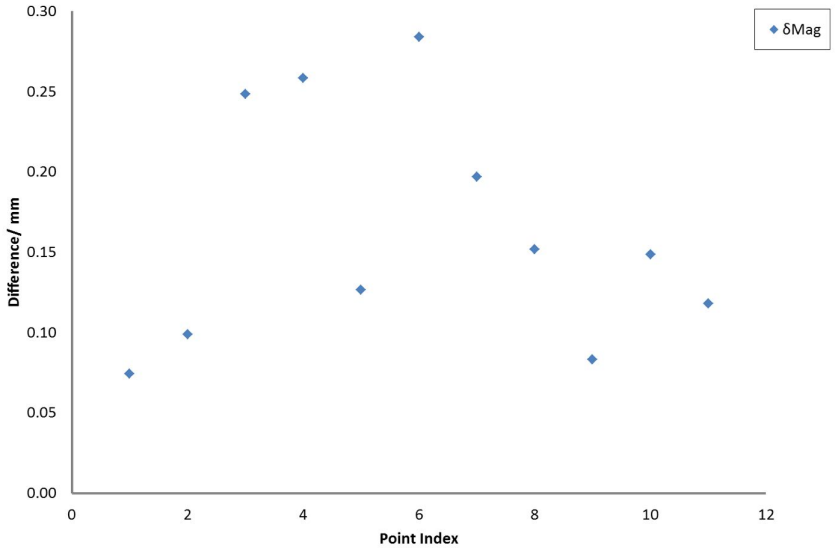


(b) Magnitude of Differences

Figure 5-5: Comparison of digital SLR and VMS bundle adjustment co-ordinates after unweighted least-squares regression with the reference network co-ordinates

The components in the photogrammetric network can be expressed as:

$$p = p_f + n \tag{5.28}$$

Table 5.12, combines the variances:

| Standard uncertainty component<br><br>$u(x_i)$ | Source<br><br>$X_i$ | Value of standard uncertainty<br><br>$u(x_i)$ | Sensitivity coefficient<br><br>$c_i = \frac{\delta f}{\delta x_i}$ | $u_i(n) = \lvert c_i \rvert u(x_i)$ |
|---|---|---|---|---|
| $u(p_f)$<br>$u(n)$ | 6DOF fit residuals<br>Reference standard network uncertainty | 186.16 µm<br>12.53 µm | 1.0<br>1.0 | 186.16<br>12.53 |
| | | | | $u_c^2(n) = \Sigma u_i^2(n) = 34\,812.92\,\mu m^2$<br>$u_c(n) = 186.58\,\mu m$ |

Table 5.12: Uncertainty contributions for post-measurement uncertainty estimate with knowledge of the reference network

The different method yield uncertainty estimates of:

VMS bundle adjustment RMS and associated contributions :106.92 µm
VMS Fit quality to reference network :186.58 µm

The high fitting or bundle adjustment residuals dominate the uncertainty budgets. This is likely to be a consequence of several limitations in comparison to commercial system, the combination of which will increase the uncertainty of the target coordination within the self-calibrating bundle adjustment process. Factors are listed as follows:

(a) Fundamental to a high quality result is the geometry of the imaging network with multiple convergent lines of sight to each target. Unlike the state of the art commercial photogrammetric system, the low cost system does not have provision to connect to a host computer and carry out on-line bundle adjustment as images are captured. This limitation means that the operator does not receive guidance as to where the photogrammetric imaging geometry should be improved during the capture process.

(b) Retro target image quality is critical for a high quality result. Whilst images were captured using retro-reflective targets and an electronic flash with the low cost system, there were no optimisations, such as multiple exposures and changes in exposure, to ensure optimal target image quality. This limitation is compounded with a reduction in retro-target image quality following the camera Beyer colour correction that is integral to the design of the DSLR sensor (Luhmann, 2010).

**Comparison to a single station laser tracker**

In order to assess the photogrammetry systems' suitability for large volume measurement, the current state of the art / industrial practice must be taken into consideration in order to make meaningful comparisons. At present a laser tracker can be used in a single station configuration or networked together to minimise point uncertainty - however the former is more common.

For completeness a single station laser tracker's uncertainty was calculated using the reference network points; Table 5.13 shows the summary. This summary is the result of ten data sets from individual tracker stations, some tracker positions are better placed than others, and this should provide a balanced residual. The uncertainty was subsequently calculated as 65.04 µm at $1\,\sigma$ using the same uncertainty budget assumptions as above.

| | Best-Fit Transformation | | | |
|---|---|---|---|---|
| Results | $X$ | $Y$ | $Z$ | Mag |
| Max Error | 0.1148 | 0.1373 | 0.0669 | 0.1840 |
| RMS Error | 0.1067 | 0.0990 | 0.0624 | 0.1584 |
| StdDev Error | 0.0339 | 0.0314 | 0.0198 | 0.0503 |

Table 5.13: Laser tracker single station average best-fit with reference network points (parameters calculated from 10 individual stations' best-fit residuals)

| | |
|---|---|
| Laser Tracker Network | :12.53 µm |
| Laser Tracker Single Station | :65.04 µm |
| System specification and associated contributions | :58.24 µm |
| V-STARS bundle adjustment RMS and associated contributions | :46.63 µm |
| V-STARTS Fit quality to reference network | :43.09 µm |
| VMS bundle adjustment RMS and associated contributions | :106.92 µm |
| VMS Fit quality to reference network | :186.58 µm |

These data demonstrate the impact of using a laser tracker in isolation when compared to a networked arrangement, although it should be noted that an industrial tracker network is unlikely to be quite as strong, as not all stations have line of sight to all targets. Nevertheless, networking instruments still yields significant improvements with respect to the associated uncertainty.

The V-STARS uncertainty consumes much of the intended tolerance budget (150 µm), this is comparable to - and less than - the laser tracker's uncertainty as single station measurement instrument. However for this application the V-STARS meets the uncertainty requirement and is a suitable substitute for the single station laser tracker measurements.

The non-commercial photogrammetric system is working within its expected uncertainty estimation from the bundle adjustment, but this far exceeds the desired uncertainty level, and tolerance band for this application: this makes confidence in achieving the tolerance impossible. In its current configuration, the system could provide low-cost measurement for less critical tolerances, e.g. ±1 mm) across the 13.5m x 8m x 3m volume used for this series of experiments.

### 5.2.3 Industrial Application of Photogrammetry

The industrial application evaluation focusses on the practicalities of using a measurement system in a realistic production environment; the measurement uncertainty has been considered in the above section, and shown to be be comparable to a single station laser tracker measurement. Off-line photogrammetry is not a practical solution for the measurement of components that have to be manually manipulated to a nominal position - a *build to CAD* process. Off-line photogrammetry requires many images to be acquired and post-processed, consequently the points of interest must be stationary. If the component has been determined out of position and must be manipulated (such as a tooling pick-up) the data acquisition, post-processing and manipulation must be iterated many times; this is a time-consuming and laborious method for setting. As a result, off-line photogrammetry is not a suitable solution or alternative to the full tooling recertification, and cannot replace/compete with the laser tracker's dynamic measurement capability. However, a *tooling health-check* measurement would be well suited to off-line photogrammetry.

The industrial application of off-line photogrammetry evaluation was carried out on the Advanced Low Cost Aircraft Structures (ALCAS) Main Assembly Jig (MAJ)

(Figure 5-6). There are two main types of Position of Interest (POIs) on the MAJ: 1) Enhanced Reference System (ERS) points, and 2) the Optical Tooling Points (OTPs) (Figure 5-7). The ERS points are a stable constellation of Spherically Mounted Retro-reflective (SMR) target nests that are arbitrarily attached onto the tooling structure, subsequently, the ERS points have been accurately measured and recorded; these are used as reference points to locate instruments to the tooling co-ordinate system, the wing geometry co-ordinate frame and ultimately, the master aircraft axis. The flags on an assembly tool are moveable components on which the pick-ups/clamps are mounted. The flags have to move in order to allow access for the components during and after the assembly process. On a traditional tool the nominally correct positions of the flags are maintained and re-gained by using dowel pins; the ALCAS assembly tooling however does not have dowelled flags and this is often the case with flexible/reconfigurable tooling. The flags are important as they hold the KCs and Interchangability (ICY) features of the assembly. Facility tooling such as: vector bars, pin nests, etc. are used to target the KC and ICY features on the flags; once targeted we can measure the point of interest (POI), collectively known as OTPs. The measured ERS networks and the OTP nominal positions are recorded and documented in documents associated to the tooling.

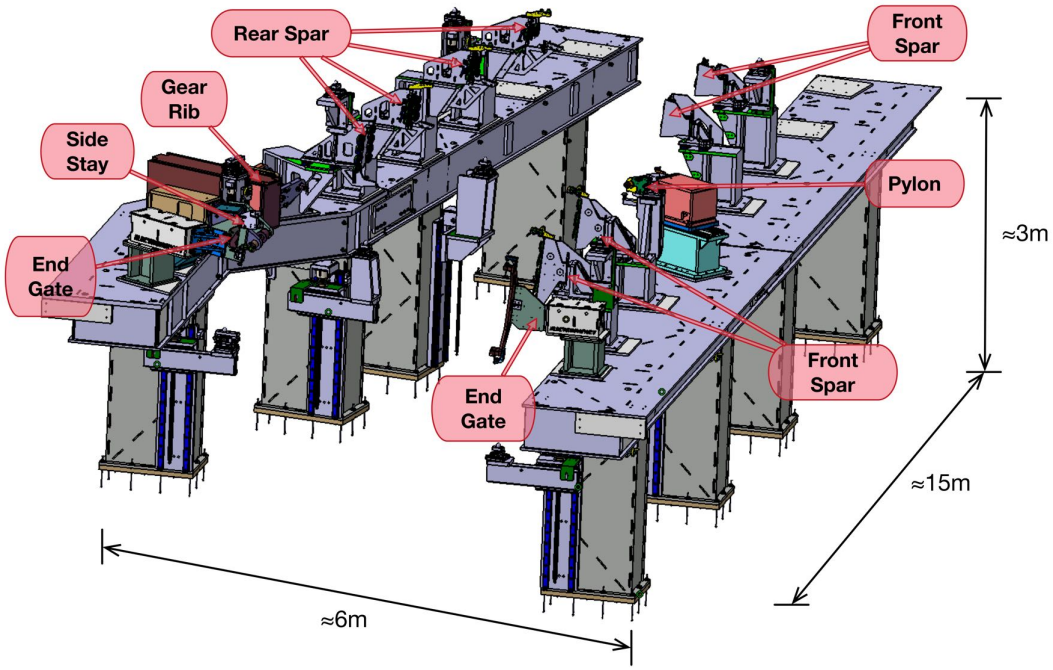


Figure 5-6: The ALCAS MAJ and flags identified

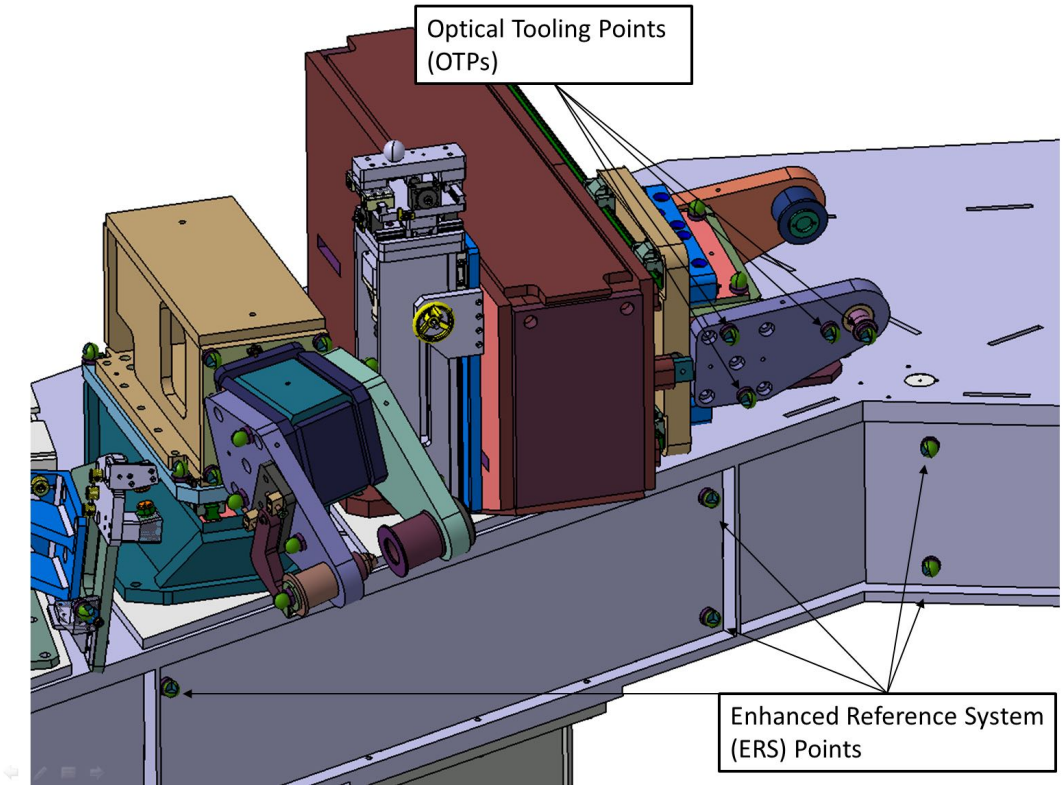


Figure 5-7: The ALCAS MAJ OTPs and ERSs surrounding the side stay flag (left) and gear rib (right)

The Health Check measurements carried out on the ALCAS MAJ measured one OTP on each flag and the two points of a sine bar on both the Gear Rib and Pylon - in order to measure the axial KC. This measurement task is particularly well suited to photogrammetry as the measurements/targets are all static. However additional photogrammetry targets had to be placed to *strengthen* the network; this is required to 'stitch' the individual images together during the *bundle adjustment*. Additional consideration should be made for the facility tooling (sine bars) and target nests, as these are specifically designed for laser tracker operations; photogrammetry could use lower cost targets and facility tooling, optimised for photogrammetry measurements. The photogrammetry systems trialled both use essentially the same method: a single roving camera taking many images which are subsequently processed as a *bundle adjustment*. The V-STARS system uses a single INCA3 camera, the bundle adjustment processed in the V-STARS proprietary software. The other set of measurements are taken using a standard off-the-shelf digital SLR camera, the subsequent bundle is processed VMS software.

The health-check measurement surveys were carried out with intentionally out-of-tolerance points, the measurement systems had to detect which points were out of tolerance; proving that they could measure and identify gross errors in the flag positions.

The health check measurement data is separated into two sets: firstly the 'best-fit' transformation, this is an unweighted least-squares regression of the measured ERS points to the nominal ERS positions. The summary of the best-fit residuals for a laser tracker are given in table 5.14; it should be noted that these residuals are quite high but still sub-250 µm, a majority of the deviation from nominal comes from the $z$-axis this is due to movement between the two gantries. It also important to recognise that a 'better' fit can be achieved by only measuring a subset of the available ERS points - for example: measuring only ERS on one gantry - however, this can be deceptive as it does not provide a better *global fit*. A satisfactory global fit will distribute the measurement discrepancies over the entire structure, without bias. Secondly, the results of the health check measurements are presented: the measured deviations of the OTPs from their nominal positions. The tolerance threshold for OTPs is 150 µm in each axis, if a deviation exceeds this then the OTP needs to be reset.

The V-STARS roving camera system measured the OTPs in 33 minutes, the best-fit (Table 5.15) seems reasonable, showing greater residuals in the $z$-axis as expected; however the measurement used only eight ERS points and is not as rigorous as the Laser Tracker's fit. The OTP measurements (Table 5.16) have identified (highlighted)

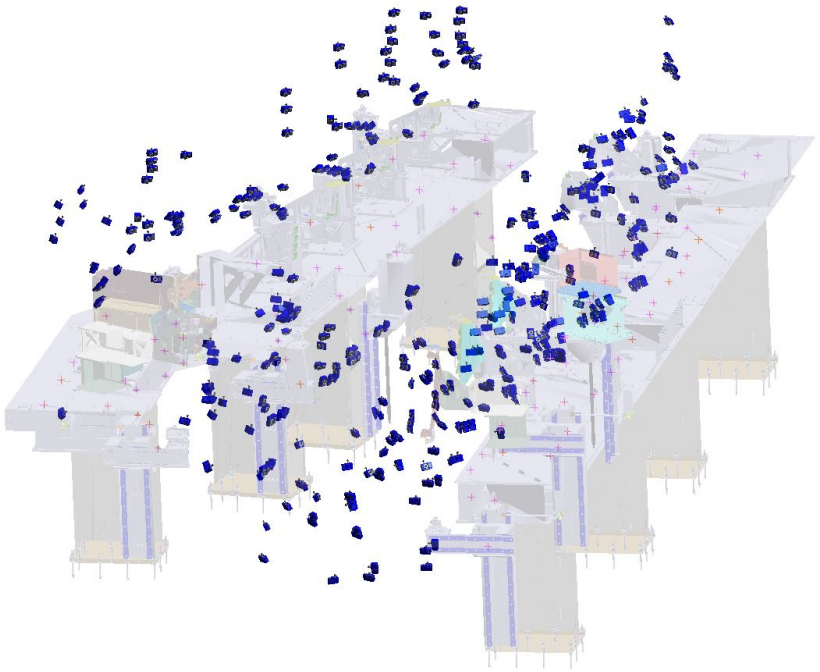

Figure 5-8: The V-STARS/S health check measurement of the ALCAS MAJ

all the out of tolerance points. The vectors generated from Table 5.16 are shown as deviations from the CAD model in Figure 5-9

| | Best-Fit Transformation | | | |
|---|---|---|---|---|
| Results | $X$ | $Y$ | $Z$ | Mag |
| Max Error | 0.1172 | 0.0564 | 0.2219 | 0.2372 |
| RMS Error | 0.0540 | 0.0297 | 0.1111 | 0.1271 |
| StdDev Error | 0.0547 | 0.0301 | 0.1126 | 0.1288 |

Table 5.14: Typical laser tracker best-fit with ALCAS JRS nominals

| | Best-Fit Transformation | | | |
|---|---|---|---|---|
| Results | $X$ | $Y$ | $Z$ | Mag |
| Max Error | 0.0933 | 0.0256 | 0.1720 | 0.1967 |
| RMS Error | 0.0625 | 0.0130 | 0.1074 | 0.1249 |
| StdDev Error | 0.0668 | 0.0139 | 0.1148 | 0.1335 |
| Max Error (all) | 0.0933 | 0.0256 | 0.1720 | 0.1967 |
| RMS Error (all) | 0.0625 | 0.0130 | 0.1074 | 0.1249 |

Table 5.15: V-STARS/S best-fit with ALCAS ERS nominals

The digital SLR/VMS fit residuals to the nominal ERS (Table 5.17) are comparable to those of the Laser Tracker and the V-STARS system (sub-250 µm) however, the comparison to the nominal positions of the OTPs (Table 5.18) shows significant deviations when not expected. *OTP809404* and *OPT809304* were within tolerance of nominal, however the digital SLR/VMS has calculated these points as out-of-tolerance. These OTPs were approximately on the $y, z$ plane, the most significant deviation was seen on the $x$ axis, this may be due to lack of resection, occlusion or lines of sight to these targets; resulting in a weak solution in the $x$ direction. This could, to some extent, be reduced if a weighted least squares fit was employed - as the $x$ axis measurements would have larger associated uncertainty. Figure 5-10 shows the graphical representations of the OTPs deviations from nominal.

| Name | Deviation from Nominal | | | |
|---|---|---|---|---|
| | $\delta X$ | $\delta Y$ | $\delta Z$ | Mag |
| OTP809404 | −0.0569 | 0.0138 | −0.1133 | 0.1275 |
| OTP809304 | −0.1239 | −0.0189 | −0.1092 | 0.1662 |
| OTP809204 | 0.0209 | 0.1032 | −0.2188 | 0.2428 |
| OTP809104 | −0.3064 | −3.2415 | 0.1353 | 3.2588 |
| OTP811304 | −0.4013 | −0.1636 | 0.0877 | 0.4422 |
| OTP811204 | 0.1271 | 0.0814 | 0.1015 | 0.1818 |
| OTP811104 | −0.0589 | −0.0206 | −0.0268 | 0.0679 |
| OTP813120 | −0.9134 | 0.2120 | −0.5651 | 1.0948 |
| OTP813121B | −0.9342 | 0.2277 | −0.7397 | 1.2131 |
| OTP817113 | −0.3347 | −0.1929 | 0.7177 | 0.8151 |
| OTP817114 | −0.2246 | −0.0148 | 0.6859 | 0.7219 |
| OTP819106 | 0.1091 | −1.9193 | −4.4987 | 4.8922 |
| OTP819109 | −0.0434 | −2.3256 | 2.6055 | 3.4927 |

Table 5.16: V-STARS/S OTP deviations from nominal

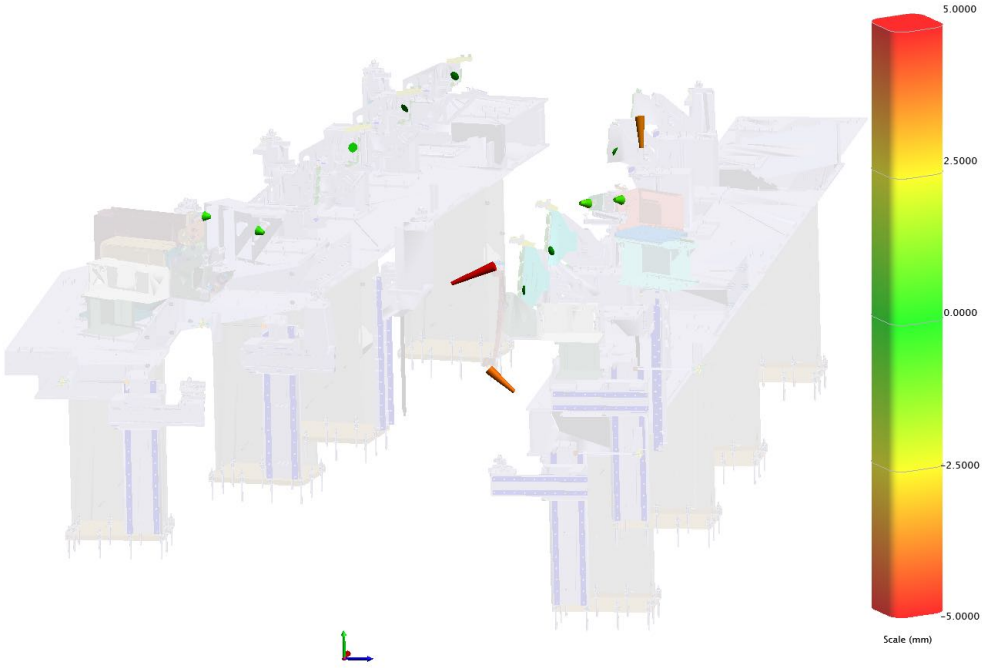


Figure 5-9: Vector plot of the V-STARS/S measured OTPs

| Results | Best-Fit Transformation $X$ | $Y$ | $Z$ | Mag |
|---|---|---|---|---|
| Max Error | 0.1529 | 0.1121 | 0.1685 | 0.1934 |
| RMS Error | 0.0537 | 0.0332 | 0.0600 | 0.0871 |
| StdDev Error | 0.0544 | 0.0336 | 0.0608 | 0.0883 |

Table 5.17: UCL digital SLR measurements best-fit with ALCAS ERS nominals

| Name | Deviation from Nominal $\delta X$ | $\delta Y$ | $\delta Z$ | Mag |
|---|---|---|---|---|
| OTP809404 | −0.5508 | −0.1470 | 0.1831 | 0.5988 |
| OTP809304 | −0.5540 | −0.0399 | 0.1665 | 0.5799 |
| OTP809204 | 0.2573 | 0.2634 | 0.3559 | 0.5120 |
| OTP809104 | −0.2402 | −4.0638 | 0.9388 | 4.1777 |
| OTP811304 | N\A | N\A | N\A | N\A |
| OTP811204 | 0.3379 | 0.0920 | 0.1638 | 0.3866 |
| OTP811104 | −0.3201 | −0.0790 | −0.3733 | 0.4981 |
| OTP813120 | −1.0214 | −0.1954 | −0.4108 | 1.1181 |
| OTP813121B | −1.1939 | 0.3890 | −0.2732 | 1.2851 |
| OTP817113 | −0.1045 | −0.1536 | 0.7382 | 0.7612 |
| OTP817114 | −0.5671 | 0.1901 | 0.4189 | 0.7302 |
| OTP819106 | −0.1468 | 0.1203 | 0.4716 | 0.5084 |
| OTP819109 | −0.1552 | 0.0413 | 0.6265 | 0.6468 |

Table 5.18: UCL digital SLR OTP deviations from nominal

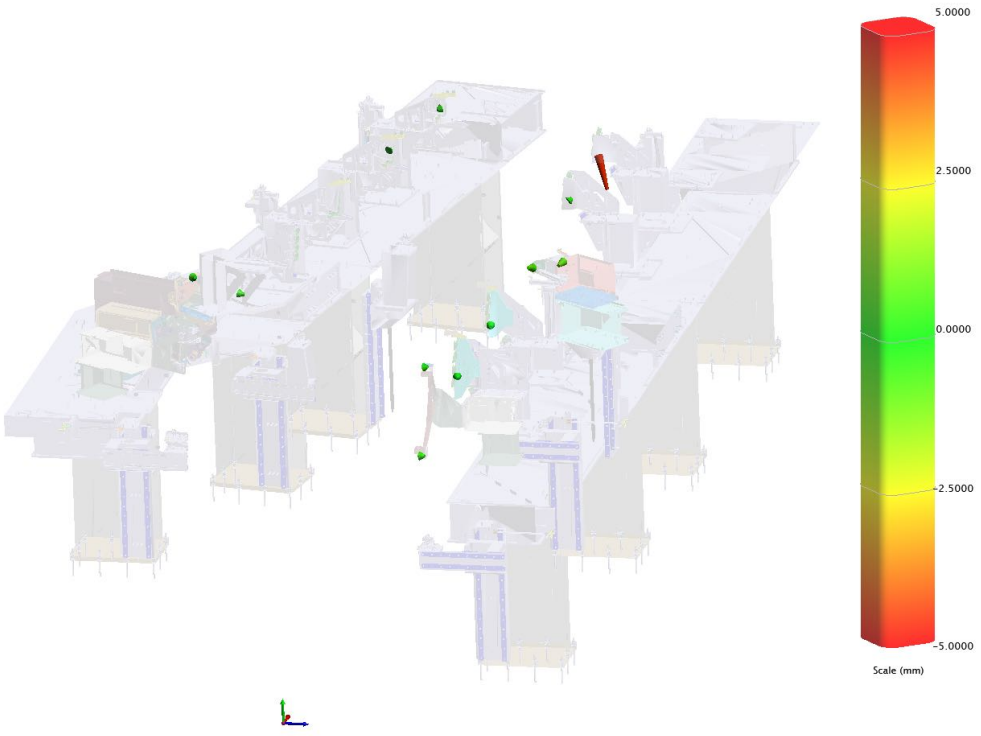


Figure 5-10: The UCL digital SLR health check measurement of the ALCAS MAJ

In order to assess the photogrammetry systems' suitability for large volume measurement, the current state of the art/ industrial practice must be taken into consideration in order to make meaningful comparisons.The uncertainty for the industrial standard and proposed LVM has been experimentally determined in Section 5.2.2.

The fixture health check measurement application is not an established method in Airbus UK or the aerospace sector at large, the accuracy of the system must be understood in order to proceed with this new application. The digital SLR an VMS could not in reality perform the health check measurement, as the hardware and software would not be a turn-key solution, requiring tailoring to this specific application. In addition the static uncertainty evaluation has shown that the uncertainty is too high for the health check measurement.

Roving camera systems on the whole, hold potential as diagnostic tool, providing a *snapshot* of the fixture condition between builds giving rise to:

- Assurance that the fixture has no gross errors before the wing build begins - reducing concessions.
- Providing an aid to accurately estimate levels of re-work; reducing time and cost.
- Providing SPC data, used for predictive fixture re-work and trend spotting.

## 5.3 Large Volume Multi-Instrument Networks

This section further the examines the use of photogrammetry in large volume aerospace tooling applications. Here we explore a data fusion approach - using laser tracker networks to establish large scale references that can subsequently be utilised by the photogrammetric bundle adjustment. This provides the foundation for the large volume metrology network element of the META Framework (Figure 5-11).

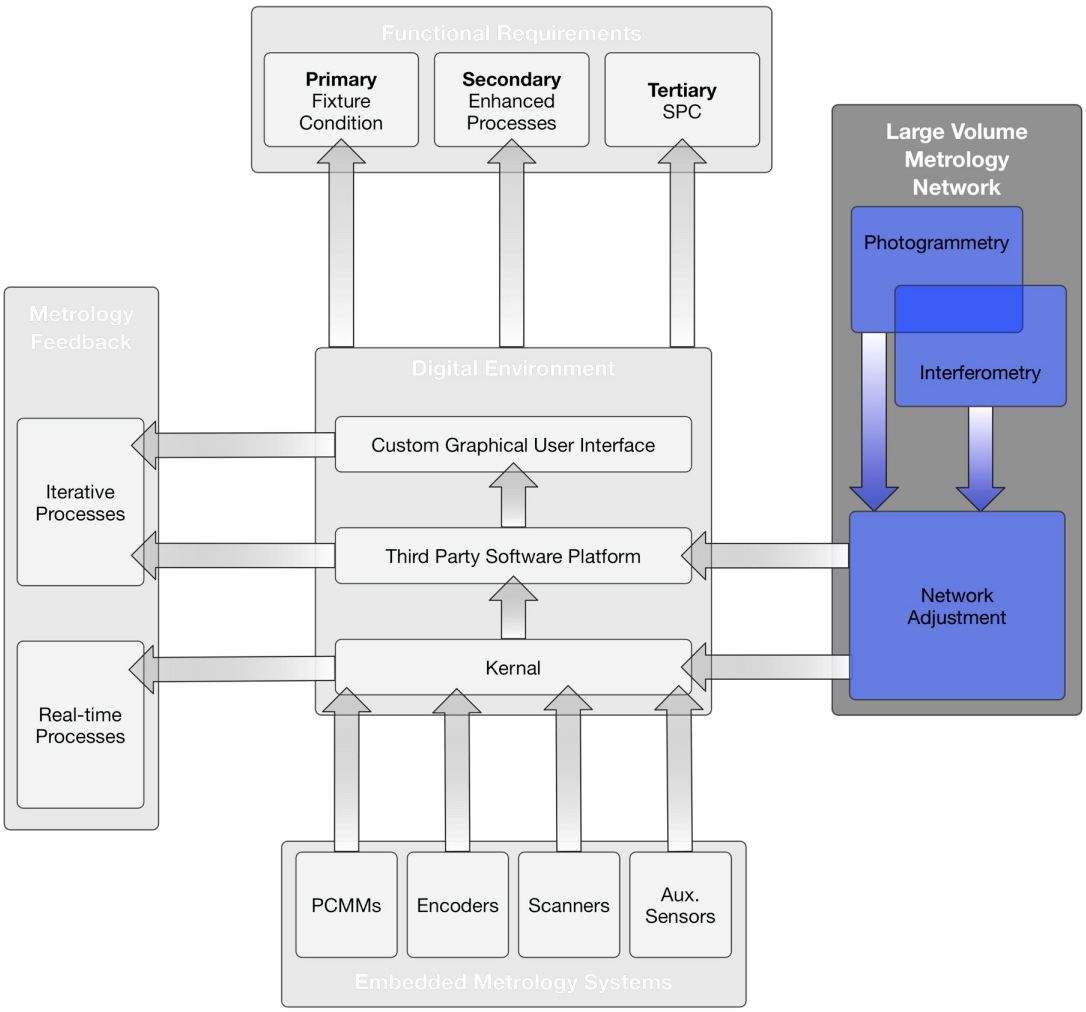


Figure 5-11: META framework highlightinglaser tracker and photogrammetric measurement networks explored within this section

Utilising the following outcomes from the previous section, the large volume metrology network should include:

- The use commercial photogrammetric equipment.
- The use of 7 DOF fits for instead of "scaling for temperature" manually (current best practice).
- The uncertainty estimate for the photogrammetric measurement uncertainty based on laser tracker network - not based on system specification or bundle adjustment metrics.

Developing the following:

- Improved the uncertainty estimate of laser tracker uncertainty
- a specific uncertainty estimation for laser tracker and photogrammetric measurements

As with the previous section, this work needs both representative scale and environmental conditions to be valid. An ideal testbed for such a network is contained within a requirement for the BLADE flight test demonstrator [1]. The BLADE project requires accurate measurement of the following features on an Airbus A340:

- Wing Sweep angle relative to the fuselage centre-line
- Front and Rear Spar positions between Rib 27 and 28 (witness planes)
- Rib 27 Position witness plane if possible
- Surface profile at Rib 27 and a band approximately 300mm inboard
- All measured points and generated planes/surfaces to be output in STEP format (.stp)
- All points should be relative to the global/Aircraft axis system.

Although additional outputs were industrially required and are outlined above (for completeness) this section is focussed on the discrete co-ordinate definition and the laser tracker/ photogrammetry measurement network.

### 5.3.1 Measurement Strategy

The scale of the measurement represents a physical challenge, with a wingspan of approximately 80 m and the upper surface/key features approximately 6 m vertically up: the wingspan is twice the scale of a traditional fixture measurement[2].

[1] the Breakthrough Laminar Aircraft Demonstrator in Europe (BLADE), aims to validate that a specific wing profile can sustain laminar flow with an acceptable stability versus in flight deformation and contamination. The project entails the removal of the outer wing-boxes, Rib 27 Outboard (OTBD), and fitting new laminar flow outer wing boxes. The new outer wing sections to be fitted have a very accurate profile and high surface finish on the upper wing surface. These wing-boxes will be dry areas (without fuel) and fully functional with Flight Test Instrumentation (FTI). The test Aircraft is A340 MSN001, the first A340 to be produce: Milestone Number (MSN) 001.

[2] the physical scale of this measurement is unprecedented within Airbus

The measurement philosophy uses a combination of laser tracker measurements and photogrammetry measurements to complement one another, the outline steps are:

1. Measure a constellation of points with a low-level of associated measurement uncertainty, using a laser tracker network; this provides known points on the upper and lower wing surfaces, key datum features, as well as creating an accurate association between Port and Starboard wings.
2. The photogrammetry system measures the upper wing profiles and sections of the fuselage. The scale required for the bundle adjustment algorithm uses the laser tracker network data. It also locates the photogrammetric measurements in the same co-ordinate system as the laser tracker network.
3. The combined data set can then locate relative to A/C geometry, as a rigid body[3].

### 5.3.2 Laser Tracker Reference Network

The aim of the laser tracker measurement network was to output a constellation of discrete points with low measurement uncertainty associated to the co-ordinate definitions, subsequently to be utilised by the photogrammetric bundle as reference points to be used as scale, the points can be subdivided as:

- Measurement of Floor Reference System (FRS)
- Measurement of wing Enhanced Reference System (ERS)
- Measurement of key features: witness planes, fuse scans, *etc.*

#### Data Acquisition

The measurement was constrained to a four day window as the Aircraft had limited availability due to a flight test schedule. The work was carried out with the support of three AUK laser tracker operators.

The laser tracker network utilised 38 positions, using two laser trackers: a Long-Range (LR) and a Mid-Range (MR) Leica Absolute Tracker 901 (AT901), with a total

[3]the Aircraft (A/C) Datum is a non-physical feature, this presents a significant challenge when associating the measurement data to the nominal design intent, this is not included in this thesis, but the step is included for reference.

of 383 discrete measurement observations, within a 80 m x 80 m x 8 m volume. Figure 5-12 shows the laser tracker stations and the measurements, the vertices of the lines indicate the stations and the lines are the measurement observations. The data was post-processed via a network adjustment.

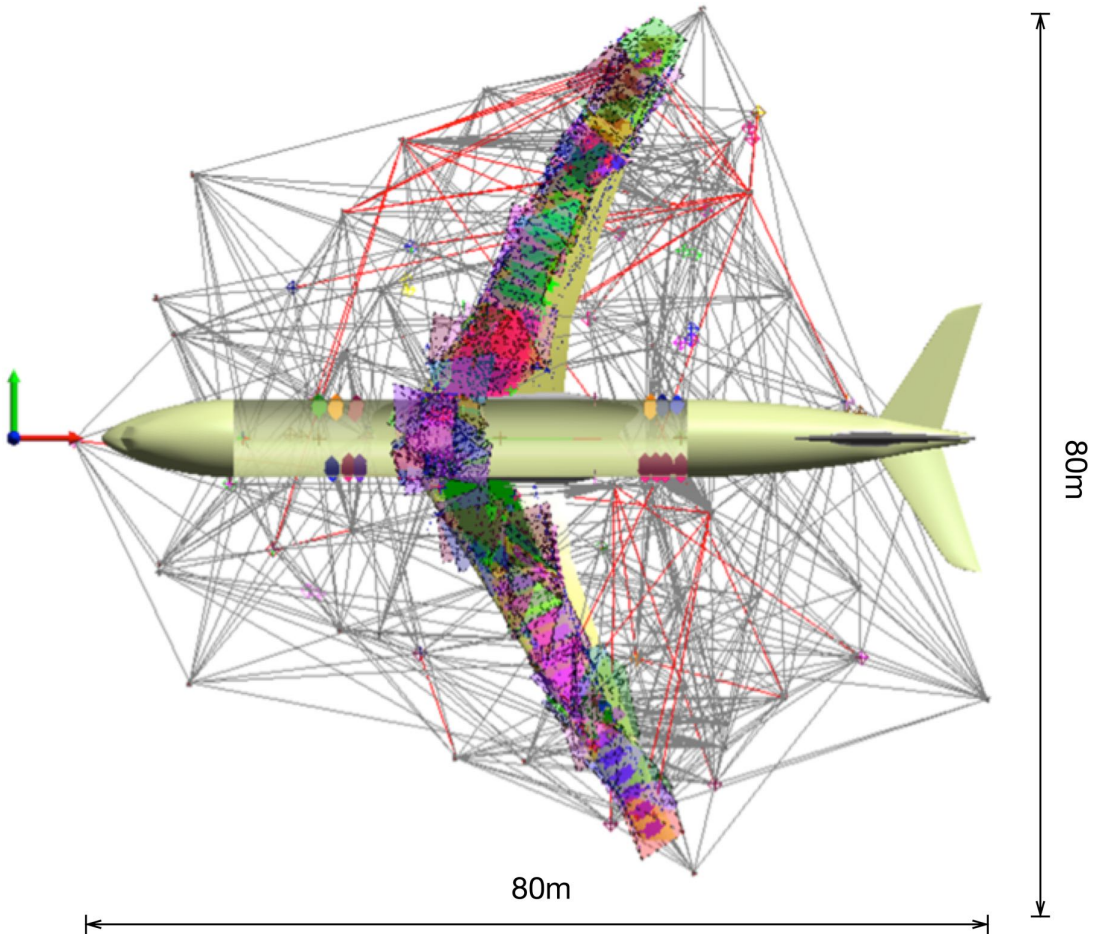


Figure 5-12: LVM network of A340MSN001

### Network Adjustment

The network adjustment improves the co-ordinate definition and reduces the uncertainty of measurement significantly from using a single laser tracker in isolation.

The current network adjustment process is standardised within an internal AUK document (Forster, 2007); this documentation was developed with assembly tooling

reference networks as the primary focus. As a consequence of the increased scale and the learning from the above section, new techniques were used - depoarting from current practice - to better estimate the network uncertainty including: i) 7 DOF network adjustment and ii) updating instrument uncertainty parameters.

**Outlier rejection**: within any large volume metrology network, poor measurements will be recorded, this can be through environment fluctuations, operator accidents, unstable structures *etc.* These 'poor' measurements must be excluded during the network adjustment as they can skew the composite point definition and mis-represent the magnitude of the associated uncertainty. However, enthusiastic and blanket removal of outliers can *weaken* a network as a whole, causing a reduction in station-to-station overlap and reduce the number of measurements used to determine the point co-ordinate definitions. On a network of this scale this removes many points that weaken the integrity of the 'optimised' co-ordinate definition, but could report good measurement residual and metrics. Over-trimming is likely to be the most dangerous scenario as unstable or non-repeatable measurement points can be missed, and trusted as having 'good' co-ordinate definition with low associated uncertainty.

The outliers are initially examined after an equal weighting least-squares best fit of the data set. This fist examination of point data provides opportunity to discarded measurements based on gross errors (>1 mm). These gross errors are attributable to component movement, debris in the target nest, operator movement, *etc.* Once these erroneous measurements are discarded outlier rejection based on the expected uncertainty can be carried out.

The outlier metric is a function of the *maximum deviation* from the optimum co-ordinate definition as a percentage of the expected uncertainty (at a $3\sigma$ level). A typical 'enthusiastic' approach is remove any and all points above 100% of there expected $3\sigma$ uncertainty values; followed re-running the best-fit without the discarded point set and the process is iterated until no points lie above the $3\sigma$ level. The maximum deviation changes with the best-fit. To ensure valid measurement data was not removed the following strategy was applied:

1. Run least-squares fit
2. Remove outliers exceeding 200% of expected uncertainty
3. Re-run least-squares fit
4. Remove outliers exceeding 150% of expected uncertainty

5. Re-run least-squares fit

6. Remove outliers exceeding 100% of expected uncertainty

Providing the following rule are not violated:

$$\begin{array}{lcl} \text{Each ERS point measurement observations} & \geq & 3, \\ \text{Each FRS point measurement observations} & \geq & 5, \\ \text{Laser tracker observations (per station)} & \geq & 5, \\ \text{Percentage of total points removed} & \leq & 10\% \end{array}$$

The different requirements for ERS and FRS measurements reflects the number of observations for the different reference points. The ERS had fewer observations due to access issues, whereas the FRS had many more observations and therefore greater redundancy.

This sequence provides a repeatable and logical approach. It first removes very few measurement observations during the initial step (<5%), eliminating the measurements that would skew the optimised co-ordinate definition. Subsequent steps (3 to 6) further remove poor measurement observations. Steps 3-6 do not effect the co-ordinate definition greatly, but does reduce the uncertainty associated with those co-ordinate definitions. Note, after these three iterations, measurement observations that exceed the 100% of expected uncertainty are still present in the network adjustment but are of a magnitude where the influence is marginal both in terms of co-ordinate definition and associated uncertainty.

**Thermal expansion**: is a major component of measurement uncertainty in LVM activities. The measurement was carried out in an uncontrolled aircraft hangar, based in Toulouse, France, during the summer months; this gave a large temperature differential from night to day. The Aircraft has a dominant material of Aluminium (*approx.* CTE of 24ppm), whereas the factory floor is concrete (*approx.* CTE of 10ppm). This creates a significant difference in expansion between the FRS targets and the wing-mounted ERS. For example, by applying a linear thermal expansion model we can see that a change in 1 °C would result in an overall expansion of around 2 mm for the aircraft and 1 mm for the floor. Perhaps, more importantly, the difference in the floor expansion and the aircraft would be in the order of 1 mm for each degree Celsius of change in the hanger. Management of thermal expansion within the network adjustment is detailed below.

**7 DOF adjustment** departs from the AUK documentation (Forster, 2007) that

describes a method for managing thermal expansion by scaling the measurements based on the average temperature of the object (this is usually performed with the temperature probe taking around 10 measurements). This uses a linear thermal expansion model. The previous section (Section 5.2) highlights that letting the scale "float" and performing a 7 DOF fit, produces smaller residuals - optimising the scaling factor - instead of manually scaling the measurement inducing further uncertainty from: the averaging techniques, operator error and temperature uncertainty.

The temperature at the first measurement position (Station 1) was recorded as 20.10 °C. This 0.10 °C from a nominal 20 °C and was within the measurement uncertainty of the temperature probe (0.5 °C). Subsequently, Station 1 was constrained (with respect to scale, position and rotation), all the other stations were free to float in terms of scale (7 DOF fit during the network adjustment), this uses just the FRS to establish scale as Station 1 only measured FRS and the FRS points are more stable and have the same CTE.

**Multiple iterations of instrument uncertainty parameters** departs from the AUK documentation (Forster, 2007) further. The least-squares regression used to combine the measurements from each station is weighted with respect to the instrument uncertainty parameters attributable to the: horizontal, vertical and distance (H, V, and D respectively) measurement components in the laser tracker. Initial values for these parameters are: H = V = 1 arcseconds, and D = 7.5 µm, from the network adjustment the *actual* instrument performance is evaluated based on the variance when combining the data sets. Current best-practice uses these actual variances to update the instrument parameters (from the default values) and re-run the network adjustment. This generates a co-ordinate definition with an associated uncertainty estimation that reflects the performance of the laser tracker(s) in the particular measurement network. This best-practice does however have some shortcomings; namely:

i) the uncertainty parameters used to update the instruments are averages of *all* the laser trackers in the network, it is unlikely that two (or more) instruments will exhibit the same uncertainty characteristics;

ii) the values are only iterated the once, this too could generate misleading uncertainty evaluations.

The ERS points were mounted on a structure that had potential to move, in order to assess the multiple iterations of instrument uncertainty parameters philosophy without a higher chance of erroneous data, the FRS subset will firstly be considered; before

expanding the philosophy to both the FRS and ERS points. Using the FRS data (23 points, spanning the 80 m range)in isolation for the network adjustment and applying the current techniques provides a baseline. Current best practice methods yield average instrument uncertainty parameters as:

| | |
|---|---|
| Horizontal | 0.8729 arcseconds |
| Vertical | 0.5837 arcseconds |
| Distance | 0.0280 mm |

Re-running the adjustment with the updated parameters the same for the LR and MR AT901, generates an average standard uncertainty of: 95.73 µm, whereas the initial network estimate, using default instrument parameters gives: 117.18 µm (18.3% difference). Using a new technique of 1) treating the as laser trackers (LR and MR AT901) as independent instruments and having differing associated uncertainties; and, 2) iterating the process until confident that the uncertainty parameters were stable between iterations (converged). Over eight network adjustments the following change of instrument parameters was observed:

The MR AT901 laser tracker:

| Iter. | H (arcseconds) | V (arcseconds) | D (mm) |
|---|---|---|---|
| 0 | 1.0000 | 1.0000 | 0.0075 |
| 1 | 0.9432 | 0.5114 | 0.0277 |
| 2 | 0.9824 | 0.4763 | 0.0357 |
| 3 | 1.0271 | 0.4430 | 0.0424 |
| 4 | 1.0334 | 0.4400 | 0.0450 |
| 5 | 1.0428 | 0.4352 | 0.0476 |
| 6 | 1.0436 | 0.4343 | 0.0488 |
| 7 | 1.0426 | 0.4342 | 0.0494 |
| 8 | 1.0416 | 0.4343 | 0.0497 |

Table 5.19: MR AT901 Laser tracker instrument uncertainty parameters for each network adjustment iteration

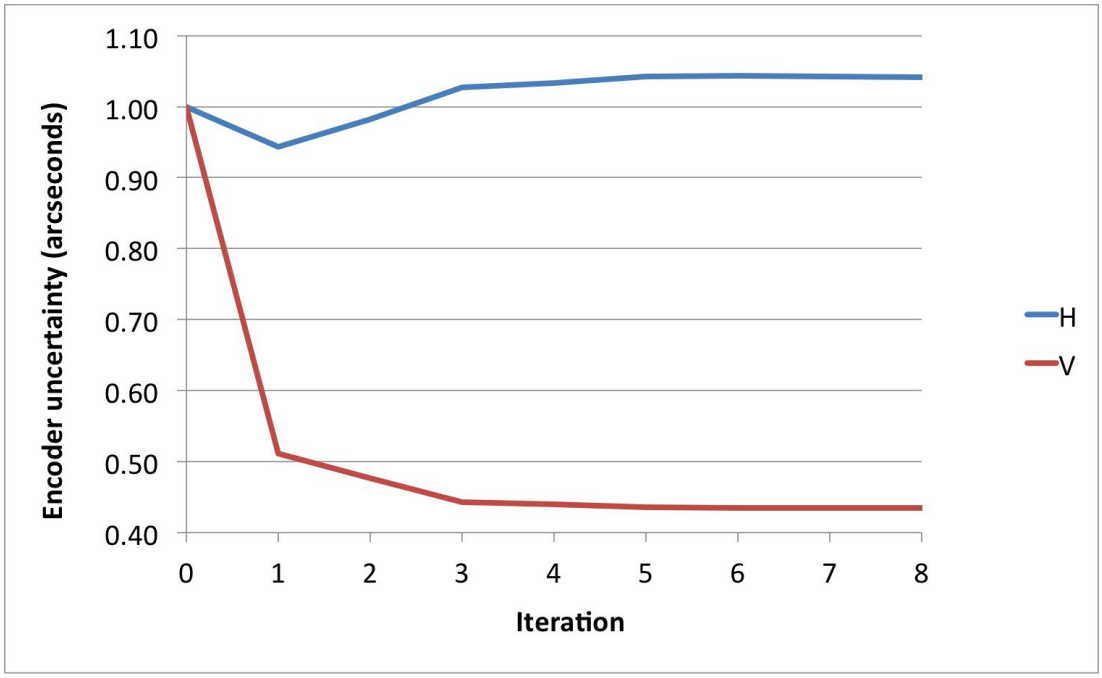


(a) Encoder uncertainty parameters

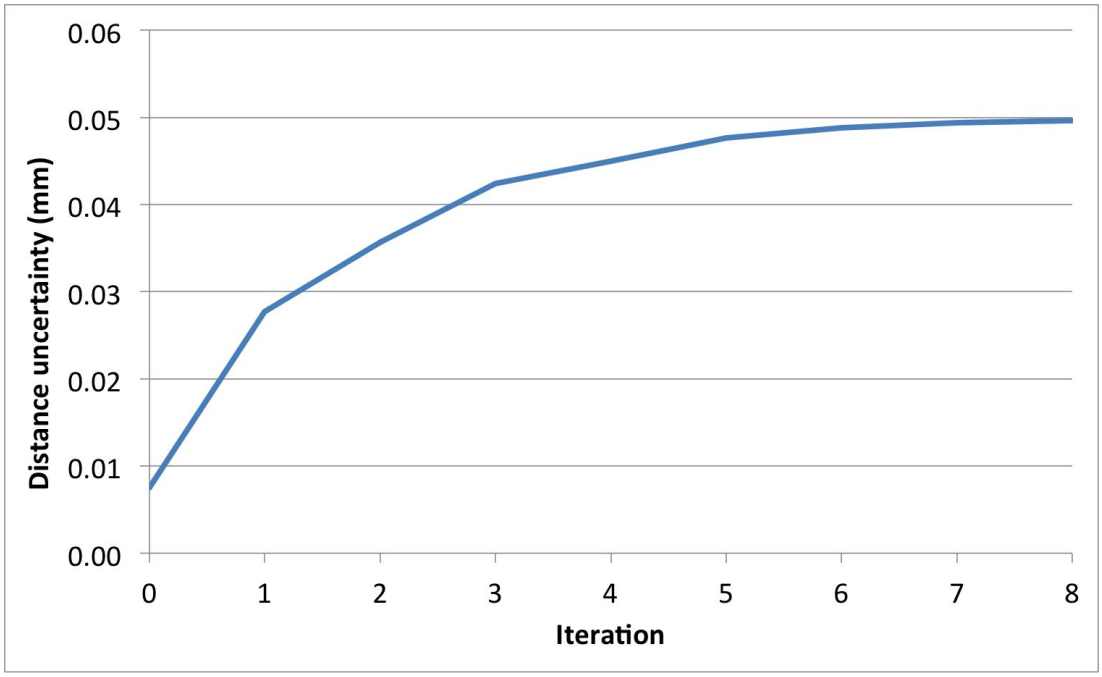


(b) Distance uncertainty parameter

Figure 5-13: MR AT901 Laser tracker instrument uncertainty parameters for each network adjustment iteration

| Iter. | dH (arcseconds) | dH% | dV (arcseconds) | dV% | dD (mm) | dD% |
|---|---|---|---|---|---|---|
| 1 | 0.05678682 | 5.7% | 0.48857424 | 48.9% | -0.0202025 | -269.4% |
| 2 | -0.03918929 | -4.2% | 0.03513835 | 6.9% | -0.00801041 | -28.9% |
| 3 | -0.04472129 | -4.6% | 0.03330259 | 7.0% | -0.00670071 | -18.8% |
| 4 | -0.00629524 | -0.6% | 0.00298612 | 0.7% | -0.00256112 | -6.0% |
| 5 | -0.00934088 | -0.9% | 0.00484306 | 1.1% | -0.00263918 | -5.9% |
| 6 | -0.00085453 | -0.1% | 0.00088376 | 0.2% | -0.00122688 | -2.6% |
| 7 | 0.00098047 | 0.1% | 0.00006106 | 0.0% | -0.00057106 | -1.2% |
| 8 | 0.00099729 | 0.1% | -0.00008300 | 0.0% | -0.00026594 | -0.5% |

Table 5.20: MR AT901 Laser tracker instrument uncertainty changes for each network adjustment iteration

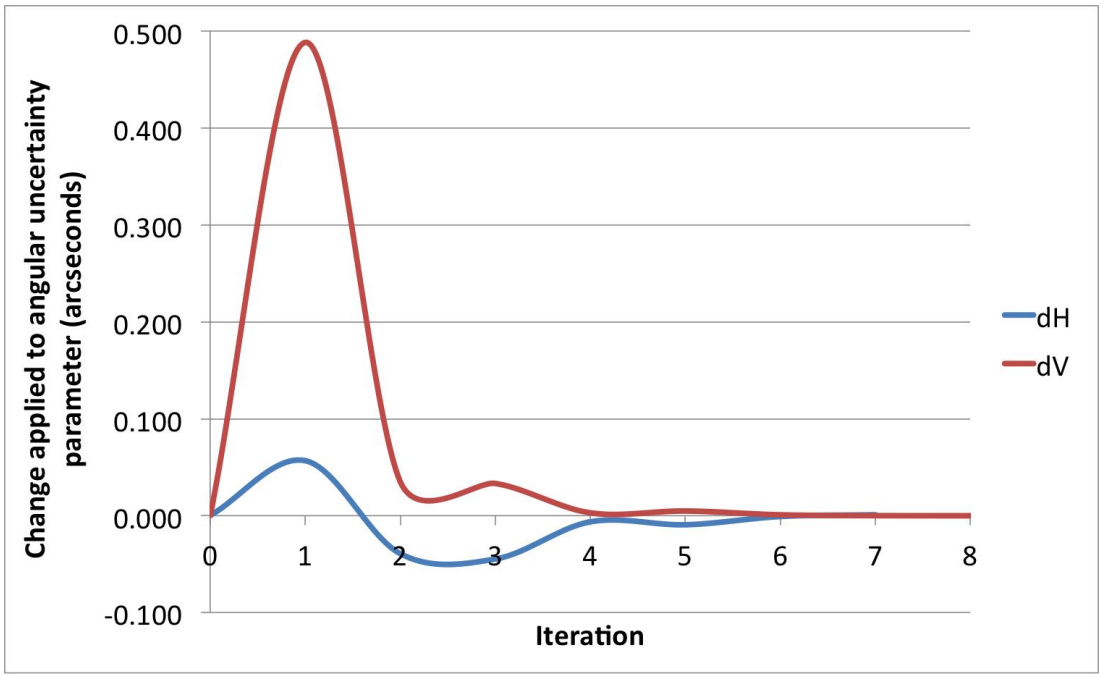


(a) Changes in encoder uncertainty parameters

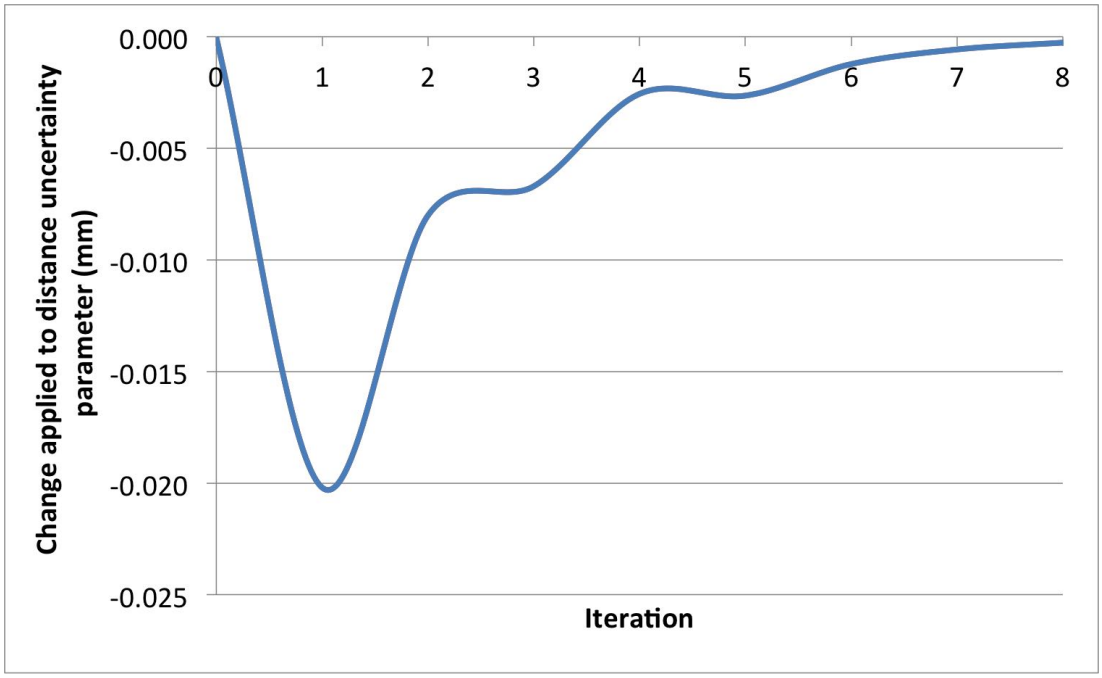


(b) Change in distance uncertainty parameter

Figure 5-14: Changes in MR AT901 Laser tracker instrument uncertainty parameters for each network adjustment iteration

The LR AT901 laser tracker:

| Iter. | H (arcseconds) | V (arcseconds) | D (mm) |
|---|---|---|---|
| 0 | 1.0000 | 1.0000 | 0.0075 |
| 1 | 0.8397 | 0.6101 | 0.0274 |
| 2 | 0.8123 | 0.5116 | 0.0383 |
| 3 | 0.7791 | 0.4381 | 0.0461 |
| 4 | 0.7637 | 0.3794 | 0.0494 |
| 5 | 0.7657 | 0.3608 | 0.0525 |
| 6 | 0.7668 | 0.3540 | 0.0539 |
| 7 | 0.7672 | 0.3513 | 0.0545 |
| 8 | 0.7673 | 0.3503 | 0.0548 |

Table 5.21: LR AT901 Laser tracker instrument uncertainty parameters for each network adjustment iteration

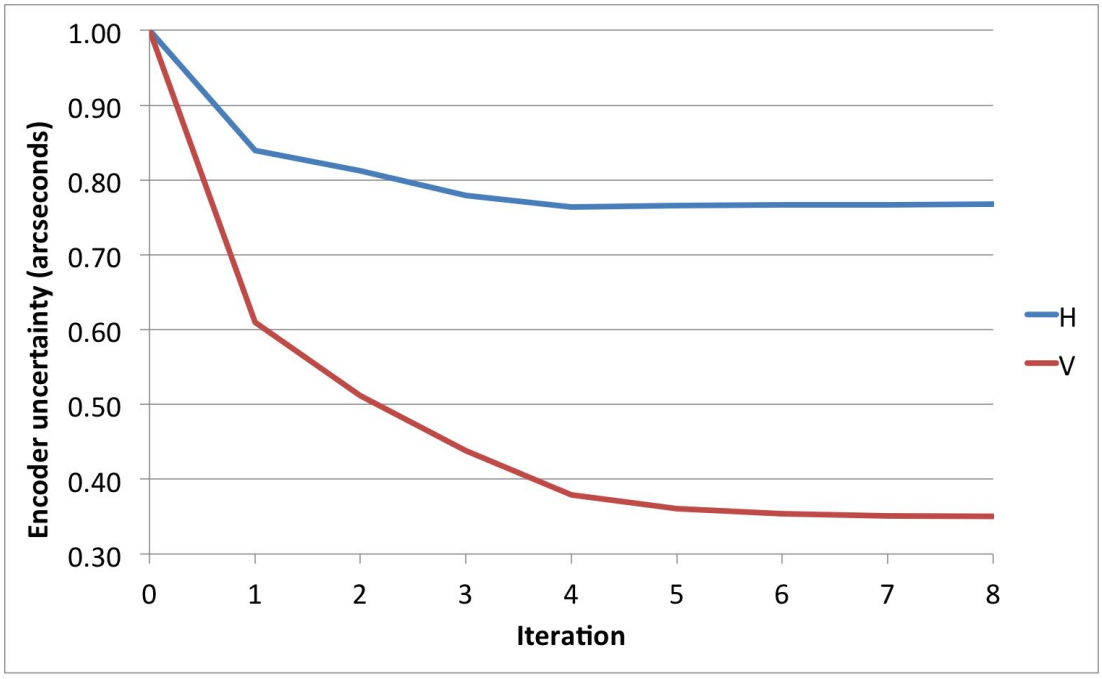


(a) Encoder uncertainty parameters

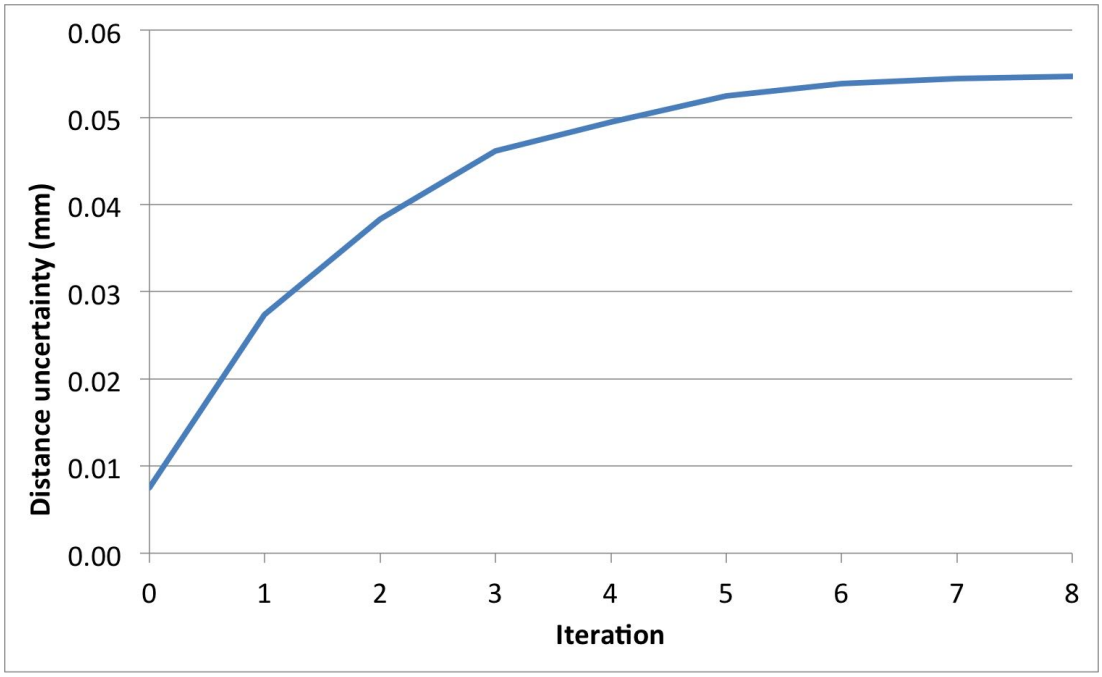


(b) Distance uncertainty parameter

Figure 5-15: LR AT901 Laser tracker instrument uncertainty parameters for each network adjustment iteration

| Iter. | dH (arcseconds) | dH% | dV (arcseconds) | dV% | dD (mm) | dD% |
|---|---|---|---|---|---|---|
| 1 | 0.16033872 | 16.0% | 0.38990300 | 39.0% | -0.01986556 | -264.9% |
| 2 | 0.02732167 | 3.3% | 0.09853050 | 16.1% | -0.01098378 | -40.1% |
| 3 | 0.03323228 | 4.1% | 0.07347922 | 14.4% | -0.00777817 | -20.3% |
| 4 | 0.01536900 | 2.0% | 0.05872778 | 13.4% | -0.00331878 | -7.2% |
| 5 | -0.00200178 | -0.3% | 0.01856117 | 4.9% | -0.00303906 | -6.1% |
| 6 | -0.00101217 | -0.1% | 0.00683650 | 1.9% | -0.00141656 | -2.7% |
| 7 | -0.00041678 | -0.1% | 0.00261206 | 0.7% | -0.00060500 | -1.1% |
| 8 | -0.00016578 | 0.0% | 0.00101578 | 0.3% | -0.00025044 | -0.5% |

Table 5.22: LR AT901 Laser tracker instrument uncertainty changes for each network adjustment iteration

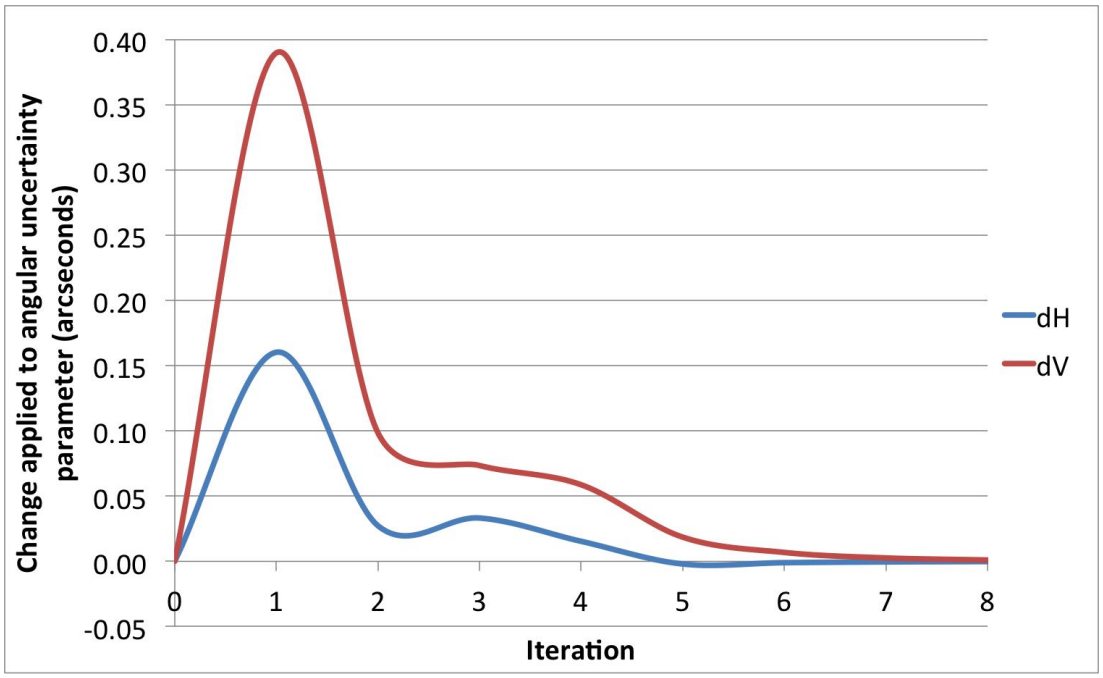


(a) Changes in encoder uncertainty parameters

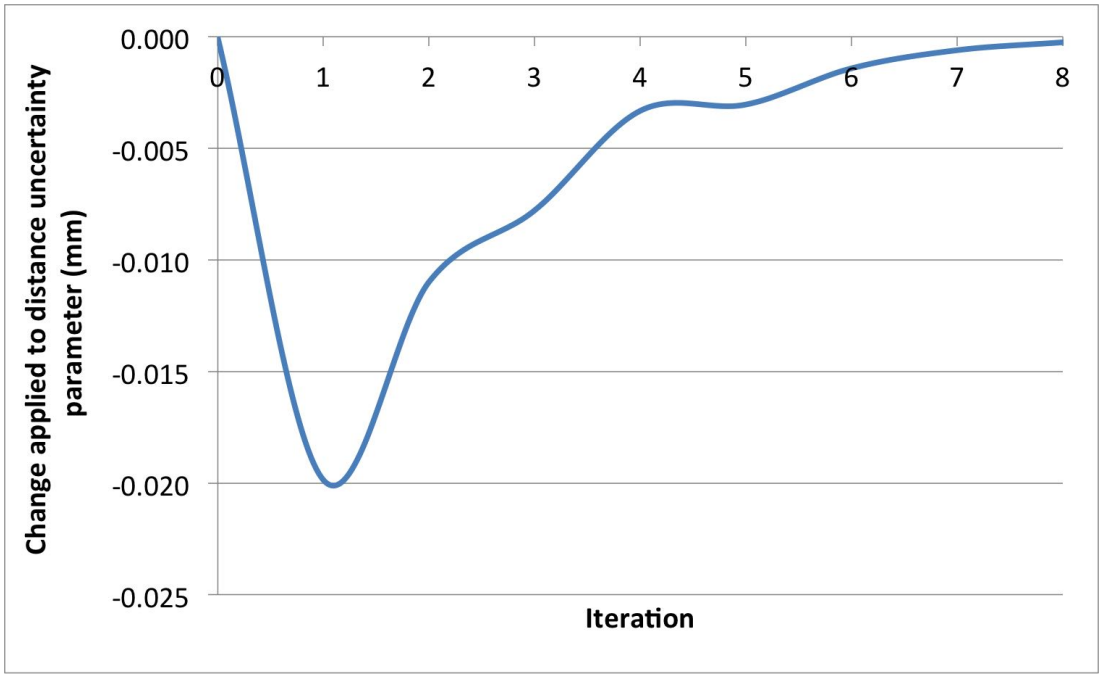


(b) Change in distance uncertainty parameter

Figure 5-16: Changes in LR AT901 Laser tracker instrument uncertainty parameters for each network adjustment iteration

To summarise:

| Uncertainty Parameter | Default Values | Current Practice | Multi-iteration | |
|---|---|---|---|---|
| | | | MR | LR |
| Horizontal (arcsecs.) | 1.0000 | 0.8729 | 1.0416 | 0.7673 |
| Vertical (arcsecs.) | 1.0000 | 0.5837 | 0.4343 | 0.3503 |
| Distance (mm) | 0.0075 | 0.0280 | 0.0497 | 0.0548 |
| Average Network (mm) | 0.1172 | 0.0957 | 0.1084 | |

Table 5.23: Summary of results with FRS network points

Table 5.3.2 illustrates that treating the instruments as independent and using multiple iterations of instrument uncertainty parameters, yields differing uncertainty estimates for each instrument. Based on a converged result of the network adjustment. In this instance both laser trackers are performing better than the specification as the

FRS points are generally planar. This planar measurement also explains the better vertical encoder uncertainty when compared to the horizontal (and the defaults values); as the horizontal encoders were exercised to a far greater extent. The distance measurement uncertainty was significantly higher than the default values, this is due to the uncontrolled factory environment and the long ranging measurements. The MR has performed worse than the LR and is expected to be exacerbated in a more 3D measurement network, such as the ERS and FRS combined network represents.

Now the ERS and FRS network can be considered as a whole, using the current techniques provides a baseline. The ERS and FRS combined dataset (54 reference points) spans a 80 m x 80 m x 6 m volume). Current best practice methods yield average instrument uncertainty parameters as:

| | |
|---|---|
| Horizontal | 1.8393 arcseconds |
| Vertical | 2.0742 arcseconds |
| Distance | 0.0825 mm |

Re-running the adjustment with the updated parameters the same for the LR and MR AT901, generates an average standard uncertainty of: 262.50 µm, whereas the initial network estimate, using default instrument parameters gives: 129.70 µm (102.4% difference). Using multiple iterations of instrument uncertainty parameters philosophy following change of instrument parameters was observed:

The MR AT901 laser tracker:

| Iter. | H (arcseconds) | V (arcseconds) | D (mm) |
|---|---|---|---|
| 0 | 1.0000 | 1.0000 | 0.0075 |
| 1 | 2.1534 | 1.8501 | 0.0839 |
| 2 | 2.0697 | 1.7774 | 0.0957 |
| 3 | 2.0314 | 1.7497 | 0.1026 |
| 4 | 2.0134 | 1.7401 | 0.1062 |
| 5 | 2.0046 | 1.7370 | 0.1079 |
| 6 | 2.0002 | 1.7363 | 0.1088 |
| 7 | 1.9980 | 1.7363 | 0.1092 |
| 8 | 1.9968 | 1.7365 | 0.1094 |
| 9 | 1.9962 | 1.7368 | 0.1095 |

Table 5.24: MR AT901 Laser tracker instrument uncertainty parameters for each network adjustment iteration

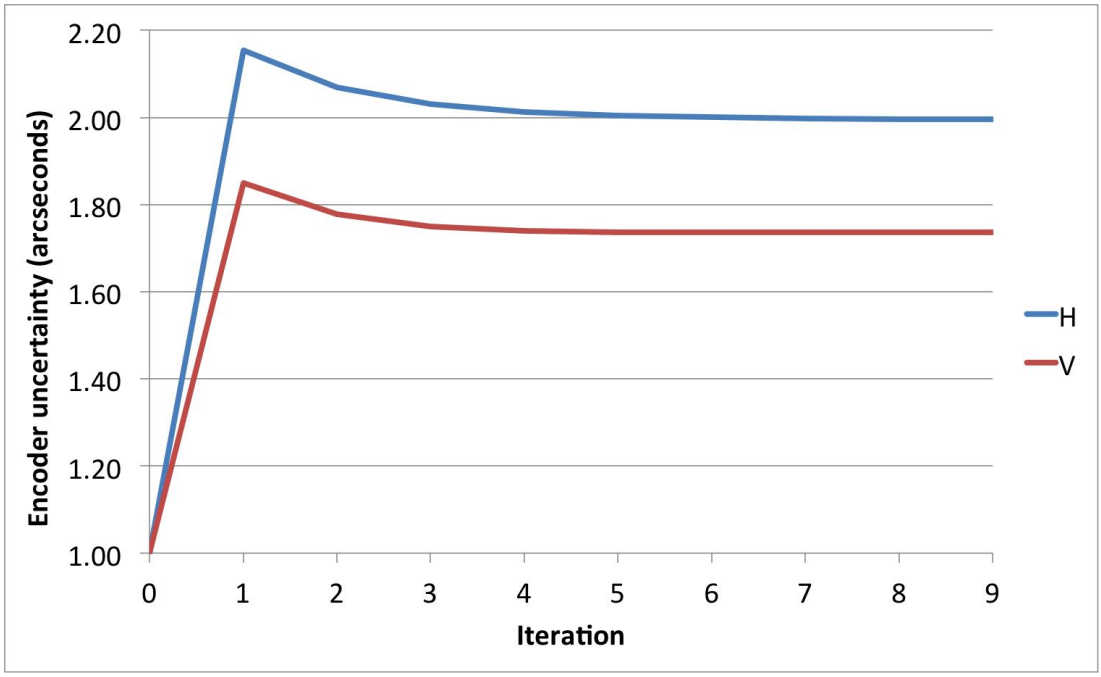


(a) Encoder uncertainty parameters

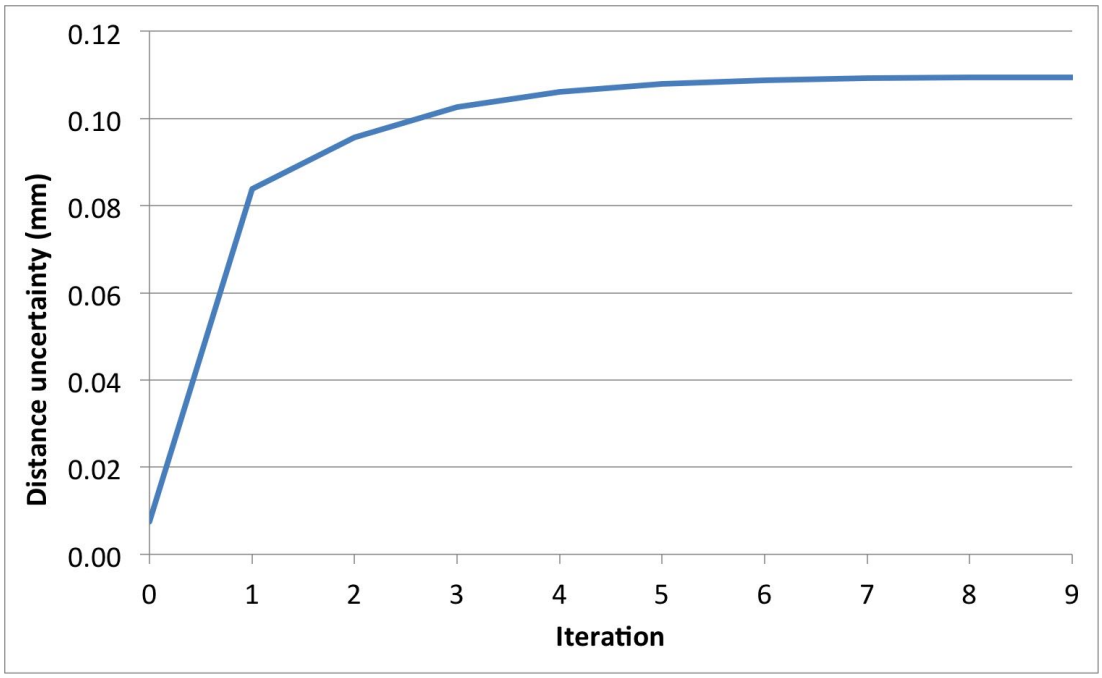


(b) Distance uncertainty parameter

Figure 5-17: MR AT901 Laser tracker instrument uncertainty parameters for each network adjustment iteration

| Iter. | dH (arcseconds) | dH% | dV (arcseconds) | dV% | dD (mm) | dD% |
|---|---|---|---|---|---|---|
| 1 | 1.15341916 | 115.3% | 0.85006863 | 85.0% | 0.07642274 | 1019.0% |
| 2 | -0.08373489 | -3.9% | -0.07270289 | -3.9% | 0.01173126 | 14.0% |
| 3 | -0.03826337 | -1.8% | -0.02764021 | -1.6% | 0.00693558 | 7.3% |
| 4 | -0.01797379 | -0.9% | -0.00963832 | -0.6% | 0.00359911 | 3.5% |
| 5 | -0.00881295 | -0.4% | -0.00308089 | -0.2% | 0.00175895 | 1.7% |
| 6 | -0.00440053 | -0.2% | -0.00071858 | 0.0% | 0.00084784 | 0.8% |
| 7 | -0.00224032 | -0.1% | 0.00004047 | 0.0% | 0.00040968 | 0.4% |
| 8 | -0.00116421 | -0.1% | 0.00021721 | 0.0% | 0.00019958 | 0.2% |
| 9 | -0.00061711 | 0.0% | 0.00020705 | 0.0% | 0.00009811 | 0.1% |

Table 5.25: MR AT901 Laser tracker instrument uncertainty changes for each network adjustment iteration

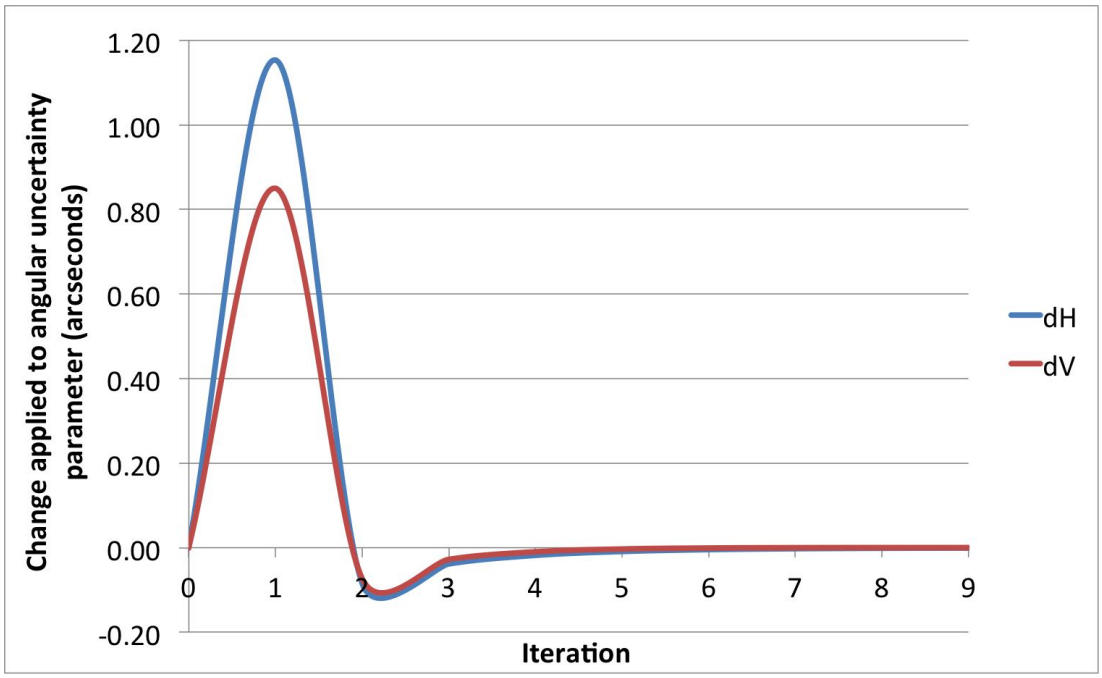


(a) Changes in encoder uncertainty parameters

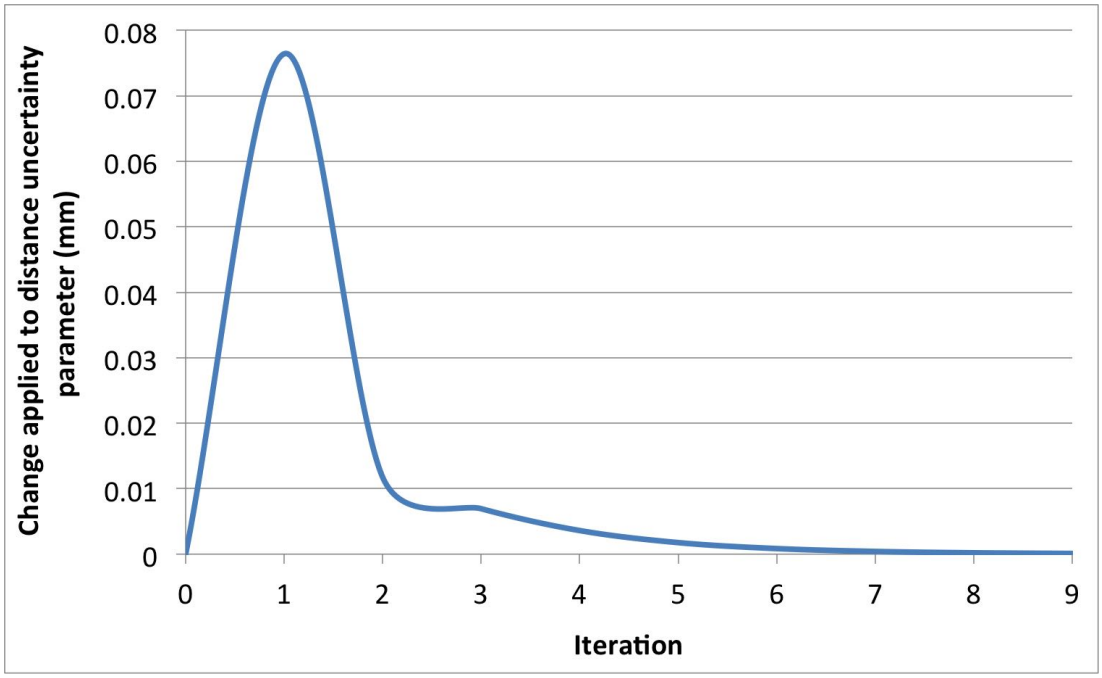


(b) Change in distance uncertainty parameter

Figure 5-18: Changes in MR AT901 Laser tracker instrument uncertainty parameters for each network adjustment iteration

The LR AT901 laser tracker:

| Iter. | H (arcseconds) | V (arcseconds) | D (mm) |
|---|---|---|---|
| 0 | 1.0000 | 1.0000 | 0.0075 |
| 1 | 1.2686 | 1.4835 | 0.0628 |
| 2 | 1.0605 | 1.3196 | 0.0688 |
| 3 | 0.9850 | 1.3365 | 0.0733 |
| 4 | 0.9529 | 1.3427 | 0.0762 |
| 5 | 0.9377 | 1.3449 | 0.0778 |
| 6 | 0.9303 | 1.3457 | 0.0787 |
| 7 | 0.9265 | 1.3460 | 0.0792 |
| 8 | 0.9245 | 1.3461 | 0.0795 |
| 9 | 0.9235 | 1.3461 | 0.0796 |

Table 5.26: LR AT901 Laser tracker instrument uncertainty parameters for each network adjustment iteration

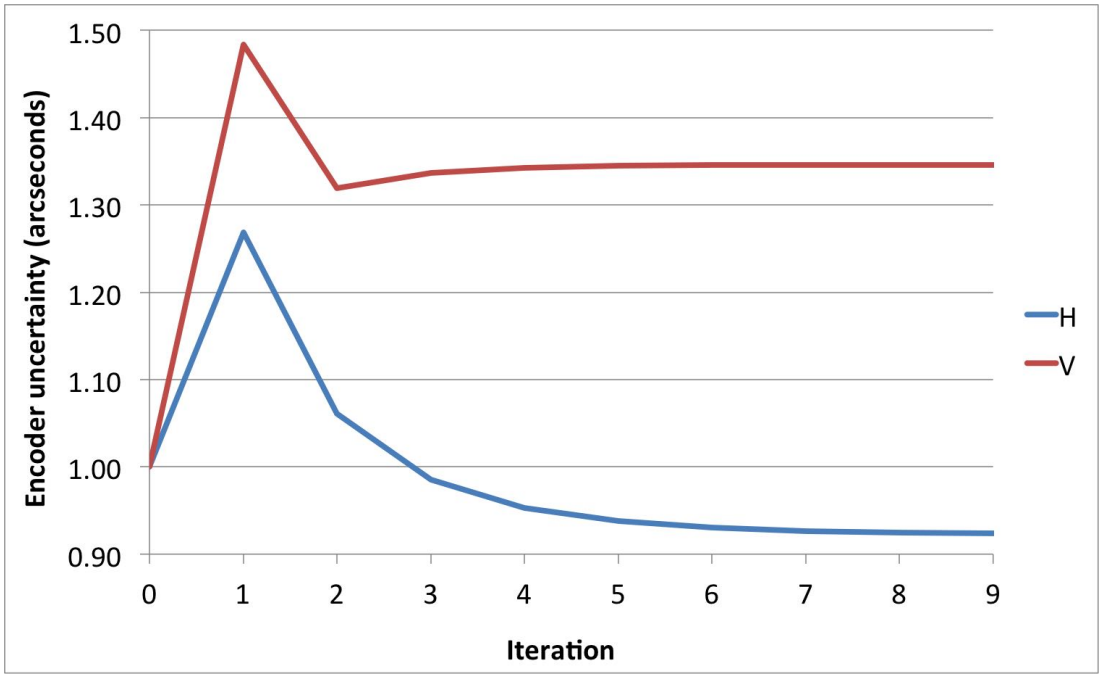


(a) Encoder uncertainty parameters

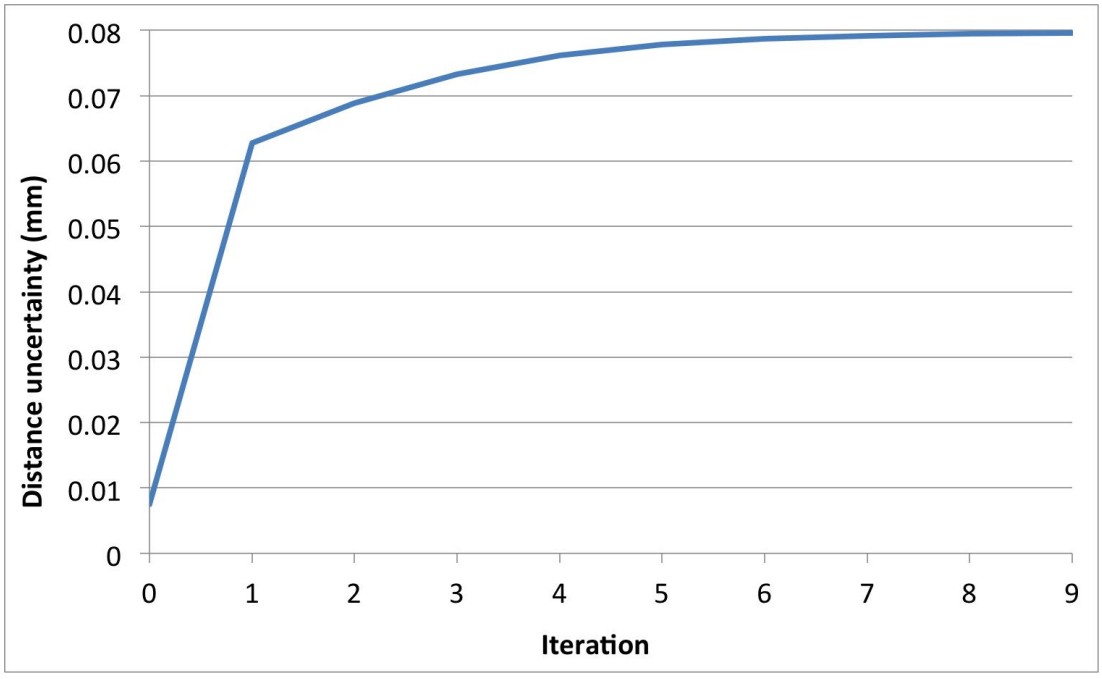


(b) Distance uncertainty parameter

Figure 5-19: LR AT901 Laser tracker instrument uncertainty parameters for each network adjustment iteration

| Iter. | dH (arcseconds) | dH% | dV (arcseconds) | dV% | dD (mm) | dD% |
|---|---|---|---|---|---|---|
| 1 | 0.26863345 | 26.9% | 0.48345675 | 48.3% | 0.05531330 | 737.5% |
| 2 | -0.20813345 | -16.4% | -0.16384505 | -11.0% | 0.00603000 | 9.6% |
| 3 | -0.07547950 | -7.1% | 0.01685560 | 1.3% | 0.00444070 | 6.5% |
| 4 | -0.03216290 | -3.3% | 0.00621305 | 0.5% | 0.00286685 | 3.9% |
| 5 | -0.01512935 | -1.6% | 0.00223465 | 0.2% | 0.00166075 | 2.2% |
| 6 | -0.00747700 | -0.8% | 0.00079920 | 0.1% | 0.00091235 | 1.2% |
| 7 | -0.00378820 | -0.4% | 0.00028315 | 0.0% | 0.00048765 | 0.6% |
| 8 | -0.00194320 | -0.2% | 0.00009735 | 0.0% | 0.00025695 | 0.3% |
| 9 | -0.00100290 | -0.1% | 0.00003060 | 0.0% | 0.00013410 | 0.2% |

Table 5.27: LR AT901 Laser tracker instrument uncertainty changes for each network adjustment iteration

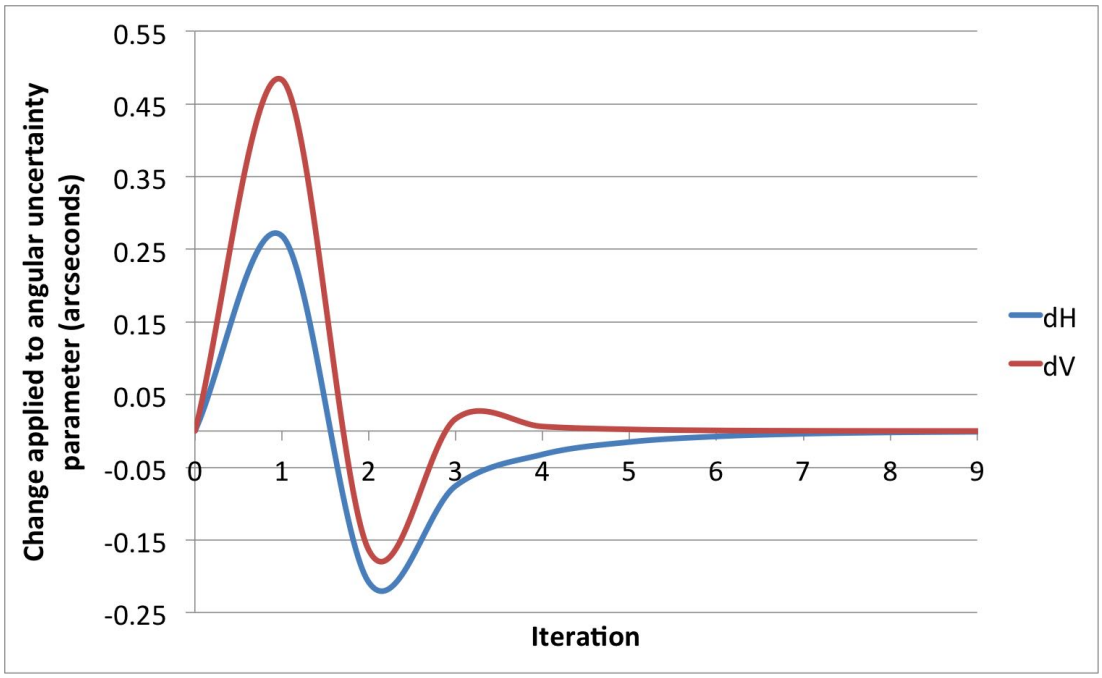


(a) Changes in encoder uncertainty parameters

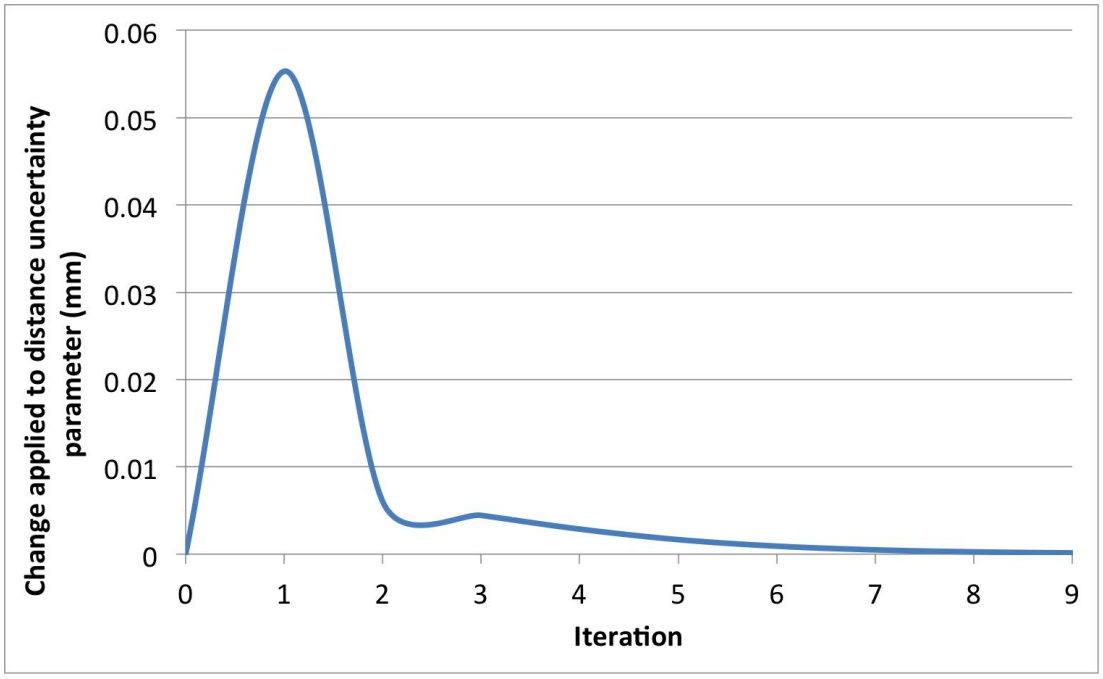


(b) Change in distance uncertainty parameter

Figure 5-20: Changes in LR AT901 Laser tracker instrument uncertainty parameters for each network adjustment iteration

To summarise:

| Uncertainty Parameter | Default Values | Current Practice | Multi-iteration MR | Multi-iteration LR |
|---|---|---|---|---|
| Horizontal (arcsecs.) | 1.0000 | 1.8393 | 1.9962 | 0.9235 |
| Vertical (arcsecs.) | 1.0000 | 2.0742 | 1.7368 | 1.3461 |
| Distance (mm) | 0.0075 | 0.0825 | 0.1095 | 0.0796 |
| Average Network (mm) | 0.1297 | 0.2625 | 0.1895 | |

Table 5.28: Summary of results with ERS and FRS network points

The results shown in Table 5.3.2 illustrate the differences in each approach and the impact on the average network uncertainty. The 3D nature of this network has increased the encoder uncertainty values, with greater uncertainty in the vertical encoders. This larger uncertainty is attributable to the unstable nature of the ERS points, and the

increased use of the vertical encoders when compared to the FRS network in isolation. As with the previous analysis, the MR is performing significantly worse the the LR laser tracker. Lastly the impact the differing approaches have on the network uncertainty has also been exacerbated, with significant differences between the three.

### Uncertainty Budget of Laser Tracker Network

The co-ordinate definition ($n$) of the points in the reference network can be expressed as:

$$n = n_m + n_t + n_n + n_{tp} \tag{5.29}$$

Where:

$n_m$ = This uncertainty source is an average of the uncertainty magnitudes associated to each of the points in the reference network. It has been determined using a Monte Carlo simulation approach on the adjusted network based on the two angular and ranging uncertainties of the laser tracker. This is a statistically determined variance and the standard uncertainty can be obtained by treating this as a normal distribution with a standard deviation of 189.5 µm.

$n_{tp}$ = The constellation of measurements is scaled using a linear expansion model based on average readings from a temperature probe. This probe has a level of associated uncertainty (0.5 °C), which in turn has a dimensional impact on the co-ordinate definitions. The sensitivity co-efficient ($c_i$) is generically defined as:

$$c_i = \frac{\delta f}{\delta x_i} = \frac{\delta f}{\delta X_i}\bigg|_{X_1=x_1 \ldots X_N=X_1} \approx \frac{\Delta f}{\Delta X_i} \tag{5.30}$$

hence, the linear expansion model given by:

$$\Delta L = \Delta T \alpha L \tag{5.31}$$

becomes,

$$\frac{\Delta L}{\Delta T} = \alpha L = c_i \tag{5.32}$$

Substituting the mean inter-point distance and a thermal co-efficient of expansion of concrete gives:

$$\begin{aligned} c_i &= 16.8256804m \times 0.18 \times 10^{-6^\circ}\mathrm{C}^{-1} && (5.33)\\ &= 166.57 \times 10^{-6} m^\circ\mathrm{C}^{-1} && (5.34)\\ &= 166.57\mu m^\circ\mathrm{C}^{-1} && (5.35) \end{aligned}$$

| Standard uncertainty component $u(x_i)$ | Source $X_i$ | Value of standard uncertainty $u(x_i)$ | Sensitivity coefficient $c_i = \frac{\delta f}{\delta x_i}$ | $u_i(n) = \lvert c_i \rvert u(x_i)$ |
|---|---|---|---|---|
| $u(n_m)$ | Network measurement | 189.50 µm | 1.0 | 189.50 |
| $u(n_t)$ | Targeting manufacturing Tolerance | 3.46 µm | 1.0 | 3.46 |
| $u(n_n)$ | Nest manufacturing tolerance | 1.48 µm | 1.0 | 1.48 |
| $u(n_{tp})$ | Temperature probe scaling | 0.5 °C | 166.57 | 83.29 |
| | | | $u_c^2(n) = \Sigma u_i^2(n) = 42\,861.16\,\mu\mathrm{m}^2$ | |
| | | | $u_c(n) = 207.03\,\mu\mathrm{m}$ | |

Table 5.29: Uncertainty contributions for laser tracker network measurement

### 5.3.3 Temperature Variation

The temperature was recorded over the course of the measurement period, the results of which can be seen in Figure 5-21. The temperature was measured across both the floor (FRS) and the wings (ERS) this remained relatively consistent between the ground and the wing, suggesting minimal thermal gradients and a stable environment considering the size and nature of the hangar. However, the temperatures of the wing and floor did begin to diverge during the third day of measurement; this is due to rapid change in weather conditions and the ambient temperature (rising). The wing has a higher thermal conductivity and lower thermal inertia (aluminium) than the factory floor (concrete), this is apparent from the graph as the temperature of the wing rises with the ambient temperature more quickly than the floor on the third day.

In the context of the measurement rapid temperature change appears to give rise to the worst case of differing temperatures on the wing to the ground.

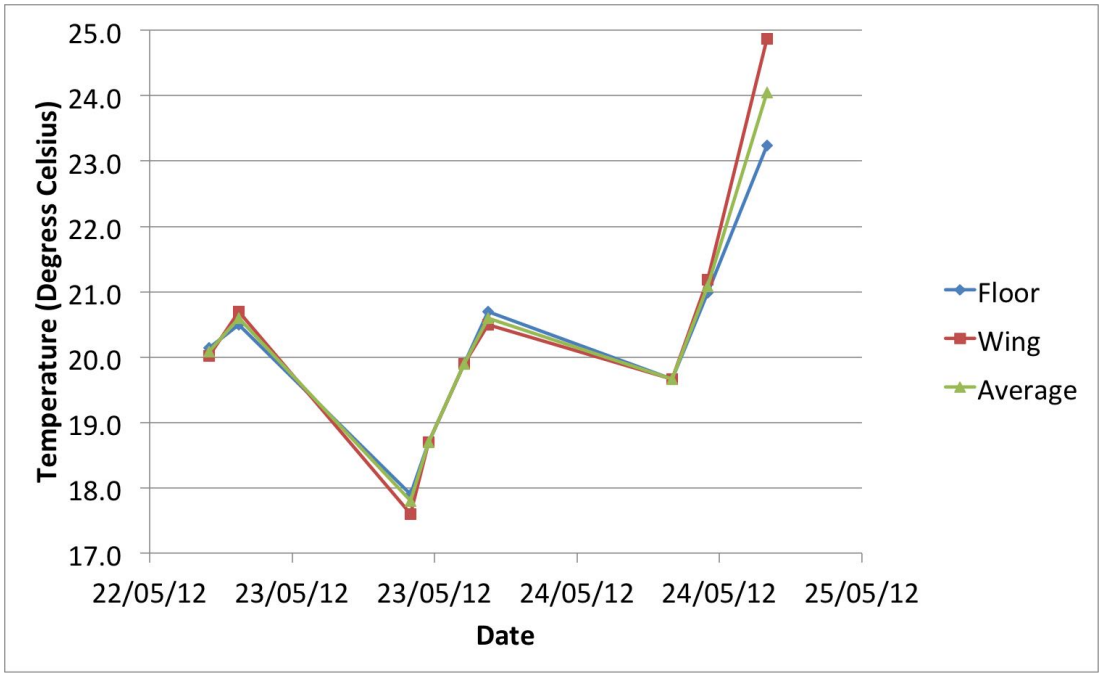


Figure 5-21: Average temperature measurements during the metrology survey

### 5.3.4 Photogrammetry Measurement

The photogrammetric survey targeted the wing surfaces and fuse for reverse engineering purposes, however the ERS were required for global orientation/location and dimensional scale for the bundle, the data requirements were:

- Measurement of ERS
- Measurement of the lower Rib 27 surface
- Measurement of the fuse/Pod area
- Measurement of the upper wing surfaces

The photogrammetry network totalled 1054 images and a measurement of over 36,000 points, this data acquisition and photogrammetric bundle adjustment was carried out by Solve Metrology using V-STARS INCA3 Cameras utilising a elevated platform for access to the upper cover and fuselage. The camera positions and a subset of the respective Fields Of View (FOV) can be seen in Figure 5-22 & Figure 5-23. The photogrammetric bundle adjustment used the co-ordinate definitions from laser tracker network to give dimensional scale to the bundle adjustment over a substantial distance. This differs from traditional methods of using small 1 m calibrated lengths and propagating the scale through the measurement volume.

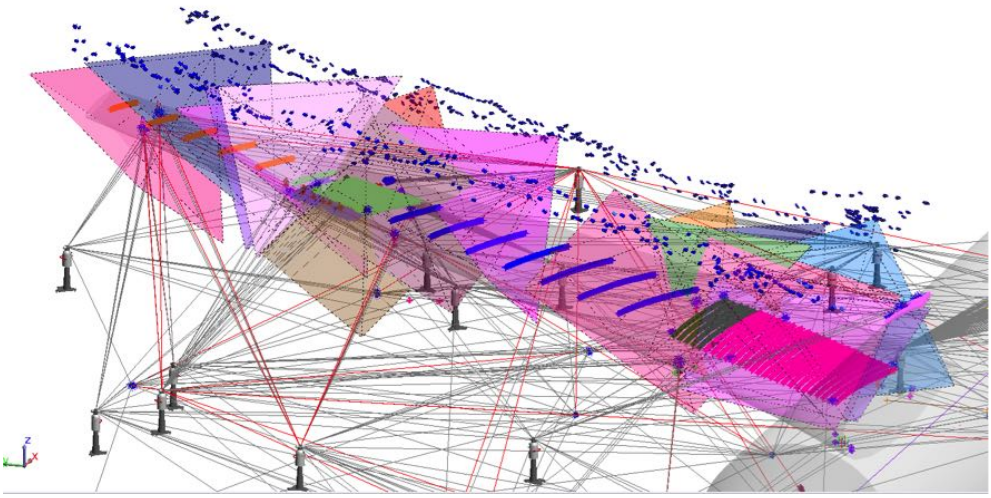

Figure 5-22: DMU showing the laser tracker and photogrammetry measurements across the 30m wing

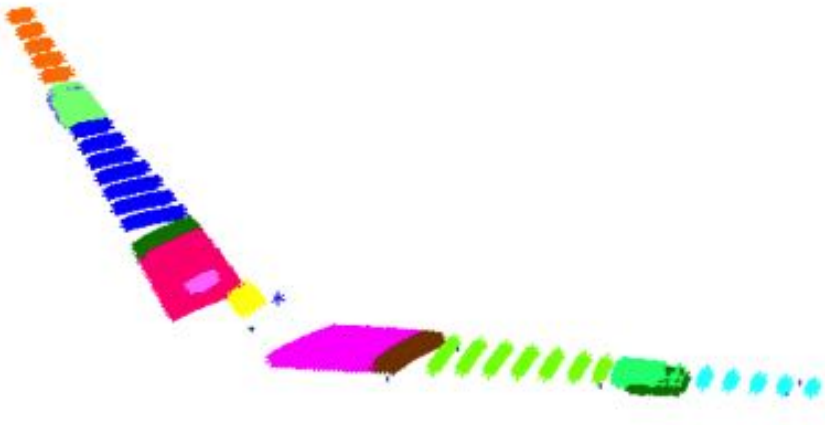

Figure 5-23: Constellation of points measured with the photogrammetry system, across wingspan of approx. 80m

### 5.3.5 Uncertainty Budget

The co-ordinate definition ($n$) of the points in the reference network can be expressed as:

$$n = n + p_{rms} + n_n + c_{td} \tag{5.36}$$

Where:

$c_{td}$ = This uncertainty value was generated as the average difference in temperature. This was 0.18 °C. To estimate the uncertainty contribution for this, By using the difference in thermal expansion coefficient from concrete and aluminium $(23.04 - 9.9) \times 10^{-6}$ and applying a linear expansion model over the mean inter-point distance of 17.62 m.

$$c_i = \frac{\delta f}{\delta x_i} = \frac{\delta f}{\delta X_i}\bigg|_{X_1 = x_1 \ldots X_N = X_1} \approx \frac{\Delta f}{\Delta X_i} \tag{5.37}$$

hence, the linear expansion model given by:

$$\Delta L = \Delta T \alpha L \tag{5.38}$$

becomes,

$$\frac{\Delta L}{\Delta T} = \alpha L = c_i \tag{5.39}$$

Substituting the mean inter-point distance and a thermal co-efficient of expansion of concrete gives:

$$\begin{aligned} c_i &= 17.6395912m \times 13.4 \times 10^{-6^\circ}\mathrm{C}^{-1} && (5.40)\\ &= 238.13 \times 10^{-6} m^\circ\mathrm{C}^{-1} && (5.41)\\ &= 238.13 \mu m^\circ\mathrm{C}^{-1} && (5.42) \end{aligned}$$

| Standard uncertainty component | Source | Value of standard uncertainty | Sensitivity coefficient | $u_i(n) = \lvert c_i \rvert u(x_i)$ |
|---|---|---|---|---|
| $u(x_i)$ | $X_i$ | $u(x_i)$ | $c_i = \frac{\delta f}{\delta x_i}$ | |
| $u(n)$ | Laser tracker network uncertainty | 207.03 µm | 1.0 | 207.03 |
| $u(p_n)$ | Targeting manufacturing Tolerance | 3.46 µm | 1.0 | 3.46 |
| $u(n_n)$ | Nest manufacturing tolerance | 1.48 µm | 1.0 | 1.48 |
| $p_{rms}$ | RMS Fitting residuals to laser tracker network | 290.53 µm | 1.0 | 290.53 |
| $u(p_{tp})$ | Temperature differential uncertainty | 0.18 °C | 238.13 µm/°C | 42.86 |
| | | | | $u_c^2(n) = \Sigma u_i^2(n) = 129\,122.67\,\mu m^2$ |
| | | | | $u_c(n) = 359.34\,\mu m$ |

Table 5.30: Uncertainty estimate of the measurement survey

Due to their esoteric nature LVM uncertainty budgets are rarely explored and documented, as a result, quantifying the magnitude of the uncertainty contributions remains a subjective process, operating within the guidelines (at a global level) set out in the GUM. The uncertainty estimation set out in this section can act as a template for future large volume laser tracker-photogrammetry metrology networks.

## 5.4 Automated Measurement of Aircraft Wing-box Assembly Tooling

Aerospace assembly jigs and fixtures can have global build tolerances of less than 250 µm, over tens of meters. The assembly tools are generally very stable structures that only require periodic checks (recertification) to ensure that the key interfaces are still within tolerance. However, assembly tooling can be compromised by the assembly process. Assembly tooling undergoes stresses from the assembly process, this includes: the weight of the component or sub-assembly, residual stresses from in-tool fastening, vibration from in-tool material removal and accidental damage. Although assembly tooling is designed to cope with these forces, unforeseen stresses and strains can cause less robust pick-ups or flags to become out of tolerance between builds. Additionally, the assembly process may require elements of the assembly tooling to be movable; these movables are then dowelled back into the nominal position when required; this process has inherent uncertainty associated with it. Periodic recertification increases risk of non-conforming assemblies and sub-assemblies moving to the next manufacturing process step undetected. In addition, assembly cannot continue during the recertification process.

As production rates increase the impact of an out of tolerance assembly tool and stopping production for rectification will become significant. Increasing recertification frequency is difficult due to the production down-time impact. The recertification process can take up to *three weeks*; this is dependent on the condition of the assembly tooling and the level of rectification work required. The level of work to correct the tooling is often estimated, and in many cases over-estimated in order to ensure the work does not run over the scheduled time frame. As the aerospace sector increases the rate of manufacture, assembly downtime will become more critical with large non-value adding associated costs. Reduction or elimination of the assembly tooling downtime due to recertification is an important step in reducing manufacturing costs and increasing conformance confidence. Rapid measurement of assembly tooling - *health checks* - are a potential solution to reducing production downtime due to recertification. Rapid assembly tooling health checks would greatly reduce the risk of out of tolerance assembly tooling in production.

The importance of fixture condition is highlighted in the META framework (Chapter 4). This section establishes a methodology for the rapid measurement of fixture condition within the META framework (Figure 5-24).

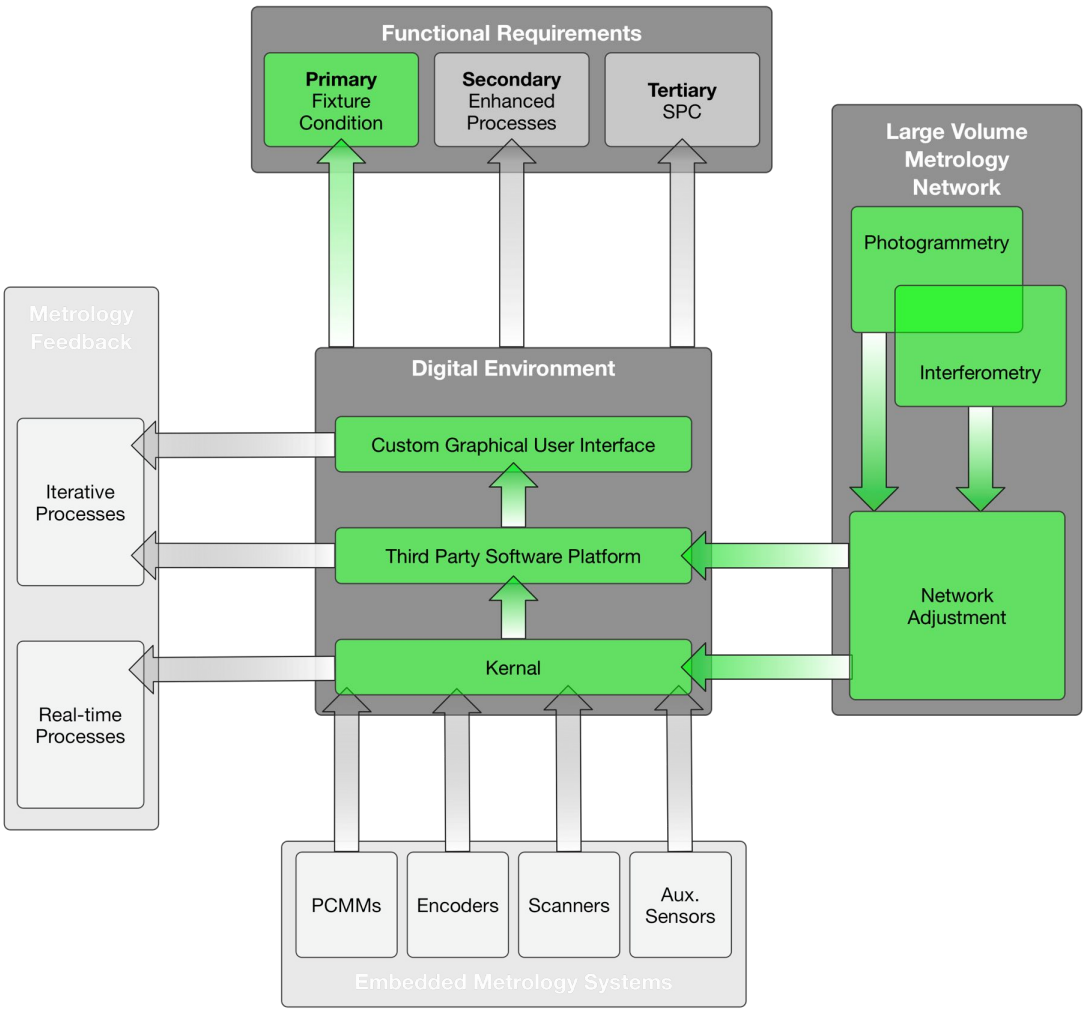


Figure 5-24: META framework elements utilised to achieve rapid health check measurement

Rapid health checks aim to verify the assembly tooling condition before *each* and *every* assembly begins in a short period of time. These health check measurements are of the key interfaces, identifying gross positional errors ($\geq 100\,\mu m$). In addition to verifying the assembly tooling condition, the health check measurements can provide useful empirical information that can be used in *predicting levels of recertification work* and problem areas within a fixture. This will make the full recertification procedure leaner as the work would be quoted and scheduled for the *actual* level of re-work/fixture condition and not the *estimated* level of work.

Current practice employs a reference network of points around the assembly tooling, this is established during the commissioning of the assembly tooling, this is called an

Enhanced Reference System (ERS). The ERS points are are arbitrarily placed around the tooling and measured using a laser tracker network as described in the previous sections. Once measured, these initial ERS co-ordinate definitions are orientated to the tooling axis system and subsequently assigned to the assembly tooling certification documentation. When re-certifying an assembly tool, it is the pick-ups that define the Key Characteristics (KC) and Interchangeability (ICY) criteria that are of interest. The KCs ensure the functional requirements of the design and the ICY criteria ensure component/ sub-assembly's compatibility. These are checked by utilising the ERS system. A laser tracker will locate its relative position by measuring a sub-set of the ERS, scaling for thermal expansion, and best-fitting to the measured points by minimising the residual fitting errors. The laser tracker is now correctly orientated within the global co-ordinate system. Each Point Of Interest (POI) - KC or ICY interface - is measured through the use of additional facility tooling, this tooling targets the specific POI indirectly with a defined offset. If the POI is out of tolerance it is then moved back into its nominal position. Figure 5-25 illustrates the current recertification process, which is described in the *Review of Industrial Practices* (Chapter 3).

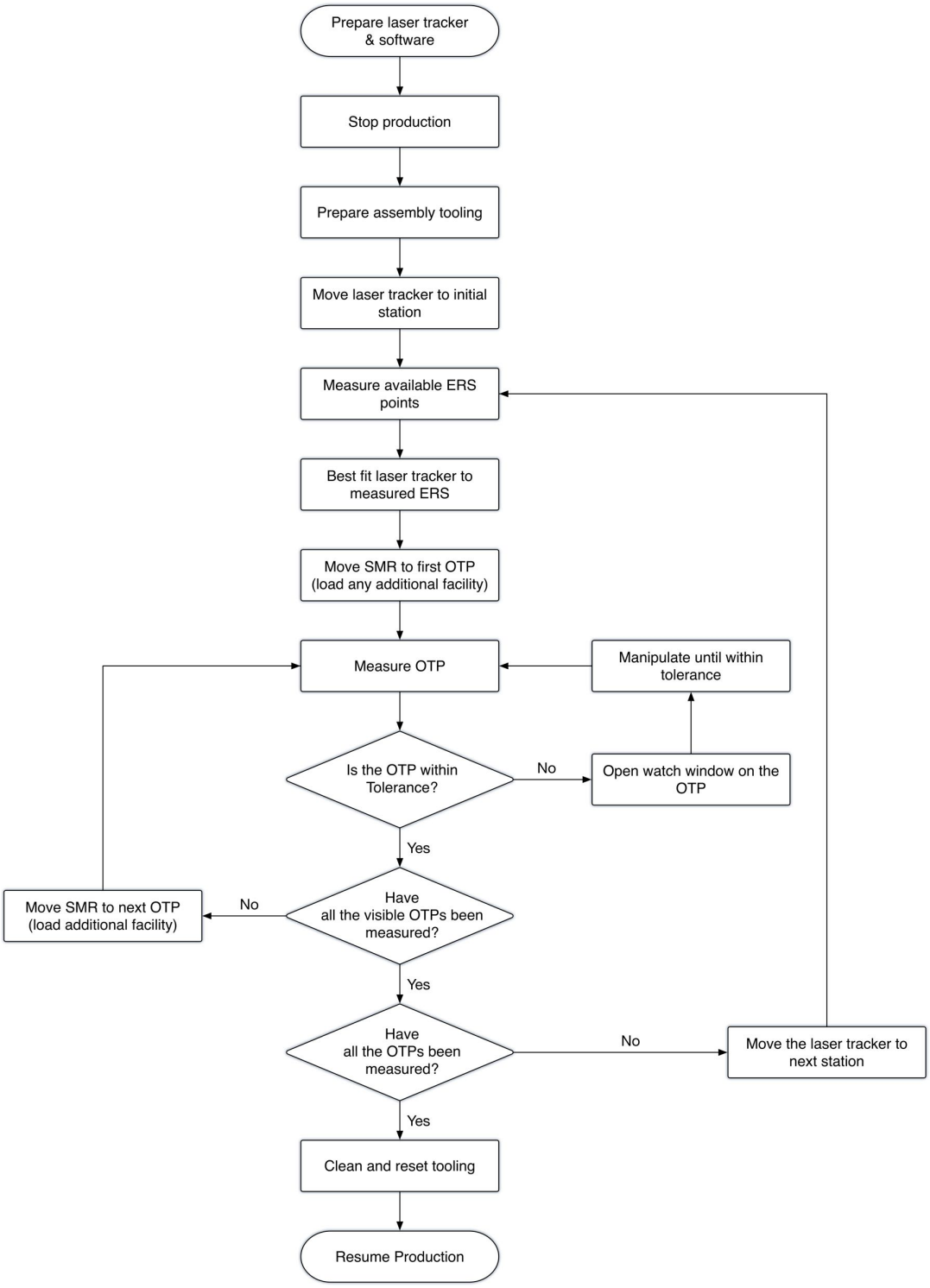


Figure 5-25: Flow chart of the current assembly tooling recertification paradigm

This process requires laser tracker operators to move a Spherically Mounted Retro-reflector (SMR) target to each measurement point, this is time consuming and best carried out with two operators. Additionally, this can be dangerous as it may require working at height.

The measurement instrument to enable rapid health checks will be photogrammetry based. Section 5.2 showed that photogrammetry can provide comparable levels of accuracy in the typical volume of the assembly tooling environment. Whilst providing the following advantages:

- Simultaneous multiple-target measurement,
- Quick measurement time,
- Inexpensive measurement targets.

These advantages, hold potential to challenge current paradigms, in particular 1) POI targeting and 2) data acquisition.

### 5.4.1 POI Targeting

#### Facility Tooling

It is current practice to indirectly measure POIs with the use of facility tooling (Figure 5-26), for better repeatability, ergonomic and instrument line of sight considerations. This additional tooling ensures that the assembly tooling pick-ups are correctly positioned with reference to the CAD nominal position of the assembly KC or ICY requirements. For example: a fixture may hold a hinge bore in an assembly, this hinge axis requires additional facility tooling to target the axis' centreline; this facility tooling could be a bush, vector bar (extrapolation) or sine bar (interpolation).

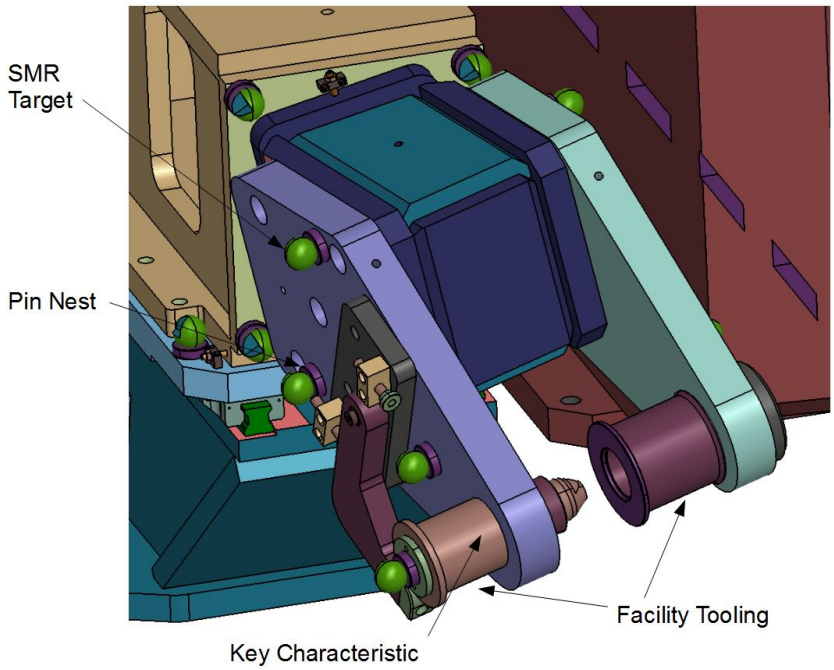


Figure 5-26: Pick-up on the ALCAS MAJ

Although features could be measured directly (in this case the hinge line bore) and the POI calculated, facility tooling ensures speed and consistency of measurement, by reducing operator judgment. However, this traditional tooling is slow and requires either many duplicate tools to be manufactured or a set of tools to be moved around the assembly tool. Simulating the common facility tools, gives a baseline POI uncertainty. Figure 5-27 shows a Monte Carlo simulation of the calculated position of the POI based on two measured points either interpolating or extrapolating the POI, the measured points have a 50 µm associated uncertainty.

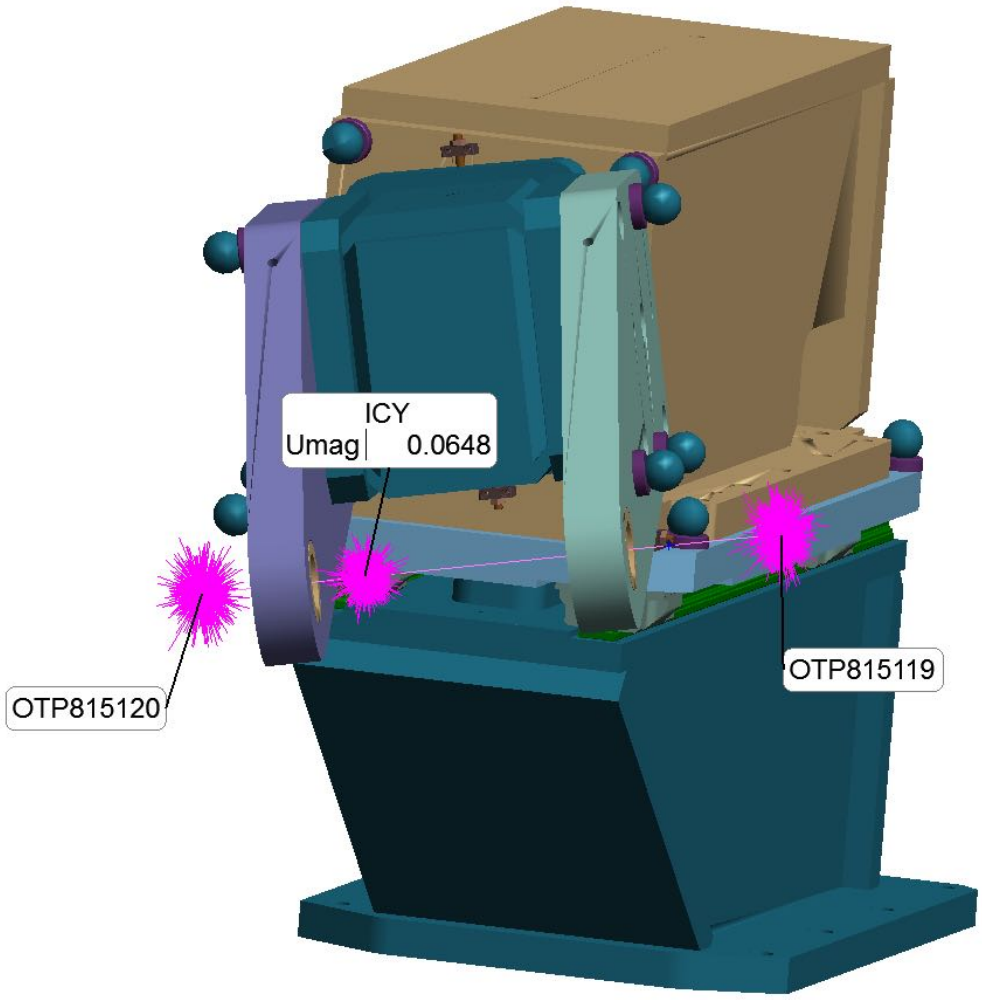


(a) Sine bar MCS of POI uncertainty

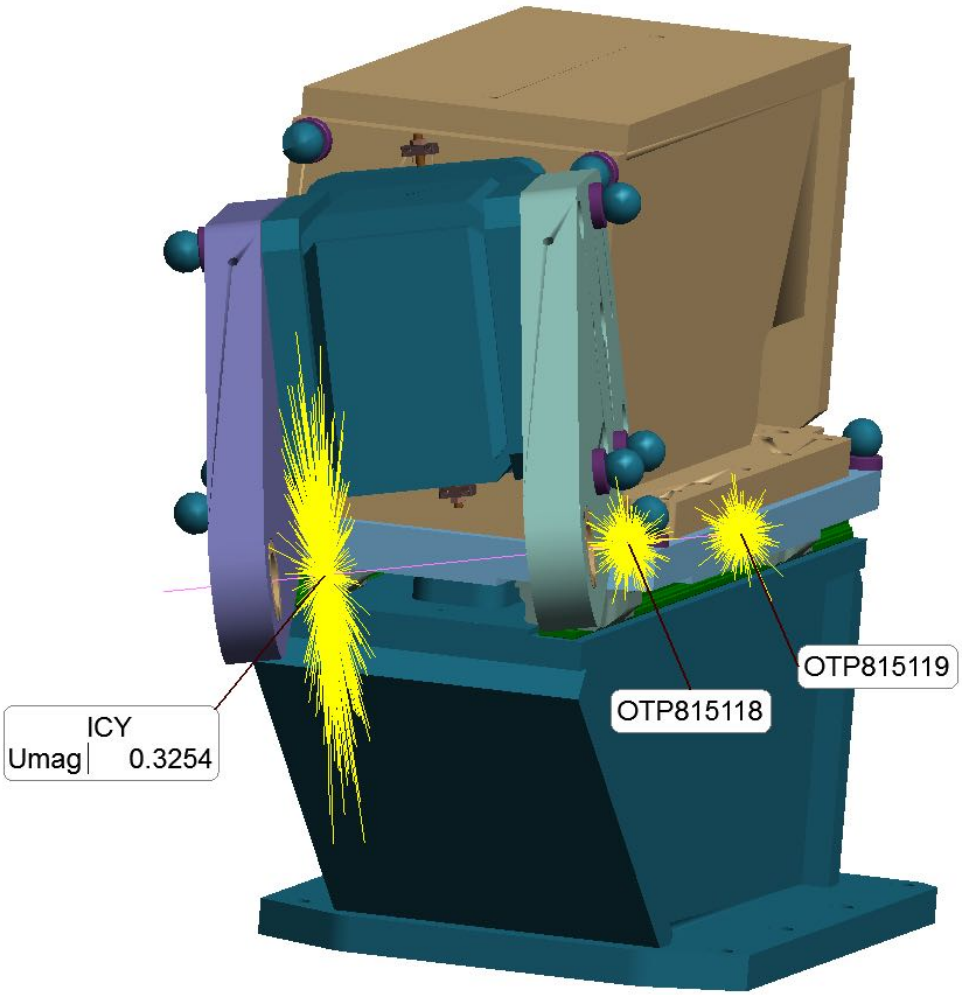


(b) Vector bar MCS of POI uncertainty

Figure 5-27: Comparison of the associated uncertainty when using facility tooling to (a) interpolate or (b) extrapolate the POI; the uncertainty fields are shown.

Intuitively the extrapolation method has a higher uncertainty than that of the interpolation method and this is confirmed in the MCS with the extrapolation method having around 5 times the associated uncertainty. However, interpolation methods are more commonly used and have an uncertainty of 64.8 µm. The different facility tools yield uncertainty estimates of:

| | |
|---|---|
| Interpolation (Sine bar) | 64.8 µm |
| Extrapolation (Vector bar) | 325.4 µm |

Photogrammetric methods could reduce the dependency of facility tooling and increase the measurement process of POIs by utilising Rigid Body Transforms (RBTs), described below.

### Rigid Body Transform

A future state using Rigid Body Transforms (RBTs) to interpolate the POI(s) negates the use of facility tooling and is enabled by employing photogrammetry.

Measuring three or more points enables the position and orientation of a rigid body to be defined in all Six Degrees Of Freedom (6DOF). If a suitably rigid structural connection exists between the measured points and the POI, then an offset can reliably be applied. This relationship has to be calibrated using facility tooling and would take place at the assembly tooling commissioning stage. As with traditional facility tools, there is potential to either: 1) interpolate, or, 2) extrapolate, the POIs co-ordinate definition. Figure 5-28 shows the uncertainty fields generate via a MSC of the two options with three targets, the uncertainty estimate of the POI are:

| | |
|---|---|
| Interpolation | 52.8 µm |
| Extrapolation | 215.4 µm |

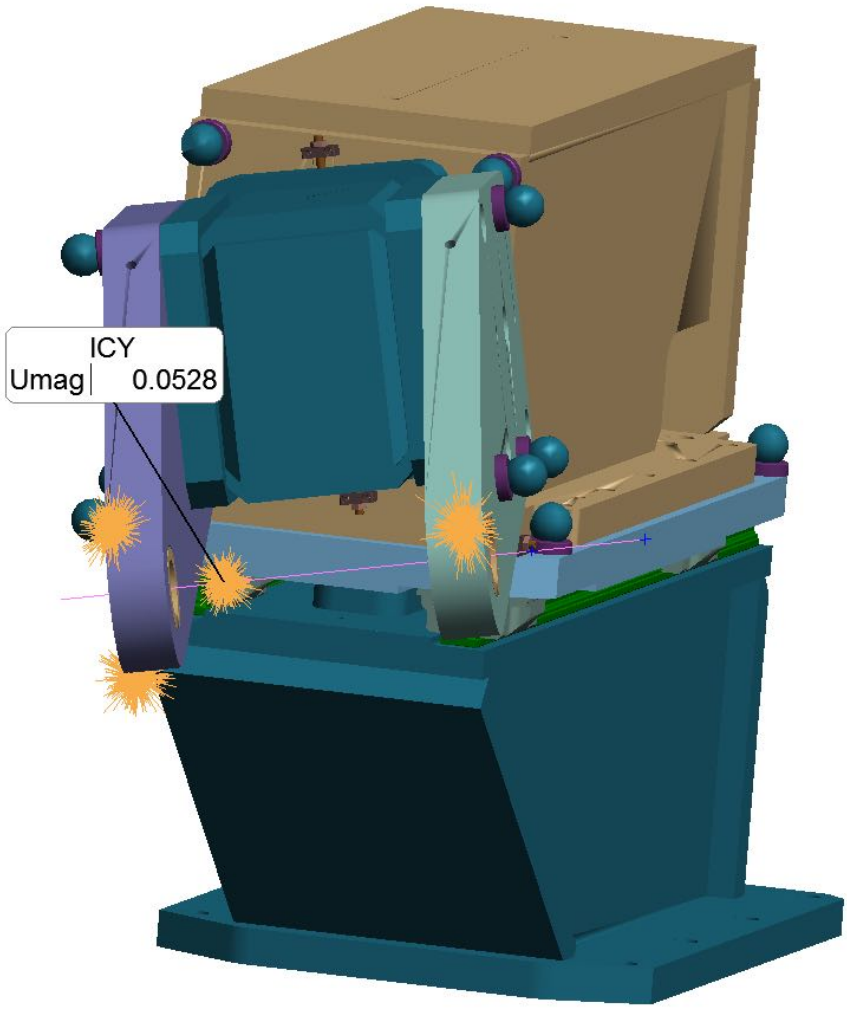


(a) MCS of POI uncertainty using 3 photogrammetry targets to interpolate

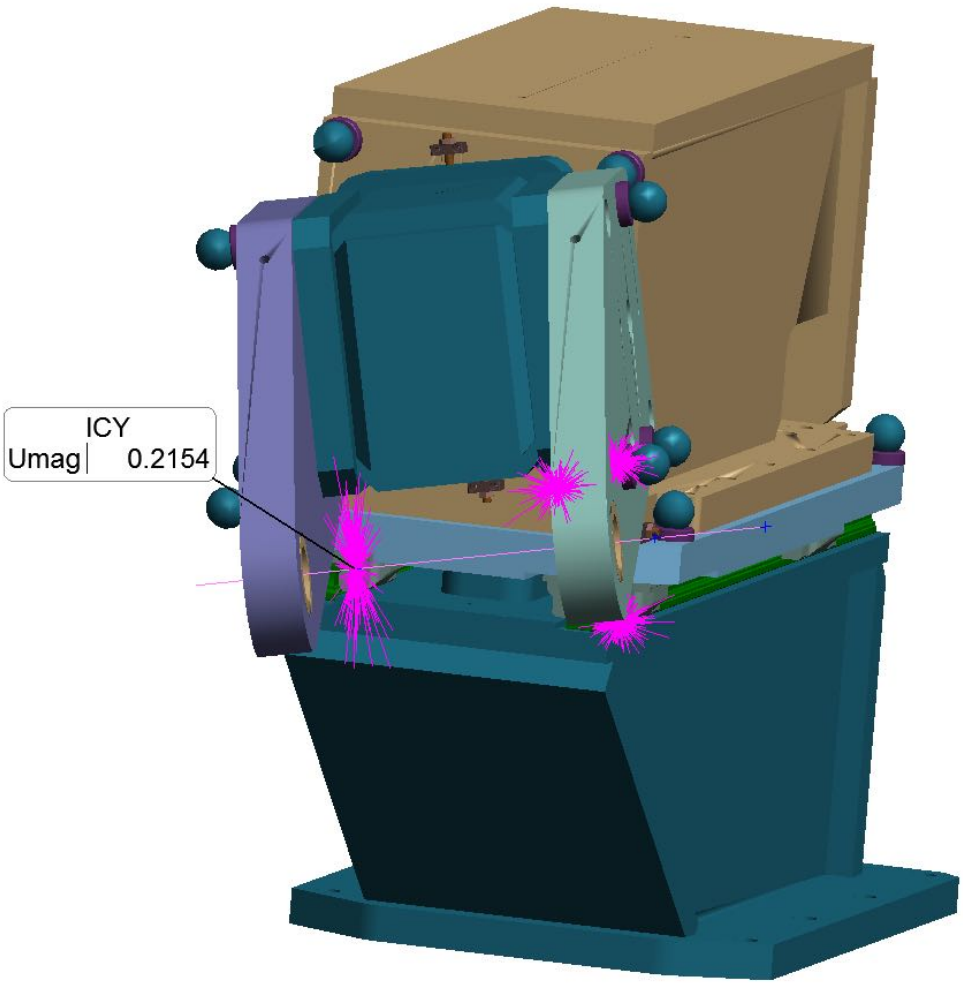


(b) MCS of POI uncertainty using 3 photogrammetry targets to extrapolate

Figure 5-28: Comparison of the associated uncertainty when using 3 photogrammetry targets to (a) interpolate or (b) extrapolate the POI; the uncertainty fields are shown.

This new POI targeting philosophy could be applied to existing fixtures and laser tracker instruments, measurements could be rapidly achieved by leaving SMR targets in-situ, however this could become prohibitively expensive if using accurately centred SMRs. An advantage of using photogrammetry for these measurements is that the targets that define the offset can be adhesive targets of negligible cost. These do not have to be in predefined positions, rather, the adhesive targets can be arbitrarily and abundantly placed around the POI(s) and subsequently calibrated relative to the POI(s). This means that tens of un-coded, single point targets can be used per POI

to ensure measurement redundancy and an increased accuracy, therefore the offsets are more accurately applied. The number of targets required to achieve a comparable uncertainty to that of the existing facility tooling is three, as demonstrated in the above MCS results. However, as photogrammetry holds the potential to measure many points simultaneously with out any adding any time for the data acquisition simulations were carried to investigate the reduction in associated uncertainty to the POI when the number of targets used in the rigid body transform was increased. These is a physical limitation on a tooling pickup as to how many targets , Figure 5-29 shows that reduction in uncertainty is significant, but with diminishing returns.

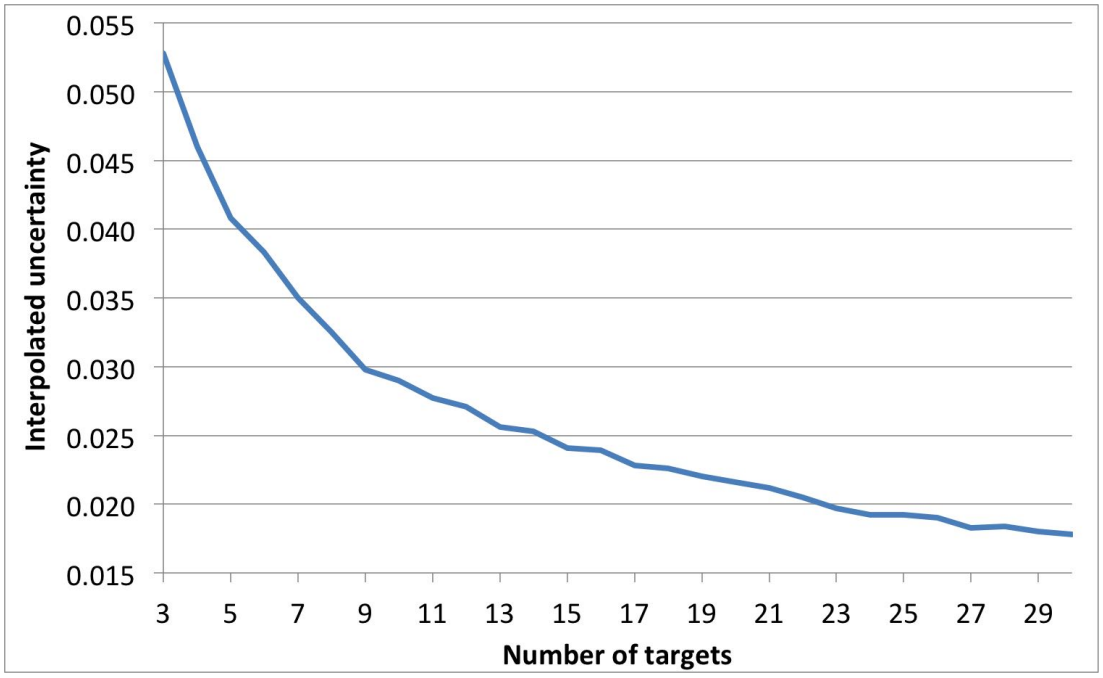


Figure 5-29: Number of photogrammetry targets affect on interpolated POI uncertainty

Figure 5-30, visually indicates the uncertainty reduction when increasing the number of targets in the rigid body transform.

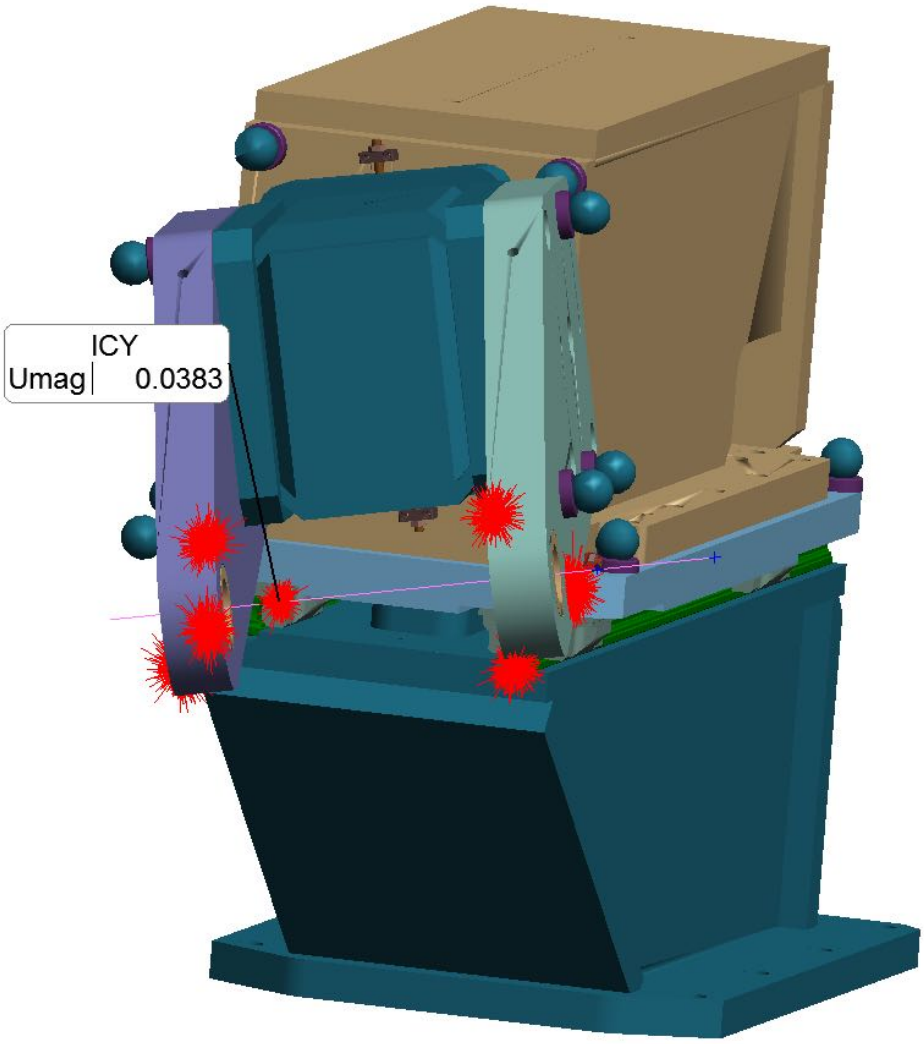


(a) MCS of POI uncertainty using 6 photogrammetry targets to interpolate

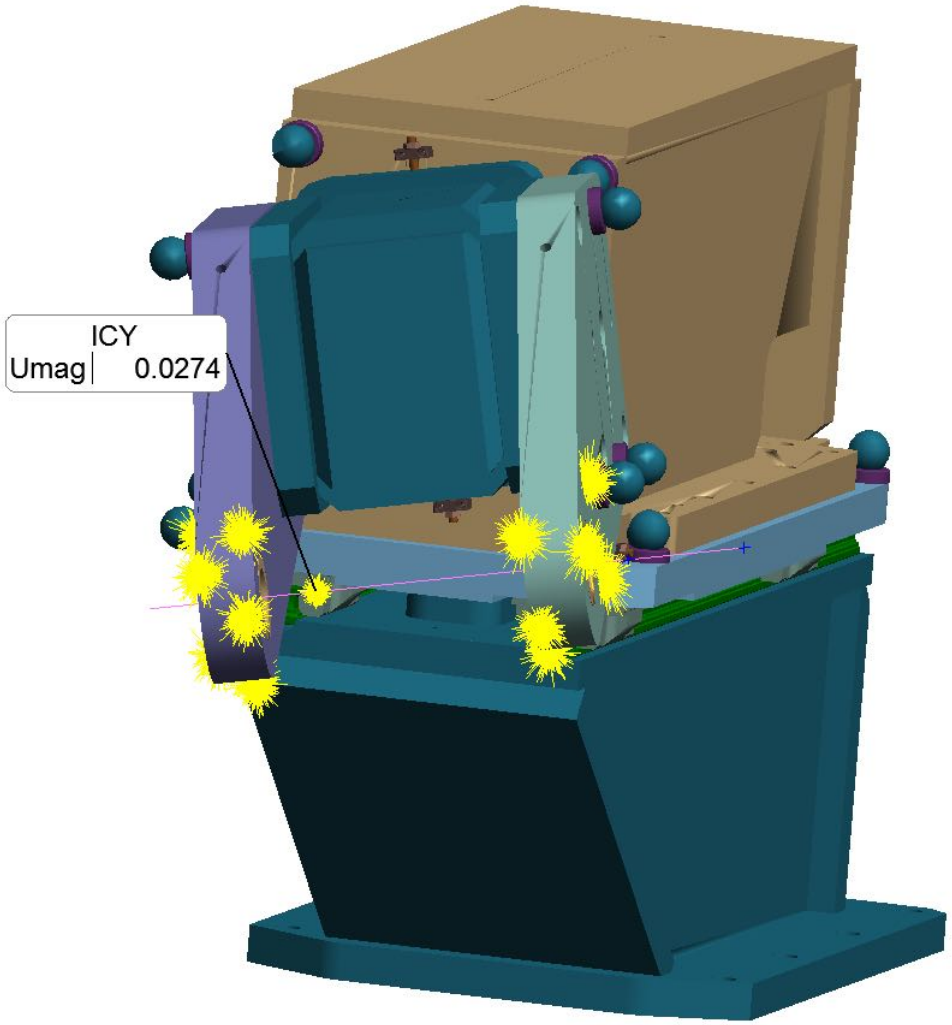


(b) MCS of POI uncertainty using 12 photogrammetry targets to extrapolate

Figure 5-30: Comparison of the associated uncertainty when interpolating the POI with photogrammetry targets; the uncertainty fields are shown.

More measurement redundancy, decreases line of sight issues as well as insuring against target damage during the assembly process. Coded targets would be deployed to enable localised system referencing and enable measurement process automation. To assess the

Facility tooling can only be used when the fixture is empty as the pick-up and POI is usually covered by components. Sufficient redundancy in photogrammetric RBTs could

facilitate health check measurements during the assembly, ensuring that the tooling has not moved during the loading and assembly processes. Consequently, concessions could be identified whilst still in-fixture.

Rigid body transforms to interpolate the POI and leaving the targets in-situ holds additional advantages such as lower measurement time and increased automation potential. Automation potential comes from negating the need to place facility tooling and manually moving an SMR to each POI. Photogrammetry systems are light and require stability over a very short time-period for each measurement image to be acquired. These attributes allow systems to be mounted onto an end effector or overhead gantry system without the difficulties of accurate positioning of creating periods of stability. This is developed further in the following section.

### 5.4.2 Automated Data Acquisition

In order to achieve a rapid health check measurement the data acquisition needs to be automated. Full automation of the data acquisition process is enabled by employing the RBT POI targeting method (described above), this should be adopted in conjunction with photogrammetric systems. In addition to simultaneous measurement, photogrammetry systems are well suited for automated data acquisition, due to the following characteristics:

- Long periods of stability are not required
- The measurement systems are light
- Targeting can remain in-situ
- The measurement process is passive
- Accurate positioning is not required
- Remote triggering and data transfer options

To automate the data acquisition, the metrology system would be attached to a serial axis industrial robot, on a rail system. The complexity and orientation of the rail system is largely dependent on the assembly tooling geometry and the factory layout/access.

### 5.4.3 Automation of Analysis

SpatialAnalyzer (SA) is the metrology software used across the aerospace sector; within SA are many instrument interfaces which enables multiple instruments from different manufacturers to be used together and networked. Additionally, SA has a scripting mechanism - *measurement plan* - that allows metrology tasks to be automated; this could be the measurement, analysis or reporting tasks. This internal scripting can be used to automate or semi-automate measurement processes.

SA MP can automate measurement processes however SA MP makes some relatively simple programming structures - such as conditional logic, loops, and mathematical operations - cumbersome and overly complicated.

The SA MP features can be accessed via the Software Developers Kit (SDK), this enables SA to be used as a platform and the functions accessed via standard programming languages such as VC++ and VB. Giving rise to a more robust method of interfacing with SA and combining the programming power of a standard programming language and an open architecture for any additional interfacing requirements. This approach was used to fully automate the data analysis. This included the following:

- Automated processing of the robot measurement images
  - Auto-loading of images
  - Image processing and bundling
  - Output results
- Analysis in SA
  - Load measurement results
  - Unified Spatial Metrology Network (USMN)/RBT process
  - Compute deviations
  - Report results and uncertainties
- RAG Health decision process
  - Load analysis results in excel
  - Run conditional logic
  - Report

A common programming language enabled the project to establish communications with the metrology software SDK, the SA SDK, and Excel to automate all aspects.

Traditionally, a fixture is either within tolerance or out of tolerance, however this does not often consider measurement or process uncertainty (Section: 2.3), with respect to the tolerance (Section: 2.4); once this measurement uncertainty is taken into consideration, a third, ambiguous state becomes necessary to indicate a scenario where the fixture may or may-not be within tolerance but a more accurate, rigorous method of measurement is required.

These these measurement outcomes: Red, Amber, Green (RAG) can be summarised as:

- `Green`: Key Characteristics (KCs) on the fixture are within tolerance of their nominal position,
- `Amber`: Unable to determine that the KCs on the fixture are within tolerance (due to measurement/process uncertainty),
- `Red`: KCs are not within tolerance of their nominal position.

The rapid fixture health check will output a simple colour indication of the fixtures' condition based on the above.

### 5.4.4 Rapid Fixture Health Checks - Generic Process

This section introduces a generic process for the implementation of rapid health check measurements for aerospace assembly tooling structures. The generic process is separated into three sections:

- Commissioning
- Rapid Health Check
- Associated Uncertainty

#### Commissioning

The steps that need to take place to enable the rapid health check are:

1. Manually measure the secondary datum structure with a laser tracker network. This is already carried out within assembly tooling commissioning. Perform a network adjustment and uncertainty estimates based on learning from Section 5.3. The output is a co-ordinate definition for the ERS and an uncertainty estimate.

2. Manually manipulate the tooling pick-ups into nominal position using traditional facility tooling and a laser tracker oriented via the ERS (secondary datum structure from step 1). The output is the OTP co-ordinate definition.

3. Position in-expensive, adhesive photogrammetry targets around the tooling pick-ups; using a minimum of 6 targets per POI and ensuring the POI is enveloped. This will ensure sufficient redundancy and that the POI is determined using interpolation (as described in subsection 5.4.1).

4. Manually measure the ERS points and photogrammetry targets with the photogrammetric system. This establishes the relationship between the expensive and limited ERS targets with the in-expensive and abundant photogrammetry targets. In turn, the relationship to the OTPs can be inferred. The ERS points from the laser tracker network measurements act as control points with the photogrammetric bundle to provide scale and a common co-ordinate system (as in Section 5.3). In addition to the co-ordinate definition, an uncertainty estimate should be established (as in Section 5.2).

5. Finally, the photogrammetry system measures the photogrammetry targets in isolations, from which the OTPs can be interpolated (via the relationship established in step 4 and RBTs see Section 5.4.1). This activity provides the resected camera positions; these positioned can be treated as Tool Centre Points (TCPs) for the serial axis robot to move to for each image capture.

these are summarised in Table 5.31:

| ID | POI | Task | Analysis | Output |
|---|---|---|---|---|
| 1 | ERS | Manual laser tracker measurement | Network adjustment | ERS co-ordinate definition and uncertainty estimate |
| 2 | OTP | Manual manipulation and laser tracker measurement of tooling pick-ups | OTP co-ordinate definition | |
| 3 | N/A | Position photogrammetry targets on tooling pick-ups | N/A | N/A |
| 4 | ERS & Photo. Targets | Manual photogrammetric measurement of ERS points and photo. targets | Bundle adjustment | Co-ordinate definition of photo. targets and uncertainty estimate |
| 5 | Photo. Targets | Manual photogrammetric measurement | Bundle adjustment & RBTs | Resected camera positions, OTP co-ordinate definition & process uncertainty estimate |

Table 5.31: Commissioning tasks required to enable rapid health check measurements

**Rapid Health Check**

The execution of the rapid health check is as follows (Figure 5-31):

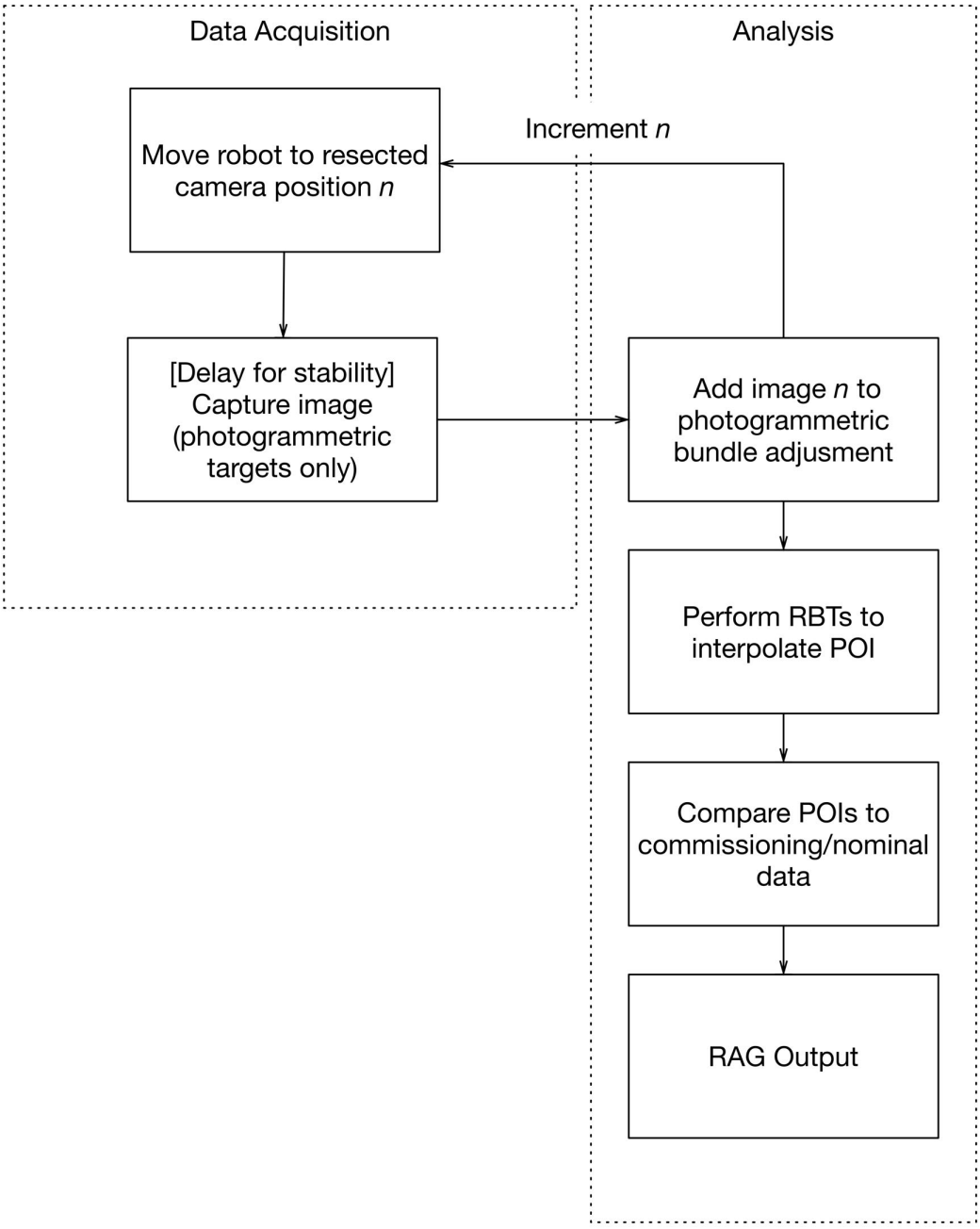


Figure 5-31: Rapid health check measurement process

### 5.4.5 Rapid Fixture Health Checks - Case Study

To demonstrate the rapid fixture health check process a strategy that used physical and digital environments was developed. This approach enabled a synergy of the data sets from both environments to give rise to a realistic process time. This was a necessity due to the financial and practical constraints with deploying automation. The physical aspects included the 'commissioning' of the RBTs, followed by the measurement of assembly tooling emulating a robot's working envelope and limitations.

The automation process can be simulated (in DELMIA) to assess the feasibility from a line of sight and access perspective as well as simulated in the time of the measurement process (Martin et al., 2011*a*,*b*,*c*; Wang, 2013). The simulation process required the demonstrator tooling (the ALCS MAJ) to be 'commissioned' to calibrate the RBTs, this is described in Section 5.4.5. The resected camera positions (to be calculated/defined) can be utilised as Tool Centre Point (TCP) or 'tag' positions for the robot's end effector for the simulation, as these are the frame positions the robot would need to achieve to take each image. The robot simulation in DELMIA featured a standard industrial serial robot, moving to each camera position and pausing to take the measurement then moving to the next camera position - simulated in real time. This enabled a measurement process time to be established. The full process and results are detailed in Section 5.4.5.

The following steps were carried out to demonstrate the commissioning process detail in Table 5.31:

1. Four laser tracker stations and facility tooling used for the measurement of the ERS (*Physical Measurement Task*).
2. The OTPs did not require any manipulation, but were measured (*Physical Measurement Task*).
3. Application of photogrammetry targets on the ALCAS fixture (coded & un-coded targets).
4. Photogrammetry measurement of the tooling, the ERS with split bearings and adhesive targets, no facility tooling (*Physical Measurement Task*)
5. Photogrammetry measurement of the jig, no split bearings or facility tooling (*Physical Measurement Task*)

This commissioning stage determined the ERS and OTP spatial relationship with a laser tracker, the relationship is parsed to the photogrammetry instrument through the measurement of the ERS. The photogrammetry system also measures the photogrammetric targets (coded and un-coded). Indirectly, the spatial relationship between the photogrammetric targets and POIs has now been established. The RBTs as described in Section 5.4.1 have now been determined. Finally, the fixture is re-measured with just the photogrammetric targets, and the resected camera positions and POIs are an output from the bundle adjustment.

The Automated data acquisition was simulated. The resected camera positions from the final photogrammetry measurement were an output from the bundle adjustment algorithm. The resected camera positions provided the TCP/Tag positions for the DELMIA simulation.The time-based simulation moved through each tag position pausing for 1 second; representative of the image capture time.

Subsequently the measurement data was automated within SA, however due to restrictions in the SDK the process still required manual intervention (although minimal). The entire process was scripted as described in Section 5.4.3. A digital mock-up (DMU) of the rcapid fixture health heck is illustrated in Figure 5-32.

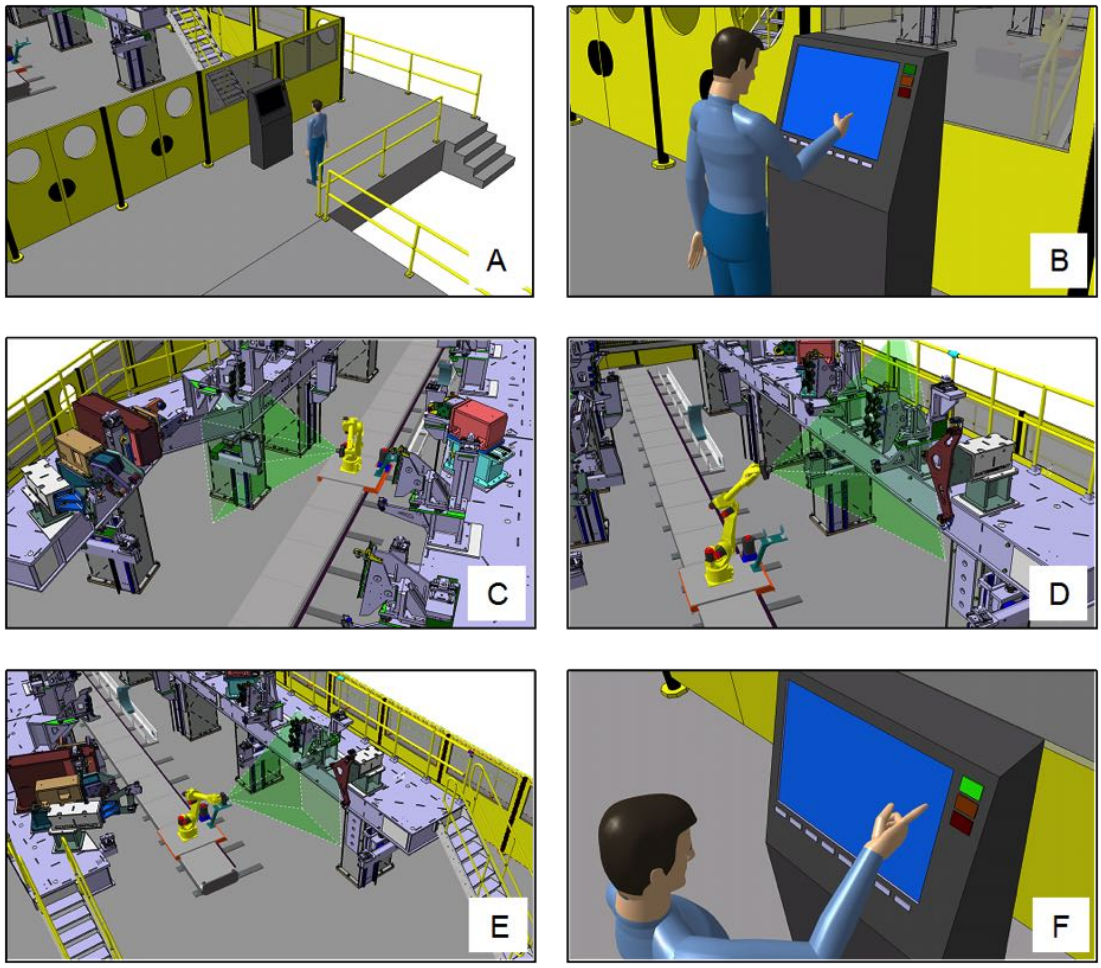


Figure 5-32: A story board of the process (Martin et al., 2011*a*), where: a, b) the operator initiates the rapid health check with a single button press; c,d,e) the serial axis robot with a mounted photogrammetry system performs the data acquisition; f) a RAG indicator of the assembly tooling condition is displayed

The breakdown of the process time can be examined in Figure 5-33; here we can see that the overall process is approximately 10 minutes, the photogrammetry processing is concurrent as the images are wirelessly transferred to the computer. Variation in the bundle adjustment and network adjustment computation has created a level of process-time uncertainty into the time estimation. However, the system could be further optimised for production deployment by: i) increasing computation power, ii) better metrology equipment (faster image acquisition and bundle adjustments), iii) optimised robot path and camera positions and iv) optimised robot dynamics (velocities and accelerations).

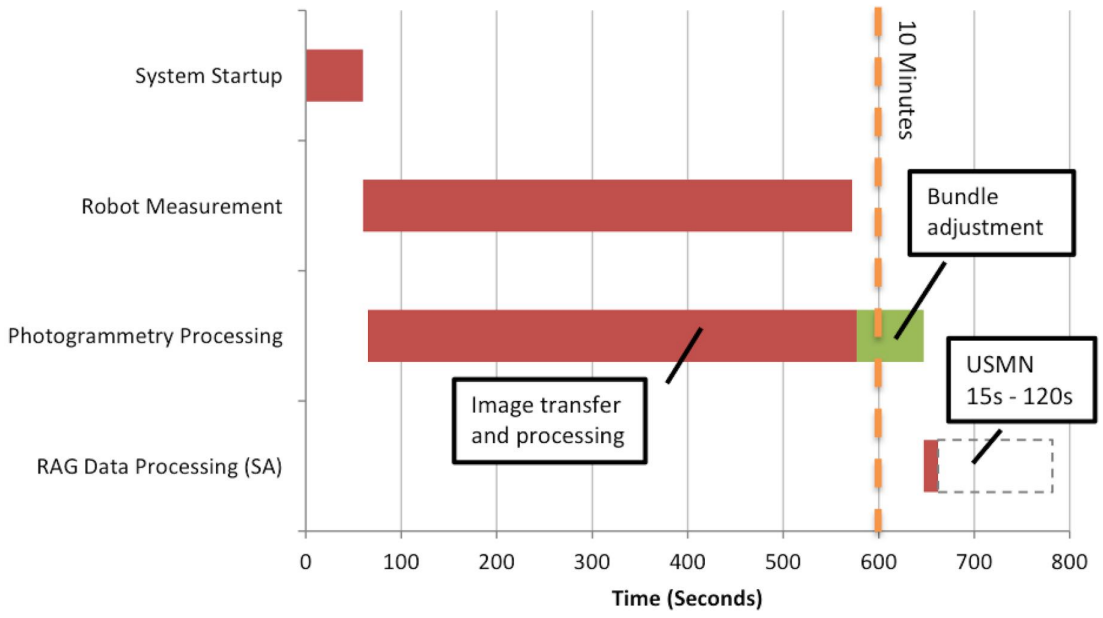


Figure 5-33: A time-based chart of the process (Martin et al., 2011*b*)

Photogrammetry systems hold the potential to rapidly verify the condition of an assembly fixture. The instrument cost is comparable to that of a laser tracker. Experimentally, the uncertainty has been shown (Section 5.2) to be similar to that of the laser tracker deployed as a single station; however the manufacturer's expectation is an instrument uncertainty greater than the laser tracker's. This could limit the health check measurement to the identification of gross errors only. Speed of measurement is a result of: leaving targets in place, multiple targets within the field of view, elimination of facility tooling and automation potential.

Through the development of rigid body transforms for this application (Section 5.4.1), the use of automation for data acquisition (Section 5.4.2) and the exploitation of scripting and programming (Section 5.4.3), the realisation of the rapid health check measurement has been demonstrated through a hybrid digital and physical simulation (Section 5.4.5). Further development work for industrial deployment includes:

- Increasing computation power,
- Better metrology equipment (faster image acquisition and bundle adjustments),
- Optimised robot dynamics (velocities and accelerations).

In general health check measurements could avoid gross positional errors within the fixture. Measurement before each build (and potentially during the build) could avoid concessions occurring between recertification periods. Health check measurements would also act as a diagnostic tool enabling recertification work to be scheduled and costed more effectively. Regular fixture measurements would also facilitate legacy data collection and statistical process control (SPC). This deeper understanding of fixture stability would inform and improve future tooling designs.

## 5.5 Chapter Summary

*Photogrammetry & Laser Tracker Performance Testing*, Section 5.2 assessed the appropriateness of photogrammetric systems - both commercial and off-the-shelf systems - as an alternative metrology technology to the traditional laser tracker for the measurement of assembly tooling. The uncertainty of the systems was both theoretically estimated and experimentally determined. The experimentally determined uncertainty estimation enabled a comparison of the photogrammetric measurement to be compared to a traceable reference network, and the uncertainty propagation and combination was carried out in line with the GUM standard. It was shown that the commercial photogrammetry system had an experimentally determined standard measurement uncertainty of 43 µm, better than control measurement using a laser tracker which had an estimated associated standard uncertainty of: 65 µm. The commercial photogrammetric system was shown to be a suitable substitute technology for tooling certification whereas the estimated standard uncertainty for the off-the-shelf system determined as 187 µm and could not be used for tooling certification purposes.

*Large Volume Multi-Instrument Networks*, Section 5.3 further explored photogrammetry as a complementary technology to laser tracker networks. Photogrammetry utilised the accurate laser tracker network, to give scale to the photogrammetric bundle adjustment over large distances (80m). The associated uncertainty estimate for the laser tracker reference network was improved by updating the individual instrument uncertainty parameters based on the instrument performance within the network adjustment and iterating until convergence. This method ensures an appropriate representation of the instrument uncertainty parameters within an industrial LVM context. The estimated uncertainty using current methods is 263 µm, whereas the new method of multiple instrument updates yields an uncertainty of 189 µm, a 28% improvement on uncertainty estimation over 80m. Subsequently, uncertainty budgets of the combined measurement process were created to accurately estimate the uncertainty. The uncer-

tainty estimation set out and documented in this section acts as a template for future large volume laser tracker-photogrammetry metrology networks.

*Automated Measurement of Aircraft Wing-box Assembly Tooling*, Section 5.4 details a process for the rapid measurement of fixture condition, employing the outcomes from the previous sections. That is, using a commercial photogrammetric system for data acquisition, utilising a network of points having a co-ordinate definition measured by a laser tracker(s), using multiple instrument updates for an accurate metrology estimate. In order to automate the data acquisition rigid body transforms (RBTs) were put forward to measure the POI, this is a new application for RBTs. The minimum number of targets used to measure the POI via RBTs was simulated to achieve a comparable accuracy to current methods. RBTs negate the need for facility tooling, and enable automated data acquisition by leaving low-cost photogrammetry targets in-situ. A commissioning methodology and process was developed and documented. A case study was used to show proof of concept through a combination of physical trials and digital simulations.

# Chapter 6

# Embedded Metrology Systems

## 6.1 Introduction

This chapter describes how digital local metrology systems can be embedded into tooling structures to negate the dependancy on in-tool manual, mechanical checks. Providing automated, faster and more robust data acquisition.

The literature review (Chapter 2) indicated that a gap exists relating to: *an integrated approach towards metrology and aerospace Wing-box assembly tooling.* This is more specifically identified in the review of industrial practices within aircraft Wing-box assembly tooling (Chapter 3), as a need to:

- Reduce manual metrology checks & reduce tooling reliance
- Enable greater automation
- More robust component placement

The META framework outlines the generic interaction of external metrology and embedded sensors within tooling (Figure 6-1). The specific metrology systems appropriate for deployment on the individual tools are unique to the requirements of that tooling structure and assembly. The META framework is best exercised through specific measurement tasks and feature checks. Industrial context and application gives rise to specific tooling and measurement requirements, representative of a production environment.

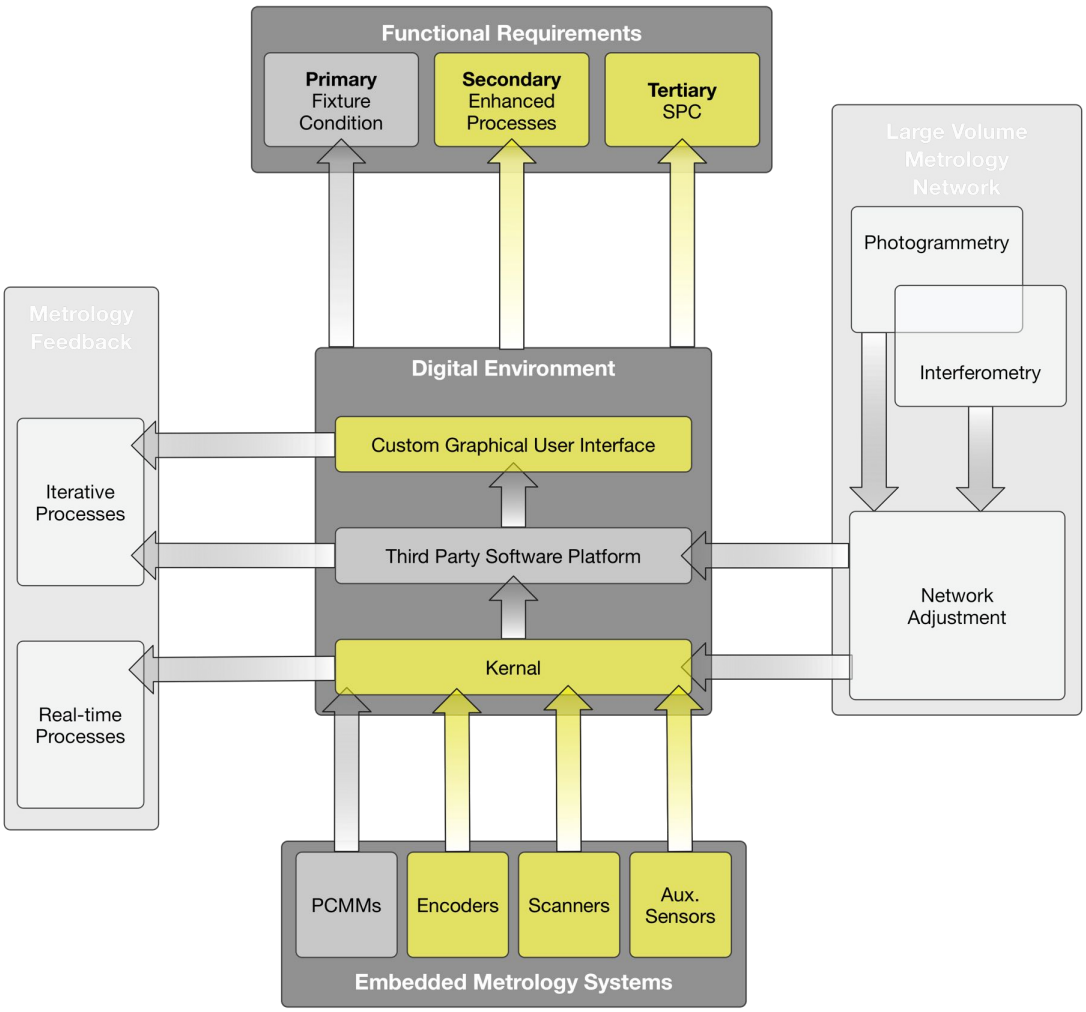


Figure 6-1: META framework

The tooling application (Section 6.2) provides context for the embedded metrology; this includes: representative tolerance requirements, inspection features, scale and geometries. This industrial context informs the down-selection of the measurement systems (Section 6.3). The measurement systems interface and communicate through a common platform detailed in Section 6.4. Subsequently, the commissioning, data acquisition and associated uncertainty for the measurement systems is discussed and quantified in the context of the proposed industrial deployment (Section 6.5), the finding are summarised in Section 6.6.

## 6.2 Tooling Application

The case study detailed in Chapter 3 outlines the requirements present on a typical aerospace fixture. The hinge brackets will provide a focus for the embedded metrology development. The positional measurements for the hinge brackets include:

- Hinge Bore Co-Axiality, controlled with concentricity tolerance (300 µm)
- Hinge Bracket/Bore Perpendicularity (10 µm)
- Hinge Bracket Step & Gap Condition (±150 µm)

The details are surmised in Figure 3-3 and the simplified geometry in the diagram below (Figure 6-2).

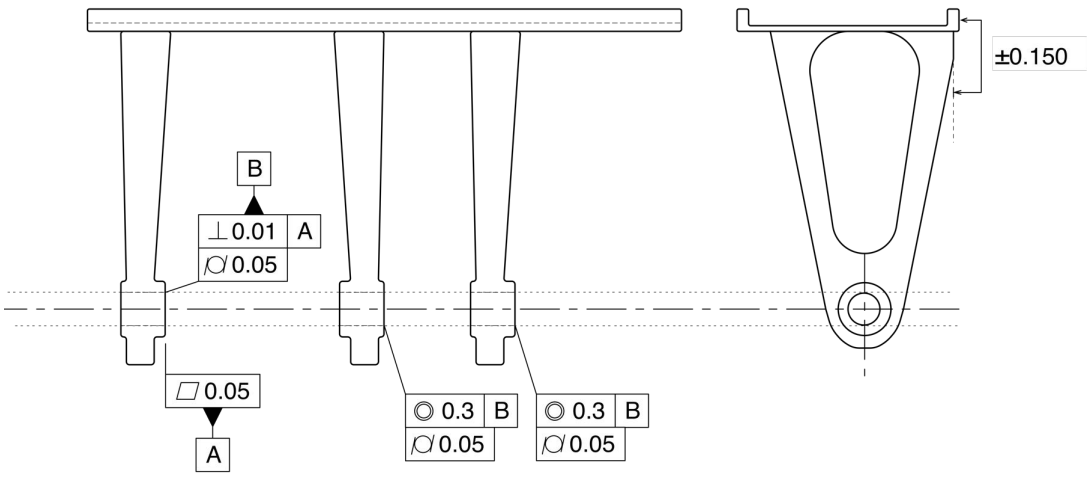


Figure 6-2: Simplified hinge-line assembly drawing

These positional checks are traditionally carried out through the setting of accurately machined pick-ups/hard tooling positioned to a setting tolerance of 150 µm with a laser tracker; this figure is the tool-setting tolerance. In reality the tool setters set

as close to nominal as possible, typically achieving sub-50 µm, however when considering the instrument and process uncertainty, the 150 µm tool setting requirement is a realistic figure to quote, as current uncertainty associated with tool-setting is 125 µm ($K = 2$) detailed in Table 6.4.

| Component | Value µm | Distribution | Divisor | Standard Uncertainty µm |
|---|---|---|---|---|
| Locating Tracker to ERS[1] | 100.00 | Normal | 2 | 50.00 |
| SMR Magnetic Nests[2] | 13.00 | Rectangular | $\sqrt{3}$ | 7.51 |
| SMR Centering[3] | 6.00 | Rectangular | $\sqrt{3}$ | 3.46 |
| Setting Tolerance[4] | 50.00 | Rectangular | $\sqrt{3}$ | 28.87 |
| Instrument Uncertainty[5] | 45.00 | Normal | 2 | 22.5 |
| | | Combined Standard Uncertainty, $u_c$ | | 62.51 |
| | | Expanded Standard Uncertainty ($K = 2$), $U_c$ | | 125.02 |

Table 6.1: Uncertainty contributions for setting the standard pick-ups

The following notes give explanation to the uncertainty contributions, used in the uncertainty budget (Table 6.1):

[1] This value represents the best-fit residuals expected during the instrument location process. This value will vary between measurements, however, this is an average expected value, derived from operator experience.

[2] Mechanical tolerance statement.

[3] Value from manufacturers statement.

[4] This is the value that the operator/tool-setter will use nominally set the tool within, according to the instrument dynamic readout.

[5] Value from manufacturers statement - at 5m.

This 150 µm (stated tool-setting tolerance) consumes a large proportion of the assembly tolerances detailed in Figure 6-2. The components are checked in-fixture with the use of gauge-plate slips, pins (Figure 3-4), and step-gauges (Figure 3-5). The motivation for implementing META in this application is to reduce these manual feature

checks: reducing time, operator dependancies and increasing repeatability of measurement and manufacturing data. In addition to the positional in-fixture checks, temperature sensors will also be incorporated.

The design intent of components, assemblies and tooling is specified with respect to the nominal temperature of 20 °C, unless stated otherwise. Components and assemblies with comparatively tight tolerances relative to their overall dimensions must consider the effects of thermal expansion and contraction. Thermal expansion and contraction has a profound effect and can readily cause an assembly to exceed its assembly tolerance. Assembly rates and the in-fixture time for the components/sub-assemblies are comparatively long in aerospace manufacture, and this creates a greater risk of thermal variation.

Airbus UK currently compensates measurement at the fixture setting stages by taking the temperature of the object (in this case the tooling) and applying a linear expansion model through the metrology software: SpatialAnalzer; the change in length due to thermal expansion ($\Delta L$) is given by:

$$\Delta L = \alpha \Delta T L_o. \tag{6.1}$$

Where $\alpha$ is the coefficient of thermal expansion (CTE); $\Delta T$ is the change in temperature and $L_o$ is the original length. CTE is given in $ppm/K$, in other words: *for every metre, the material will expand by $\alpha$ micrometers per Kelvin.*

However, this compensation does not eradicate the effects of thermal expansion/ contraction completely. Additionally, the scaling of a fixture to its CAD nominal state, which may not be appropriate; for example, an aluminium assembly built in a steel fixture will have a different CTE (see Table 6.2) and hence scaling the *fixture* to nominal will not scale the *assembly* to nominal; hence a disparity will occur. Although a full exploration of the thermal effects on fixtures is out of the scope of this research, automated temperature data collection is carried out.

| Material | Coefficient of Thermal Expansion ($\alpha$) $10^{-6}/K$ |
|---|---|
| Steel (Structural A36) | 12.0 |
| Aluminium Alloy (6061-T6) | 24.0 |
| Invar | 1.5 |
| CFRP | 3.0 |
| Granite | 7.5 |

Table 6.2: Typical CTE Values of materials

## 6.3 Measurement Systems

Positional measurement systems are required to replace the hard tooling and gauges found in traditional tooling. These systems are performing local, relative measurements. Referencing these local checks back to the global Aircraft (A/C) or Wing Datum structure would be carried out during the commissioning stage and is captured in *Deployment of Embedded Metrology* (Section 6.5). The systems that are to be demonstrated include:

**On-Track, OT4040 Bore Alignment:** this system will be implemented to measure the bore co-axiality of the hinge-line, replacing the pin diameters identified in the *Review of Industrial Practices within Aircraft Wing-box Assembly Tooling*, (Chapter 3).

The Bore Alignment system (Figure 6-3) generates a nominal alignment axis from the laser source. Transparent targets (Figure 6-4) sit in the feature of interest - in this case a hinge bore - and intercept the reference laser axis. The targets allow a two dimensional displacement to be described in a plane ($x$,$y$) normal to the nominal laser axis (Figure 6-5). The system can be used independently with a digital read-out box for each sensor or integrated into a PC-based, custom GUI. Subsequently, the individual hinge-line bore pick-ups can be manipulated (manually or with automation) using the output to determine the direction and magnitude required to achieve co-axiality.

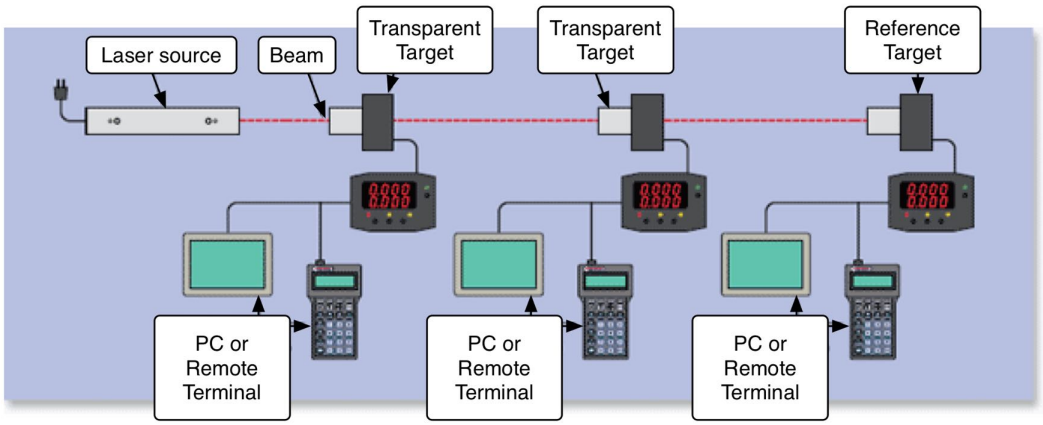


Figure 6-3: Schematic of the OT4040 operation (OnTrak, 2014)

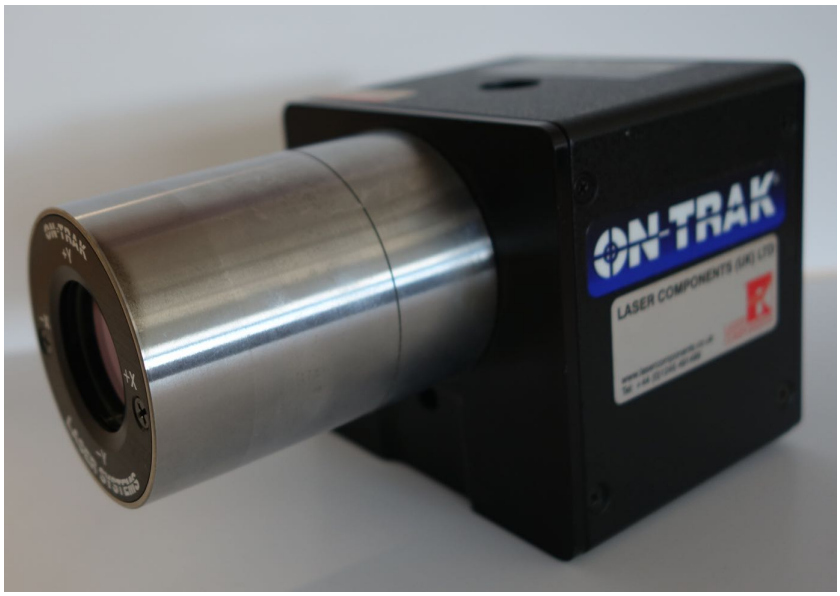


(a) Transparent target - isometric view


(b) Transparent target - front elevation

Figure 6-4: Images of the OT4040 transparent targets

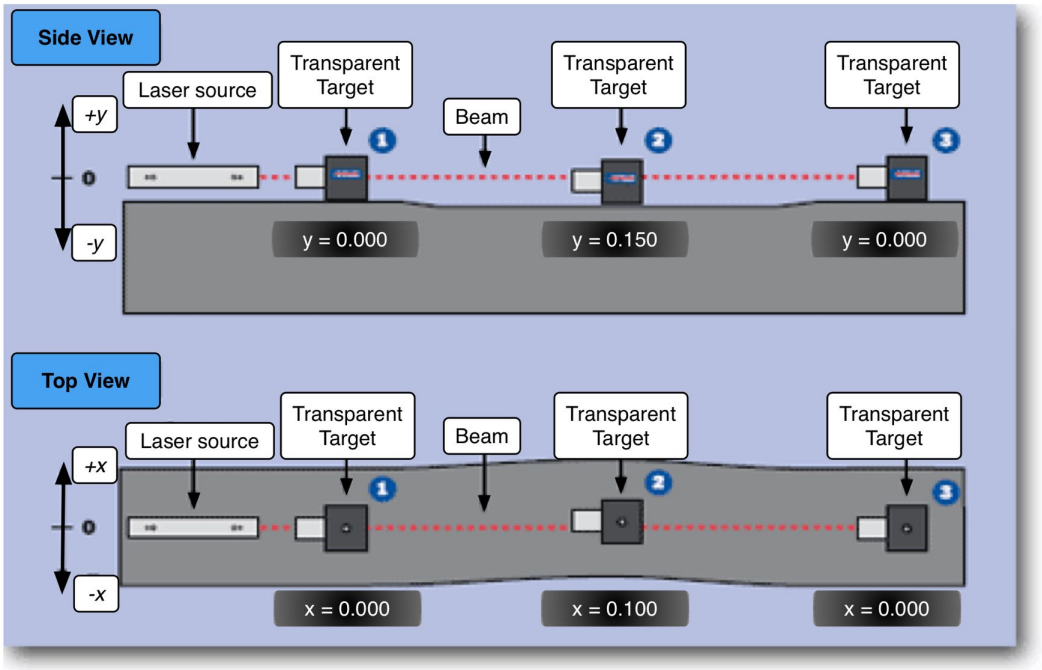


Figure 6-5: Measured deviation from the OT4040 system (OnTrak, 2014)

**Solartron, Linear Variable Differential Transformers (LVDTs):** these linear displacement (*1D*) measurement devices can be configured to measure a number of features. For the measurement of the features identified in Figure 6-2 the LVDTs will be configured to measure the perpendicularity of the Datum face **B** with respect to Datum **A**. Secondly, the LVDTs will be configured to measure the step condition between the Rear Spar and the Hinge Bracket on the upper surface. The deployment of the LVDTs, replaces the slip gauges and step gauges observed in the *Review of Industrial Practices within Aircraft Wing-box Assembly Tooling*, (Chapter 3).

To achieve the perpendicularity measurement the LVDTs have been configured as in Figure 6-6 & 6-7, this determines three points to define a plane (Datum **B**), which must be compared to Datum Feature **A**.

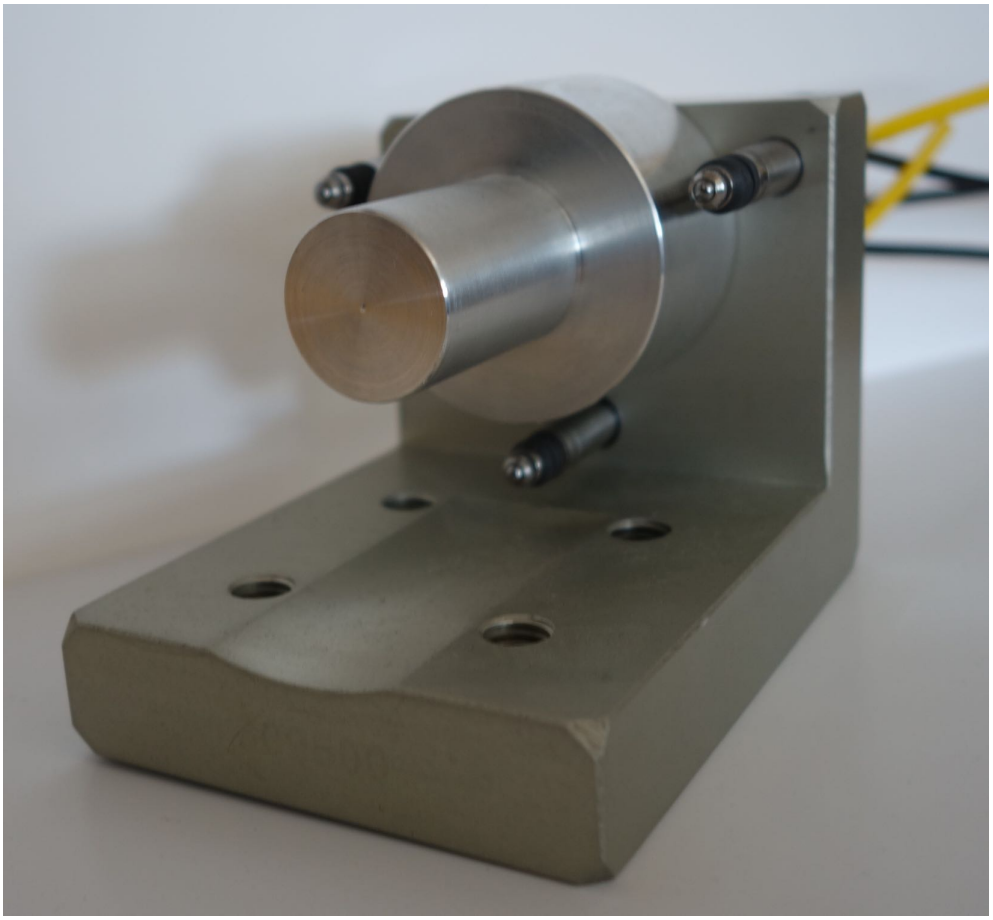

Figure 6-6: Configuration of LVDTs in the hinge-line pick-up

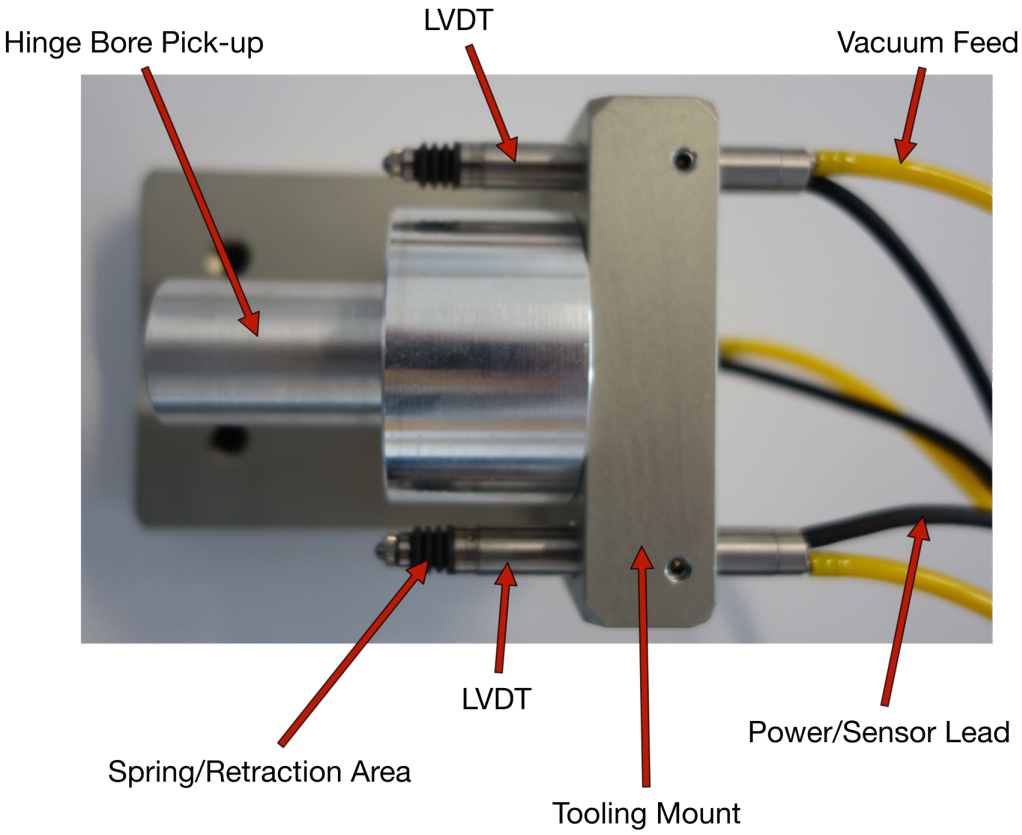


Figure 6-7: Annotated configuration of LVDTs on the pick-up

To measure the step condition, a single LVDT will probe the spar web, and another LVDT will probe the hinge bracket.

The LVDTs natively interface through Solatron's proprietary software or through a macro within a Microsoft Excel spreadsheet; however, communications can be established through a custom GUI via the SDK. Vacuum-retractable, spring-return LVDTs were employed to avoid damage during the component placement and removal operations.

**Third Dimension, GapGun:** is a commercially available laser line scanner from Third Dimension, used for the measurement of steps, gaps, profile, radii and other features that can be determined by a laser-line. The interface and processing unit is

integrated into the handle on which the sensor is mounted (Figure 6-8). The sensor will be detached and mounted to measure the step condition, as an alternative to the LVDTs.

Figure 6-8: Image of the GapGun's detachable sensor/head (ThirdDimension, 2014)

The thermal sensors are intended to be deployed to passively record the thermal condition of the fixture. The temperature sensors will monitor the fixture; when the temperature range reaches an unacceptable level the interface will indicate to the operator that the tolerances have been exceeded through material expansion. The unacceptable level will be defined by applying a linear expansion model of the thermal disparity, and finding the temperature limits required to maintain the tolerances.

**4G Metrology, ScAlert:** is a wireless temperature monitoring system (Figure 6-9) that is calibrated and traceable to the national measurement standards. As well as being integrated into a single interface, the sensors were positioned on a large scale fixture to collect representative data. The sensors were left in-situ for two weeks, to assess the extent of the temperature fluctuations over time.

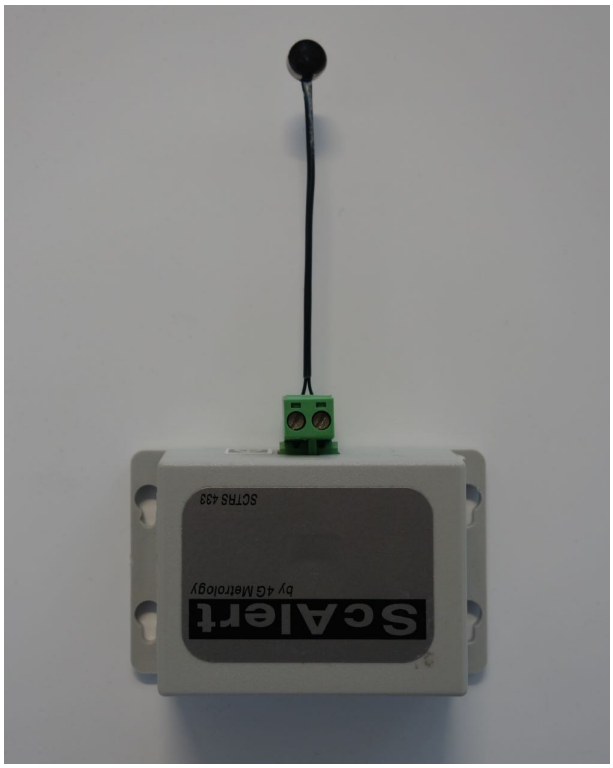


Figure 6-9: Image the ScAlert sensor

## 6.4 Interface & Communications

As a continuation of the Red, Amber and Green (RAG) Metrology philosophy introduced in Section 5.4, the interface for the embedded metrology utilises the same principles:

- User-friendly operation, requiring no specific metrology training,
- Simple output (Red, Amber or Green),
- Reduced measurement time.

The integration of the hardware is illustrated in figure 6-10, the control box houses the individual peripherals required for each metrology system.

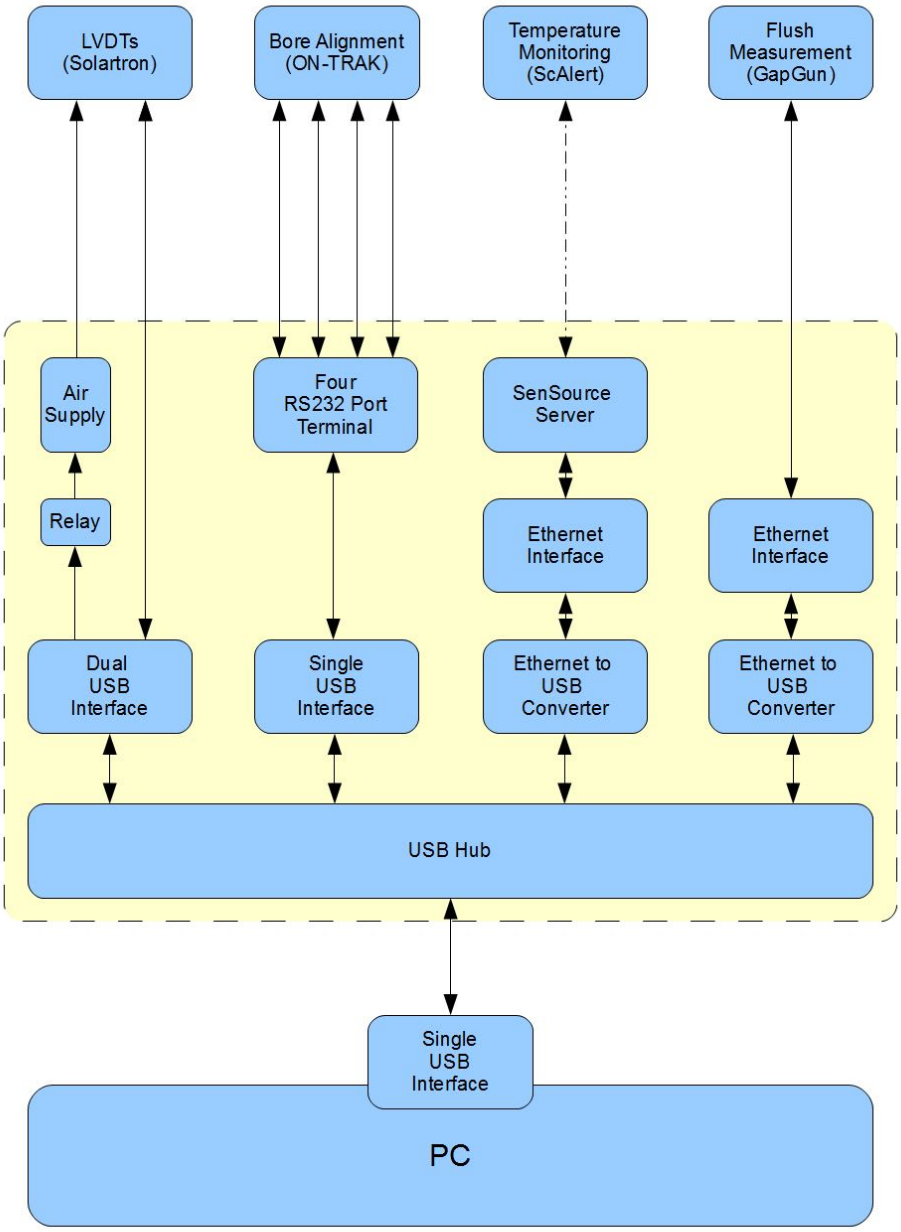


Figure 6-10: Schematic of distributed metrology network hardware integration

The embedded metrology graphical user interface (GUI) was written in Visual C#, this enabled all the instruments and sensors to communicate in one environment

(Figure 6-11). The GUI has a simple workflow with additional options and tabs for Metrology specialists, that can be deactivated for shop-floor operations. The embedded metrology GUI was designed with the intention of using a touch-screen input. The workflow for operators is simply:

`Initialise Sensors` ⇒`Engage LVDTs` ⇒ `Check Assembly`

**Initialise Sensors:** Starts and checks communications with the distributed sensors,

**Engage LVDTs:** releases the vacuum on the LVDTs,

**Check Assembly:** retrieves current values of the measurement sensors, and reports the output and result.

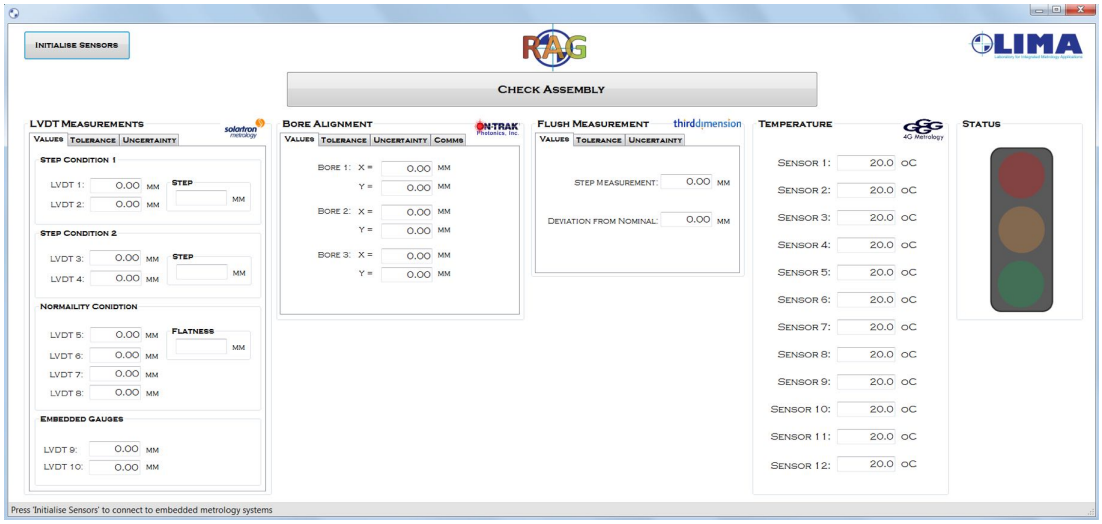


Figure 6-11: Embedded metrology graphical user interface (GUI)

The output for each of the individual positional/thermal checks the value is populated in the corresponding field and the box changes colour to indicate either:

- `Green`: Components on the fixture are within tolerance of their nominal position,
- `Amber`: Unable to determine that the components on the fixture are within tolerance (due to measurement/process uncertainty),

- `Red`: Components are not within tolerance of their nominal position.

The `Status` field gives the global summary using simple conditional logic, with the Red, Amber and Green (RAG) traffic-light system indicating whether the assembly is:

- `Green`: All individual positional/thermal checks are green
- `Amber`: At least one or more of the individual positional/thermal checks is amber, the remaining individual positional/thermal checks are green.
- `Red`: At least one or more of the individual positional/thermal checks is red.

The additional input tabs and fields within the GUI allow the individual instrument uncertainty values and the tolerance requirements to be changed. These values are used to compute the RAG outputs.

## 6.5 Deployment of Embedded Metrology

### 6.5.1 On-Track, OT4040 Bore Alignment

**Commissioning** the system requires the laser source to be aligned to the nominal hinge axis. This needs to be completed at the tool-build and setting phase when the traditional 'pick-ups' would be fine tuned and pinned off. This setting process would be carried out using a laser tracker. Once aligned correctly, the transparent targets are placed into the hinge pick-ups. This would not add any significant time to the commissioning process.

**In-Fixture Measurement** is carried out via the RAG interface, with rapid data acquisition. Giving a two dimensional deviation from nominal the acceptance limits of which are interpreted from the GD&T requirement stated in Figure 6-2; a concentricity tolerance of 300 µm translates into a deviation tolerance of ±150 µm in both axes ($x$,$y$).

**Uncertainty of Measurement** the bore alignment system has an instrument uncertainty of 50 µm, this is appropriate for achieving the GD&T concentricity requirement. However in addition to this local datum structure and tolerance requirement, the pick-ups have a global positioning tolerance to satisfy. This is relative to *Wing Axis* which in turn is related to the *Aircraft (A/C) Axis*. Tool setting tolerances are between 150 µm to 250 µm, dependent on Aircraft family. A large component of uncertainty associated

with the deployment of bore alignment systems can be attributed to the setting of the laser source: *the virtual hinge-line*. Other components include the tolerance build-up experienced by the seating-interface of the targets within the pick-ups, however these are mechanical machining tolerances that can be considered as negligible contributions in the context of large volume metrology, as the uncertainty contribution is less than 5%; in accordance with M3003 (UKAS, 2012) and GUM (*ISO/IEC Guide 98-3:2008 Uncertainty of measurement – Part 3: Guide to the expression of uncertainty in measurement (GUM)*, 2008). There are two methods for setting the laser source/hinge-line, illustrating the importance of measurement strategy and the consideration of measurement uncertainty. Firstly, consider the setting of the laser source as in Figure 6-12.

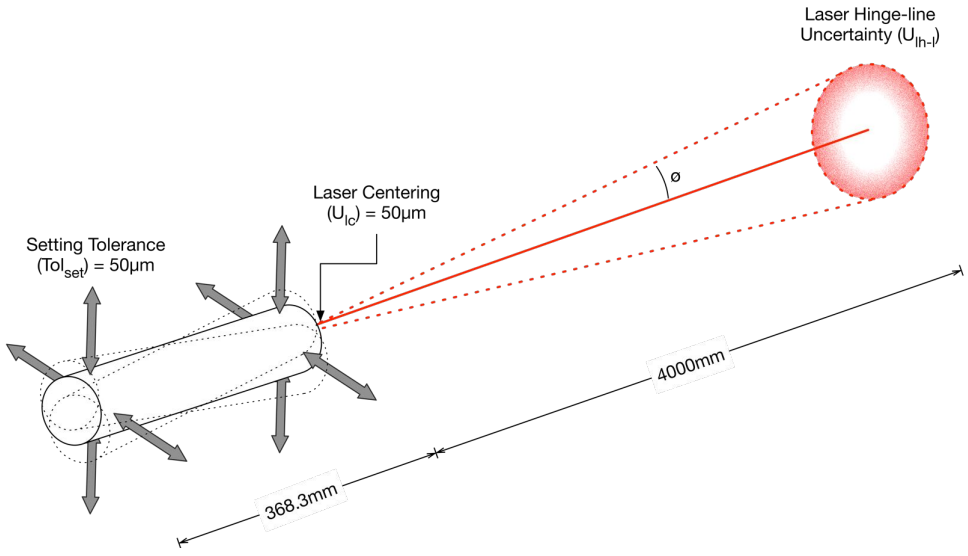


Figure 6-12: Setting laser source uncertainty

The laser source is set as a pick-up, and is traditionally set by: 1) the laser tracker locates to an ERS/JRS, 2) dynamic measurement of the pick-up is compared to the CAD nominal, 3) the pick-up is adjusted to manipulate the laser source until the setting tolerance has been achieved, 4) pick-up is fixed. The uncertainty budget for this process is detailed in Table 6.3

| Component | Value µm | Distribution | Divisor | Standard Uncertainty µm |
|---|---|---|---|---|
| Locating Tracker to ERS[1] | 100.00 | Normal | 2 | 50.00 |
| SMR Magnetic Nests[2] | 13.00 | Rectangular | $\sqrt{3}$ | 7.51 |
| SMR Centering[3] | 6.00 | Rectangular | $\sqrt{3}$ | 3.46 |
| Setting Tolerance[4] | 50.00 | Rectangular | $\sqrt{3}$ | 28.87 |
| Instrument Uncertainty[5] | 45.00 | Normal | 2 | 22.5 |
| Laser Centering[6] | 50.00 | Rectangular | $\sqrt{3}$ | 28.87 |
| | Combined Standard Uncertainty, $u_c$ | | | 68.86 |
| | Expanded Standard Uncertainty ($K = 2$), $U_c$ | | | 137.71 |

Table 6.3: Uncertainty contributions for setting the laser hinge-line

The following notes give explanation to the uncertainty contributions, used in the uncertainty budget (Table 6.3):

[1] This value represents the best-fit residuals expected during the instrument location process. This value will vary between measurements, however, this is an average expected value, derived from operator experience.

[2] Mechanical tolerance statement.

[3] Value from manufacturers statement.

[4] This is the value that the operator/tool-setter will use nominally set the tool within, according to the instrument dynamic readout.

[5] Value from manufacturers statement - at 5m.

[6] Value from manufacturers statement.

The setting process of the laser source could give rise to a ±137.71 µm deviation. This can be considered as the worst-case miss-alignment of the laser source, an unlikely outcome, but with severe consequences. In this condition the laser source is mis-aligned by an angle of $0.043^o$, which, over the 4m hinge bay would cause a deviation from nominal of 2.99 mm. The co-axility of the hinge bore could be accurately maintained and verified but the global tolerance could not be met with confidence.

A more robust method of setting the nominal hinge-line is to begin by positioning the Reference Target at the terminal hinge-bore pick-up (Figure 6-13).

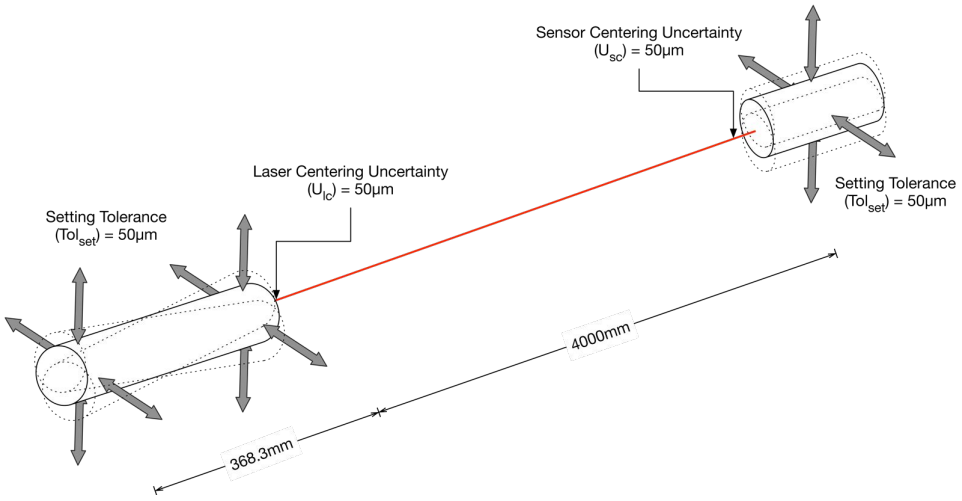


Figure 6-13: Setting laser source uncertainty and reference target

Table 6.4 details the uncertainty contributions for the setting of the reference target.

| Component | Value µm | Distribution | Divisor | Standard Uncertainty µm |
|---|---|---|---|---|
| Locating Tracker to ERS[1] | 100.00 | Normal | 2 | 50.00 |
| SMR Magnetic Nests[2] | 13.00 | Rectangular | $\sqrt{3}$ | 7.51 |
| SMR Centering[3] | 6.00 | Rectangular | $\sqrt{3}$ | 3.46 |
| Setting Tolerance[4] | 50.00 | Rectangular | $\sqrt{3}$ | 28.87 |
| Instrument Uncertainty[5] | 45.00 | Normal | 2 | 22.5 |
| Reference Target Centering[6] | 50.00 | Rectangular | $\sqrt{3}$ | 28.87 |
| | | Combined Standard Uncertainty, $u_c$ | | 68.86 |
| | | Expanded Standard Uncertainty ($K = 2$), $U_c$ | | 137.71 |

Table 6.4: Uncertainty contributions for setting the reference target

The following notes give explanation to the uncertainty contributions, used in the uncertainty budget (Table 6.4):

[1] This value represents the best-fit residuals expected during the instrument location process. This value will vary between measurements, however, this is an average expected value, derived from operator experience.

[2] Mechanical tolerance statement.

[3] Value from manufacturers statement.

[4] This is the value that the operator/tool-setter will use nominally set the tool within, according to the instrument dynamic readout.

[5] Value from manufacturers statement - at 5m.

[6] Value from manufacturers statement.

The laser source can be set with the laser tracker as detailed in Table 6.3. Simultaneously, the reference target can be used to manipulate the laser source further (through dynamic updates) this negates any large angular deviations/errors being introduced to the laser source. Figure 6-14 illustrates the constraints. The reference target has been set to within the setting uncertainty; further sources for uncertainty are the centering accuracy of the laser source (50 µm) and the instrument uncertainty (a further 50 µm); the interaction of these sources is captured in Figure 6-14, from which it can be seen that the 50 µm can be simply combined to the setting tolerance in accordance with GUM (*ISO/IEC Guide 98-3:2008 Uncertainty of measurement – Part 3: Guide to the expression of uncertainty in measurement (GUM)*, 2008), Table 6.5.

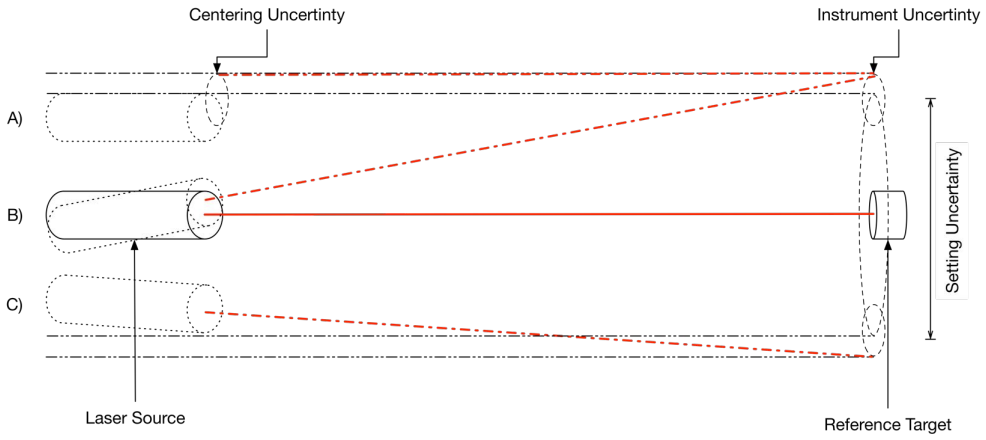


Figure 6-14: Commissioning the laser source using the reference target

| Component | Value μm | Distribution | Divisor | Standard Uncertainty μm |
|---|---|---|---|---|
| Setting via Laser Tracker Uncertainty[1] | 137.71 | Normal | 2 | 68.86 |
| Centering Uncertainty | 50.00 | Normal | 2 | 25.00 |
| | | Combined Standard Uncertainty, $u_c$ | | 73.25 |
| | | Expanded Standard Uncertainty ($K = 2$), $U_c$ | | 156.51 |

Table 6.5: Uncertainty contributions for setting the laser source

The following notes give explanation to the uncertainty contributions, used in the uncertainty budget (Table 6.5):

[1] This value is taken from Table 6.3 & 6.4.

### 6.5.2 Solartron, LVDTs for Perpendicularity

**Commissioning** the nominal position of the LVDTs must be carried out. This is the position/reading when the LVDTs are in contact with a plane that is perpendicular to the hinge bore. This can be achieved in one of two ways, either: 1) the LVDTs are accurately positioned (micron level) within the pick-up, or, 2) the LVDTs are placed within the pick-up at millimetre level accuracy, and subsequently calibrated with a gauge plate. It is the latter that will be explored here as this method is less time and cost intensive, additionally, the pick-ups can be re-calibrated *in-situ* using this method.

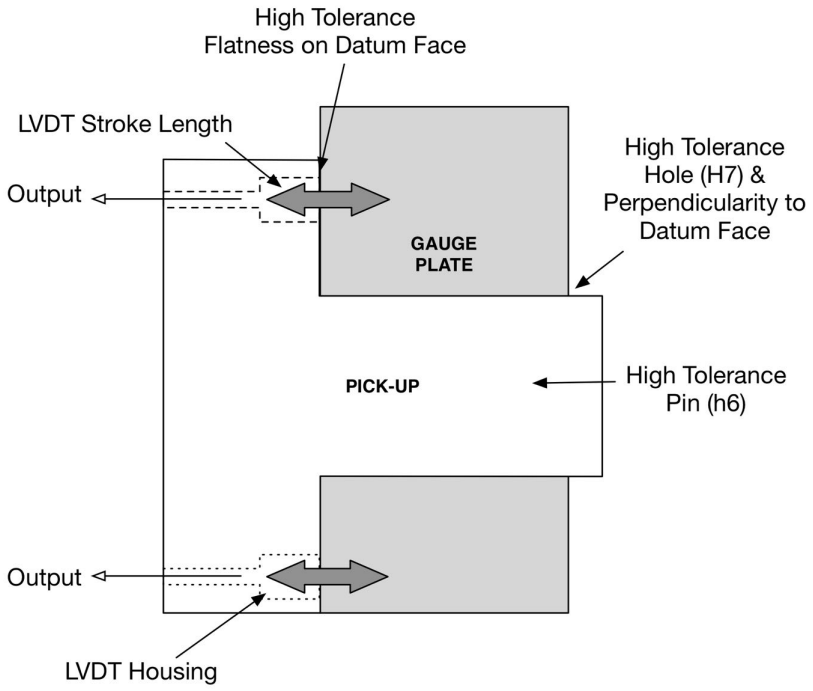


Figure 6-15: Commissioning the LVDT perpendicularity measurement

Figure 6-15 illustrates the calibration method. Using an accurately machined section of gauge-plate (readily available at low-cost) the LVDTs are 'zeroed' through the software. Hence, the perpendicular plane has been recorded, and can be described using the co-ordinate definitions detailed in Figure 6-16. This strategy negates the requirement for accurate placement of the LVDTs, as any error in assembling the pick-up is calibrated out.

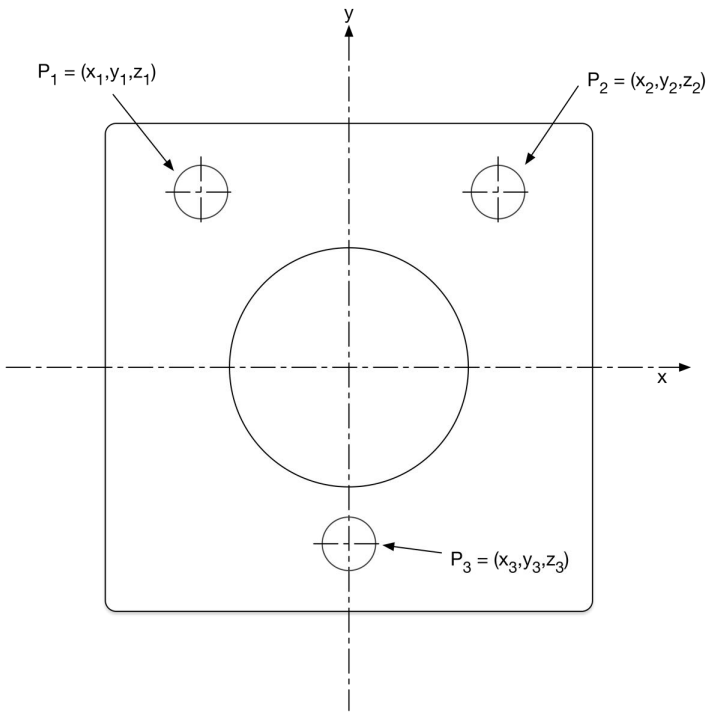


Figure 6-16: LVDTs co-ordinate definition

The general equation for a plane from three points $P_1$, $P_2$ and $P_3$, with co-ordinates $(x_1, y_1, z_1)$, $(x_2, y_2, z_2)$, and $(x_3, y_3, z_3)$, respectively, is:

$$\begin{vmatrix} x - x_1 & y - y_1 & z - z_1 \\ x_2 - x_1 & y_2 - y_1 & z_2 - z_1 \\ x_3 - x_1 & y_3 - y_1 & z_3 - z_1 \end{vmatrix} = 0. \tag{6.2}$$

Hence the perpendicular (zeroed LVDTs) plane has the equation:

$$\begin{vmatrix} x - x_1 & y - y_1 & z \\ x_2 - x_1 & y_2 - y_1 & 0 \\ x_3 - x_1 & y_3 - y_1 & 0 \end{vmatrix} = 0. \tag{6.3}$$

Solving gives:

$$z((x_2 - x_1)(y_3 - y_1) - (y_2 - y_1)(x_3 - x_1)) = 0, \tag{6.4}$$

if $P_1$ is the origin, such that: $P_1 = x_1, y_1, z_1 = 0, 0, 0$, then Equation 6.4 becomes:

$$\begin{aligned} z((x_2 - 0)(y_3 - 0) - (y_2 - 0)(x_3 - 0) = 0, \\ z(x_2 y_3 - y_2 x_3) = 0. \end{aligned} \tag{6.5}$$

This is our calibrated nominal plane; where $x_2 y_3 - y_2 x_3$ can be considered as our $C$, in the general equation of a plane:

$$Ax + By + Cz + D = 0. \tag{6.6}$$

**In-Fixture Measurement** is carried out via feedback from the LVDTs; If the hinge-bore is perpendicular to the Datum face [**B**] then the LVDTs will read a zero $z$ displacement, as in Figure 6-17. However, to varying degrees the hinge-bore will exhibit a level of non-perpendicularity. Figure 6-18 illustrates the isolated roll and pitch implications if the bore is non-perpendicular in a single axis, however the non-conformance is likely to be in both axes, causing a compound plane angle.

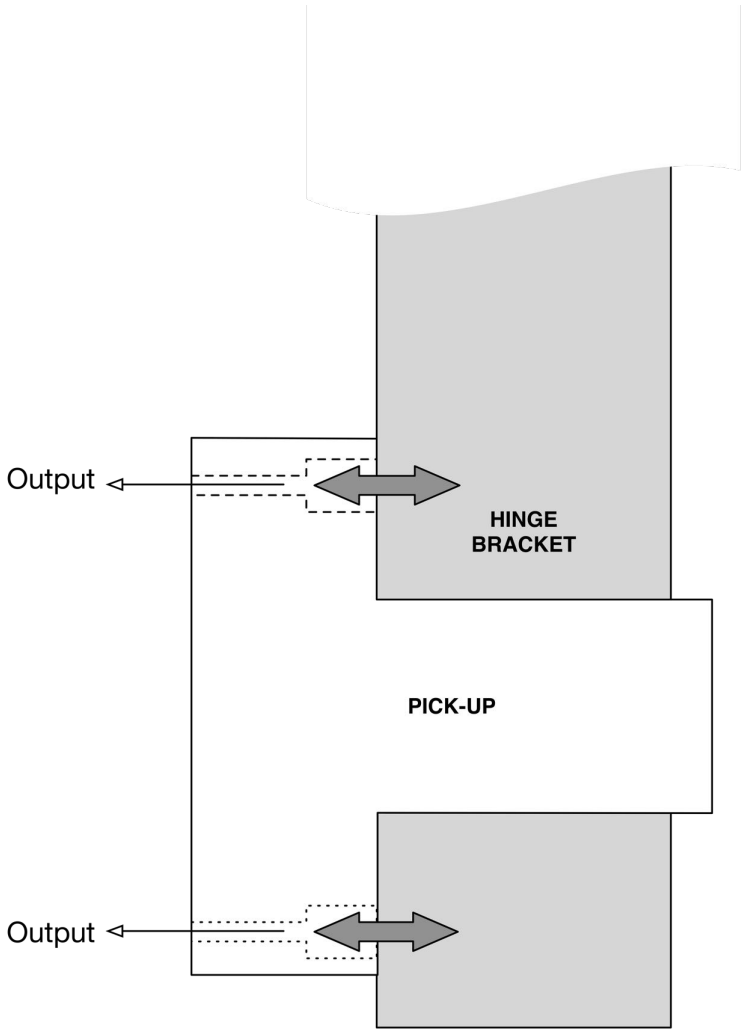


Figure 6-17: Nominal LVDT perpendicularity measurement

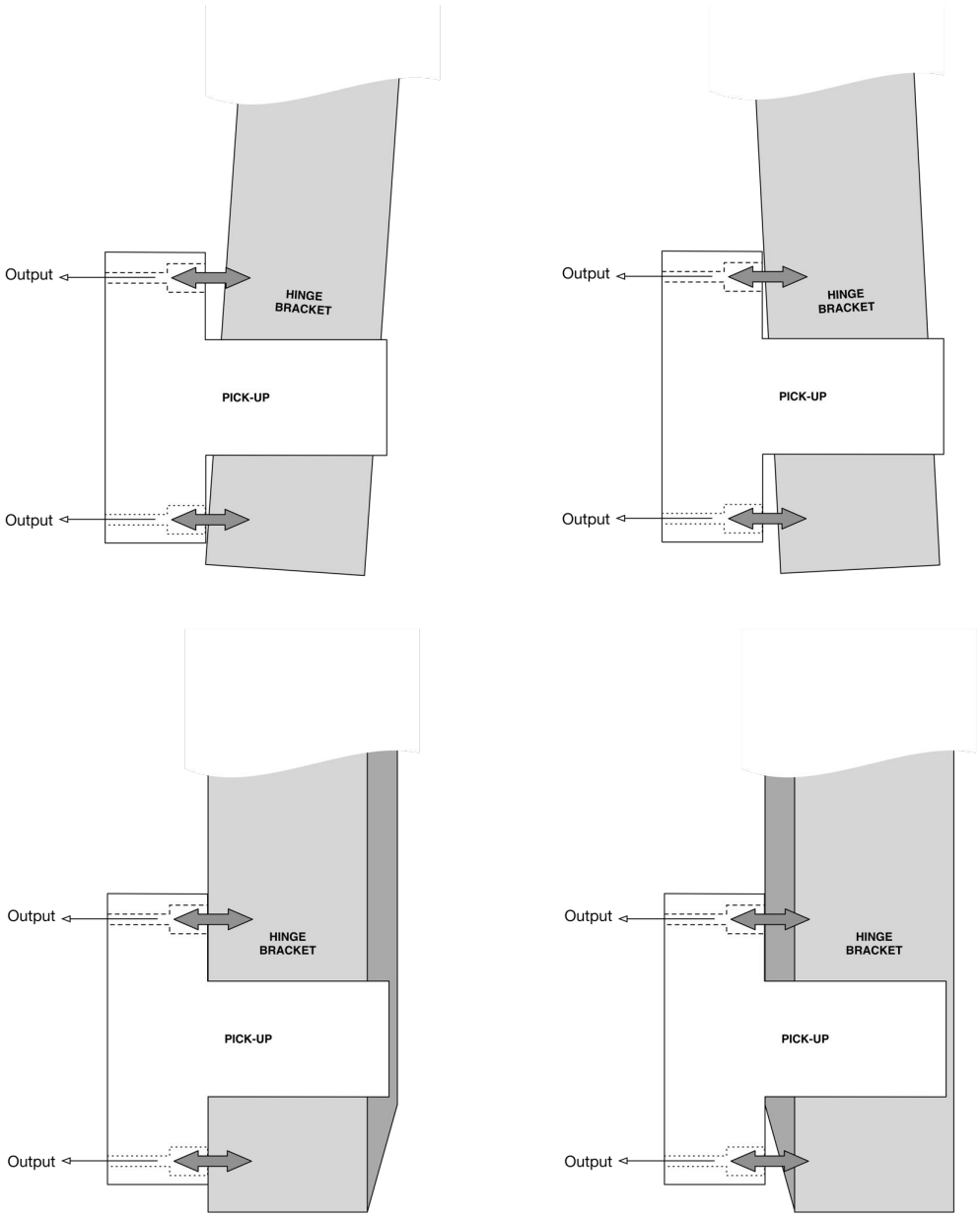


Figure 6-18: LVDT perpendicularity measurement with non-perpendicular hole

The plane's equation is calculated as:

$$\begin{vmatrix} x - x_1 & y - y_1 & z - z_{d1} \\ x_2 - x_1 & y_2 - y_1 & z_{d2} - z_{d1} \\ x_3 - x_1 & y_3 - y_1 & z_{d3} - z_{d1} \end{vmatrix} = 0, \tag{6.7}$$

using the convention introducing in Figure 6-19 and keeping $P_1$ as our origin, Equation 6.8 becomes:

$$\begin{vmatrix} x & y & z - z_{d1} \\ x_2 & y_2 & z_{d2} - z_{d1} \\ x_3 & y_3 & z_{d3} - z_{d1} \end{vmatrix} = 0. \tag{6.8}$$

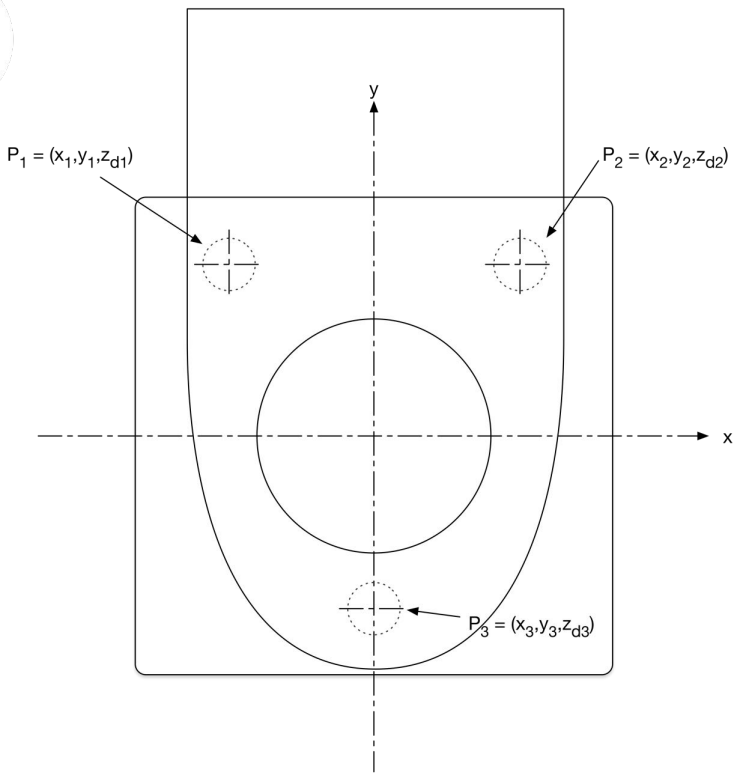


Figure 6-19: LVDT measurement

The angle between planes two planes, in the general forms $A_1x + B_1y + C_1z + D_1 = 0$, and $A_2x + B_2y + C_2z + D_2 = 0$ is given by:

$$\cos\theta = \frac{A_1A_2 + B_1B_2 + C_1C_2}{\sqrt{(A_1^2 + B_1^2 + C_1^2)(A_2^2 + B_2^2 + C_2^2)}}. \tag{6.9}$$

From the calibration process (6.4) we have: $A_1 = 0$, $B_1 = 0$, and $C_1 = x_2y_3 - y_2x_3$, so Equation 6.9 becomes:

$$\cos\theta = \frac{C_1C_2}{C_1\sqrt{A_2^2 + B_2^2 + C_2^2}}. \tag{6.10}$$

As the $x, y$ values remain the same, $C_1 = C_2 = C$, so Equation 6.10 becomes:

$$\cos\theta = \frac{C}{\sqrt{A_2^2 + B_2^2 + C^2}}. \tag{6.11}$$

The general solution to Equation 6.8 is given by:

$$\begin{aligned}(x - x_1)(((y_2 - y_1)(z_{d3} - z_{d1})) - ((z_{d2} - z_{d1})(y_3 - y_1)))-\\ (y - y_1)(((x_2 - x_1)(z_{d3} - z_{d1})) - ((z_{d2} - z_{d1})(x_3 - x_1)))-\\ (z - z_{d1})(((x_2 - x_1)(y_3 - y_1)) - ((y_2 - y_1)(x_3 - x_1))) = 0.\end{aligned} \tag{6.12}$$

With $P_1$ as the origin, Equation 6.12 reduces to:

$$\begin{aligned}x(y_2(z_{d3} - z_{d1}) - y_3(z_{d2} - z_{d1})) - y(x_2(z_{d3} - z_{d1}) - x_3(z_{d2} - z_{d1}))-\\ (z - z_{d1})(y_3x_2 - x_3y_2) = 0.\end{aligned} \tag{6.13}$$

Hence the measurement angle of the plane can be described as:

$$\cos\theta = \frac{C}{\sqrt{A_2^2 + B_2^2 + C^2}}, \tag{6.14}$$

where:

$$\begin{aligned} A_2 &= y_2(z_{d3} - z_{d1}) - y_3(z_{d2} - z_{d1}), \\ B_2 &= x_2(z_{d3} - z_{d1}) - x_3(z_{d2} - z_{d1}), \text{ and} \\ C &= y_3 x_2 - x_3 y_2. \end{aligned} \tag{6.15}$$

The variables: $x_{2,3}$ and $y_{2,3}$ are the positions of LVDTs 2 and 3, respectively; and $z_{d1,d2,d3}$ are given by the displacements measured by LVDTs 1,2 and 3 respectively.

The angle, $\theta$, gives a value that represents the planar deviation from the nominal/perpendicular plane. However, the GD&T definition of perpendicularity is defined through dimensional (and not angular) values; Figure 6-20 illustrates the definition in the context of the tooling situation (described in Figure 6-2).

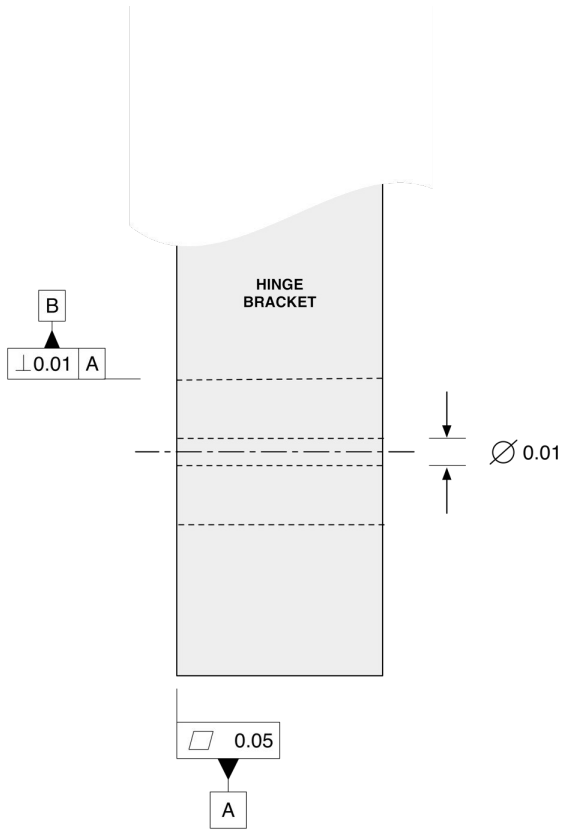


Figure 6-20: Perpendicularity tolerance effect on positioning of the nominal axis

Figure 6-20 shows how the central axis of the bore can not deviate by more than than a co-axial cylinder of 10 µm diameter. This has been simplified further in Figure 6-21; this illustrates the angular deviation of the datum plane as a consequence of maximum and minimum dimensional deviation of the central axis.

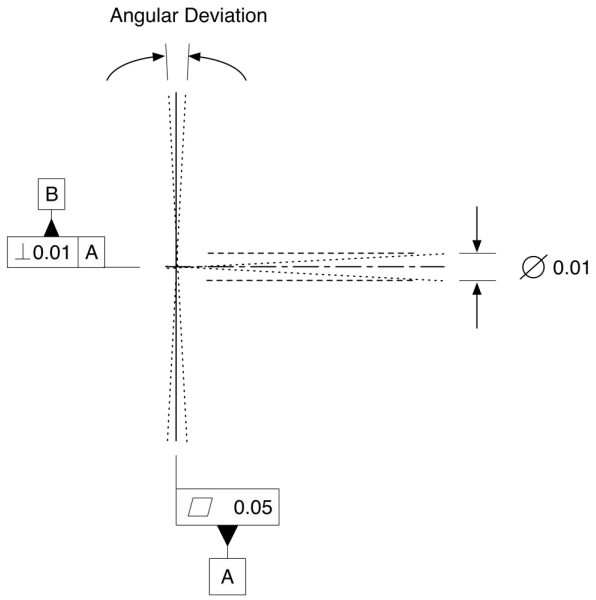


Figure 6-21: Perpendicularity tolerance effect on positioning of the nominal axis, in the $x, z$ plane

Assuming a Bore length of 100 mm, then the maximum planar deviation is $\pm 2.86648 \times 10^{-3}$ °.

**Uncertainty of Measurement** for determining the perpendicularity of the bore has number of contributions. These include:

- The commissioning gauge plate,
- The machining of the LVDT bores, and bore pick-up,
- The LVDTs' uncertainty of measurement.

These components of uncertainty interact with, and impact Equations 6.13 & 6.15 to determine the plane-to-plane angle. However, the commissioning gauge plate has

a significantly better associated uncertainty than the rest of the system, and so, can be considered as insignificant. Machining positional tolerances of 10 µm are readily achievable on modern machine tools, this will impact the $x_{2,3}$ and $y_{2,3}$ values, however the impact on the plane measurement is likely to be small, if not insignificant. The remaining machining tolerances, such as cylindricality and bore pick-up perpendicularity are sufficiently small to be considered insignificant.

The interaction of the variables and associated uncertainty can be modelled within a Monte Carlo Simulation. The MCS will consider the following inputs:

**Positional** $x_2, x_3, y_2, y_3$ with their associated machining tolerance/uncertainty (uniform/rectangular distributions): $u_{x2}, u_{x3}, u_{y2}, u_{y3}$, respectively.

**Measurement** $z_{d1}, z_{d2}, z_{d3}$ have a normally distributed associated measurement/instrument uncertainty: $U_{zd1}, U_{zd2}, U_{zd3}$, respectively.

To assess the sensitivity of the positional tolerance/uncertainty we set (in the $x, y$ plane): $P_1 = (0, 0); P_2 = (100, 0)$ & $P_3 = (50, -50)$ all in mm. The parameters: $z_{d1}, z_{d2}$ & $z_{d3}$ will be given values of 0,2,3 µm, respectively, if the plane-to-plane angle would be equal to zero any $x, y$ positional uncertainty would have no effect as the uncertainty would be *in-plane*. These LVDT values give an angular deviation close to the tolerance limit; hence, represent a near worst-case. $U_{zd1}, U_{zd2}$ & $U_{zd3}$ will be set to zero, without the interjection of measurement uncertainty the simulation will show the effect of only adding a positional uncertainty of 10 µm (that is, for parameters: $u_{x2}, u_{x3}, u_{y2}, u_{y3}$). The MCS is executed with 10,000 iterations, the results are as shown in Figure 6-22. A standard deviation of $2.7301031 \times 10^{-7}$ °, this is proportionally small, and can be considered as an insignificant uncertainty contribution.

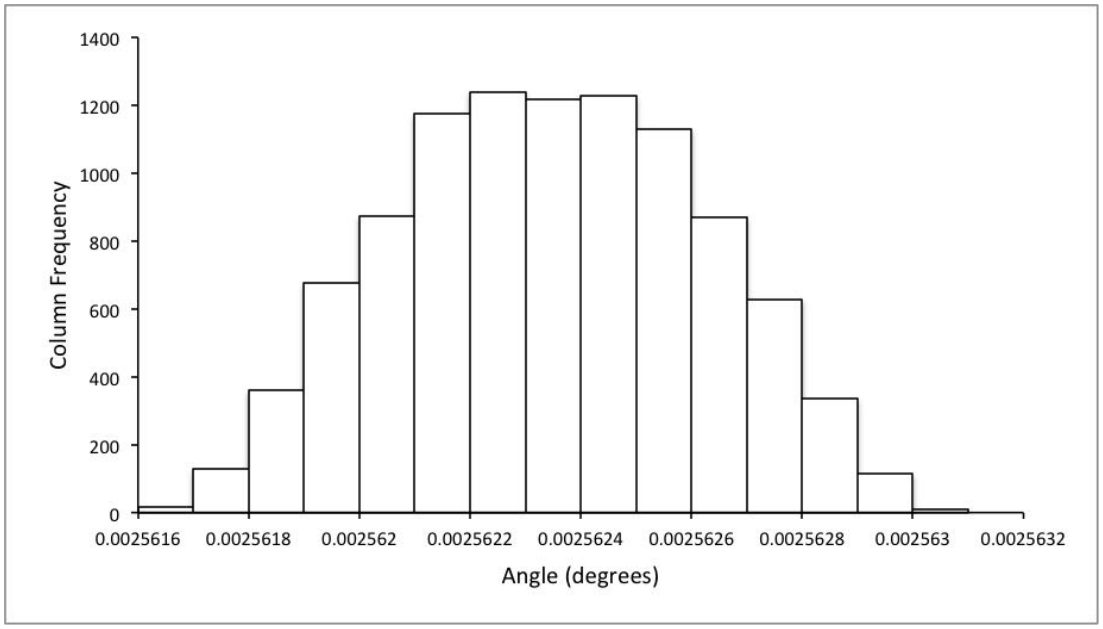


Figure 6-22: Effect of machining uncertainty on plane angular measurement

Hence the MCS now can be run, excluding the *positional* uncertainty contribution - $u_{x2}, u_{x3}, u_{y2}, u_{y3}$ - and only include the *measurement* uncertainties: $U_{zd1}, U_{zd2}$ & $U_{zd3}$. These are set at 0.235 µm at 1 sigma, this is from the instruments' calibration certificate. The highest standard deviation $3.30 \times 10^{-5}$ °; this represents less than 1.15% of the perpendicular tolerance.

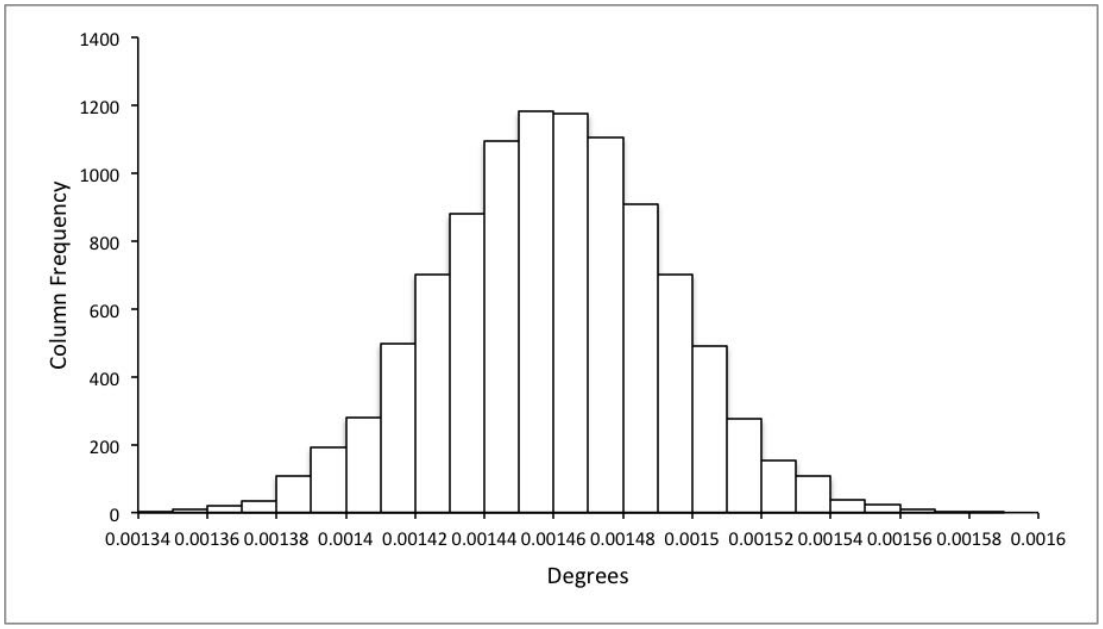


Figure 6-23: Effect of machining uncertainty on plane angular measurement

### 6.5.3 Solartron, LVDTs for Step Condition

**Commissioning** the step measurement LVDTs use a similar philosophy to the above perpendicularity measurement. The LDVTs are 'zeroed' using a gauge plate, once a nominal *flush* condition has been established the step measurement is simply computed. Figure 6-24 illustrates the commissioning stage.

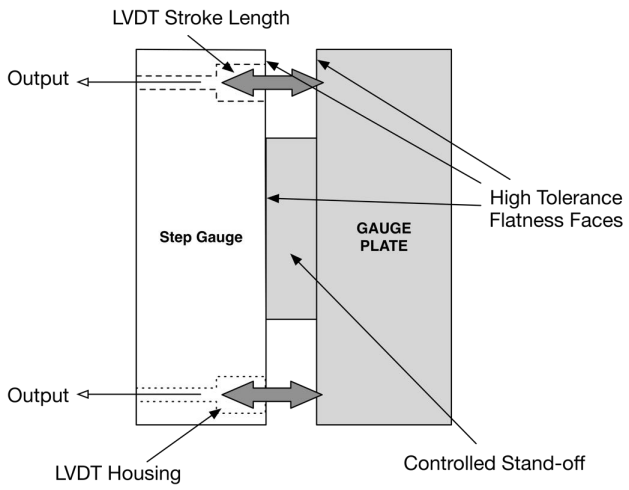


Figure 6-24: Commissioning the LVDT step gauge

**In-Fixture Measurement** is simply the difference between the LVDT readings. This gives the value of the step.

**Uncertainty of Measurement** The uncertainty of the step measurement has the following components. They include:

- LVDT instrument uncertainty (0.235 µm at 1 sigma),
- Perpendicularity of LVDTs creating a Cosine error along the stroke length (Figure 6-25),
- Planar setting of the pick-up (Table 6.6), subsequent Cosine error (Figure 6-26).

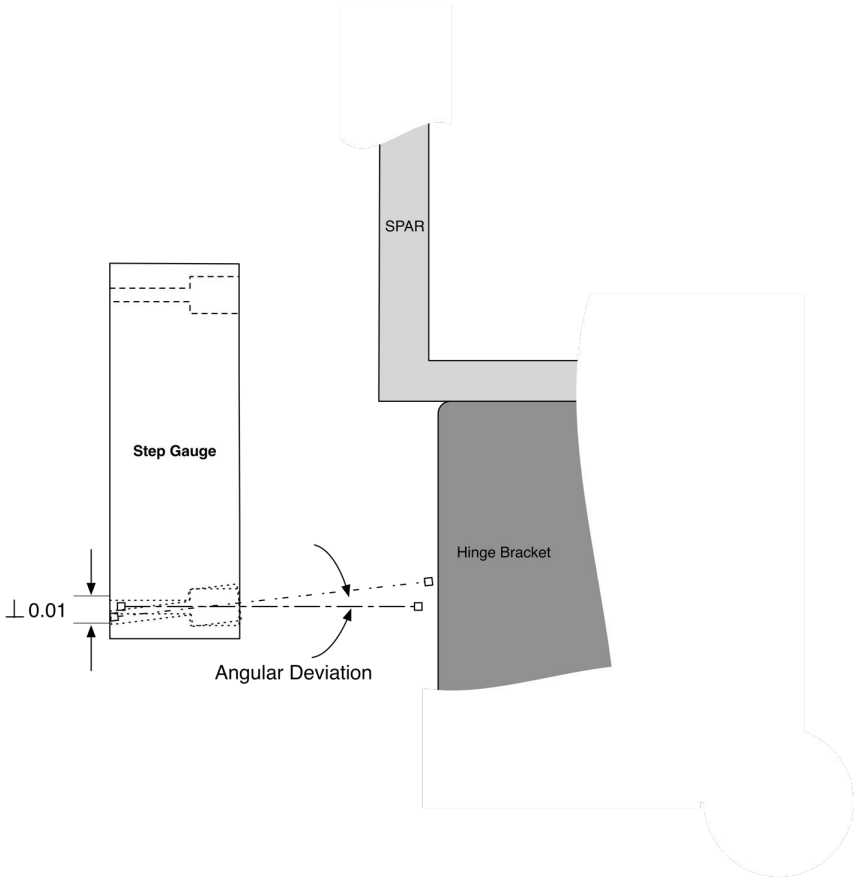


Figure 6-25: Uncertainty associated with the perpendicularity LVDT step gauge

Assuming a maximum LVDT stroke length of 10mm and a perpendicularity tolerance of 10 µm, and a LVDT body length 50mm; with respect to Figure 6-25 this gives an angular deviation of:

$$\tan^{-1} = \frac{0.01}{50} = 0.0115°. \tag{6.16}$$

Over a 10mm stroke length this Cosine error translates to:

$$10\cos(0.0115) = 9.9999998mm. \tag{6.17}$$

This leads to a Cosine error due to machining tolerances of 0.0002 µm; this can be considered as negligible when compared to the desired tolerance of 150 µm.

| Component | Value μm | Distribution | Divisor | Standard Uncertainty μm |
|---|---|---|---|---|
| SMR Centering[1] | 6.00 | Rectangular | $\sqrt{3}$ | 3.46 |
| Setting Tolerance[2] | 50.00 | Rectangular | $\sqrt{3}$ | 28.87 |
| Instrument Uncertainty[3] | 45.00 | Normal | 2 | 22.50 |
| | | Combined Standard Uncertainty, $u_c$ | | 36.76 |
| | | Expanded Standard Uncertainty $(K = 2), U_c$ | | 73.53 |

Table 6.6: Uncertainty contributions for setting a planar surface

[1] Mechanical tolerance statement.

[2] This is the value that the operator/tool-setter will use to set the tool within nominal, according to the instrument dynamic readout.

[3] Value from manufacturers statement - at 5m.

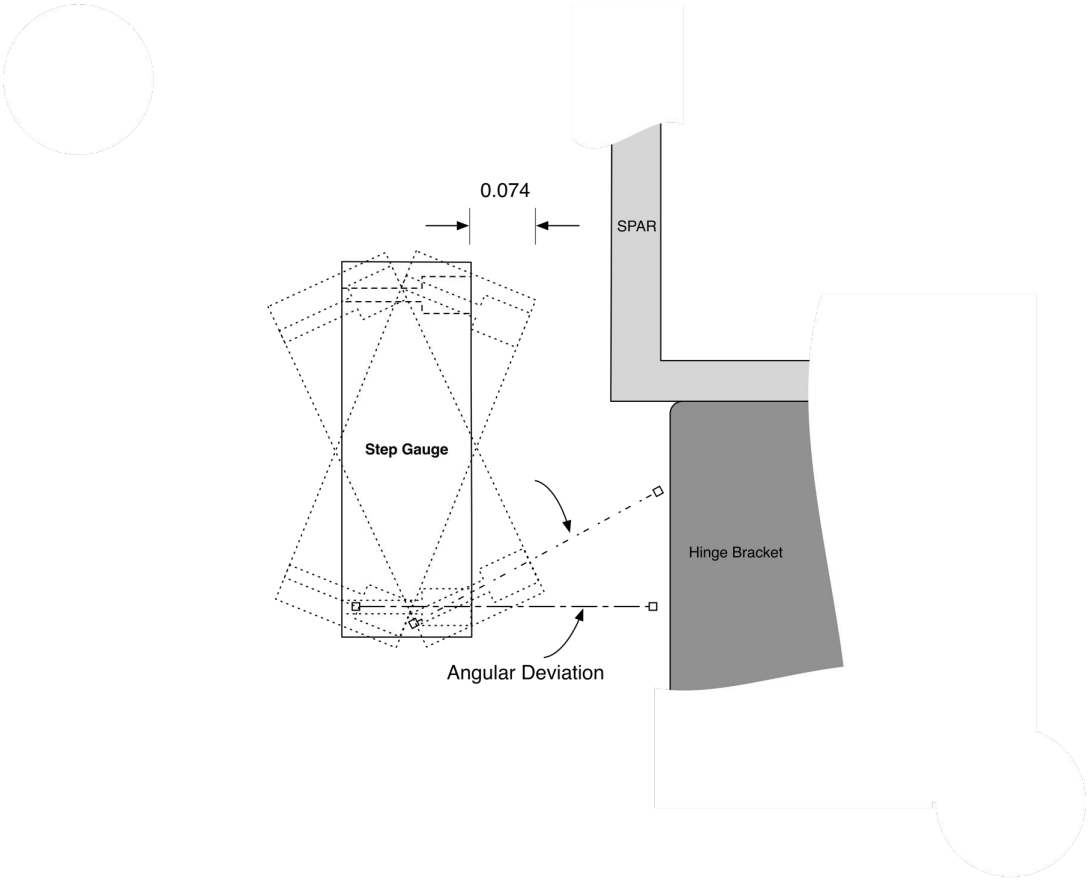


Figure 6-26: Uncertainty of setting the LVDT step gauge

With a planar setting of 74 µm, over a length of 150mm between LVDTs gives rise to a maximum angular deviation of:

$$\sin^{-1} = \frac{0.074}{150} = 0.0282^{\circ}, \tag{6.18}$$

this translates to a Cosine error of:

$$10\cos(0.0282) = 9.999998783mm. \tag{6.19}$$

This gives an uncertainty of 0.001 22 µm, and hence can be considered insignificant. Combining the uncertainties gives a local step measurement uncertainty of less than a single micron; consequently we can consider the measurement uncertainty as insignificant when assessing the 150 µm tolerance applied to the step condition.

**Third Dimension, GapGun**

The GapGun is an off-the-shelf solution for Step and Gap measurement; although included in the RAG interface, the system was commissioned via the manufacturer as part of an Airbus activity,

### 6.5.4 4G Metrology, ScAlert

**Commissioning** the temperature sensors is achieved by attaching the thermistors to the jig structure using adhesive tape with a thermal compound to improve conductivity from the fixture to sensor; these sensors are positioned close the the Jig Reference System (JRS, also known as the ERS) and represent working envelope/volume of the tooling. The sensors were distributed on the ALCAS assembly tooling introduced in Section 5.2.3.

**In-Fixture Measurement** can be carried out periodically and logged in the server, or, the measurement is retrieved via the RAG interface when the *Check Assembly* button is pressed.

**Uncertainty of Measurement**: the stated uncertainty of the temperature sensors - from the calibration certificate - is $\pm 0.5\,^{\circ}\mathrm{C}$. For a steel fixture this gives rise to a dimensional uncertainty of $\pm 6\,\mu\mathrm{m/m}$, based on a linear expansion model and a CTE of 12ppm/K. The temperature sensors were distributed through a fixture in an uncontrolled factory environment, this enabled data to be passively collected to help inform the necessity for thermal monitoring within fixtures. Figure 6-27 shows the position of the temperature sensors distributed on the ALCAS fixture.

The temperatures recorded over the period are shown in Figure 6-28. Figure 6-28(a) shows the individual temperature readings over a two week period. There is a consistent difference in temperature, however the temperature differences are not as expected: the lower temperatures are not always at the lowest points and higher temperatures are not always higher up; as an example: the *AUK F-12* sensor is consistently at the highest temperature, however, this sensor is low down and towards the back of the facility; a sensor in this position would be expected to have one of the lowest temperatures - this higher temperature may be due to a thermal current from a heater or a local heat source (such as a automation controller). The largest sensor differences are shown in Figure 6-28(b), with the high and low points indicated, as well as the average temperature.

The differences in the temperature readings average at $1.5\,^{\circ}\mathrm{C}$, with a thermal dis-

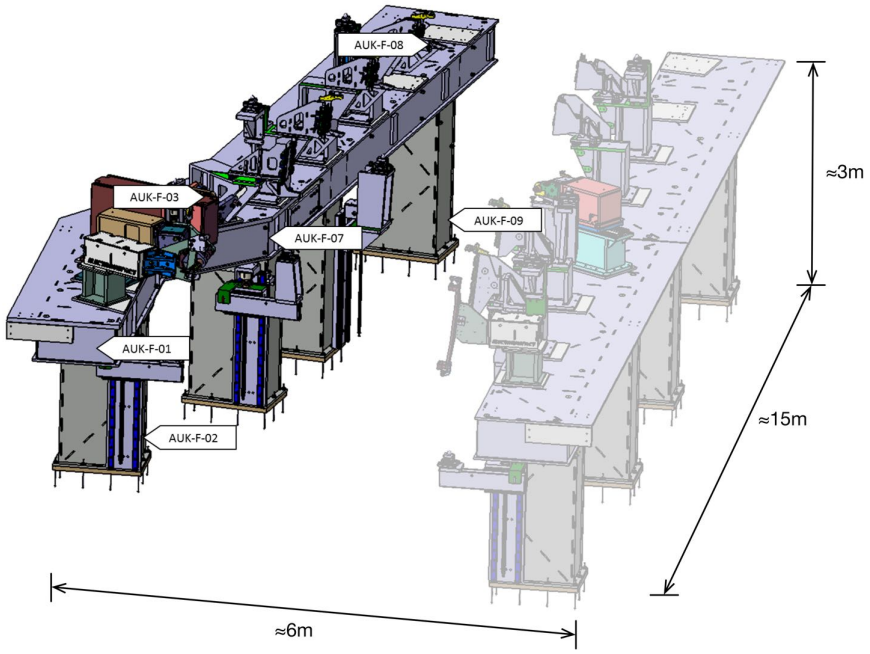


(a) Trailing Edge

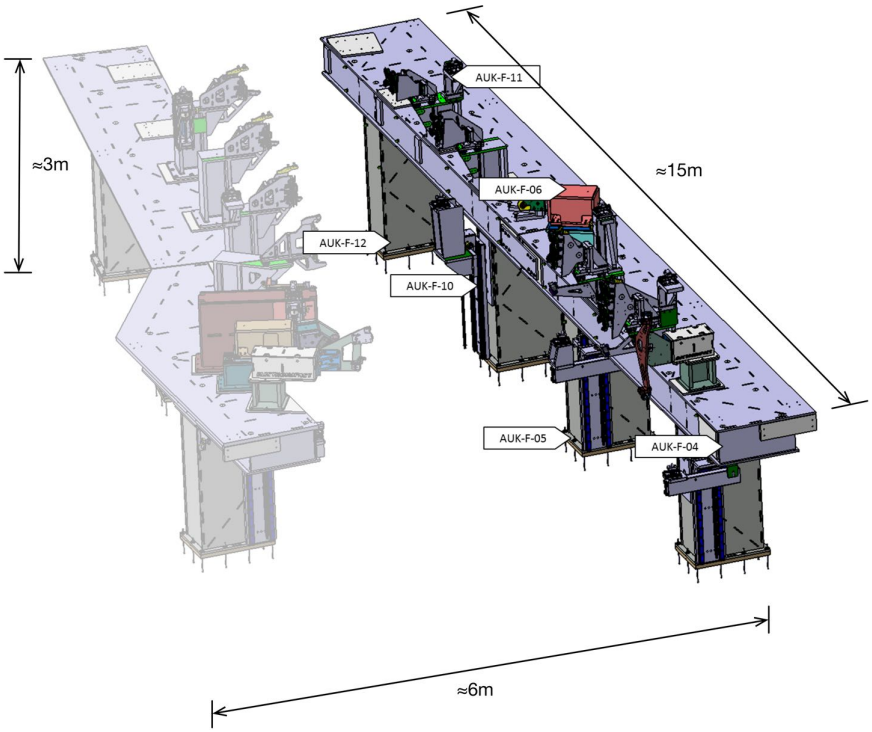


(b) Leading Edge

Figure 6-27: Positions of ScAlert sensors on the ALCAS MAJ

parity of between 0.8-2.5 °C. This has a significant impact on the the fixtures ability to hold the assembly tolerances. The differences incurred are significant in comparison to the design tolerances, and without considering the thermal expansion, tolerances would easily be exceeded. However, in this context the sensor uncertainty of ±0.5 °C is too large and could be significantly impacting the recorded measurements. Consequently the thermal measurements and the approximation of the linear expansion model, can identify gross errors and thermal issues within the fixture.

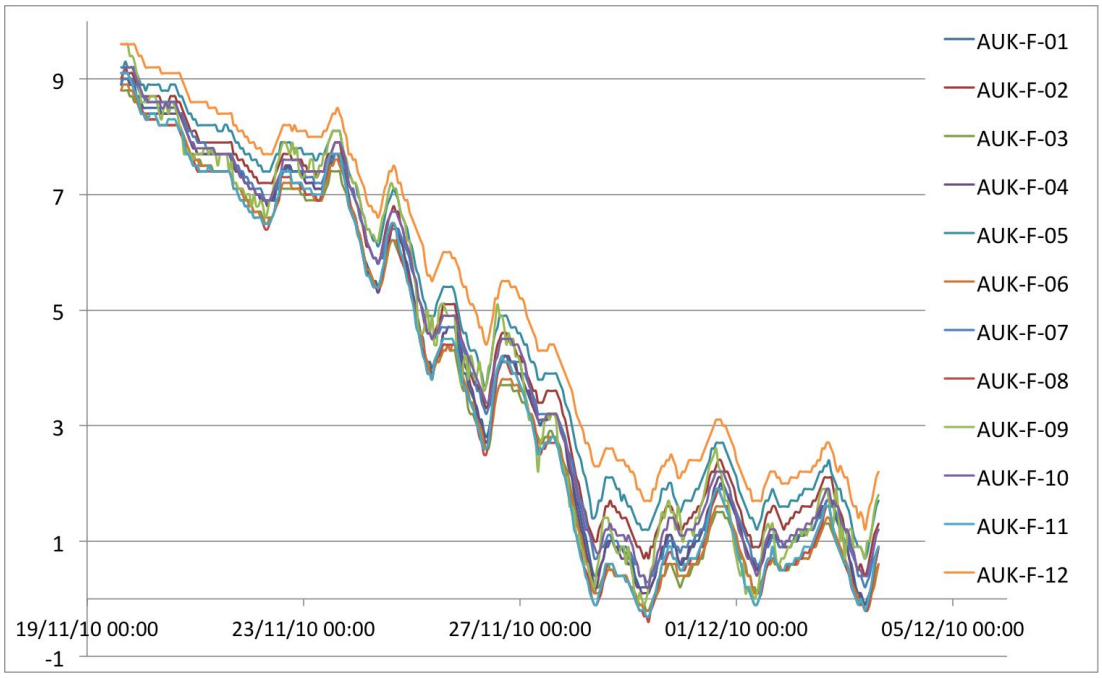


(a) Individual sensor readings

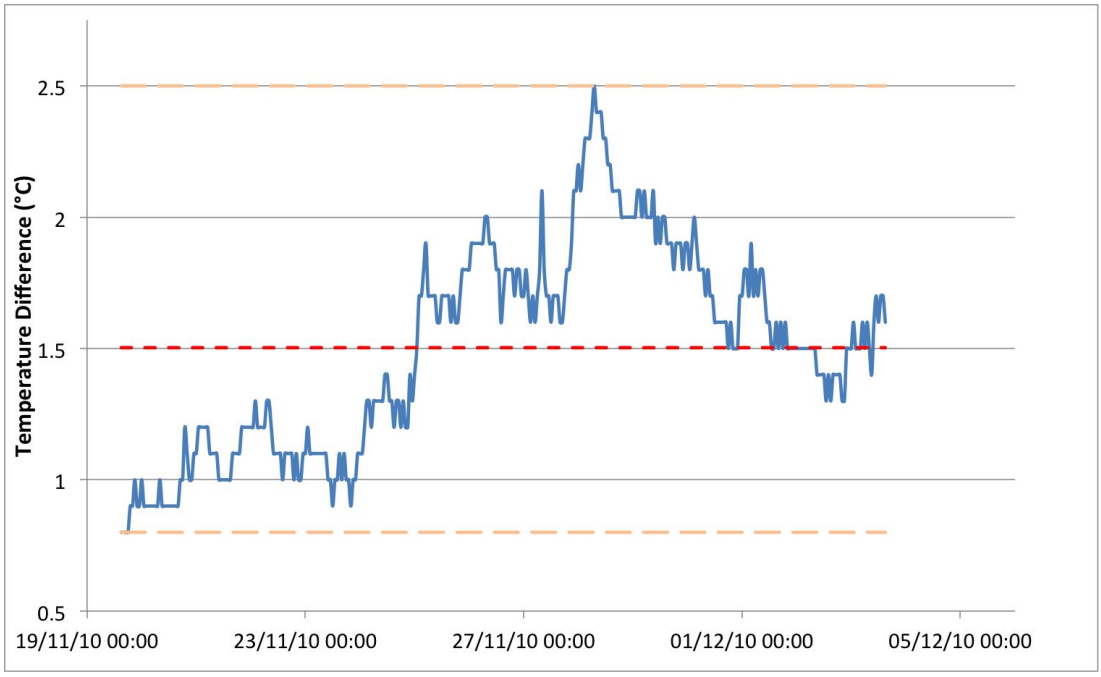


(b) Difference in temperature sensor extremities on ALCAS MAJ

Figure 6-28: The temperature measurement of the ALCAS MAJ

## 6.6 Chapter Summary

This chapter has suggested how embedding metrology into tooling can automate in-fixture feature checks such as interchangeability (ICY) requirements and Key Characteristics (KCs). Embedded metrology systems increase the data collection opportunities with aerospace manufacture, giving *accurate* and *quantitive* data, not just a binary data set typical of in-fixture gauge measurements. Additionally, digital sensors remove operator dependancies and therefore increases repeatability (within the limits of the measurement uncertainty). Lastly, data is acquired quickly (2-6 seconds), and does not require specialist operator intervention. It follows that automated data collection can enable active tooling, that is: tooling that manipulates the component or assembly autonomously, this is detailed in *Metrology Feedback* (Chapter 7).

Figure 6-11 shows the elements of the META framework, handled by the positional embedded metrology systems examined in this section. These embedded systems have been examined from an uncertainty of measurement perspective and have shown to exhibit better *local GD&T* uncertainties than setting to a global datum structure such as Wing or A/C Axis.

# Chapter 7

# Metrology Feedback

## 7.1 Introduction

This chapter shows how metrology feedback can be used to automate the positioning of tooling pick-ups with the use of metrology feedback, by targeting the key manufacturing feature *not* the nominal tooling position.

The literature review (Chapter 2) indicated that a gap exists relating to: *an integrated approach towards metrology and aerospace Wing-box assembly tooling* This is more specifically identified in the review of industrial practices within aircraft Wing-box assembly tooling (Chapter 3), as a need to:

- Reduce manual metrology checks & reduce tooling reliance
- Enable greater automation
- More robust component placement

The requirements can be addressed with the META framework (Figure 7-1). This chapter details a coupon study of automation within assembly tooling, sometimes referred to as: *live fixturing*. This example shows that automated pick-ups can perform fixture-setting, correction and measurement. The research uses a measurement instrument to control the position of an actuated tooling flag, the flag will automatically adjust until the Key Characteristic (KC) of the part/assembly is within tolerance of its nominal position (closed loop control). In the case of this study the actuated flag is

a Hexapod (also known as a Stewart platform) from Physik Instrumente (PI) and the KC is the hinge line axis that runs through the hinge bracket's bore.

For this trial a hexapod was used to provide 6DOF manipulation of the component. The DOF could be isolated as required. The 6DOF capability of the hexapod also enables the tooling be assembled with more open tolerances, in both position and orientation (see Section 7.2).

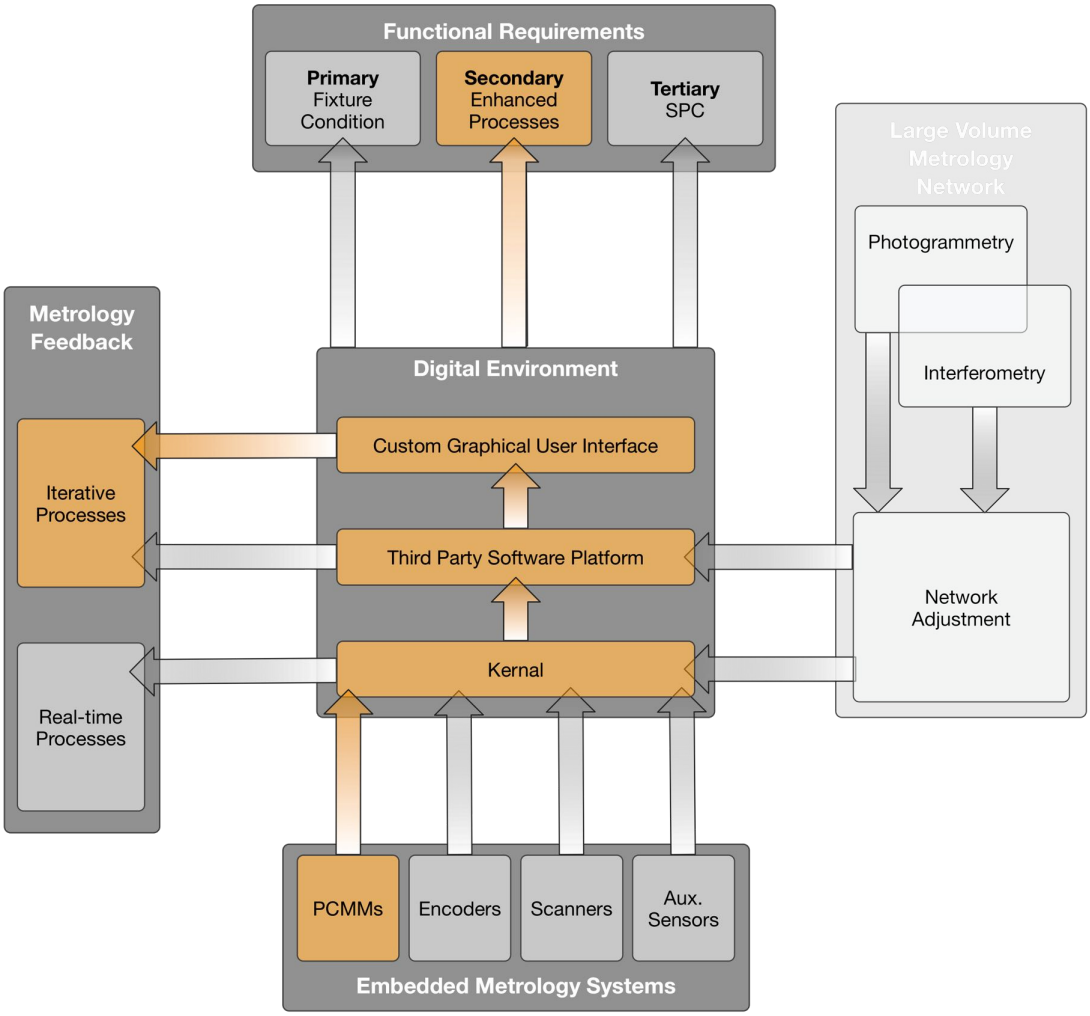


Figure 7-1: Automation requirements addressed with the META framework

This trial was carried out concurrently with the *Airbus Tooling Hub* activities, at the Centre for Aerospace Manufacturing based at the University of Nottingham (UoN).

## 7.2 Hexapod Location

The methods used to build the trial fixture (Figure 7-2) cannot perfectly align the native co-ordinate frame of the hexapod (Figure 7-3) to the jig co-ordinate base-frame; aligning these frames accurately would be a time consuming and laborious exercise. A more robust and quicker method is to identify the location and orientation of the hexapod's frame and transform the relevant information into the jig co-ordinate system when required; if calculations are completed with an appropriate degree of accuracy no loss of information will occur when changing from frame-to-frame. This method allows the hexapod to be approximately placed in its nominal position without considering the hexapod's position and orientation.

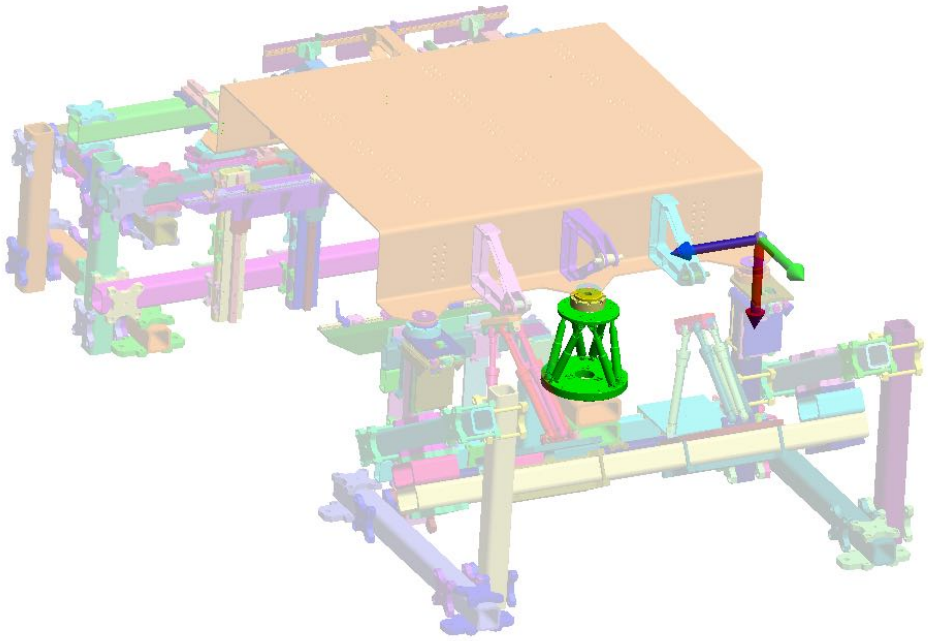

Figure 7-2: Location of study on University of Nottingham demonstration fixture and jig co-ordinate frame

The hexapod is moved to the extreme of each axis in isolation using PI's proprietary software interface (Figure 7-4); each axis extremity is measured using a *Leica AT901* laser tracker and SpatialAnalyzer (SA). This enables the definition of the working envelope ($x$ = ±50mm, y±50mm, z=±25mm) and the creation of the physical, native co-ordinate frame of the hexapod relative to the fixture's co-ordinate frame. Subsequently, the hexapod can be manoeuvred into its CAD nominal position by ob-

Figure 7-3: Native hexapod co-ordinate frame in its CAD nominal position

taining the translations $[x, y, z]^T$ and rotations $[\alpha, \beta, \gamma]^T$ from the SA function: "compare to CAD". This method is consistent with the fixture build philosophy used for the construction of the fixture. In turn the physical location of hexapod's frame can be compared to the CAD nominal location of the hexapod frame (Figure 7-5). The transformation matrix from native to CAD nominal (Equation: 7.1) gives us the offsets required to reach the intended CAD nominal position.

$$T = \begin{bmatrix} \cos\alpha\cos\beta & cos\alpha\sin\beta\sin\gamma - \sin\alpha\cos\gamma & cos\alpha\sin\beta\cos\gamma + \sin\alpha\sin\gamma & x_t \\ \sin\alpha\cos\beta & sin\alpha\sin\beta\sin\gamma + \cos\alpha\cos\gamma & sin\alpha\sin\beta\cos\gamma - \cos\alpha\sin\gamma & y_t \\ -\sin\beta & \cos\beta\sin\gamma & \cos\beta\cos\gamma & z_t \\ 0 & 0 & 0 & 1 \end{bmatrix} \tag{7.1}$$

This is a specific transformation matrix that uses the sequence: rotate about $x$ $(\alpha)$, followed by $y$ rotation $(\beta)$, then rotated about $z$ $(\gamma)$, finally, performing a translation in $x, y, z$; this is the sequence that the SA software uses. The offsets required in this case by the hexapod are $[x, y, z, \alpha, \beta, \gamma]^T = [20.439, 1.3195, 0.3847, -0.25, -0.10, 0]^T$, and the subsequent transformation matrix is:

$$T_H = \begin{bmatrix} 0.999998 & 0.000008 & -0.001745 & 20.439000 \\ 0.000000 & 0.999990 & 0.004363 & 1.319500 \\ 0.001745 & -0.004363 & 0.999989 & 0.384700 \\ 0.000000 & 0.000000 & 0.000000 & 1.000000 \end{bmatrix} \tag{7.2}$$

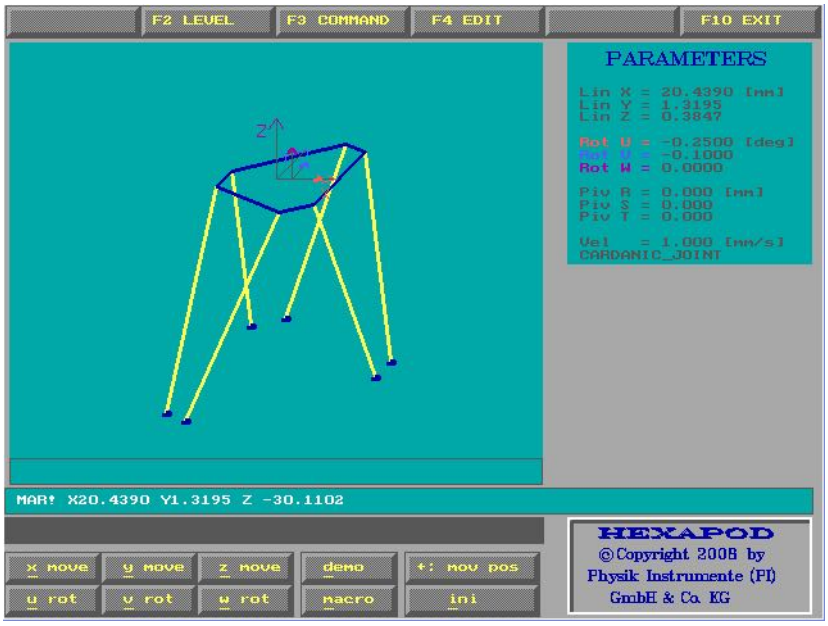


Figure 7-4: PI hexapod controller interface

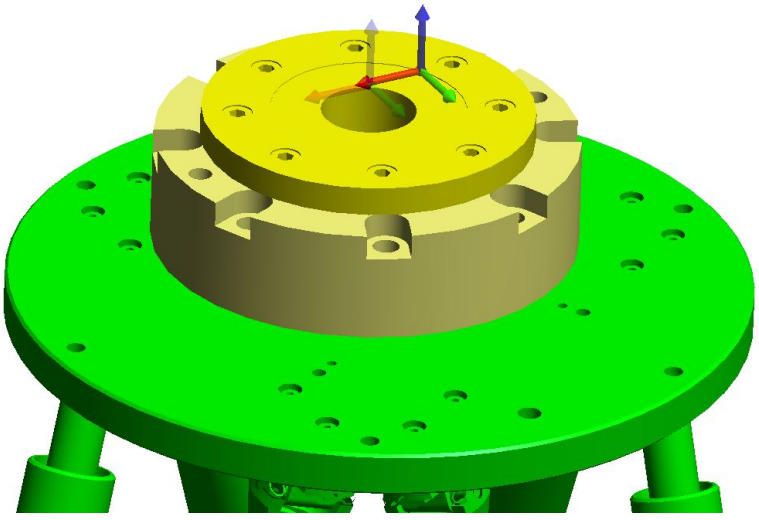

Figure 7-5: Actual position of the hexapod's native co-ordinate frame

## 7.3 Hexapod Communication & Control

The measurement information from the laser tracker continuously streams to SA. SA converts the native spherical co-ordinates (Section 2.4.2) from the laser tracker to the Cartesian co-ordinates required for the hexapod control. This post-processed data is streamed via a User Datagram Protocol (UDP) to a bespoke program created by the author designed to bridge the interface gap between the PI hexapod interface and SA. The interface program (Figure 7-6) samples the UDP data stream, checks whether the KC is within tolerance, sends the required corrective movement to the hexapod and checks whether the hexapod is stationary before iterating. The communication paths between the hardware and software are shown in Figure 7-7. The program also enabled the control of a selection of parameters, such as: the tolerance threshold, hexapod velocity, enabling and disabling the hexapod's degrees of freedom and closed or open loop control; the latter is discussed in Section 7.4.

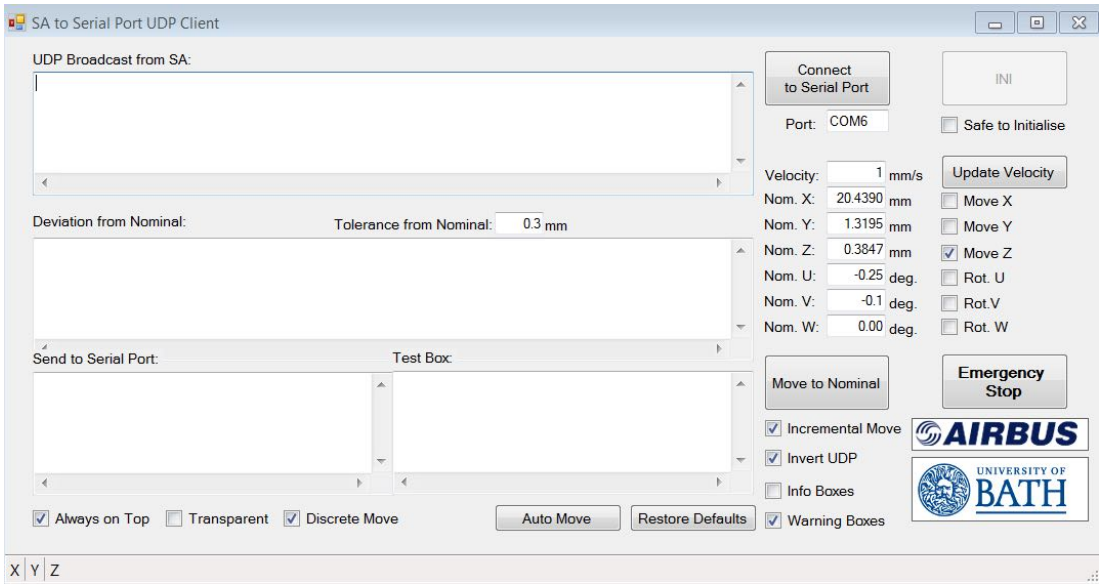


Figure 7-6: META GUI created for hexapod control

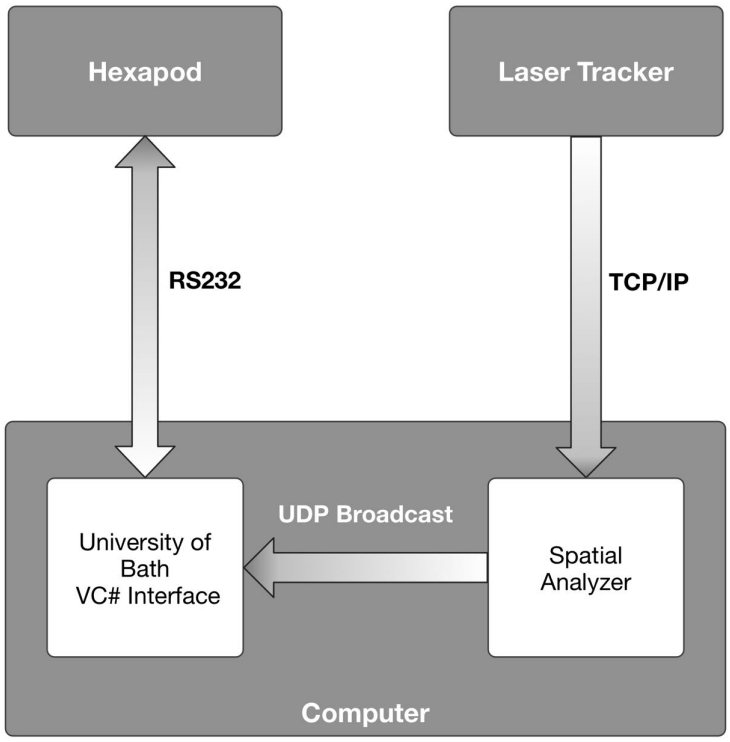


Figure 7-7: Schematic of hardware/software communication

## 7.4 Metrological Feedback

The metrology requirement is to measure the deviation from the hinge bracket's bore to its nominal CAD position; the hexapod will move accordingly, attempting to reclaim the hinge line's CAD nominal position. The hexapod is attached to the spar via a *zero point clamp* (Figure 7-8); there is a substantial offset from the point of attachment to the point of interest (POI) (Figure 7-9), and between hexapod and the POI are compliant connective elements: zero point clamp, spar, hinge bracket and vector bar. As the relationship between the hexapod and the POI cannot be considered as a rigid body, the metrology feedback will have to be in a closed loop (Figure 7-10(a)); if however there was a rigid relationship or a predictable relationship between the movement of the hexapod and the POI, the PI hexapod is accurate enough to support an open loop system - this is quicker and less resource intensive (Figure 7-10(b)).

An open loop system is advantageous when considering measurement resources and time; a closed loop system requires continuous measurement, whereas an open loop system requires a single measurement. If many POIs require measurement and actuation, closed loop systems are *bottlenecked* by the metrology resource as it is unfeasible from a cost perspective to dedicate a laser tracker to each pick-up. One way to partially mitigate this resource limitation is to employ an open loop system; as the measurement system can sequentially measure each POI. However, the cost savings presented by reducing the number of metrology systems is offset against the high accuracy actuators an open loop system requires. Due to the compliance of large aerospace components it is unlikely that a truly open-loop system would be achievable. Hence a method that uses periodic feedback could be more appropriate, that is, a single measurement system cycling through the POIs.

Figure 7-9 highlights the hexapod's native co-ordinate frame after the origin has been translated to the POI; it follows that measurements taken from this new co-ordinate frame are essentially deviations from the POIs nominal position. Consequently, the co-ordinates - and hence the deviations from nominal - are streamed from SA via the UDP.

The measurement instrument used for the trial was a *Leica LT500* laser tracker, this was a readily available instrument with an acceptable accuracy capable of real-time, three dimensional measurement. 3D co-ordinates were assumed as appropriate since the compliance of the material is limited to two dimensions and this research assessed the feasibility of reclaiming the hinge line. Figure 7-11 shows the laser tracker

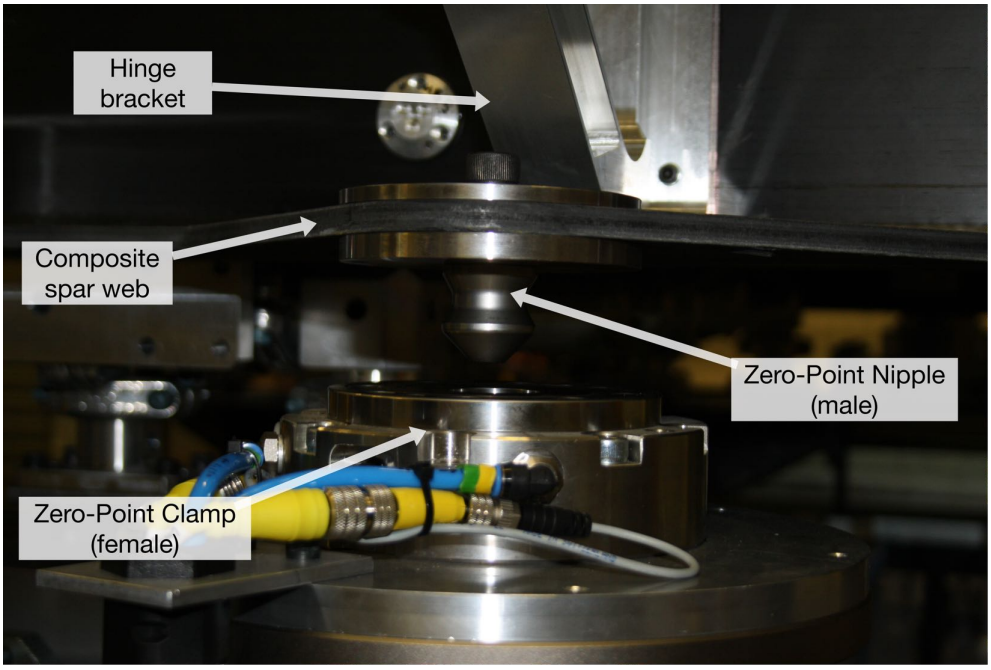


Figure 7-8: Close-up of the zero-point clamp

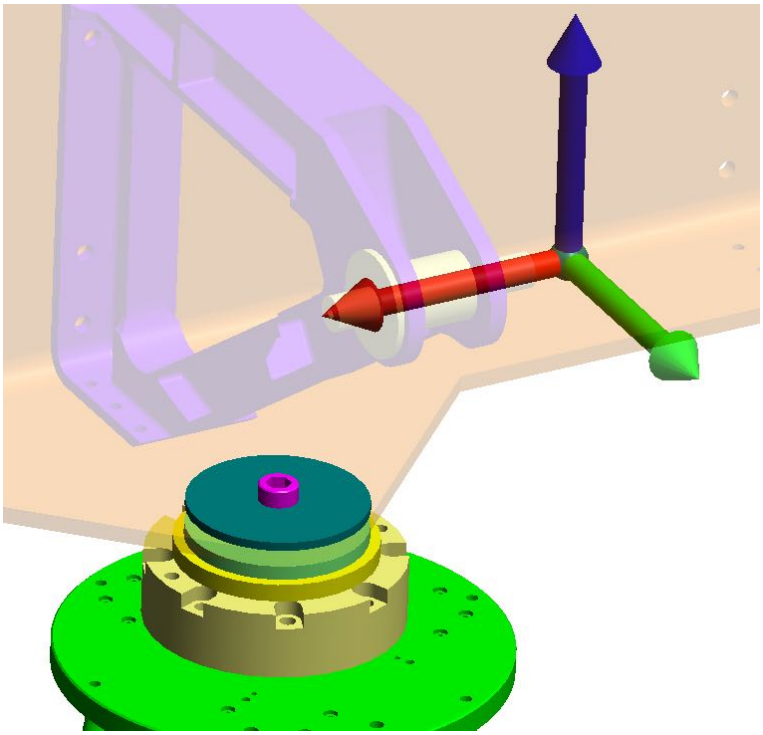

Figure 7-9: Hexapod's native co-ordinate frame after transformation to CAD nominal position of hinge-line axis

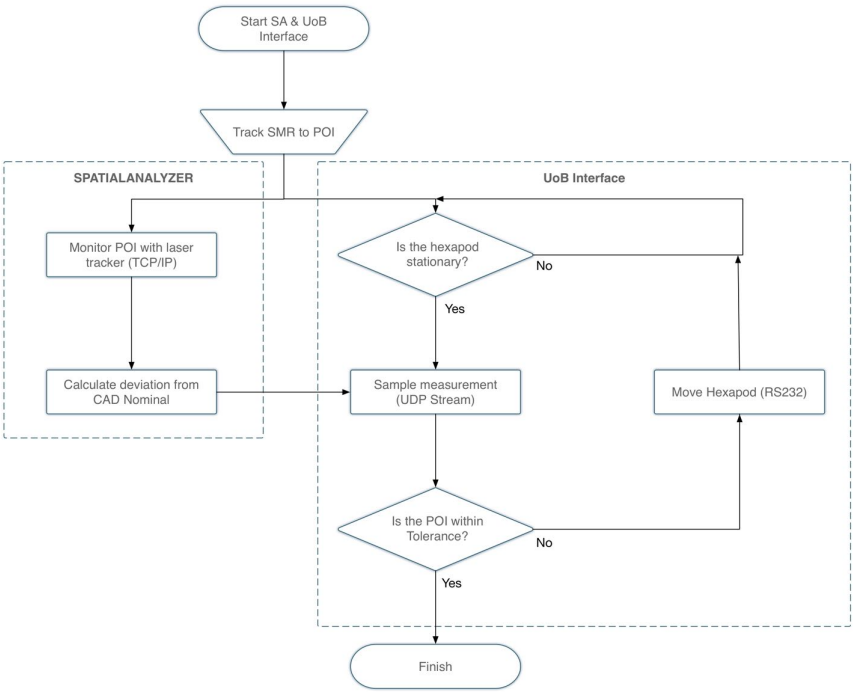


(a) Closed loop control of hexapod

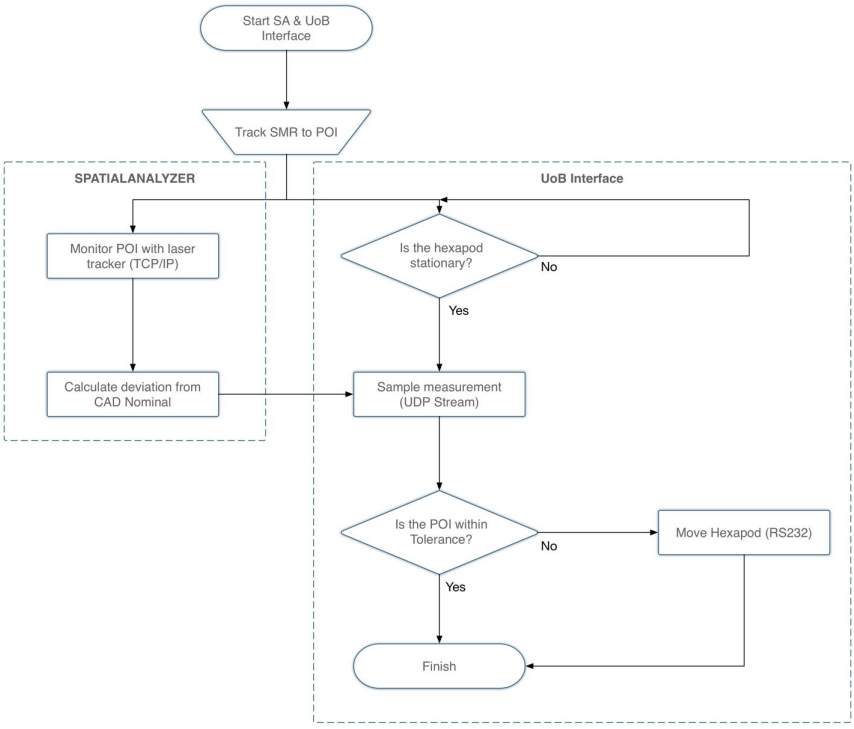


(b) Open loop control of hexapod

Figure 7-10: Metrology feedback

measurement target in relation to the zero-point clamp attachment point.

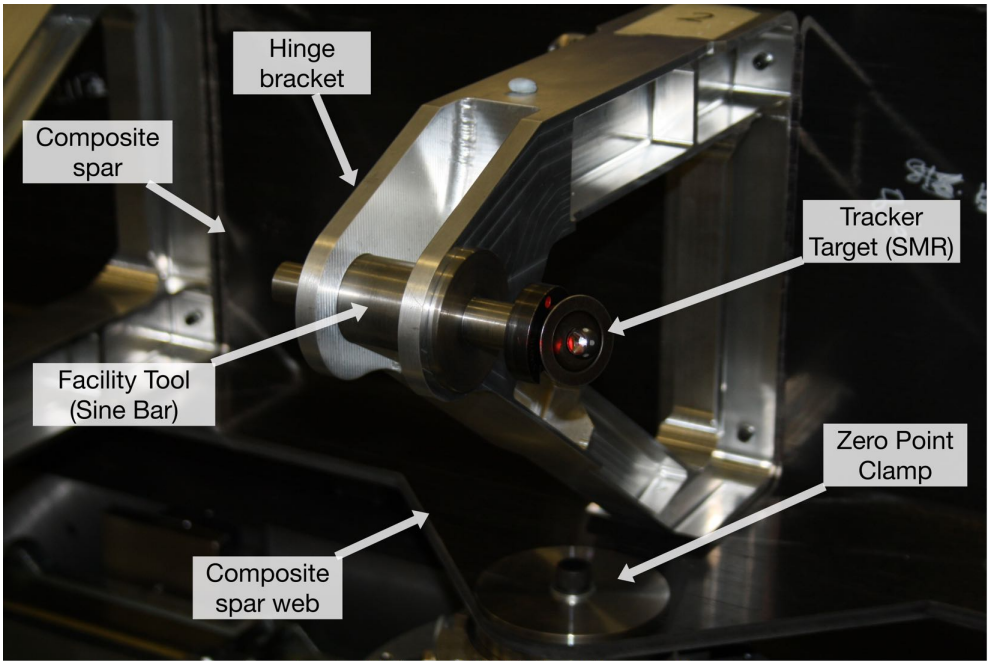


Figure 7-11: Facility tooling for targeting the hinge line

The trial engaged the hexapod's $y$ (chord-wise) and $z$ axis (vertically up) in isolation as these axes had the largest deviations from CAD nominal. The stiffness and stress impact of movement along the wing-box's span-wise ($x$) direction was unknown and the risk to the component was high, as the longitudinal movement was likely to add additional stress to the fasteners as the structure had high rigidity in this plane. Rotational movements were excluded at this stage because only one POI in 3D was monitored, rotational movement is more appropriate when best-fitting multiple points or with 6DOF metrological feedback.

## 7.5 Results

The closed loop configuration of the hexapod achieved the designated tolerance threshold of $\leq$300 µm. The largest out of tolerance axis was $z$. The closed loop configuration moved the POI a total of 0.421mm in the $y$-axis and negative 1.572mm in the $z$- axis; the hexapod achieved the stated tolerance threshold within two iterative cycles this is summarised in Figure 7-12.

The hexapod's internal encoders registered a movement of 1.103mm in the $y$-axis (Figure 7-13) and negative 2.412mm in the $z$-axis (Figure 7-14); this difference can be attributed to the material compliance. The compliance was observed as the gap between the hinge rib base and spar web closed-up during manipulation. This supports the assertion that the POI and hexapod do not act as a rigid body.

However, Figure 7-13 and Figure 7-14 show that after 5 iterations the deviation between the POI and hexapod displacements begin to level out, reducing the significance of the component deflection and offset.

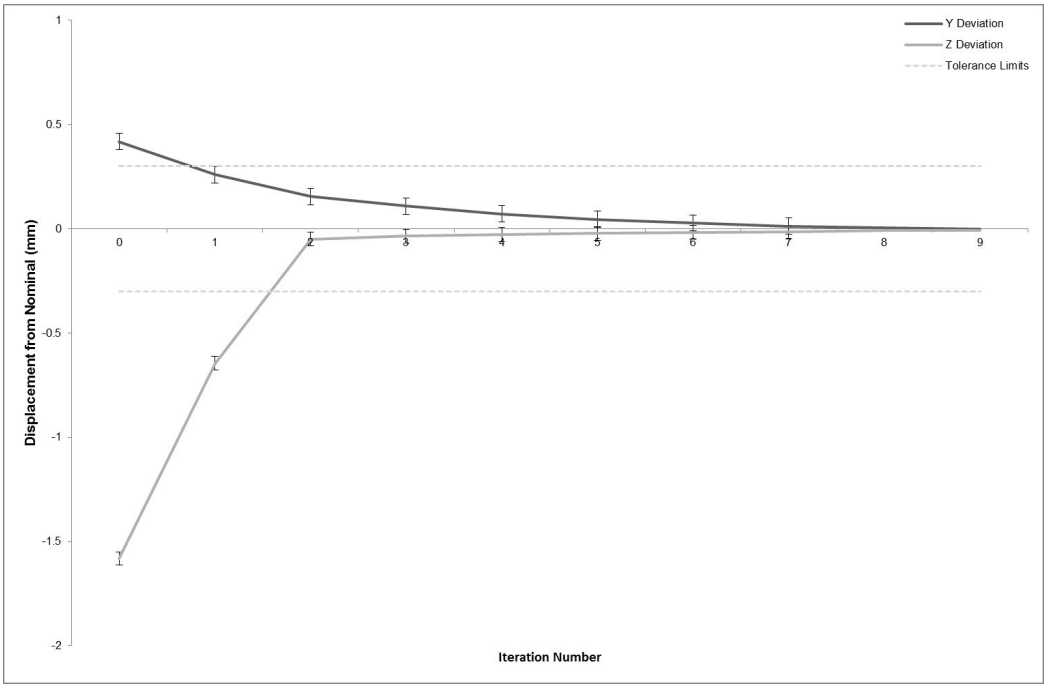


Figure 7-12: POI deviations from nominal

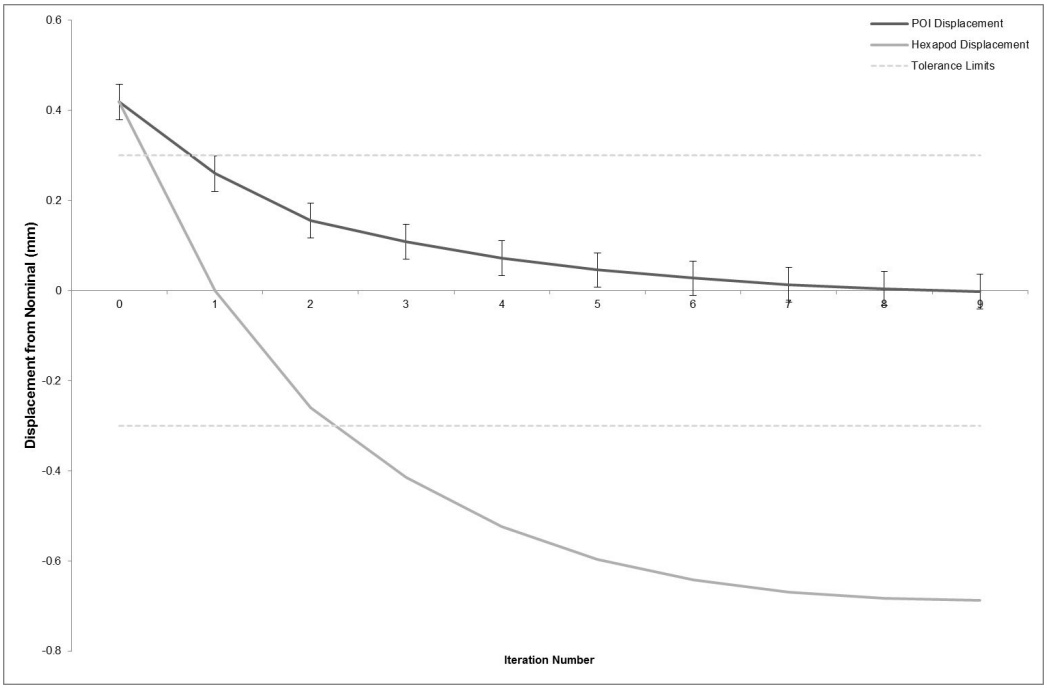


Figure 7-13: POI and hexapod displacement relative to nominal - $Y$ Axis

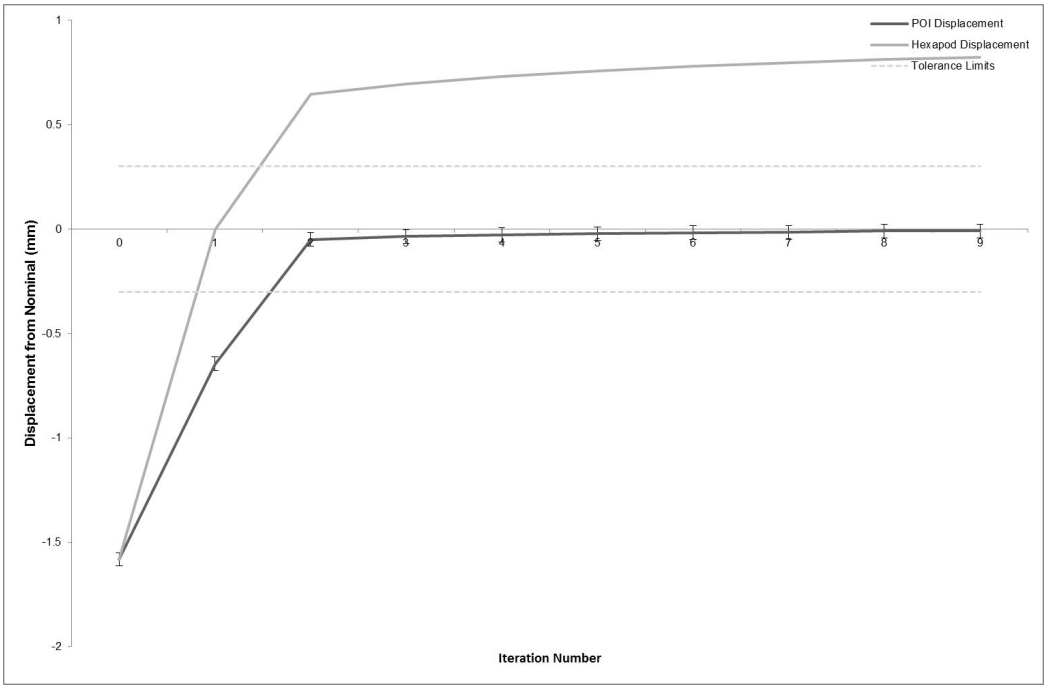


Figure 7-14: POI and hexapod displacement relative to nominal - $Z$ Axis

## 7.6 Chapter Summary

This chapter has suggested how metrology can be integrated into tooling to enable a *live* fixturing philosophy. Which, in turn can facilitate the use of reconfigurable and less inherently-accurate tooling, relying on *in-process* metrology and not traditional tool setting techniques.

# Chapter 8

# Discussion

## 8.1 Introduction

The presented research has explored the interaction between metrology and tooling within the context of Wing-box assembly. Firstly, the emphasis has been on how to increase manufacturing confidence with respect to tooling conformance, through increased use of metrology. Secondly, to improve the manufacturing process for aero-structures, specifically: the assembly of wing-boxes through the novel deployment of metrology within the tooling environment.

The following objectives were set out in Section 1.4:

i) To create a generic framework for the integration of metrology and assembly tooling; accommodating the multi-disciplinary, high resource needs of aerospace wing-box manufacture.

ii) To define the sources of uncertainty on large scale, multi-instrument measurement networks in non-controlled environments.

iii) To establish a method for the rapid measurement of Wing-box assembly tooling.

iv) To reduce the dependency on manual, mechanical in-tool checks for component placement and assembly conformance. Quantify the associated uncertainty for integrating these techniques

## 8.2 Research Contribution

*Metrology Enhanced Tooling for Aerospace (META) Framework* (Chapter 4): meets *Objective i* through the creation of a new framework (Figure 8-1) for integrating metrology into the tooling environment. The literature review identified a lack of an integrated approach towards metrology and aerospace Wing-box assembly tooling, the META framework addresses this research gap. The META framework maps the interaction of sensors within the tooling environment and provides a framework for the deployment of metrology within the assembly tooling of aero-structures. Consequently the META framework facilitates fixture condition checks, in-fixture conformance checks and automation.

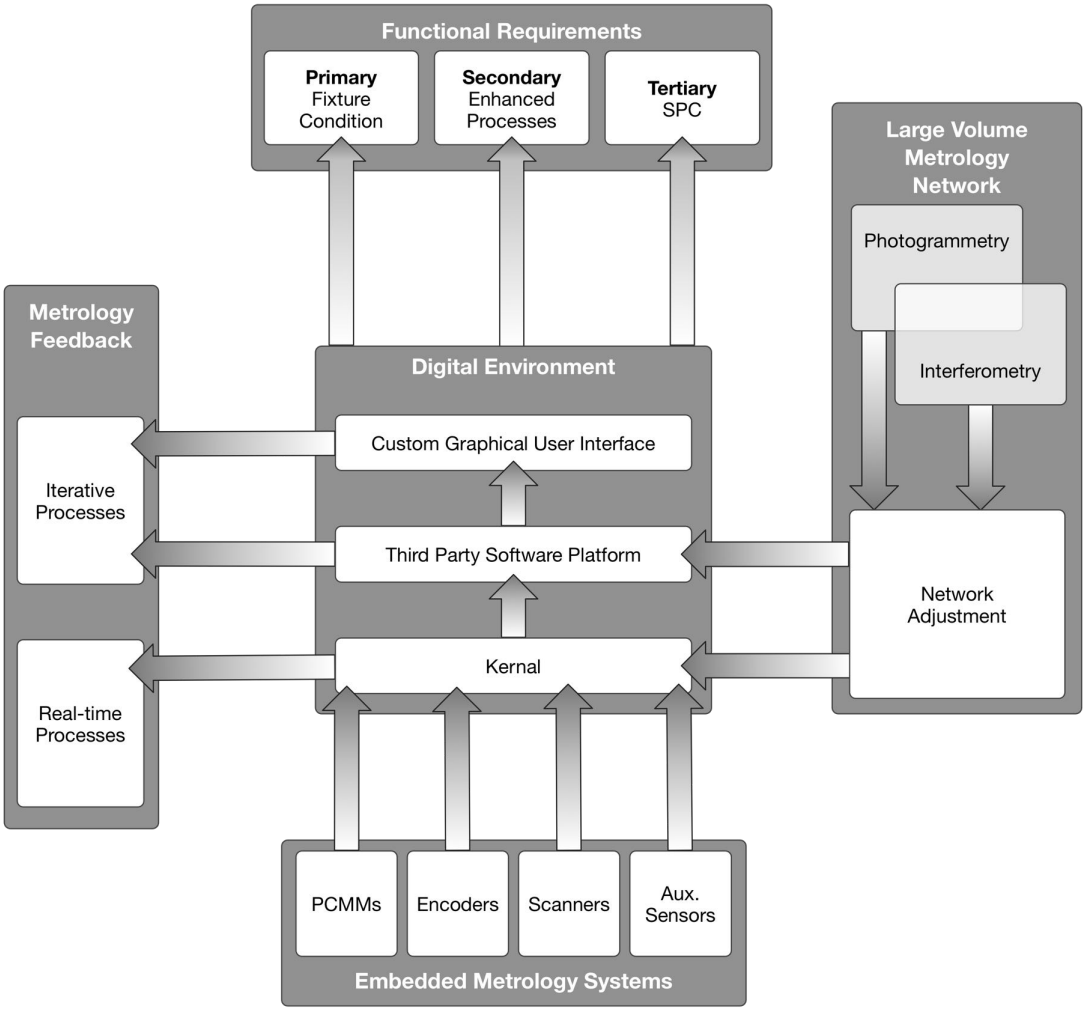


Figure 8-1: META framework

The practicalities, such as: the scale, cost and logistics prevent the holistic testing of the framework. As a consequence Chapters 5, 6 and 7 test elements of the framework in isolation.

*Large Volume Metrology Network* (Chapter 5): primarily meets *Objective ii & iii* through the development of a process for the rapid measurement of fixture condition. In addition the work links back to the META framework (*Objective i*), examining the large volume metrology network component. The research has been presented in Sections 5.2, 5.3 and 5.4 the contribution is outlined below:

- *Photogrammetry & Laser Tracker Performance Testing*: examined the suitability of photogrammetry as an alternative metrology instrument for the measurement of assembly tooling structures. The research presented a capability investigation assessing the use of commercial and non-commercial photogrammetry systems. The uncertainty of the photogrammetry systems was estimated theoretically and experimentally. It was shown that the commercial photogrammetry system had an experimentally determined measurement uncertainty of 43 µm, performing 34% better than current - laser tracker - technologies. Whereas the off-the-shelf photogrammetry system was determined as having a measurement uncertainty of 187 µm and could not be used for tooling certification. The commercial photogrammetric system was shown to be a suitable substitute technology for tooling certification.

- *Large Volume Multi-Instrument Networks*: determined the associated uncertainty when using laser tracker and photogrammetry systems as complementary technologies for large volume measurements. The laser tracker reference network gave global scale to the photogrammetric bundle. The estimation for the reference network uncertainty was improved by updating the individual instrument uncertainty parameters. These updates were based on the instrument performance within the network adjustment; this presents a new method for ensuring appropriate representation of the instrument uncertainty parameters within an industrial LVM context. The estimated uncertainty using current practice methods is 263 µm, whereas the multiple instrument updates method yields an uncertainty of 189 µm: a 28% improvement on uncertainty estimation over the 80m x 80m x 6m volume.

  The uncertainty budgets of the combined measurement network were developed and documented to accurately represent the overall measurement performance. The uncertainty estimation set out in this section can act as s template for future

large volume laser tracker-photogrammetry complementary metrology networks.

- *Automated Measurement of Aircraft Wing-box Assembly Tooling*: details a process for the rapid measurement of fixture condition, employing the outcomes from the above two previous sections. Namely: 1) using a commercial photogrammetric system for data acquisition that was tested and the uncertainty experimentally derived; and, 2) utilising a network of points having a co-ordinate definition measured by a laser tracker(s), using multiple instrument updates for an accurate metrology estimate.

  In addition, rigid body transforms (RBTs) were put forward in a novel application: to measure the position of interest (POI) and remove the need for traditional facility tooling during the recertification process. The minimum number of targets required to measure the POI via RBTs was simulated to achieve a comparable accuracy to current methods. RBTs enable automated data acquisition by leaving low-cost photogrammetry targets in-situ. A commissioning methodology and process was developed and documented. A case study was used to show proof of concept through a combination of physical trials and digital simulations.

*Embedded Metrology Systems* (Chapter 6): primarily meets *Objective iv* by illustrating how digital local metrology systems can be embedded into tooling structures to negate the dependancy on in-tool manual, mechanical checks. Providing automated, faster and more robust data acquisition. Embedded metrology systems also address an element of the META framework (*Objective i*), further increasing the data collection opportunities within aerospace manufacture, giving *accurate* and *quantitive* data, not just a binary data set typical of in-fixture gauge measurements. Additionally, digital sensors remove operator dependencies and therefore increases repeatability (within the limits of the measurement uncertainty). These embedded systems have been examined from an uncertainty of measurement perspective and have shown to exhibit better *local GD&T* uncertainties than setting to a global datum structure such as Wing or A/C Axis.

*Metrology Feedback* (Chapter 7), primarily meets *Objective iv*. The chapter demonstrates the control of a hexapod/Stewart platform with metrology, integrated into assembly tooling to enable a *live* fixturing philosophy. Both closed and open loop control of an active tooling pick-up (a hexapod) was shown. The novelty of this technique lies in measurement of the assembly key characteristics and manipulating the assembly to the CAD nominal geometry as opposed to targeting and/or setting the tooling into a nominal state.

## 8.3 Research Limitations

This section discusses the limitations of the contributions within this body of research. Each contribution shall be discussed in turn, in the order in which they have been presented.

### 8.3.1 Metrology Enhanced Tooling for Aerospace (META) Framework

The META framework has many permutations and can be adapted to suit any number of aerospace assembly tooling applications each with bespoke requirements. As such this research is not exhaustive and has the following limitations within the context of the META framework:

- Development of metrology hardware for real-time, highly accurate, ubiquitous LVM.
- An exhaustive experimentation of each framework permutation.
- A full-scale physical trial, this is impractical, therefore a mix of digital. simulation, physical trials and proof of concept was presented.
- Real-time metrology control of automation solutions.

### 8.3.2 Large Volume Metrology Network

The *Photogrammetry and Laser Tracker Performance Testing* (Section 5.2) has the following limitations:

- Limited instruments, the test only exercises two photogrammetry systems, and one laser tracker. This is a limitation as other systems will have performance variations. They are however representative of the state of the art in photogrammetry and laser tracking.
- The tests were carried out as a static points measurement. Although this is appropriate for the generation of co-ordinate reference systems, laser trackers are also used in a dynamic capacity (e.g. building to CAD).

- The test could be increased in scale as the 14.5m maximum test distance is the equivalent to a short-haul, single isle aircraft variant - such as the Airbus 320 - reference system. However larger Aircraft could have fixtures in excess of 30m - such as the Airbus 380 - performance of the instruments at this scale is not independently documented.

The limitations of the uncertainty estimation research presented in *Large Volume Multi-Instrument Networks* are:

- The introduction of multiple iterations of the instrument uncertainty parameters during the network adjustment for better uncertainty estimation is more involved than current techniques.
- The requirement for high-accuracy large co-ordinate reference systems is limited to a few industries, principally aerospace; therefore it would have to be adopted by the industry primes such as Airbus, and disseminated through their supply chain where appropriate.

The contribution developed via the *Automated Measurement of Aircraft Wing-box Assembly Tooling* is generic in principle using photogrammetry as an end-effector, the fixture commissioning process, and the use of 'Virtual' facility-tooling; however, there are limitations with:

- The temporal simulation, as simulation is bespoke to the fixture.
- Practical implementation limitations *could* exist as aerospace wing-box assembly tooling varies in both scale and geometry, hence no generic automation paths can be created but are bespoke for each fixture.

### 8.3.3 Embedded Metrology Systems

The embedded metrology does not have generic solutions for *all* tooling scenarios. Consequently the research has been limited by:

- Using a subset of features that are inspected in-tool.
- The approach/metrology system adopted for this research was not a flexible, which is acceptable for the current paradigm: large fixtures, with life spans of over 10 years.

- The temperature monitoring data is collected passively and recorded as a 'Tertiary' function
- Is limited as industrial assembly tooling varies in scale, geometry and inspection requirements. Hence the software capability and industrial deployment are unknown for a full-scale aerospace wing-box assembly fixture, although, the research has not indicated any scale-up problems.

### 8.3.4 Metrology Feedback

The metrology feedback research presented illustrates how metrology can be used to automate the assembly tooling environment, however it is not exhaustive. The study was limited by scale and complexity, depending on the adopted method, either:

- The closed loop model is limited by metrology resources, or,
- The open loop model is limited by actuator positional accuracy (if sufficiently stiff).

# Chapter 9

# Conclusions

Following the research contribution and limitations a number of conclusions can be drawn, subsequently the future work pertaining to this body of research has been detailed (Section 9.1). The following conclusions have been formulated:

- The literature review identified three significant knowledge gaps specifically: i) a lack of uncertainty estimation for methods for large volume multi-instrument networks within industrial processes; ii) no integrated approach towards metrology and Wing-box assembly tooling; and that, iii) examination of the metrology requirements within the aerospace industry with respect to large scale assembly tooling remains undocumented.
- The review of current industrial practices gave a complementary perspective with the following desirable future metrology requirements with respect to the assembly tooling environment:
  - Reduce manual metrology checks,
  - Enable greater automation,
  - More robust component placement,
  - Detect concessions earlier,
  - Increase in SPC data collection,
  - Ensuring component/sub-assembly placement is correct,
  - Reduce tooling reliance,
  - Reduce jig recertification time.

- A framework entitled Metrology Enhanced Tooling for Aerospace (META) has been established as part of the major research output from this body of work. The META framework was developed to provide a holistic view for the deployment of metrology in assembly tooling structures. It has shown to be of strong potential for use as an industrial tool.

- It was shown that commercial photogrammetry systems though experimental validation perform with a better associated uncertainty than that of the current technologies. However, a photogrammetry system comprised from off-the-shelf equipment was experimentally validated and demonstrated to perform with an associated uncertainty that is not sufficient for assembly tooling recertification.

- Improving the uncertainty estimation during network adjustments, was achieved by updating and iterating the instrument uncertainty parameters based on the performance within the network adjustment. It was shown to improve the network uncertainty estimate significantly when compared to current practice.

- The effectiveness of rigid body transforms (RBTs) was simulated for deployment in a novel application, where low-cost photogrammetric targets could negate the need for facility tooling to target the position of interest. The simulated uncertainty was shown to be at an acceptable level. This facilitated automated data acquisition.

- To realise the rapid measurement of assembly tooling, a generic commissioning methodology and measurement strategy was established by utilising photogrammetry, automation and RBTs. This enables an increase in manufacturing confidence with respect to tooling conformance, through regular and rapid 'health-check' measurements of the tooling.

- The commissioning methodology and measurement strategy was demonstrated in a case study, through a combination of physical measurement and digital automation simulation to prove the process time was greatly decreased from current methods.

- Local embedded metrology systems were developed for a subset of in-tool feature checks and the uncertainty quantified to illustrate how digital, automated in-tool component checks could be realised. These metrology systems had an estimated measurement uncertainty that represented an improvement over the current manufacturing paradigm.

- The performance capability of the control of a tooling pick-up (hexapod) based on metrology feedback, was demonstrated. The pick-up manipulated the *assembly* to its measured nominal position, not the nominal *tooling* position.

## 9.1 Future Work

A significant proportion of the future challenges that are presented in aerospace assembly tooling originate from the increasing need to accelerate manufacturing processes and product variation. Faster manufacturing rates exaggerate the non-value added impact of metrology activities. An increased manufacturing rate is achieved by either: adding more assembly tooling, or, increasing the through-put of existing assembly tooling. More assembly tooling will increase the requirement for in-fixture measurements and resource; whereas, an increased tooling through-put will further the financial impact of the tooling down-time associated with the recertification process. Additionally, the future design and architecture of aircraft will impact the metrological requirements, this could be tighter tolerances to achieve laminar flow, or to allow composite manufacture. As such, there are a number of future challenges to overcome.

### 9.1.1 META Framework Development

The Metrology Enhanced Tooling for Aerospace (META) Framework has a number of future activities to further develop. This includes scaling the research to full size, with many hundreds of features. The metrology requirements could be grouped, for example by feature-type or GD&T classification. Subsequently, the associated embedded metrology solution could be developed for each group. This would lead towards a standard set of tools and principles for reference when designing tooling and embedding metrology. Automation within the tooling environment has several research areas to be addressed, including: real-time feedback for material removal operations, stress analysis associated with component and assembly manipulation, data-driven manufacturing and understanding the cost implications/business case. As well as fundamental development of *accurate, cost-effective and ubiquitous metrology systems* similar to iGPS, wMPS, POSEYE, MScMS-II, *etc.* (but with a suitable accuracy level) is important in driving down the impact metrology tasks have on manufacturing processes. This future-state of metrology equipment is an enabler to fully realise the META Framework presented in this thesis; specifically enhancing the active tooling potential and jig/fixture condition monitoring. In the absence of such technology, tooling measure-

ment presents an interim solution.

### 9.1.2 Rapid Tooling Measurement

The next stages for rapid tooling measurement would be a series of integrated solutions leading to full-scale deployment, in an industrial setting of the rapid recertification process using photogrammetry, automation and 'virtual' facility tooling in order to further development. Subsequently future work on the implications monitoring of large-scale tooling could lead to more intelligent use of data; the data/information could be passed downstream to drive active tooling pick-ups, adjusting to suit component and sub-assembly variation.

### 9.1.3 Increasing Accuracy of Large Volume Metrology Networks

Thermal variation provides a significant level of uncertainty in the measurement processes, particularly of large volumes. Future research into the impact of thermal variation on large scale fixtures is a necessity when tighter manufacturing tolerances are required. Wing-sized, temperature controlled environments are costly, and are likely to be a last resort. A more intelligent tooling system could reduce thermal effects significantly. This is unlikely to eradicate the thermal effects completely, but rather reduce the expansion/contraction to a manageable level. However this has inherent challenges, these include:

- Material differences between: tooling and assembly components
- Non-linear behaviour of material expansion
- Non-uniform distribution of temperature.

# Bibliography


Anon (2009), 'GPS: Serving the World'. http://www.gps.gov/; accessed 15/06/2009.

*ASME B89.4.19-2006 Performance Evaluation of Laser-Based Spherical Coordinate Measurements Systems* (2006).

Bakker, O., Papastathis, T., Popov, A. and Ratchev, S. (2013), 'Active fixturing: literature review and future research directions', *International Journal of Production Research* **51**(11), 3171–3190. DOI: 10.1080/00207543.2012.695893.

Bell, S. (2001), *A Beginner's Guide to Uncertainty of Measurement*, Vol. 11 of *Measurement Good Practice Guide*, National Physical Laboratory, Teddington, UK.

Bolton, W. (1999), *Mechatronics: Electronic Control Systems in Mechanical and Electrical Engineering*, 2nd edn, Pearson Education Limited, Harlow.

Bone, G. M. and Capson, D. (2003), 'Vision-guided fixtureless assembly of automotive components', *Robotics and Computer-Integrated Manufacturing* **19**(1-2), 79–87.

Boyes, W. E. (1980), *Jigs and Fixtures*, Society of Manufacturing Engineers, Michigan.

Bracht, U. and Masurat, T. (2005), 'The digital factory between vision and reality', *Computers in Industry* **56**(4), 325–333. DOI: 10.1016/j.compind.2005.01.008.

BSI (1980), 'General metrology: Part 2: Vocabulary of legal metrology (VLM)'.

BSI (1995*a*), 'General Metrology: Part 1: Basic and General Terms (VIM)'.

BSI (1995*b*), 'General Metrology: Part 3: Guide to the expression of uncertainty in measurement (GUM)'.

BSI (1995*c*), 'PD 6461-1:1995 General metrology. Basic and general terms (VIM)'. BSI Choice not to adopt new ISO standard.

BSI (2004), 'General metrology: Part 4: Practical guide to measurement uncertainty'.

Burley, G., Odi, R., Naing, S., Williamson, A. and Corbett, J. (1999), Jigless aerospace manufacture - the enabling technologies, Technical report, SAE International.

Butterfield, J., Crosby, S., Curran, R., Price, M., Armstrong, C. G., Raghunathan, S., McAleenan, D. and Gibson, C. (2007), 'Optimization of aircraft fuselage assembly process using digital manufacturing', *Journal of Computing and Information Science in Engineering* **7**(3), 269–275.

Calkins, J. M. (2002), Quantifying Coordinate Uncertainty Fields in Coupled Spatial Measurement systems, PhD thesis, Mechanical Engineering, The Virginia Polytechnic Institute and State University.

Calkins, J. and Sandwith, S. (2007), 'Integrating certified lengths to strengthen metrology network uncertainty', *Journal of the Coordinate Metrology Systems Conference (CMSC)* .

Christensen, K. and Flynn, R. (2012), 'Developing a control network crossing a thermal boundary: A wing jig case study with best practices', *Journal of the Coordinate Metrology Systems Conference* **7**(2).

Corona-Castuera, J., Rios-Cabrera, R., Lopez-Juarez, I. and Peña-Cabrera, M. (2005), *An Approach for Intelligent Fixtureless Assembly: Issues and Experiments*, Vol. 3789, Springer Berlin Heidelberg, pp. 1052–1061.

Curran, R., Gomis, G., Castagne, S., Butterfield, J., Edgar, T., Higgins, C. and McKeever, C. (2007), 'Integrated digital design for manufacture for reduced life cycle cost', *International Journal of Production Economics* **109**(1-2), 27–40. DOI: 10.1016/j.ijpe.2006.11.010.

Deng, H. and Melkote, S. N. (2006), 'Determination of minimum clamping forces for dynamically stable fixturing', *International Journal of Machine Tools and Manufacture* **46**(7-8), 847–857.

Durrantwhyte, H. F. (1988), 'Sensor models and multisensor integration', *International Journal of Robotics Research* **7**(6), 97–113.

Faro (2014), 'Faro Arms: Portable Coordinate Measurement'. http://www.faro.com/products/metrology/faroarm-measuring-arm/overview; accessed: 06/03/2014.

Faro (2015), 'The new FARO Vantage Laser Tracker'.
$http://blog-uk.faro.com/2012/09/join-this-webinar-about-the-new-laser-tracker-vantage/_dsc9906_dxo/$;
accessed: 10/12/2015.

Flack, D. and Hannaford, J. (2005), *Measurement Good Practice Guide No. 80: Fundamental Good Practice in Dimensional Metrology*, National Physical Laboratory, Teddington, UK.

Forbes, A. B. (2012), 'Large-scale dimensional metrology (LSDM): from tapes and theodolites to multi-sensor systems', *Measurement Science and Technology* **23**(2).

Forbes, A. B. and Harris, P. M. (2009), 'Uncertainty associated with co-ordinate measurements', *Measurement* **42**(10), 1473–1477.

Forster, K. (2007), Unified spatial metrology network user manual: Issue 2, Technical Report Manufacturing Instruction No. 8-289, Airbus, Filton, UK.

Franceschini, F., Maisano, D. and Mastrogiacomo, L. (2014), 'Cooperative diagnostics for distributed large-scale dimensional metrology systems based on triangulation', *Proceedings of the Institution of Mechanical Engineers, Part B: Journal of Engineering Manufacture* **228**(4), 479–492. DOI: 10.1177/0954405413505849.

Geodetic Systems (2014), 'Picture perfect measurements'.
http://www.geodetic.com/products/systems/v-stars-s.aspx;
accessed: 06/03/2014.

*Geodetic Systems Inc* (2010).

Ghilani, C. D. (2010), *Adjustment Computations: Spatial Data Analysis*, fifth edn, John Wiley & Sons, Inc., New York.

Gibson, S. M., Coe, P. A., Mitra, A., Howell, D. F. and Nickerson, R. B. (2005), 'Coordinate measurement in 2-D and 3-D geometries using frequency scanning interferometry', *Optics and Lasers in Engineering* **44**(1), 79–95.

Glazebrook, C. (2006), Technology maturity report - metrology, Technical report, Airbus, Filton, UK.

Gooch, R. (1998), 'Optical metrology in manufacturing automation', *Sensor Review* **18**(2), 81–87.

Hirai, A., Kajima, M. and Telada, S. (2009), *Handbook of Optical Metrology: Displacement, Pulse Method*, CRC Press, Boca Ranton, p. 405.

Huang, Y.-b., Lan, Y.-b., Hoffmann, W. C. and Lacey, R. E. (2007), 'Multisensor data fusion for high quality data analysis and processing in measurement and instrumentation', *Journal of Bionic Engineering* **4**(1), 53–62.

Hughes, B., Sun, W., Forbes, A. and Lewis, A. (2010), 'Determining laser tracker alignment errors using a network measurement', *Measurement Science and Technology* **22**(4).

Hughes, E. B., Forbes, A. B., Sun, W., Maropoulos, P., Muelaner, J., Jamshidi, J. and Wang, Z. (2010), iGPS capability study, Technical report, National Physical Laboratory, Teddington, UK.

International Organization of Legal Metrology (2000), 'International vocabulary of terms in legal metrology (VIML)'.

*ISO/IEC Guide 98-1:2009 Uncertainty of measurement – Part 1: Introduction to the expression of uncertainty in measurement* (2009).

*ISO/IEC Guide 98-3:2008/Suppliment 1:2008 Propagation of distributions using a Monte Carlo method* (2008).

*ISO/IEC Guide 98-3:2008 Uncertainty of measurement – Part 3: Guide to the expression of uncertainty in measurement (GUM)* (2008).

*ISO/IEC Guide 99:2007 International vocabulary of metrology – Basic and general concepts and associated terms (VIM)* (2007).

Jamshidi, J., Kayani, A., Iravani, P., Maropoulos, P. G. and Summers, M. D. (2010), 'Manufacturing and assembly automation by integrated metrology systems for aircraft wing fabrication', *Proceedings of the Institution of Mechanical Engineers, Part B: Journal of Engineering Manufacture* **224**(1), 25–36. DOI: 10.1243/09544054JEM1280.

Jones, G. (2010), *CPR1037: Measurement Process Control using Laser Trackers, Laser Radars and CMMs*, issue 7 edn, Airbus, Filton, UK.

Kihlman, H. (2002), Affordable Reconfigurable Assembly Tooling - an aircraft development and manufacturing perspective, PhD thesis, Linkoping University, Sweden.

Kihlman, H., Loser, R., Cooke, A., Sunnanbo, A. and Von Arb, K. (2004), Metrology-integrated industrial robots: calibration, implementation and testing, *in* 'Proceedings of the 35th ISR (International Symposium on Robotics)'.

Kirkup, L. and Frenkel, B. (2006), *An Introduction to Uncertainty in Measurement*, Cambridge University Press, Cambridge.

Kyle, S., Loser, R. and Warren, D. (1997), Automated part positioning with the laser tracker, *in* '5th International Workshop on Accelerator Alignment'.

Leica Geosystems (2009), 'A Case Study: For Airbus Broughton, Leica T-Probe is the "MissingEvolutionary Link" in Tooling'.
$http://www.leica-geosystems.com/en/For-Airbus-Broughton-Leica-T-Probe-is-the-Missing-Evolutionary-Link-in-Tooling$64391.htm
accessed: 20/06/2009.

Leica Geosystems (2014*a*), 'Leica Nova TS50: True precision, true perfection'.
http://www.leica-geosystems.co.uk/en/Leica-Nova-$TS50_1$03594.htm;
accessed: 06/03/2014.

Leica Geosystems (2014*b*), 'Leica TM6100A Industrial Theodolite'.
http://www.leica-geosystems.co.uk/en/Leica-$TM6100A$788.htm;
accessed: 06/03/2014.

*Leica Absolute Tracker AT401: White Paper* (2010), Technical report, Leica Geosystems.

*Leica Geosystems: PCMM System Specifications* (2009).

*Leica Geosystems: Red-Ring Reflectors Specification (RRR)* (2010).

Leopold, J., Poppitz, A., Klarner, M., Schmidt, A. K. and Berger, J. (2008), 'Interaction between machining and new fixturing principles for aerospace structures', *International Journal of Material Forming* **1**, 531–533.

Li, Y., Jian, J., Yan, R. and Liao, W. (2009), 'Aircraft tooling collaborative design based on multi-agent and PDM', *Concurrent Engineering Research and Applications* **17**(2), 139–146.

Luhmann, T. (2010), 'Close range photogrammetry for industrial applications', *ISPRS Journal of Photogrammetry and Remote Sensing* **65**(6), 558–569.

Luhmann, T., Robson, S., Kyle, S. and Harley, I. (2006), *Close Range Photogrammetry: Principles, Methods and Applications*, Whittles Publishing, Caithness.

Maisano, D. A., Jamshidi, J., Franceschini, F., Maropoulos, P. G., Mastrogiacomo, L., Mileham, A. R. and Owen, G. W. (2009), 'A comparison of two distributed large-volume measurement systems: The mobile spatial co-ordinate measuring system and the indoor global positioning system', *Proceedings of the Institution of Mechanical Engineers, Part B: Journal of Engineering Manufacture* **223**(5), 511–521. DOI: 10.1243/09544054JEM1271.

Maropoulos, P. G. and Ceglarek, D. (2010), 'Design verification and validation in product lifecycle', *CIRP Annals - Manufacturing Technology* **59**(2), 740–759.

Maropoulos, P. G., Guo, Y., Jamshidi, J. and Cai, B. (2008), 'Large volume metrology process models: A framework for integrating measurement with assembly planning', *CIRP Annals - Manufacturing Technology* **57**(1), 477–480.

Martin, O., Wang, Z. and Maropoulos, P. (2011*a*), Red, Amber and Green Metrology 2011: Health Check Proposal Red, Amber and Green Metrology: Health Check Proposal, Technical report, LIMA: University of Bath.

Martin, O., Wang, Z. and Maropoulos, P. (2011*b*), Red, Amber and Green Metrology 2011: Health Check Proposal Red, Amber and Green Metrology: Rapid Fixture Health Check Interim Report, Technical report, LIMA: University of Bath.

Martin, O., Wang, Z. and Maropoulos, P. (2011*c*), Red, Amber and Green Metrology 2011: Rapid Fixture Health Check Results Report, Technical report, LIMA: University of Bath.

MEEQ (2007), 'MEEQ: Measurement Equipment - Consistency Check of Features'.

Mei, Z. and Maropoulos, P. G. (2014), 'Review of the application of flexible, measurement-assisted assembly technology in aircraft manufacturing', *Proceedings of the Institution of Mechanical Engineers, Part B: Journal of Engineering Manufacture* **228**(10), 1185–1197.

Metris (2009), 'Laser Radar'. www.metris.com/laserradar/features; accessed: 20/06/2009.

Mikhail, E. M., Bethel, J. S. and McGlone, J. C. (2001), *Introduction To Modern Photogrammetry*, John Wiley & Sons, Inc., New York.

Millar, A. and Kihlman, H. (2009), Reconfigurable flexible tooling for aerospace wing assembly, Technical Report 2009-01-3243, SAE International.

Mizell, D. W. (1994), Virtual reality and augmented reality in aircraft design and manufacturing, *in* 'WESCON/94. 'Idea/Microelectronics'. Conference Record', p. 91.

Molloy, O., Tilley, S. and Warman, E. A. (1998), *Design for Manufacture and Assembly: Concepts, Architectures and Implementation*, Chapman & Hall, London, p. 9.

Muelaner, J. E. and Maropoulos, P. G. (2010), 'Design for measurement assisted determinate assembly (MADA) of large composite structures', *Journal of the Coordinate Metrology Systems Conference* .

Muelaner, J. E., Wang, Z., Jamshidi, J., Maropoulos, P. G., Mileham, A. M., Hughes, E. B. and Forbes, A. B. (2009), 'Study of the uncertainty of angle measurement for a rotary-laser automatic theodolite (R-LAT)', *Proceedings of the Institution of Mechanical Engineers, Part B: Journal of Engineering Manufacture* (223(B3)), 217–229.

Muelaner, J. E., Wang, Z. and Maropoulos, P. G. (2011), 'Concepts for and analysis of a high accuracy and high capacity (HAHC) aerospace robot', *Proceedings of the Institution of Mechanical Engineers, Part B: Journal of Engineering Manufacture* **225**(8), 1393–1399. DOI: 10.1177/0954405411406939.

Muelaner, J. E., Wang, Z., Martin, O., Jamshidi, J. and Maropoulos, P. G. (2010), 'Estimation of uncertainty in three-dimensional coordinate measurement by comparison with calibrated points', *Measurement Science and Technology* (2).

Muelaner, J., Martin, O. and Maropoulos, P. (2013), 'Achieving low cost and high quality aero structure assembly through integrated digital metrology systems', *Procedia CIRP* **7**(0), 688 – 693. Forty Sixth CIRP Conference on Manufacturing Systems 2013.

Muelaner, J. and Robson, S. (2008), No. 8: Large volume measurement technologies (10m+), Technical Report 8, Airbus, Filton, UK.

Munoz, D., Bouchereau, F., Vargas, C. and Enriquez, R. (2009), *Position Location Techniques and Applications: Terrestrial-Based Location Systems*, Academic Press, Oxford, pp. 153–206.

Muralikrishnan, B., Sawyer, D., Blackburn, C., Phillips, S., Borchardt, B. and Estler, W. T. (2009), 'ASME B89.4.19 performance evaluation tests and geometric misalign-

ments in laser trackers', *Journal of Research of the National Institute of Standards and Technology* **114**(1), 15.

Nikon Metrology (2010), 'Nikon Metrology Solutions'.

Norman, A., Schönberg, A., Gorlach, I. and Schmitt, R. (2013), 'Validation of iGPS as an external measurement system for cooperative robot positioning', *The International Journal of Advanced Manufacturing Technology* **64**(1-4), 427–446.

NPL (2014), 'Large volume dimensional metrology'. http://www.npl.co.uk/science-technology/dimensional/research/large-volume-dimensional-metrology; accessed: 10/10/2014.

OnTrak (2014), 'The OT-4040, portable, two dimensional alignment.'. http://www.on-trak.com/ot4040.html; accessed: 01/09/2014.

Pavese, F. (2009), *An Introduction to Data Modeling Principles in Metrology and Testing*, Modeling and Simulation in Science, Engineering and Technology, Birkhäuser Boston, pp. 1–30.

Peggs, G. N., Maropoulos, P. G., Hughes, E. B., Forbes, A. B., Robson, S., Ziebart, M. and Muralikrishnan, B. (2009), 'Recent developments in large-scale dimensional metrology', *Proceedings of the Institution of Mechanical Engineers, Part B: Journal of Engineering Manufacture* **223**(6), 571–595.

Pertile, M., De Cecco, M. and Baglivo, L. (2009), Description and application of a new method for uncertainty evaluation in two-dimensional indirect measurement, IEEE International Workshop on Advanced Methods for Uncertainty Estimation in Measurement, AMUEM 2009, IEEE Computer Society, pp. 16–21.

Plut, W. J. and Bone, G. M. (1997), 3D flexible fixturing using a multi-degree of freedom gripper for robotic fixtureless assembly, *in* 'Proceedings of IEEE Robotics and Automation International Conference', Vol. 1, pp. 379–384 vol.1.

Pollock, H. W. (1988), *Tool Design 2nd Ed.*, Prentice Hall, New Jersey.

Predmore, C. R. (2010), 'Bundle adjustment of multi-position measurements using the mahalanobis distance', *Precision Engineering* **34**(1), 113–123.

Rajan, V. N., Sivasubramanian, K. and Fernandez, J. E. (1999), 'Accessibility and ergonomic analysis of assembly product and jig designs', *International Journal of Industrial Ergonomics* **23**(5-6), 473–487.

Rong, Y., Huang, S. H. and Hou, Z. (2005), *Advanced Computer-Aided Fixture Design*, Materials & Mechanical, Elsevier Inc. Academic Press.

Rooks, B. (2005), 'Assembly in aerospace features at iee seminar', *Assembly Automation* **25**(2), 108–111.

Rossi, G. B. (2009), *Data Modeling for Metrology and Testing in Measurement Science*, Modeling and Simulation in Science, Engineering and Technology, Birkhäuser Boston, pp. 1–40.

Saadat, M. and Cretin, C. (2002), 'Dimensional variations during airbus wing assembly', *Assembly Automation* **22**(3), 270–279.

Schodel, R. (2009), *Handbook of Optical Metrology: Principles and Applications*, CRC Press, Boca Ranton, chapter Length and Size, pp. 381–5.

Schwenke, H., Neuschaefer-Rube, U., Pfeifer, T. and Kunzmann, H. (2002), 'Optical methods for dimensional metrology in production engineering', *CIRP Annals - Manufacturing Technology* **51**(2), 685–699. DOI: 10.1016/S0007-8506(07)61707-7.

Shakarji, C. (2015), Special test service for spatialanalyzer, Technical Report 683/287163-15, NIST, Maryland, USA.

Sharke, P. (2003), 'Measuring across space and time', *Mechanical Engineering* **125**(1), 48.

Steele, A. G. and Douglas, R. J. (2009), *Monte Carlo Modeling of Randomness*, Modeling and Simulation in Science, Engineering and Technology, Birkhäuser, Boston, pp. 1–41.

Sugo, N. (2007), *Metrology Handbook: The science of measurement*, 1st edn, Mitutoyo Ltd., Reading, UK, p. 173.

ThirdDimension (2014), 'Vchange sensors'.
http://www.third.com/us/products/sensors/vchange-sensors;
accessed: 01/09/2014.

Tomlinson, D. and Singh, R. (2008), Optimised tooling solutions benchmarking, Technical report, Airbus, Filton, UK.

UKAS (2012), M3003: The expression of uncertainty and confidence in measurement, Technical report, United Kingdom Accreditation Service.

Vilbaste, M., Slavin, G., Saks, O., Pihl, V. and Leito, I. (2010), 'Can coverage factor 2 be interpreted as an equivalent to 95% coverage level in uncertainty estimation? two case studies', *Measurement* **43**(3), 392–399.

Wang, Z. (2013), Large Volume Metrology Assisted Production of Aero-structures, PhD thesis, Mechanical Engineering, University of Bath, UK.

Webb, P., Ye, C., To, M., Al-Thraa, S. and Kayani, A. (2009), A framework for the fusion of multiple metrology sources for measurement-assisted assembly, SAE International, Warrendale, Pennsylvania, USA.

Weckenmann, A., Jiang, X., Sommer, K. D., Neuschaefer-Rube, U., Seewig, J., Shaw, L. and Estler, T. (2009), 'Multisensor data fusion in dimensional metrology', *CIRP Annals - Manufacturing Technology* **58**(2), 701–721.

Wendt, K. and Gerwien, N. (2015), Evaluation software for coordinate measuring machines, Technical Report PTB-5.3-2015-052, PTB, Berlin, Germany.

Wöhlke, G. and Schiller, E. (2005), 'Digital planning validation in automotive industry', *Computers in Industry* **56**(4), 393–405. DOI: 10.1016/j.compind.2005.01.010.

Xue, B., Zhu, J., Zhao, Z., Wu, J., Liu, Z. and Wang, Q. (2014), 'Validation and mathematical model of workspace measuring and positioning system as an integrated metrology system for improving industrial robot positioning', *Proceedings of the Institution of Mechanical Engineers, Part B: Journal of Engineering Manufacture* **228**(3), 422–440. DOI: 10.1177/0954405413499901.

# Appendix A

# Publications

## A.1 Journal Papers

1. Maropoulos, P. G.; Muelaner, J. E.; Summers, M. D. and **Martin, O. C.**. (2014). *A New Paradigm in Large-Scale Assembly-Research Priorities in Measurement Assisted Assembly.* The International Journal of Advanced Manufacturing Technology, 70 (1-4), pp. 621-633.

2. Vichare, P.; **Martin, O.** and Jamshidi, J. (2013). *Dimensional Management for Aerospace Assemblies: Framework Implementation with Case-Based Scenarios for Simulation and Measurement of In-Process Assembly Variations.* The International Journal of Advanced Manufacturing Technology, DOI: 10.1007/s00170-013-5262-9, 70(1-4), pp 215-225.

3. Maropoulos, P.G.; Vichare, P.; **Martin, O.**; Muelaner, J.; Summers, M. and Kayani, A. (2011). *Early Design Verification of Complex Assembly Variability Using a Hybrid - Model Based and Physical Testing - Methodology.* CIRP Annals-Manufacturing Technology, 60(1), pp 207-210.

4. Muelaner, J.E.; Wang, Z.; **Martin, O.**; Jamshidi, J. and Maropoulos, P. (2010). *Verification of the Indoor GPS System, by Comparison with Calibrated Coordinates and by Angular Reference.* Journal of Intelligent Manufacturing, DOI: 10.1007/s10845-010-0488-y.

5. Muelaner, J.E.; Wang, Z.; **Martin, O.**; Jamshidi, J. and Maropoulos, P.G. (2010). *Estimation of Uncertainty in Three Dimensional Coordinate Measure-*

*ment by Comparison with Calibrated Points.* Measurement Science and Technology, 21(2): pp.025106

## A.2 Conference Papers & Presentations

1. Cote, G.; Kayani, A.; **Martin, O.**; Huckin, L. and El-Nounu, A. (2013). *Digital Metrology Workbench for Large Volume Aerospace Assembly*, Manufacturing/Materials/Structures: Metrology Automated Systems (Technical Session), AeroTech SAE International Conference. Montreal, Canada. PRESENTATION ONLY

2. Muelaner, J.E.; **Martin, O.** and Maropoulos, P.G. (2013). *Achieving Low Cost and High Quality Aero Structure Assembly through Integrated Digital Metrology Systems* The 46th CIRP Conference on Manufacturing Systems 2013 (CMS2013) in Portugal

3. Cote, G.; **Martin, O.**; Kayani, A.; Huckin, L. and El-Nounu, A. (2013) *Digital Metrology Workbench for Large Volume Aerospace Assembly.*1st CASI Aerospace Manufacturing Technologies Symposium Toronto, April 30th - May 2nd.

4. Muelaner, J.E.; **Martin, O.** and Maropoulos, P. (2011) *Metrology Enhanced Tooling for Aerospace (META): Strategies for Improved Accuracy of Jig Built Structures.* AeroTech SAE International Conference. Toulouse, France. DOI: 10.4271/2011-01-2556.

5. **Martin, O.** and Toutt, M. (2012) *BLADE: Metrology Survey of A340 MSN001*, Large Volume Metrology Conference (LVMC), Chester, UK. PRESENTATION ONLY

6. Bakker, O. J.; Jayaweera, N.; **Martin, O.**; Turnock, A.; Helgosson, P.; Smith, T.; Popov, A.; Ratchev, S.; Tomlinson, D.; Wright, J. and Summers, M. (2011) *Fixturing and Tooling for Wing Assembly with Reconfigurable Datum System Pickup.* AeroTech SAE International Conference. Toulouse, France. DOI: 10.4271/2011-01-2556.

7. **Martin, O.**; Muelaner, J.; Wang, Z.; Kayani, A.; Tomlinson, D. and Maropoulos, P.G. (2011). *Metrology Enhanced Tooling for Aerospace (META): A Live Fixturing Wing Box Assembly Case Study.* Proceedings of the 7th International Conference on Digital Enterprise Technology. Athens, Greece. pp. 83-92.

8. Vichare, P.; **Martin, O.**; Jamshidi, J. and Maropoulos, P.G. (2011) *Dimensional Management in Aerospace Assemblies: Case Based Scenarios for Simulation and Measurement of Assembly Variations.* Proceedings of the 7th International Conference on Digital Enterprise Technology. Athens, Greece. pp. 522-531.

9. Muelaner, J.; **Martin, O.**; Kayani, A. and Maropoulos, P.G. (2011) *Measurement Assisted Assembly and the Roadmap to Part-to-Part Assembly.* Proceedings of the 7th International Conference on Digital Enterprise Technology. Athens, Greece. pp. 11-19.

10. **Martin, O.**; Muelaner, J.E. and Maropoulos, P. (2010). *The Metrology Enhanced Tooling for Aerospace (META) Framework.* In: Proceedings of the 36th International MATADOR Conference, Manchester, UK, pp.363-366.

## A.3 Industrial Reports

1. Muelaner, J. E. ;Maropoulos, P.G and **Martin, O.** (2012) *The State of the Art in Large Volume Metrology for Civil Nuclear New Build.* LIMA Group Report, December 2012.

2. **Martin, O.** & Toutt, M. (2012) *Breakthrough Laminar Aircraft Demonstrator in Europe (BLADE): Metrology Survey of A340 MSN001.* LIMA Group Report, October 2012.

3. Muelaner, J.; Vichare, P.; **Martin, O.** and Maropoulos, P.G. (2011). *ALCAS Wing Build Tolerance Evaluation*, LIMA Group Report, April 2011.

4. **Martin, O.**; Muelaner, J. and Maropoulos, P.G. (2011). *Red, Amber, Green Metrology: a Sub-System Capability Study.* LIMA Group Report, November 2011.

5. **Martin, O.**; Gathercole, N.; Almond, D. and Maropoulos, P.G. (2011).*Coating Thickness Measurement Test Report for Lightning Strike Protection.* LIMA Group Report, October 2011.

6. Hughes, B.; Muelaner, J.E. and **Martin, O.** (2010). *ViewNet Reference Network Survey.* National Physical Laboratory Report: ENG 22, January 2010.

7. Muelaner, J.; **Martin, O.** (2010) *State of the Art Review of Reconfigurable Tooling for Bracket Bonding Fixtures at EADS Astrium.* LIMA Group Report, December 2010.

# Appendix B

# Equal-Weight 2D Coordinate Fitting: an Example

Consider the observations detailed in the follow table (Table B.1):

| | Control | | Measured | |
|---|---|---|---|---|
| Point | X | Y | X | Y |
| $a$ | 10 | 20 | 1196.2218 | 626.4105 |
| $b$ | 20 | 30 | 1198.9510 | 643.2460 |
| $c$ | 50 | 40 | 1221.6652 | 673.8653 |
| $d$ | 30 | 100 | 1160.7042 | 718.8989 |
| $e$ | 60 | 20 | 1245.1344 | 661.1202 |

Table B.1: Control and measured 2D point coordinates

Populating the $A$ matrix gives:

$$A = \begin{pmatrix} 1196.2218 & -626.4105 & 1 & 0 \\ 626.4105 & 1196.2218 & 0 & 1 \\ 1198.951 & -643.246 & 1 & 0 \\ 643.246 & 1198.951 & 0 & 1 \\ 1221.6652 & -673.8653 & 1 & 0 \\ 673.8653 & 1221.6652 & 0 & 1 \\ 1160.7042 & -718.8989 & 1 & 0 \\ 718.8989 & 1160.7042 & 0 & 1 \\ 1245.1344 & -661.1202 & 1 & 0 \\ 661.1202 & 1245.1344 & 0 & 1 \end{pmatrix} L = \begin{pmatrix} 10 \\ 20 \\ 20 \\ 30 \\ 50 \\ 40 \\ 30 \\ 100 \\ 60 \\ 20 \end{pmatrix}. \tag{B.1}$$

Using equation 2.38 gives:

$$X = \begin{pmatrix} 0.6820 \\ -0.4791 \\ -1106.0000 \\ 165.7900 \end{pmatrix}. \tag{B.2}$$

Substituting into equations 2.44 and 2.45 gives: the rotation about the $z - axis$, $\theta$ as $-35.0884$ and the $Scale$, $S$, as 0.8335; the $x - transformation = -1106.0000$ and the $y - transformation = 165.7900$.

The fit residuals, $V$, are found using equation 2.46:

$$V = \begin{bmatrix} v_{X_a} \\ v_{Y_a} \\ v_{X_b} \\ v_{Y_b} \\ v_{X_c} \\ v_{Y_c} \\ v_{X_d} \\ v_{Y_d} \\ v_{X_e} \\ v_{Y_e} \end{bmatrix} = \begin{pmatrix} -0.0202 \\ -0.1373 \\ -0.0922 \\ 0.0376 \\ 0.0709 \\ 0.0379 \\ 0.0704 \\ -0.0383 \\ -0.0289 \\ 0.1001 \end{pmatrix}. \tag{B.3}$$